Consortium Members

CCI_Sea_Level_Bridging_Phase PART 1: New Coastal Sea Level Products

SL_cci BP Part I: New coastal sea level products

Chronology Issues:			
Issue:	Date:	Reason for change:	Author
1.0	19/01/2019	Creation	Anny Cazenave, Florence Marti, Florence Birol Marcello Passaro Jean-François Legeais
2.0	31/03/2019	Includes finalised results	Anny Cazenave, Florence Marti,
2.1	31/03/2019	Last update: answer to review comments	Anny Cazenave, Florence Birol Jean-François Legeais

People involved in this issue:		
Written by (*):	Anny Cazenave, Florence Marti, Florence Birol, Marcello Passaro, Luciana Fenoglio-Marc	Date + Initials:(visa or ref)
Checked by (*):	JF Legeais	Date + Initial:(visa ou ref)
Approved by (*):	JF Legeais	Date + Initial:(visa ou ref)
Application authorized by (*):	J. Benveniste	Date + Initial:(visa ou ref)

**In the opposite box: Last and First name of the person + company if different from CLS*

Index Sheet:	
Context:	Sl_cci
Keywords:	Oceanography sea level sea level
Hyperlink:	

Distribution:		
Company	Means of distribution	Names
CLS	Notification	

Table des matières

List of abbreviations and acronyms

AL	AltiKa
ALES	Adaptive Leading Edge Subwaveform
CCI	Climate Change Initiative
CTOH	Centre de Topographie, d'Océanographie et Hydrologie
DD	Delay Doppler
ECMWF	European Centre for Medium Range Weather Forecast
ESA	European Space Agency
ESRIN	European Space Research Institute
FES	Finite Element Solution
GDR	Geophysical Data Record
GFO	GeoSat Follow-On
GPD	GNSS Path Delay
GSHHG	Global Self-consistent Hierarchical High resolution Geography database
LEGOS	Laboratoire d'Etudes en Geophysique et Océanographie Spatiale
LRM	Low Resolution Mode
MSSH	Mean Sea Surface Height
NEA	North East Atlantic
PODAAC	Physical Oceanography Distributed Active Archive Center
RMS	Root Mean Square
SAR	Synthetic Aperture Radar
SARAL	Satellite with ARgos and ALtimetry
SGDR	Sensor Geophysical Data Record
SL_cci	Sea Level Climate Change Initiative
STAR	Spatio-Temporal Altimeter waveform Retracking
TG	Tide Gauge
TUM	Technical University Munich
SLA	Sea Level Anomaly
SSB	Sea State Bias
SSH	Sea Surface Height
STD	Standard Deviation
SWH	Significant Wave Height
WAF	Western Africa region
XT	XTrack: Across Track

1. Introduction

During the 1st phase (2011-2013) of the CCI sea level project, new, optimized algorithms have been selected for the production of a first set of sea level gridded time series (Ablain et al., 2017, Quartly et al., 2017). During phase II (2014-2016), the sea level time series produced during phase I have been extended and some algorithms have been improved. Therefore, a full reprocessing of monthly sea level gridded time series was carried out over 1993-2015 and this dataset is now freely available for the users (Legeais et al., 2018). This new product benefits from the development of improved radar altimeter standards, leading to better sea level data and reduced altimetry errors.
The CCI sea level project has benefited from a 1-year extension (from March 2018 to March 2019), with two main objectives:

- Characterization of altimetry errors on the CCI sea level products at global and regional scales
- Production of new sea level datasets dedicated to coastal applications in a few selected coastal areas

In the context of these additional activities (called SL_cci_Bridging Phase), it was indeed proposed to investigate the rate of sea level change in selected coastal zones, combining the recent technical advances allowed by different efforts done in the coastal altimetry community. Retracked altimetry data from LRM missions provided by TUM (Passaro et al., 2018), obtained using the ALES retracker and geophysical corrections dedicated to coastal areas were combined using the X-TRACK processing algorithm developed at LEGOS/CTOH (Birol et al., 2017). In this 1-year project, focus was made in 3 pilot regions: western Africa, Mediterranean Sea and northeastern Europe (Fig.1). Two LRM missions have been considered: Jason-1 and Jason-2, over the period from July 2002 to June 2016 (eg 14 full years). Only along-track sea level products have been produced.
In this technical document, the coastal sea level production system is presented in section 2. The ALES retracking and processing component and the X-Track processing component are successively described and then, the coastal sea level products derived from the combined use of these processing components are presented. In section 3, preliminary results on the coastal sea level changes obtained with these new data are presented. A separated document (Part II) presents the validation results obtained with different approaches.

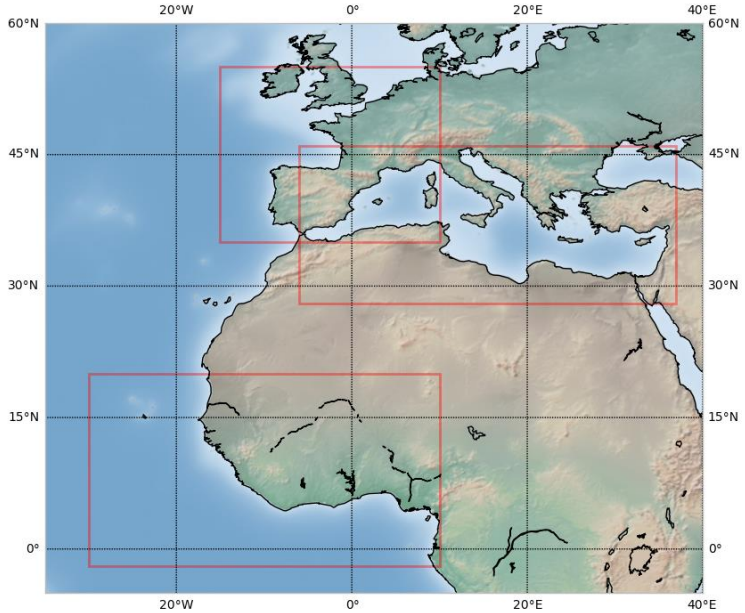

Fig.1: The three pilot regions considered for the CCI Sea Level 'Bridging Phase' project

2. Description of the coastal sea level production system

2.1. The ALES retracking and processing component

2.1.1 The ALES retracking system

The main issue in using the coastal altimetry data, from a signal processing point of view, is the deviation of the waveform shape from the model adopted in the open ocean. For conventional altimetry, new subwaveform partitioning and fitting have been designed to tackle inhomogeneities in the satellite footprint typical of coastal waters, due to presence of land or patches of calm water. Among those, the Adaptive Leading Edge Subwaveform (ALES) has been the one of the few examples of a retracking approach that led not only to validation studies, but also to oceanographic applications and to the development of a global retracked open ocean and coastal dataset based on a single retracking strategy. Indeed the strength of this algorithm relies its reliability in both open ocean and coastal conditions, without the need to change strategy depending on the waveform shape. In ALES, the width of the subwaveform is adapted depending on the sea state, in order to produce estimations that have noise performances similar to the ones of the Sensor Geophysical Data Records (SGDR) products in the open ocean.

An extensive work in checking the comparability of ALES sea level measurements with tide gauges (TG) and the improvements compared to the standards has been conducted in Passaro et al. (2014) and Passaro et al. (2015). The ALES altimetry product has consistently increased the quality and the quantity of altimetry measurements in the coastal ocean. It has been validated with respect to in-situ data in several regions, showing constant improvements in terms of accuracy when compared to the standards. For example, comparing sea level measurements along a track from Jason-1 altimeter with the Trieste TG at the closest location (~7.5 km from the coast), the ALES time series had a correlation coefficient of 0.93 as opposed to 0.60 of the SGDR product. Recently, Piccioni et al. (2018) have demonstrated that the use of ALES data instead of the original SGDR in a tidal model constantly improves the estimations.

In this project, no changes in the retracking algorithm were planned. The algorithm has been already described in details in Passaro et al. (2014), Passaro et al. (2015) and in the document CLS-SLCCI-17-0003 of the previous phase of SL_cci. Data format and output were set among the project partners and the ALES output for the selected regions, augmented with the Sea State Bias correction developed in this project and described in the next section, was provided for all the requested missions to the project partners.

2.1.2 The Sea State Bias correction

The Sea State Bias (SSB) is among the time-variable corrections that are applied to sea surface height estimates from satellite altimetry. With a mean of 5 cm and a time-variable standard deviation of 2 to 5 cm in the open ocean (Andersen and Scharroo, 2011), it is currently one of the largest sources of uncertainty linked with the altimetric signal (Pires et al., 2016). SSB is linked with both the signal processing of the radar echo and the physics of the measurement; its correct interpretation and the understanding of its coastal variability are essential to produce more accurate and more precise sea level estimations.

If SSB is still uncertain in the open ocean, this is even truer in the coastal environment, where since more than ten years the altimetry community is trying to improve the sea level estimates that were previously discarded due to interferences in the signal and scarce reliability of the corrections, including SSB. The physical effects related to the interaction of the radar echo with the crests and throughs of the waves and the numerical effects due to the way the altimeter tracks the echoes (both components of the SSB corrections) need to be reviewed for an altimetry product in the coastal ocean. Unlike in the open ocean, the shape of the waves is influenced by shoaling, refraction and bottom

friction in the shelf seas and by depth-induced wave breaking and triad wave-wave interaction in waters shallower than 20-30 m. Moreover, the traditional open-ocean retrackers are not able to estimate correctly in the coastal zone the significant wave height (SWH) and wind speed, on which the parametric relation that is used to compute SSB is not anymore valid. Finally, since the SSB models are empirically computed from altimetry observations, other components of the residual altimetric error might have a dependence on sea state that varies depending on the regions, such as tidal correction, which are also computed by means of altimetric data and are much less known in shelf seas than in open ocean. Therefore, correcting for the SSB using a model computed on a global scale might not be enough representative, in particular for shelf seas.

For these reasons, we aim in this work at computing a high-frequency (HF) and retracker-dependent SSB correction in order to improve the performances of HF altimetry data. Although initially not planned in the project, we have chosen to expand the study by attempting the computation of a specific regional SSB correction, as an initial test to test its usefulness for the next phases of SL_cci. The region of study concerning the evaluation of the results is the Mediterranean Sea (Med), i.e. one of the SL_cci selected region of study.

Three different SSB corrections are applied to derive the sea level anomalies (SLA) in this study:
1) 1-Hz SSB is the SSB correction available at low frequency (LF) in the SGDR product. The correction is derived using the methodology described in Gaspar et al. (2002) and Labroue et al. (2004) and updated in Tran et al. (2010). This methodology adopts a non-parametric estimation: a statistical technique (kernel smoothing) is used to solve a large system of linear equations based on the observations and on a set of weights. The result is a 2D map of the SSB against wind speed and SWH.

2) 20-Hz SSB is the SSB correction derived by using the same 2D map from Tran et al. (2010) and obtained by courtesy of Ngan Tran from Collecte Localisation Satellites, but computed for each HF point using the HF wind speed and SWH estimations from SGDR and ALES. The computation of the current SSB model is based on an empirical relationship between three retracked parameters. While part of it is due to the physics of the waves and will manifest itself at LF, the model contains also a relation that is due to the correlated errors in the estimation, which is performed at HF. Applying the SSB model at LF therefore means assuming that the error component of the sea level estimation related to the sea state exists only at long wavelengths, reducing its impact on the short-wavelength components.

3) Reg SSB is the SSB correction derived using the regional parametric models computed using the Fu-Glazman (FG) model proposed in Fu and Glazman (1991), and then applied to each HF point using the HF wind speed and SWH estimations from SGDR and ALES.

Two noise statistics are employed to evaluate the precision of the dataset. Firstly, the high-rate noise is computed by considering the differences between consecutive HF SLA values, since SLA is not supposed to change significantly in 300 to 350 m, which is the distance between one measurement and the next. This reference of noise was first used in Passaro et al. (2014). Secondly, the difference in SLA variance between different datasets, i.e. SLA dataset corrected with the described SSB models, is computed on a 1-degree grid. This metric has also been widely used in evaluation of SSB corrections (Tran et al., 2010); for our purpose we use the latest formulation proposed by Pires et al. (2016): the scaled SLA variance differences, which illustrate the impact of different SLAs relative to the regional variability.

Firstly we consider the noise quantified as difference of consecutive HF SLA measurements. We estimate for each cycle the average noise binned in 25-cm intervals of SWH. Then, results are averaged over all the cycles and displayed in Figure 2 with respect to the SWH. The more irregular lines seen at higher SWH are due to the decrease in available measurements. The application of the 20-Hz SSB decreases both the noise at low sea states and the slope of the noise curve. This corresponds to the effect observed by Garcia et al. (2014) when applying a 2-pass retracker to decouple SWH and range estimation and is again proof that SSB should be applied at HF, because it includes retracking errors that are strongly sea-state dependent. On top of that, further improvement of the same kind is brought when the Reg SSB model is applied. This means that our regional high-frequency empirical parametrical SSB correction is superior to the global non-parametric SSB model, even if the latter is applied at HF. It must be stressed that the metrics used in this study, which follow what is done in previous works on the corrections to the range estimated by radar altimetry, are focused on

improvements of the precision, i.e. the repeatability of a HF sea level estimate, which can be quantified by a reduction in the HF variance. An evaluation of the improvement in accuracy shall rely on external data, such as tide gauges, and can be the subject of a future validation study involving other regions as well.

To better quantify this improvement, we compute the scaled SLA variance difference in the two regions of study on a 1-degree grid in Figure 3. The comparison is performed by choosing a reference and a challenger dataset: in this way, the upper panel show the performances of the 20-Hz SSB taking the 1-Hz SSB as a reference; the middle panel show the performances of the Reg SSB taking the 20-Hz SSB as a reference; finally the lower panel shows the performances of the Reg SSB taking the 1-Hz SSB as a reference and therefore summarize the overall improvement. The decrease in variance is ubiquitous also within the domain.

To summarise using the averaged statistics the simple application of an SSB correction based on HF data improves the precision of HF sea level data by 14%. We notice how the improvement shown by the 20-Hz SSB for SGDR is similar to the one reported by Zaron et al. (2016) in their North Pacific test region, which indicates that this application is an alternative method to reduce the retracker-related noise. Subsequently, the re-computation of a parametric regional SSB model improves it overall by 29%.

In conclusion, in the context of this project it has been demonstrated that as a first step the SSB correction should be computed and applied using the high-rate measurements of SWH and backscatter coefficient. This is because a high-rate application of the SSB correction reduces the correlated errors between range and wave height estimations. Encouraging preliminary results are also found using a recomputed regional model for the specific retracker (ALES on Jason-2). The future challenges will be therefore the development of different ALES SSB regional solutions for LRM altimetry, including the interpretation of possible differences according to the selected regions, and the development of a SSB correction for the DD retracking.

This study constitutes the bulk of the recent publication Passaro et al. (2018), partially funded by this project, which contains further details and analysis. The 20-Hz SSB based on ALES was applied to the full dataset provided to the Consortium in this project. The additional Reg SSB was only applied to the specific test area (Mediterranean Sea).

2.1.3 Overall Performance Analysis

An overall performance analysis was performed globally on Jason-1 and Jason-2 by comparing crossover differences using the SGDR strategy (standard retracking + standard sea state bias correction) with the strategy followed in this project (ALES retracking + high rate sea state bias correction).

To obtain the 1-Hz sea surface heights we first subtract the estimated range from the orbital altitude and then we correct for pole tide, ocean tide, solid earth tide, geophysical effects (ionospheric delays, wet and dry tropospheric delays), dynamic atmosphere and sea state bias (using the original or the recomputed correction depending on the experiment). Finally, the median value of the screened 20-hz points within the 1-hz block is taken.

The 1-Hz points are used to perform a crossover analysis. This is a standard practice in altimetry and has been used is several publications as a key indicator of the data quality for altimetric missions (Ablain et al., 2010). In order to reduce the impact of oceanic variability, crossovers are taken into consideration if the time lag between the two passes is shorter than 10 days. Crossovers are here defined as all the available 1-Hz points of two crossing tracks that are closer than 5 km.

Figure 4 shows, for each cycle of J1 and J2 reprocessed in this project, the median of the STD of the crossover differences. For J1 in the global ocean, this value is 9.27 cm for SGDR and 7.99 cm for ALES; for J2 we have 9.86 cm for SGDR and 8.17 for ALES. This corresponds to a 30% improvement in

variance, which is mostly due to the application of the Sea State Bias using the high-rate SWH and Wind estimations from ALES. Moreover, if we define as “outliers” the points in which the crossover differences exceed 50 cm or are not computable because the measurement is missing, we find out that in the coastal area within 20 km from the coast ALES has 6% less outliers than SGDR in Jason-1 and 10% less in Jason-2 (see Figure 5).

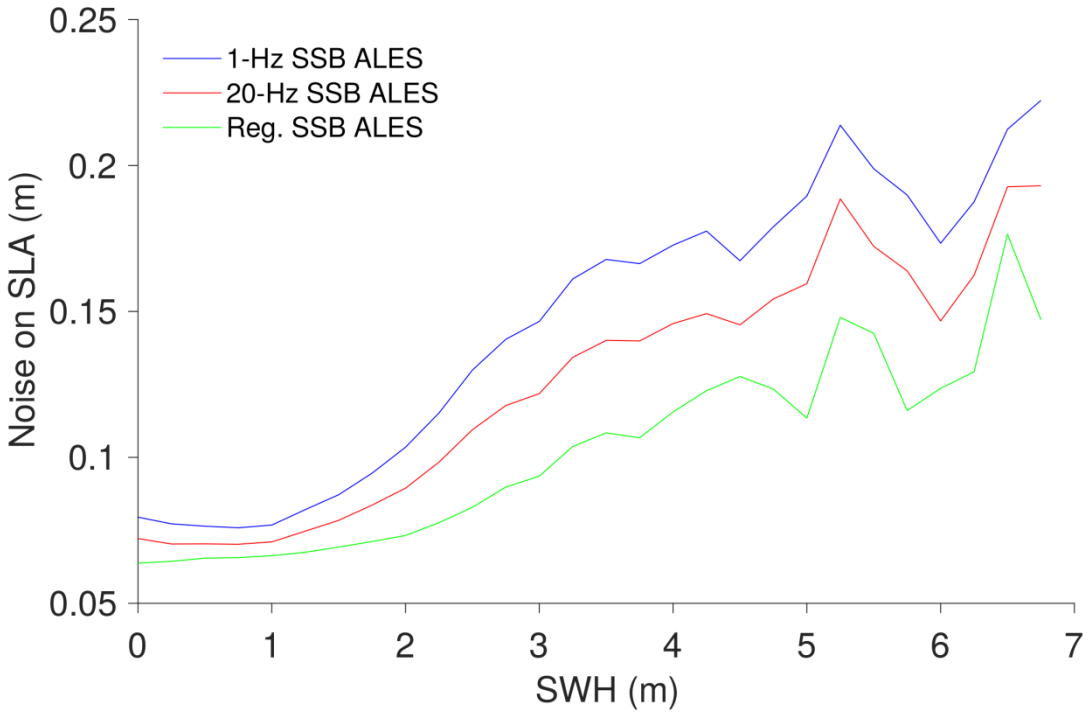

Figure 2: Noise of the sea level anomalies computed as difference between consecutive high-rate estimations using different SSB corrections analyzed in this study in Med. Continuous lines refer to SGDR data, while dashed lines refer to ALES data. The sea level anomalies were corrected with the original 1-Hz SSB correction (blue), with the 20-Hz SSB correction (red) and with the regional SSB correction (green)

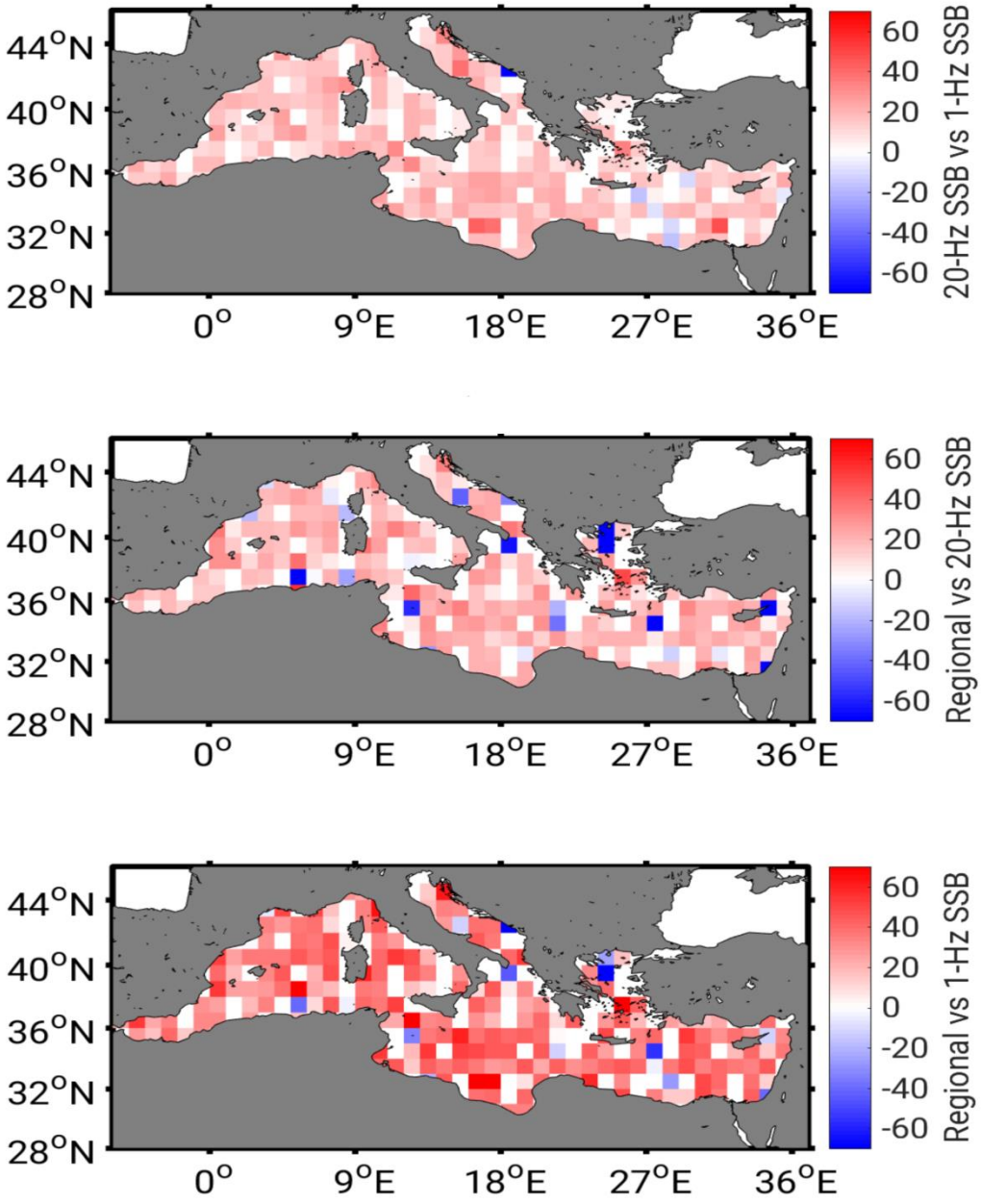

Figure 3: Percentage of scaled sea level anomalies (SLA) variance differences between a challenger and a reference model. Upper panel: SLAs computed with 20-Hz SSB correction (challenger) against the ones computed with the original 1-Hz correction (reference). Middle Panel: SLAs computed with 20-Hz SSB correction (challenger) against the ones computed with the regional SSB correction (reference). Lower Panel: SLAs computed with regional SSB correction (challenger) against the ones computed with the original 1-Hz correction (reference). Red squares represent regions with a lower SLA variance for the challenger, i.e. an improvement in the noise statistics with respect to the reference. The dataset used is the SGDR.

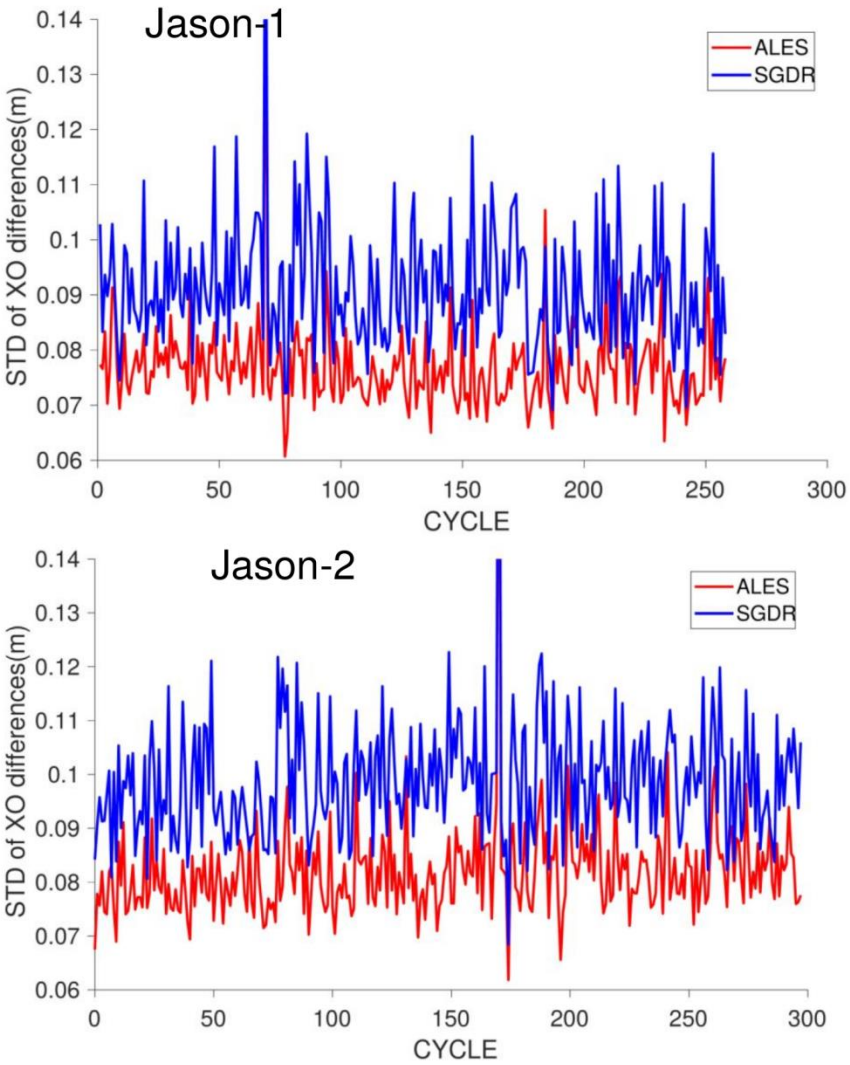

Figure 4: Global average by cycle of the Standard Deviation of the crossover differences for the SGDR dataset and the ALES dataset corrected for the high-rate Sea State Bias correction.

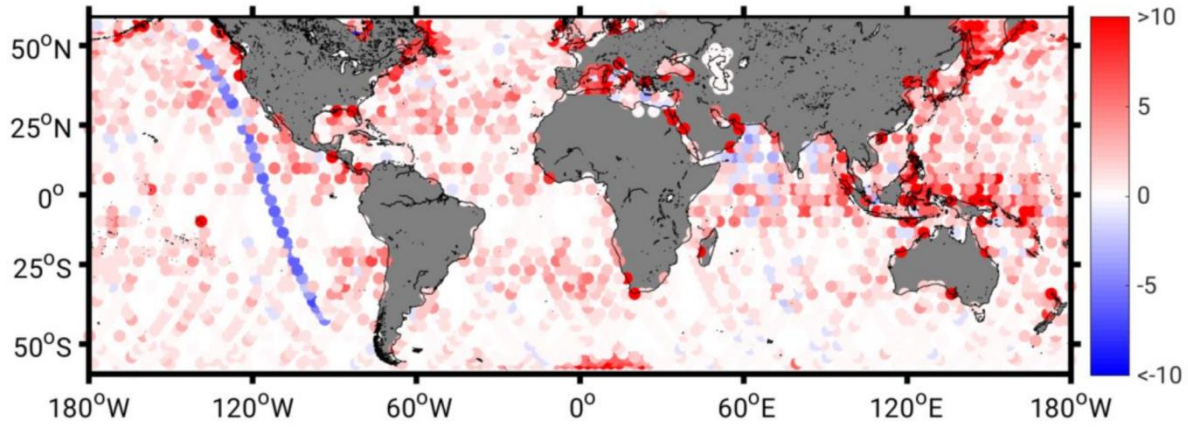

Figure 5: Difference between the number of outliers at crossover points in SGDR and ALES dataset corrected for the high-rate Sea State Bias correction.

2.2 The X-TRACK processing component

During the last decade, the LEGOS/CTOH developed the "X-TRACK" processing system in order to optimize the computation of L3 altimetry products for regional and coastal applications. Today, X-TRACK already provides homogeneous 1-Hz sea level data, computed from standard L2 GDRs data and improved geophysical corrections, covering the global coastal ocean and most of the LRM missions, as well as associated fully documented algorithms. The corresponding X-TRACK R&D coastal altimetry product is freely distributed by the operational AVISO+ service and has already been used by many scientific users for different types of applications (more than 60 refereed publications). In the context of this project, a new version of the X-TRACK processing chain has been developed in order to enhance the capabilities of satellite altimetry along coastlines, by using 1) high-rate (i.e. 20-Hz) altimeter measurements instead of the 1-Hz ranges and 2) the ALES retracked data instead of the standard GDR products.

The X-TRACK processing system is described in details in Vignudelli et al. (2005), Roblou et al. (2011) and Birol et al. (2017). Here we will only provide a brief description. The X-TRACK processing system works on a regional basis (the regional domain can be easily defined before the processing in a parameter file). It first reads parameters from the L2 products for each altimetry mission plus additional state-of-the-art geophysical corrections and auxiliary informations used during the processing phase (as the distance to the coast). Since altimetry observations degrade in accuracy near the coast, the processing first selects valid ocean data. Then, a precise land mask and a dedicated editing strategy are used. The latter includes two steps. The first step is to impose editing criteria, both on the altimeter measurements and corrections, designed to be more restrictive than the standard ones (AVISO, 1996). These threshold criteria have been chosen after series of tests for each parameter, in order to ensure that all outliers are totally removed. The behavior of all corrections is analyzed along the track, taking into account their individual characteristics. Each correction is edited in a different way (Birol el al., 2017). Abrupt changes are assumed to be associated with erroneous data. Outliers are removed. Since the editing process lead to the rejection of all altimeter measurements for which at least one correction is considered as wrong, this method rejects much more data than the classical ones, even if the altimeter measurement is meaningful. Thus, in a second step, all corrections are recomputed using interpolation/extrapolation methods, based on valid data for each correction. This strategy is very efficient in recovering a lot of good altimeter measurements flagged in the standard product because of a deficient correction. Once the corrected sea surface heights (SSHs) are computed, they are projected onto fixed points along the nominal ground track of the altimeter satellite and converted into SLAs by subtracting a precise mean sea surface height. The

latter is computed at the fixed nominal points, by inversion of all the available SSH measurements along the repeated ground tracks of the considered altimetry mission. A quadratic function is fitted to the corrected SSHs values around the nominal points to correct the cross-track and along-track variations between the observation and the nominal points and the corresponding values computed at the nominal points are defined as the MSSH. This procedure is important, since in coastal areas where topographic gradients can be large, use of a standard mean sea surface leads to significant errors in SLAs because of poor spatial resolution (Vignudelli et al., 2005). On request, the along-track SLA can be further spatially filtered to remove the background noise. (in option, corresponding to the filtered version of the X-TRACK SLA product). Therefore, a low-pass Loess filter is used in the alongtrack direction; by default a 40 km cutoff frequency is used but the latter can be adapted to optimize the signal-over noise ratio corresponding to the data set processed (e.g. the altimetry mission and the region). This optimal cutoff frequency can be quantified by spectral analysis. Note that we do not plan to use this filtering option in the context of this project unless it is explicitly requested by ESA or by the validation team. Figure 6 summarizes the different processing steps of the X-TRACK system.

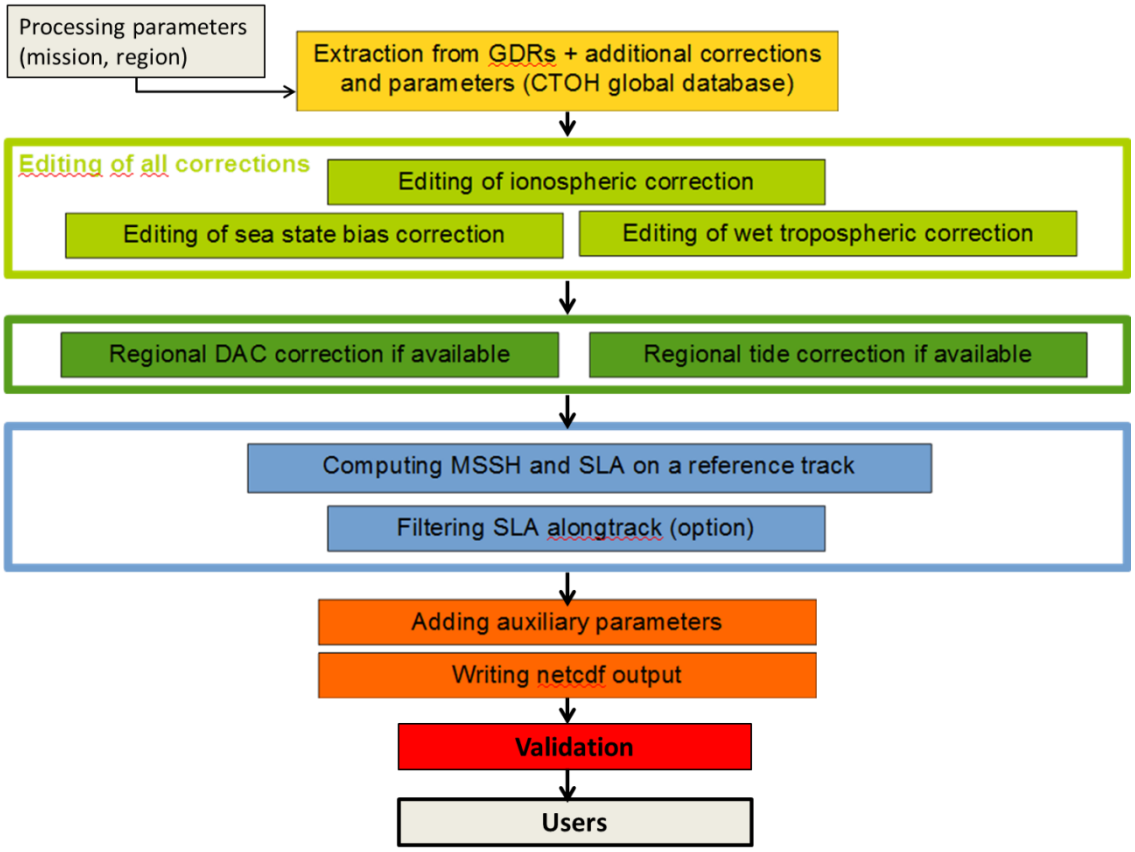

Figure 6: Processing steps of the X-TRACK system.

2.3 The ALES/X-TRACK product obtained from the merging of both processing components

2.3.1 Description

The X-TRACK processing system has been designed to provide along-track SLA time series at 1-Hz along the track for different LRM missions (T/P, GFO, Envisat, Jason-1,2,3 and SARAL/AltiKa). In the

context of the SL_cci “Bridging phase” project, all algorithms have been rewritten and adapted in order to compute high-frequency (i.e. 20-Hz) altimeter measurements, and to take advantage of the ALES retracker. The editing step has been redefined, as well as the set of geophysical corrections (listed in Table 1), and the computation of the Mean sea Surface Height (MSSH) is now at 20-Hz. A first version of this new system has been produced for the 3 pilot regions. Both Jason 1 and Jason2 data have been reprocessed, from cycle 1 to 258 and from cycle 1 to cycle 293, respectively. In a second time, for each of the three test regions considered in the project, both altimeter missions have been combined in a single homogeneous sea level time series by using a regional bias between Jason2 and Jason1 computed with the following methodology:

1. calculation of the mean sea level over the region considered for both Jason2 cycles 1 to 19 and Jason1 cycles 240 to 258, excluding all the data located at a distance < 50 km from land and altimetry points where we have less than 80% of the SL data considered as valid in the time series.
2. calculation of the difference between the resulting J2 and J1 mean sea levels. The regional bias (Jason 2 versus Jason 1) obtained are: -6.1244 cm for the Mediterranean Sea, -5.9164 cm for the North East Atlantic and -5.533 cm for the Western Africa. Jason-2 SL data were then connected to Jason-1 on Jason-2 cycle 21 by subtracting the regional bias to Jason-2.

Note that a new release of the product, based on the GPD+ and FES2014 for the wet tropospheric and tidal corrections, respectively, is under processing and will be available at the end of the project.

Corrections	**Jason-1**	**Jason-2**
Ionosphere	From dual-frequency altimeter range measurements	
Dry troposphere	From ECMWF model	
Wet troposphere	From radiometer	
Sea state bias	SSB ALES (see section 2.1.2)	
Solid tides	From tide potential model (Schureman 1958)	
Pole tides	From Wahr, 1985	
Loading effect	From FES1999 (Lefèvre et al., 2002)	
Atmospheric Correction	From TUGOm 2D global models for periods smaller than 20 days (Carrere and Lyard 2003) + Inverted barometer for periods greater than 20 days, derived from ECMWF pressure.	
Ocean Tide	From FES 2012 (Carrère et al., 2012)	

Table 1: List of corrections used in the computation of ALES/X-TRACK SLA.

2.3.2 Performance

A first performance analysis of the new ALES/X-TRACK product was performed for both Jason-1 and Jason-2 and for the three test regions by comparing the regionally averaged distance to the coast of the first SL point available in the resulting L3 product, where more than 50%/80%/95% of data are considered as physically consistent in the time series. The distance to coast is computed from the last

version of the GSHHG product (version 2.3.7 Released June 15, 2017 , http://www.soest.hawaii.edu/wessel/gshhg/). In order to analyse the respective gain associated to the use of high-frequency (i.e. 20-Hz) altimeter measurements, and to the use of the ALES retracker, we have produced and analysed 3 datasets (for each region and for both Jason1 and jason2):

- the standard 1-Hz X-TRACK product computed from the 1-Hz measurements provided from GDRs products (called XT 1Hz hereinafter),
- a 20-Hz X-TRACK product version computed from the 20-Hz measurements provided from GDRs products (called XT 20Hz hereinafter),
- the combined 20-Hz ALES/X-TRACK product computed from the 20-Hz measurements retracked with ALES (called XT/AL 20Hz hereinafter),

In terms of geophysical corrections, they are the same for the three datasets, except for XT/AL 20Hz, where the ALES SSB is used.

All the results are shown in figure 7. For the case where more than 80% of the data are considered as physically consistent in the time series, they are also provided in Table 2.

In summary, in terms of coastal data availability, we observe a very significant gain in performance in the new combined ALES/X-TRACK product for both Jason-1 and Jason-2. In Jason-2, in average, we have now more than 80% of SL observations in the time series up to 2 km / 4 km from land with Jason-2 / Jason-1, instead of 6 km / 7 km in the X-TRACK product which is distributed today. Results are lower in the Western Africa region for a reason which is still unknown but under analysis. It could be partly due to the GSHHG product used in the computation of the diagnostic, since it appears to be less accurate in that area than along European shelves. The performance of the new ALES/X-TRACK product and the gain in geophysical information associated will be further analysed in the next sections.

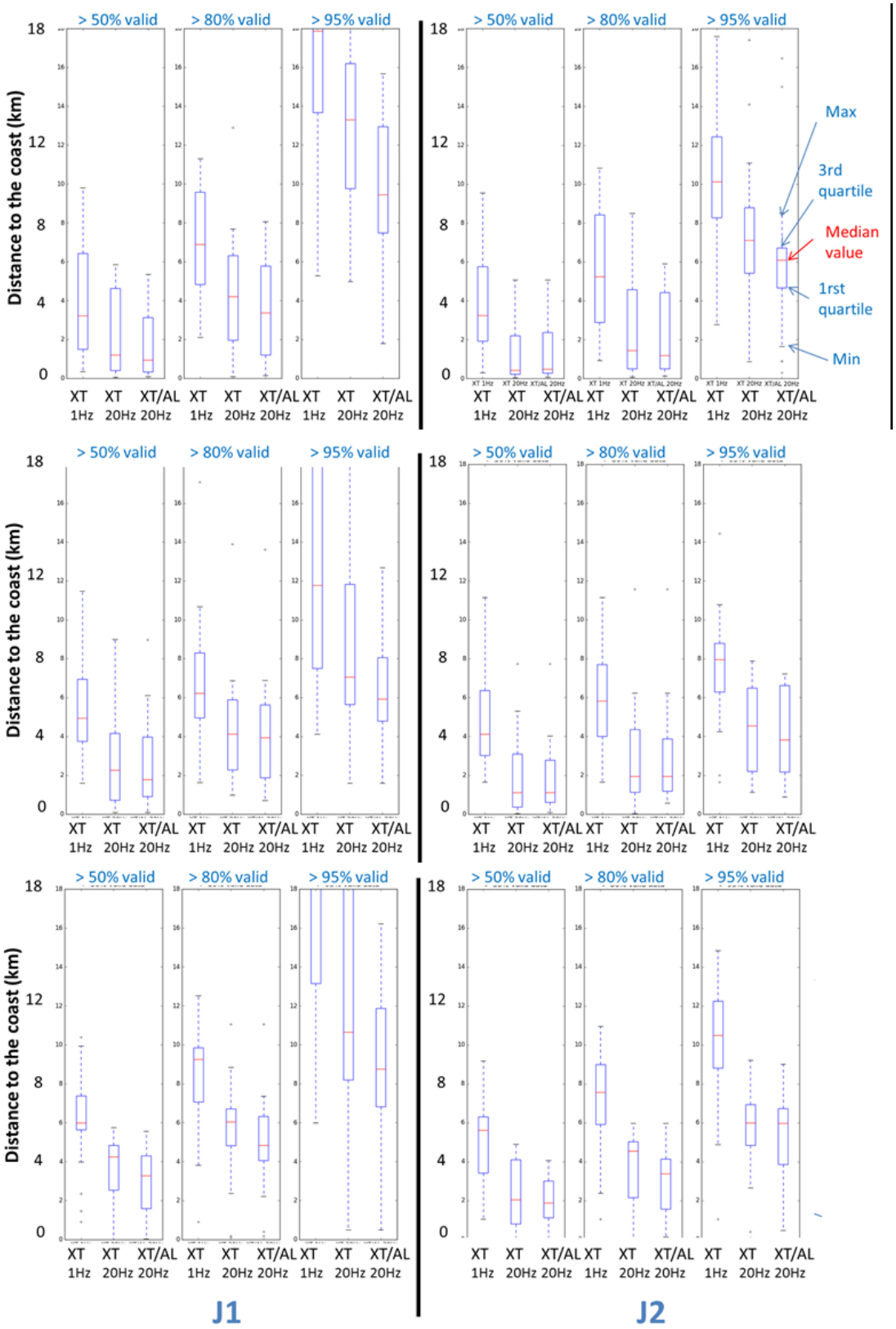

Figure 7: Mean distance to the coast (in km) of the first SL point available in the L3 product, where more than 50%/80%/95% of data are considered as physically consistent in the time series for the Mediterranean sea (top), the North East Atlantic (middle) and the Western African coast (bottom) and for three different data sets: the standard 1-Hz X-TRACK product (XT 1Hz), the 20 Hz version of X-TRACK (XT 20Hz) and the combined ALES/X-TRACK product (XT/AL 20Hz). Results are provided in the form of whisker plots.

Region	Mission	XT 1Hz	XT 20Hz	XT/AL 20Hz
MEDSEA	J1	6,9	4,2	3,4
	J2	5,2	1,4	1,2
NEA	J1	6,2	4,1	3,9
	J2	5,8	1,9	1,9
WAF	J1	9,3	6,1	4,8
	J2	7,6	4,5	3,4
ALL	J1	7,47	4,8	4,03
	J2	6,2	2,6	2,17

Table 2: Mean distance to the coast (in km) of the first SL point available in the L3 product, where more 80% of data are considered as physically consistent in the time series as a function of the mission and the region considered.

3. Coastal sea level trends in the pilot regions: Results

In the context of the additional activities (Bridging Phase) of the ESA CCI Sea Level Project, it was proposed to investigate the rate of sea level change in selected coastal zones, combining retracked altimetry data from LRM missions (using the ALES retracked products provided by TUM, Passaro et al., 2018a,b,c) and geophysical corrections dedicated to coastal areas (using the X-TRACK products developed at LEGOS/CTOH, Birol et al., 2017). In this 1-year project, focus was made in 3 regions: western Africa, northeastern Europe and Mediterranean Sea (see Fig.1 above). Here we present coastal sea level results obtained by the project in the 3 pilot regions, using Jason-1 and Jason-2 satellite tracks from July 2002 to June 2016 (14 full years).

3.1 Data

For both Jason-1 and Jason-2 missions, we considered 20 Hz along-track sea surface height data based on the merging of XTRACK products with the ALES retracker (resolution ~350 m). For each Jason-1/2 track, data of individual cycles were projected onto a 'mean' profile (after rigorous editing), and sea level anomalies –SLA- (with respect to the mean profile, see section 2.2 for details concerning the mean profile computation) were estimated for each cycle. In the following, we use these SLA data.

We also considered the C3S (Copernicus Climate Change Service) multi mission gridded product to estimate the regional sea level trends for the period 2002-2016. The corresponding trend maps are shown in Fig.8, Fig.9 and Fig.10 over the western tropical Atlantic, Northern Europe and Mediterranean Sea, respectively. On each map, the Jason tracks coverage are superimposed.

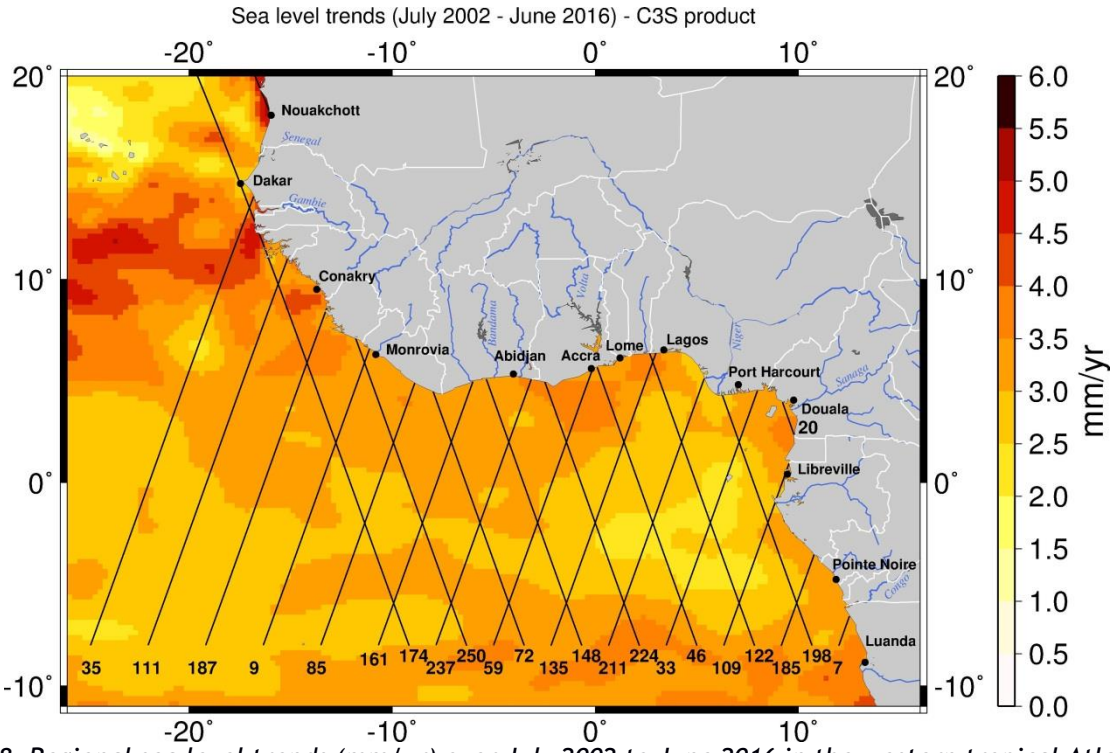

Fig.8: Regional sea level trends (mm/yr) over July 2002 to June 2016 in the western tropical Atlantic from the C3S gridded product. The Jason-1/2 track coverage is superimposed. Numbers identify the track numbers.

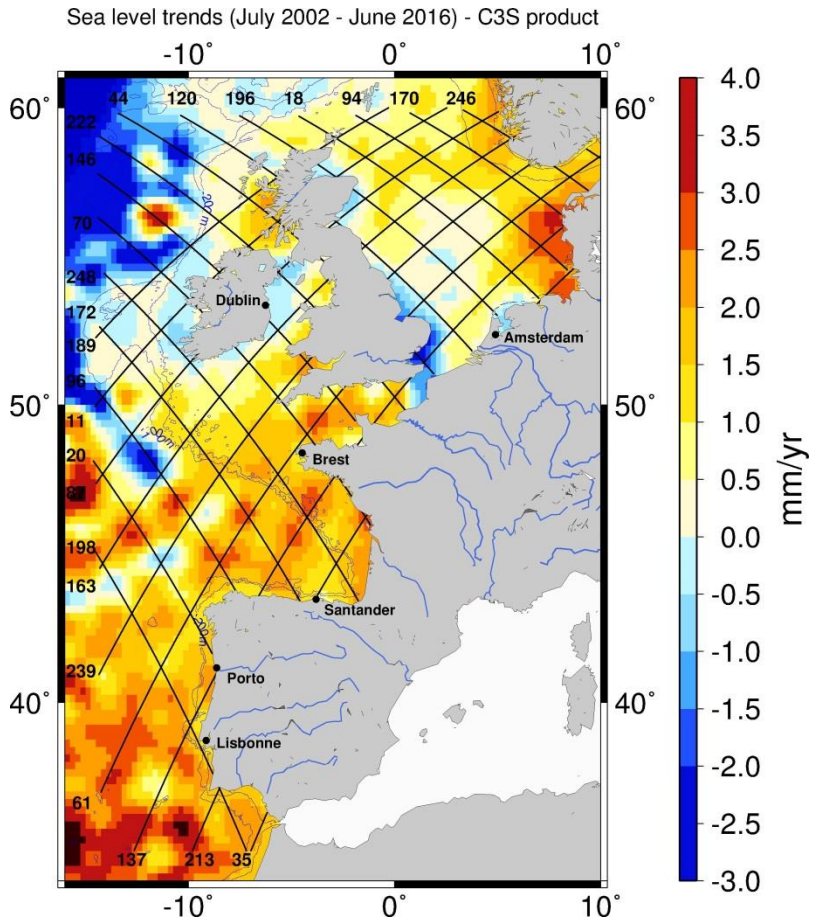

Fig.9: Regional sea level trends (mm/yr) over July 2002 to June 2016 over Northern Europe from the C3S gridded product. The Jason-1/2 track coverage is superimposed. Numbers identify the track numbers.

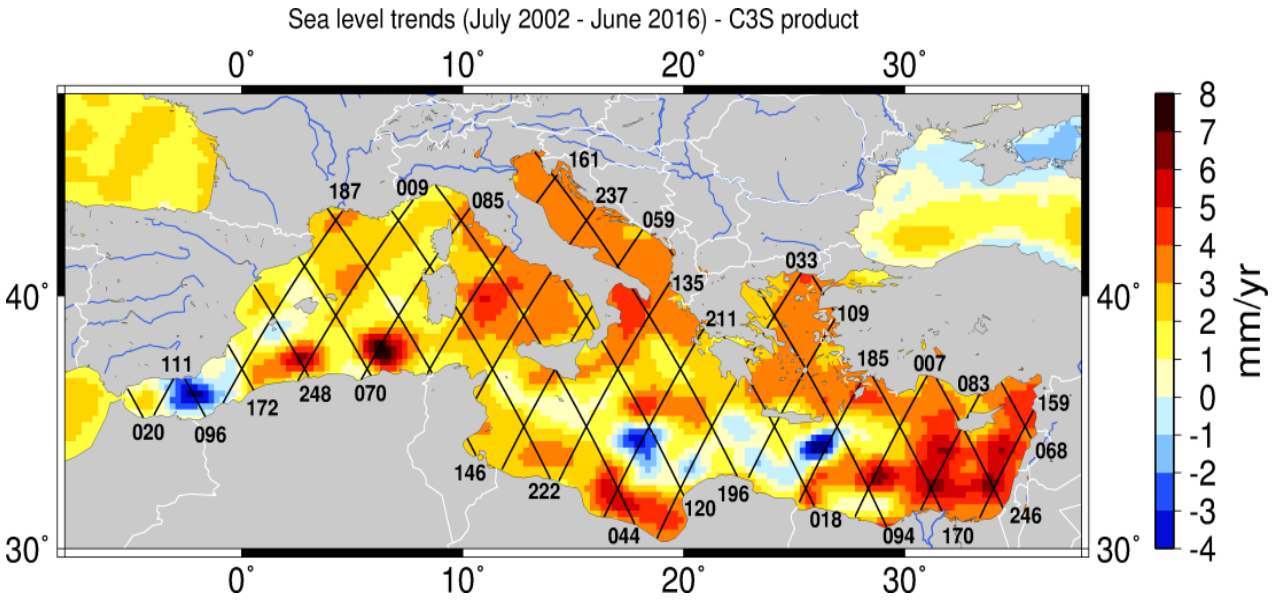

Fig.10: Regional sea level trends (mm/yr) over July 2002 to June 2016 over the Mediterranean Sea from the C3S gridded product. The Jason-1/2 track coverage is superimposed. Numbers identify the track numbers.

3.2 Open ocean and coastal sea level trends along the Jason-1/2 tracks: Method

We computed sea level trends over the 14-year period along all Jason tracks crossing the coast, as shown in Fig.8-10. For each track, sea level trends were computed over successive segments of varying lengths along different portions of the profile from the open ocean to the coast. Constant length segments were considered along the tracks, starting from the closest 20-Hz point to the coast. The construction of the segments along each track is illustrated on Fig.11.
We successively considered three spatial scales to estimate the along track evolution of the sea level trends:
(a) The entire track over the selected region; trends computed along 50 km-long segments
(b) The first 50 km from the coast; trends computed along 2 km-long segments
Each segment is characterized by a center which corresponds to the location of the nearest point to the middle of the segment.
An additional case (c) was considered:
(c) The first 15 km from the coast; trends computed at individual 20 Hz point location
For all cases (a), (b) and (c), SLA time-series were monthly averaged, all orbital cycles from July 2002 to June 2016 were considered and SLA mean was removed on the period.
For cases (a) and (b), the SLA data were spatially averaged along the segment length for each orbital cycle.
Trends were then computed after removing the annual and semi-annual signals.

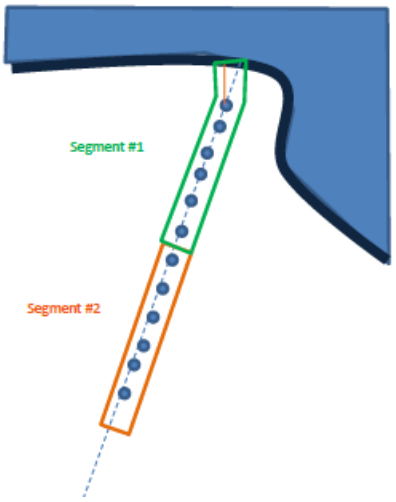

Fig.11: Sketch illustrating the along-track segment construction

3.3. Open ocean and coastal sea level trends along the Jason-1/2 tracks: Results for the western African coasts

In the following, we discuss for each Jason-1/2 track a series of figures that are presented in annex. They are organized as follows:

- **Annex A**: First series of figures, called **Fig.12** (1 page per satellite track; the tracks are ranked from west to east for the ascending profile, and from east to west for the descending profiles). The content of the figures is the following:

(a) Upper panel: Sea level trends (colored circles) computed over the 14-year time span at each 20 Hz point for the closest track portion to the coast (a few km). White triangles identify points with non-significant trend estimates (SLA data too scattered or not enough numerous for a robust trend estimation). The background map shows the geographical setting based on a recent version of Google Earth.
(b) Lower panel: Associated sea level trend uncertainties (+/- 1 standard error) (note the change in color scale)
An example is shown below:

- **Annex B:** Second series of figures, called **Fig.13** (1 page per satellite track; the tracks are ranked from west to east for the ascending profile, and from east to west for the descending profiles). The content of the figure is as follows:

(a) Upper left panel: Sea level trends (colored circles) computed over the 14-year time span at each 20 Hz point for the closest track portion to the coast (a few km). White triangles identify points with non-significant trend estimates (SLA data too scattered or not enough numerous for a robust trend estimation). The background map shows the geographical setting based on a recent version of Google Earth.
(b) Upper right panel: Associated sea level trend uncertainties (+/- 1 standard error) (note the change in color scale)
(c) SLA time series (blue dots) since June 2002 for the closest 20 Hz point to the coast (distance indicated in the heading). Red dots are outliers identified by simple statistical test based on the time series RMS (SLA values larger than 2 RMS are excluded). In green is shown the regression line computed over the 14-year time span (excluding the outliers). The corresponding trend value and associated error (+/-1 standard deviation) is indicated in the legend of the figure.
(d) Same as (c) for the second closest point to the coast
(e) Same as (c) for the third closest point to the coast
(f) Sea level trend values (green dots) and associated formal error (+/-1 standard deviation; shaded area) as a function of distance to the coast (last 15 km) estimated at each 20-Hz point.

An example is given below for panels c to f:

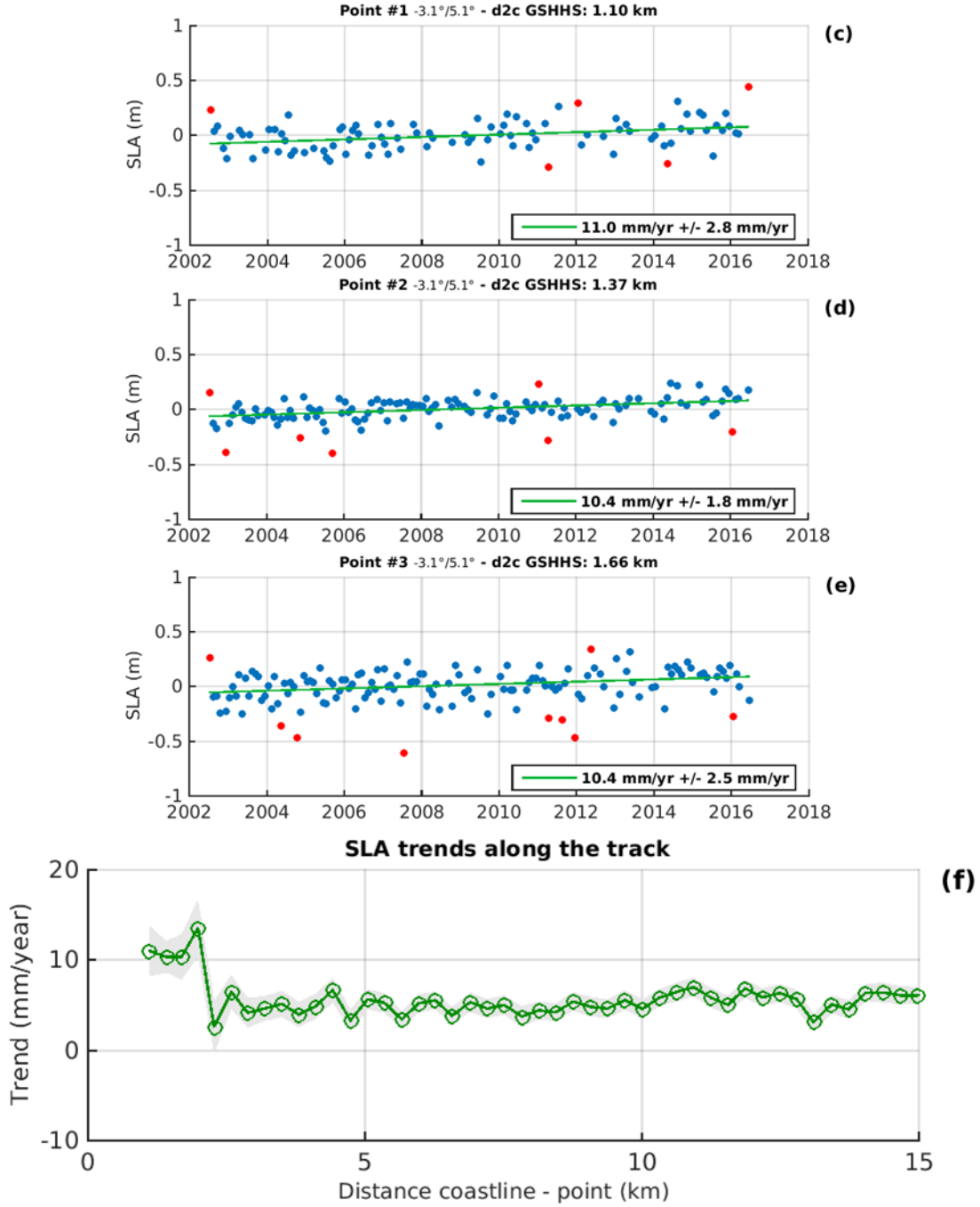

- **ANNEX C**: Third series of figures, called **Fig.14** (3 tracks per page):

(a) Sea level trends computed over successive 50 km-long segments along the entire track length (green curve); Regional trends interpolated from the C3S gridded data (red curve).
(b) Same as (a) but for the last 50 km portion of the track towards the coast, with trends computed by averaging SLA data over successive 2-km long segments.

An example is given below:

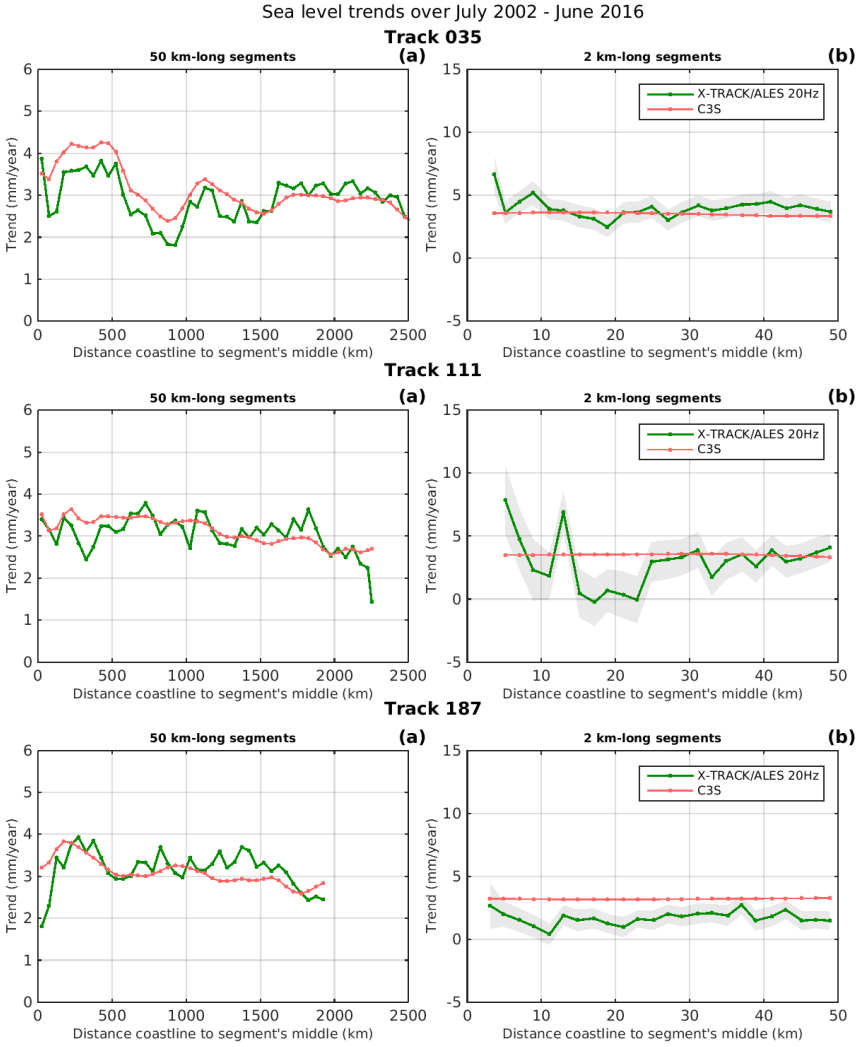

Finally **Figure 15.** shows the distribution of the closest distances to coast reached by the XTRACK/ALES 20-Hz data (i.e., distance to coast of the first valid point) for all Jason tracks considered in the study region (left panel) and associated trend estimates over 2002-2016 (right panel).

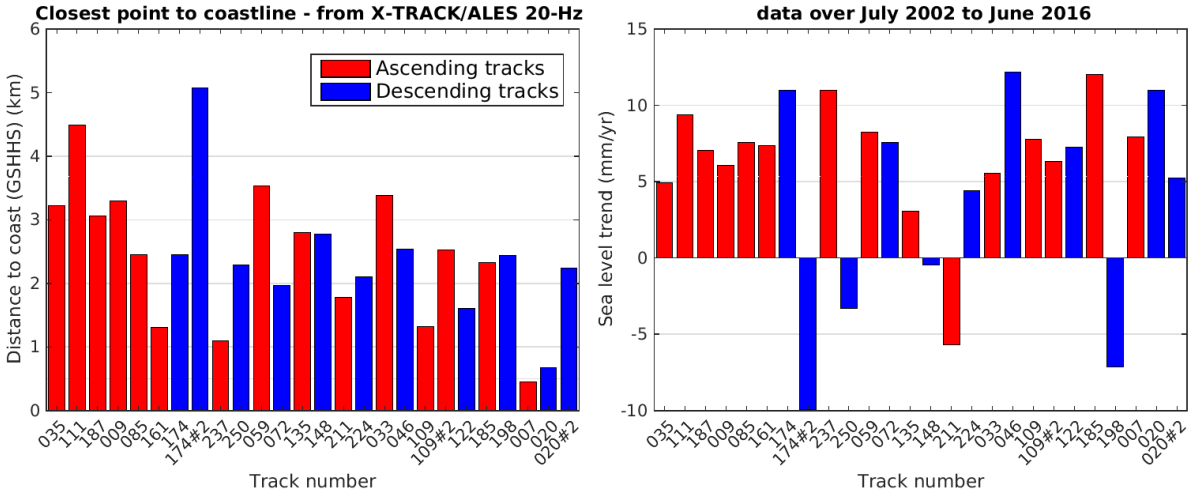

Fig.15: distribution of the closest distances to coast reached by the XTRACK/ALES 20-Hz data (i.e., distance to coast of the first valid point) for all Jason tracks considered in the study region (left panel) and associated trend estimates over 2002-2016 (right panel).

3.4: Open ocean and coastal sea level trends along the Jason-1/2 tracks: A few results for Northern Europe

Results were obtained for the northwestern Europe region following the same method than for western Africa and Mediterranean Sea region. In the following, we discuss for each Jason-1/2 track a series of figures that are presented in annex. Note that contrary to the western Africa case, **all** individual 20-Hz points, including outliers, have been kept to compute the trend. They are organized as follows:

- **Annex D**: First series of figures, called **Fig.16** (1 page per satellite track; the tracks are ranked from west to east for the ascending profile, and from east to west for the descending profiles). The content of the figures is the following:

*(a) Upper panel: Sea level trends (colored circles) computed over the 14-year time span at each 20 Hz point for the closest track portion to the coast (a few km). **Non-significant trends are not identified as they were from the western Africa case**. The background map shows the geographical setting based on a recent version of Google Earth.*

(b) Lower panel: Associated sea level trend uncertainties (+/- 1 standard error) (note the change in color scale compared to panel - color scales for trend uncertainties are identical for western Africa and northern Europe cases)
An example is shown below:

Annex E: Second series of figures, called **Fig.17** (1 page per satellite track; the tracks are ranked from west to east for the ascending profile, and from east to west for the descending profiles). The content of the figure is as follows:

(a) Upper left panel: Sea level trends (colored circles) computed over the 14-year time span at each 20 Hz point for the closest track portion to the coast (a few km) The background map shows the geographical setting based on a recent version of Google Earth.
(b) Upper right panel: Associated sea level trend uncertainties (+/- 1 standard error) (note the change in color scale)
(c) SLA time series (blue dots) since June 2002 for the closest 20 Hz point to the coast (distance indicated in the heading). Red dots are outliers identified by a simple statistical test based on the time series RMS (SLA values larger than 2 RMS are excluded). In green is shown the regression line computed over the 14-year time span (excluding the outliers). The corresponding trend value and associated error (+/-1 standard deviation) is indicated in the legend of the figure.
(d) Same as (c) for the second closest point to the coast
(e) Same as (c) for the third closest point to the coast
(f) Sea level trend values (green dots) and associated formal error (+/-1 standard deviation; shaded area) as a function of distance to the coast (last 15 km) estimated at each 20-Hz point.

An example is given below for panels c to f:

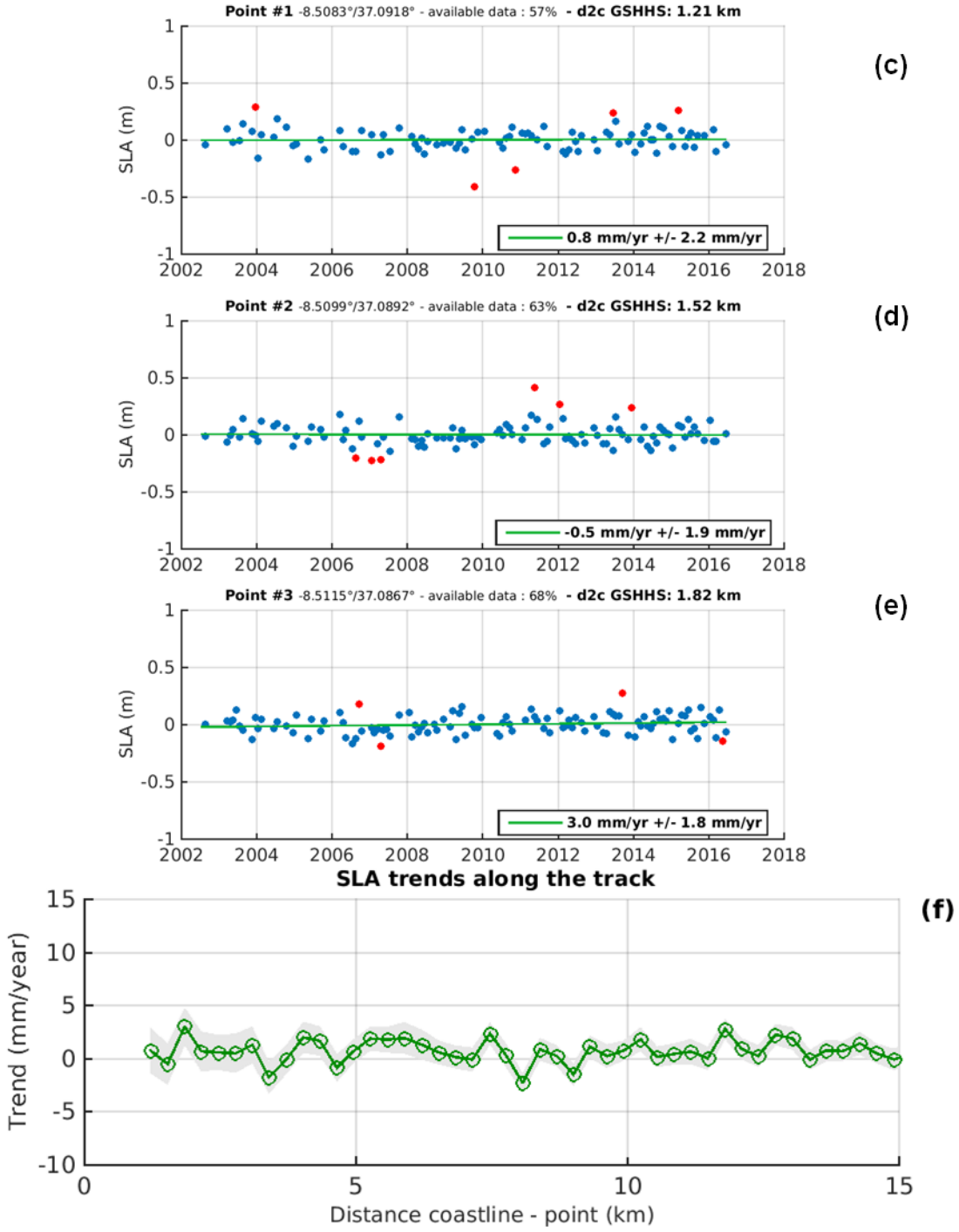

3.5: Open ocean and coastal sea level trends along the Jason-1/2 tracks: Results for the Mediterranean Sea

Results were obtained for the Mediterranean Sea region following the same method than for western Africa and northern Europe region.
In the following, we discuss for each Jason-1/2 track a series of figures that are presented in annex.

The geography of the region implies that tracks approach coasts at different locations. To distinguish the various coasts, tracks are cut into portions located between two strips of land. Portions are defined starting from the north of the track. For each portion, the satellite passes by land twice, at the north and the south of the portion.
Finally, **each intersection between track and land** (larger than about 20 km) **was given a name** in the following format: "track_number #portion_number north/south_position" (e.g.: 085 #1 N). If only one portion is identified, the name becomes "track_number north/south_position" (e.g.: 111 S).

Note that contrary to the western African case, all individual 20-Hz points are kept (including outliers) to compute the trend. They are organized as follows:

- **Annex F:** Series of figures, called **Fig.18** (8 tracks per page; the tracks are ranked from west to east for the ascending profile, and from east to west for the descending profiles - for each track, all portions are treated), showing *sea level trend values and associated formal error (+/-1 standard deviation; vertical black line) as a function of distance to the coast (last 15 km) estimated at each 20-Hz point* (similar to Annex B (f) and Annex E (f)). An example is given below:

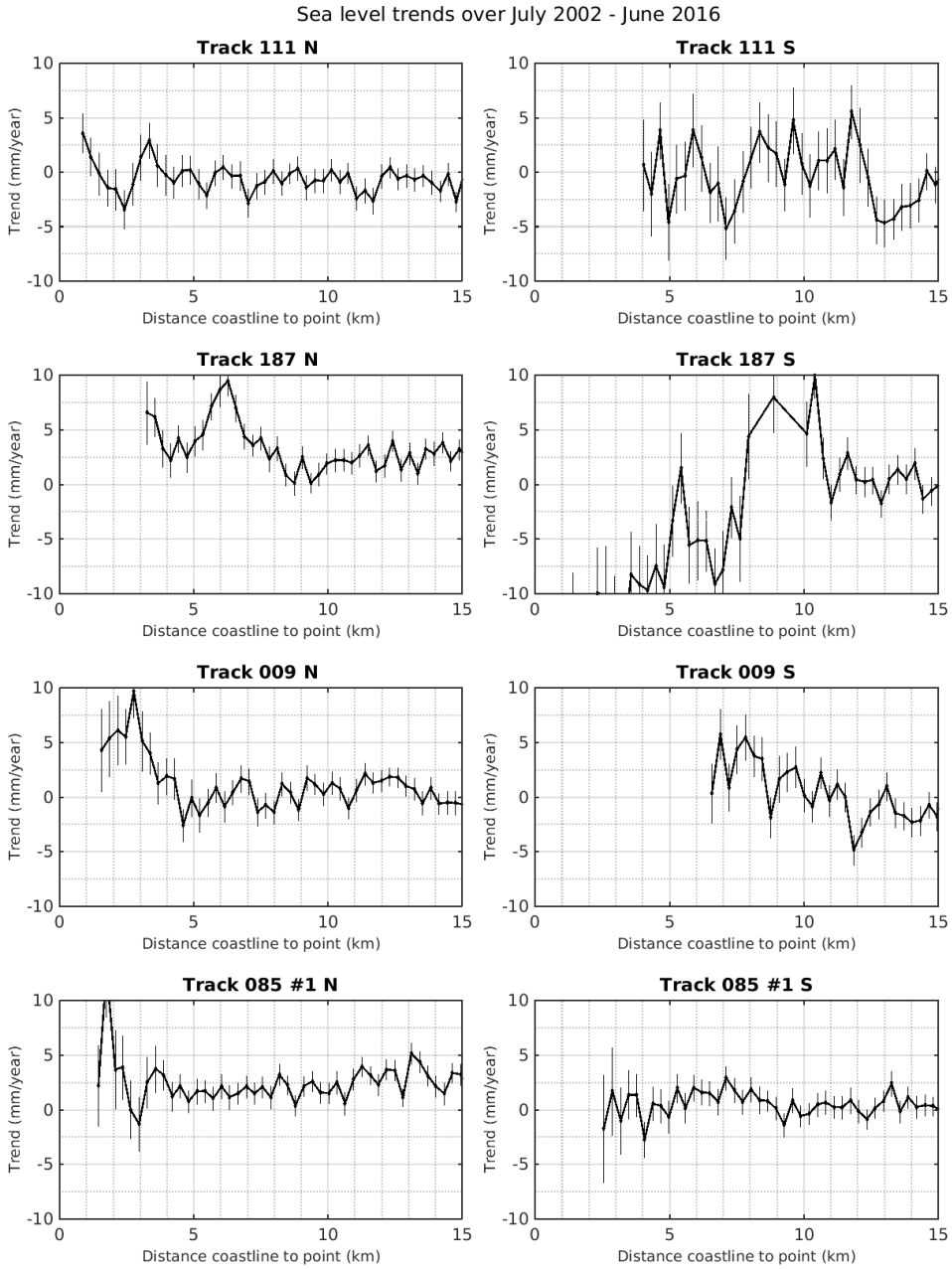

Figure 19 presents the distribution of the distances to coast reached by the closest X-TRACK/ALES 20-Hz data to shore (left panel). Only the track portions for which data are available under 2 km from coast are shown in the histogram: there are 34 of them. 64 track portions present data under 4 km from coast.

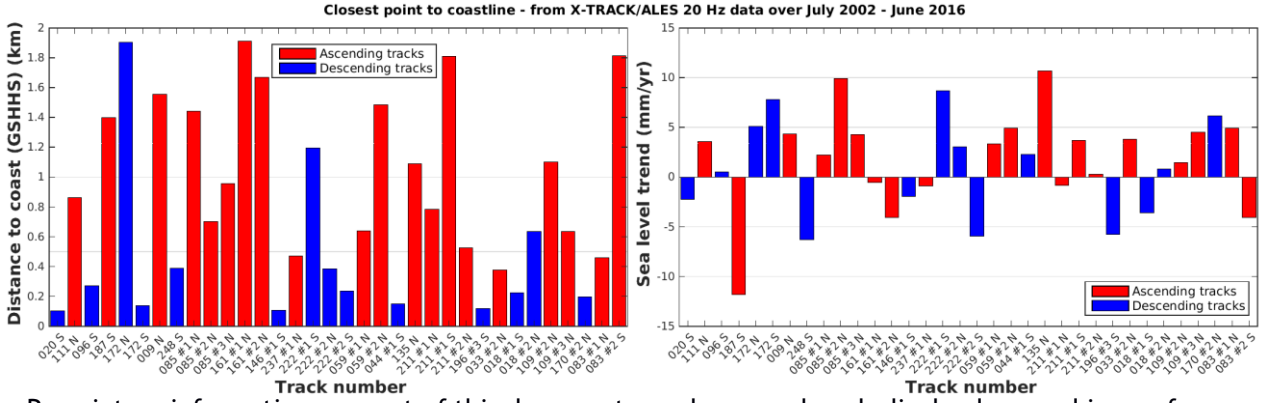

Fig.19: distribution of the distances to coast reached by the XTRACK/ALES 20-Hz data (i.e., distance to coast of the first valid point) for the selected track portions (available data under 2 km from coast) in the study region (left panel) and associated trend estimates over July 2002 - June 2016 (right panel).

Figure 20 shows which track portions present data under 2 km from coast, *i.e.* the track portions introduced above in Fig. 19. This study region is characterized by a high number of tide gauges. Almost all are located in the northern shore. Green triangles represent the tide gauges which data are available over 2002-2015 (most of Italian tide gauges do not have data over the year 2016).

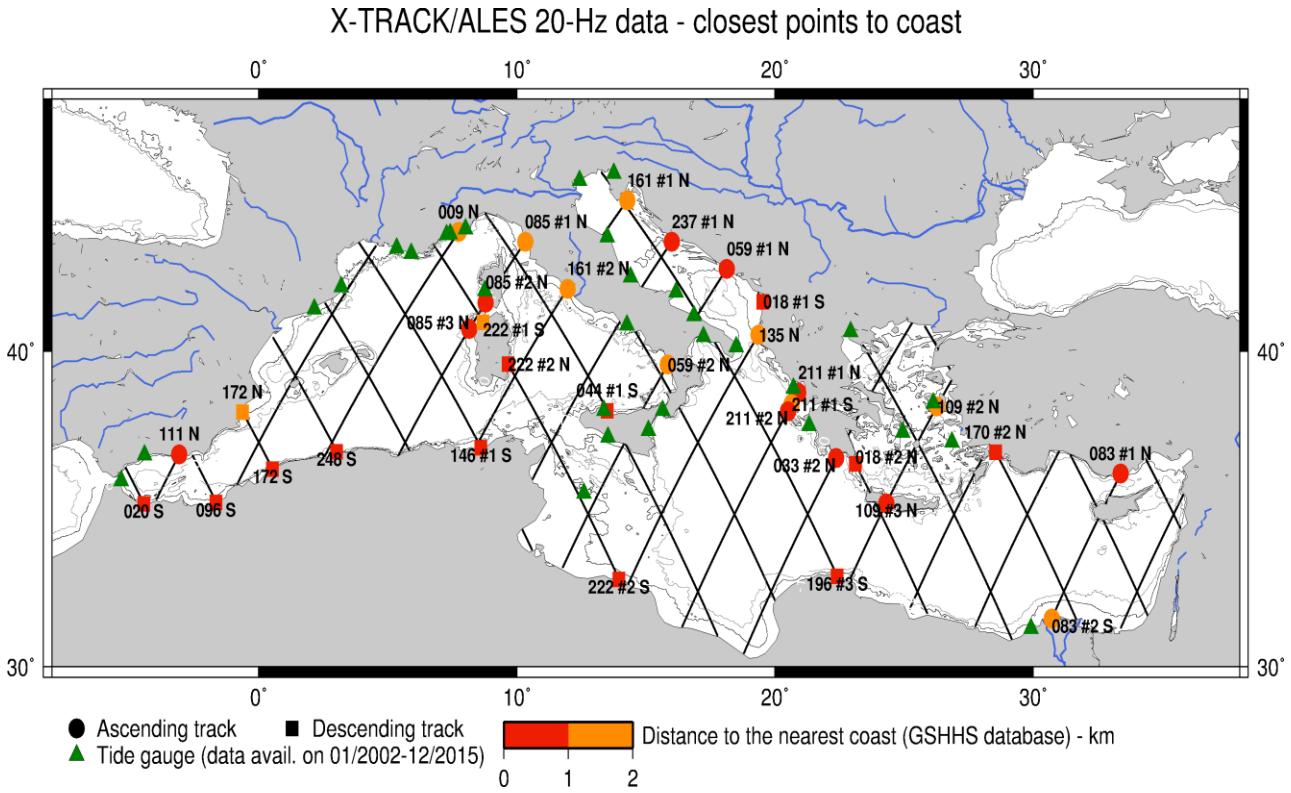

Fig.20: Location of the track portions that presents X-TRACK/ALES 20-Hz data available under 2 km from coast over the Mediterranean Sea region. Circles correspond to ascending tracks and squares to descending ones. Numbers identify the track portions. Portions where data are available under 1 km from coast are drawn in red (and orange under 2 km from coast). The Jason-1/2 track coverage is superimposed. Green triangles locate tide gauges which sea level time-series are available on January 2002 – December 2015 (https://www.psmsl.org).

Annex G: Series of figures, called **Fig.21** (1 portion per page; the tracks are ranked from west to east). The content of the figure is as follows:
(a) Sea level trend values (green dots) and associated formal error (+/-1 standard deviation; vertical black line) as a function of distance to the coast (last 15 km) estimated at each 20-Hz point.
(b) SLA time series (blue dots) from July 2002 to June 2016 for the closest 20-Hz point to the coast (distance indicated in the heading). Red dots are outliers identified by simple statistical test based on the time series RMS (SLA values larger than 2 RMS are excluded). In green is shown the regression line computed over the 14-year time span (excluding the outliers). The corresponding trend value and associated error (+/-1 standard deviation) is indicated in the legend of the figure.
(c) Sea level trends (colored circles) computed over the 14-year time span at each 20 Hz point for the closest track portion to the coast (a few km) The background map shows the geographical setting based on a recent version of Google Earth.

An example is given below:

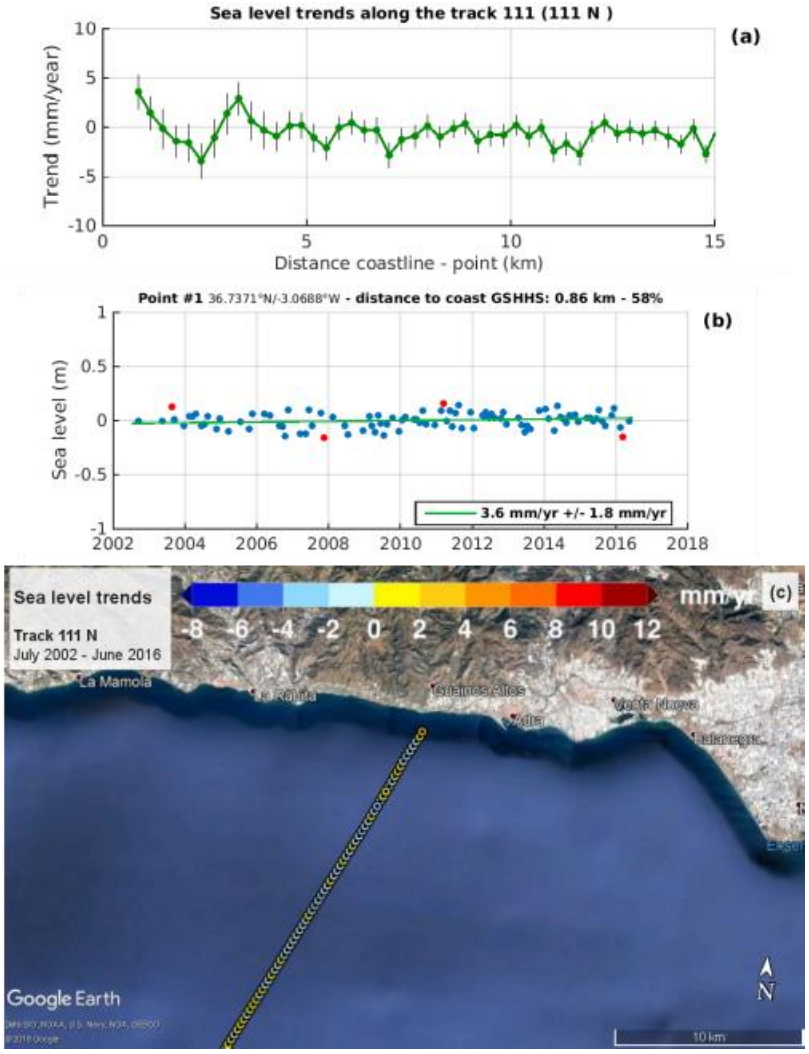

An independent analysis of the SLA data has been carried out at University Bonn for the Mediterranean and North seas. The data used are J1 and J2 data over the time interval from July 2002 to June 2016.

The following two aspects have been investigated:

(1) sea level trend and its error and

(2) the distance to coast of valid points of the time-series. To evaluate the validity of the point we compute its correlation with a near tide gauge. For this second aspect we have compared the actual XTRACK/ALES release (SLCCI Bridging Phase version October 2018) to similar J2 products, namely the PODAAC/ALES (downloaded December 2018) and the Bonn/STAR (Roscher et al., 2017) products. The geophysical corrections in PODAAC/ALES (1) and Bonn/STAR (3) are aligned together but are not fully aligned with XTRACK/ALES (2). However, these differences are negligible and do not influence the results. Instead, the main difference comes from the retrackers and these should be investigated further.

The linear trend and its standard error have been estimated at each 20 Hz point. No further selection criteria have been applied. In the Mediterranean Sea trends are mainly positive in the Adriatic and in the eastern basin and negative in the western and central basin. The trend is in the range of -/+ 4 mm/yr at most of the locations but reaches higher unrealistic values (up to 25 mm/yr) near coasts. Corresponding results are presented in Annex I.

4. Synthesis; Concluding remarks and future work

In this 1-year project, we have produced results of contemporary coastal sea level changes along the coasts of western Africa, Mediterranean Sea and Northern Europe, obtained from a dedicated reprocessing of satellite altimetry data. High sampling rate (20-Hz) sea level data from the Jason-1 and Jason-2 missions over a 14-year-long time span (July 2002 to June 2016) were considered. The data were first retracked using the ALES adaptative leading edge subwaveform retracker. The X-TRACK processing system developed to optimize the completeness and accuracy of the corrected sea level time series in coastal ocean areas was then applied. From the 14-year long sea level time series finally obtained, we estimated sea level trends along the Jason-1 & 2 tracks covering the 3 study regions. We analyzed regional variations in sea level trends, with a focus on the changes observed between the open ocean to the coastal zone. Compared to the conventional 1-Hz sea level products dedicated to open ocean applications, the retracked 20-Hz measurements used in this study allowed us to retrieve valid sea level information much closer to the coast (less than 3-4 km to the coast, depending on the satellite track location). In the study regions, results show that over the 14-year period, sea level trends close to the coast are generally significantly different than offshore.
An article has been submitted to 'Advance in Space Research' for the sea level results along the coasts of Western Africa. It is given in Annex J. Another one is in preparation for the Mediterranean Sea and Northern Europe.

The present work will be extended in the context of the CCI+ 'Sea Level' project. It will focus on the following issues:

- Development a database of coastal sea level products in a number of world coastal zones selected for their vulnerability to global warming and sea level rise, using retracked data from LRM altimetry missions and SAR altimetry from the Sentinel 3A and 3B missions, as well as dedicated coastal geophysical corrections. The study period will be 2002-present. LRM data from Jason-1/2/3 missions, Envisat and Saral/Altika will be processed (in addition to the SAR data on Sentinel-3A/B)

- Combination of the coastal altimetry products with up-to-date gridded sea level products (i.e., the SL_cci augmented by the C3S sea level data) in a 'seamless' global grid with varying spatial resolution (higher resolution near the coast)

- Interpretation of sea level trends in the coastal zones using additional data sets and model results (e.g., for waves, for the effect of river runoff in estuaries, and density changes due to small scale coastal currents, etc.).

References

Ablain M., S. Philipps, N. Picot and E. Bronner, 2010: Jason-2 Global Statistical Assessment and Cross-Calibration with Jason-1, Marine Geodesy, vol 33, supplement 1, pp 162-185.

Ablain, M., Legeais, J.F., Prandi, P., Fenoglio-Marc L., Marcos M., Benveniste J., Cazenave A. (2017), Satellite Altimetry-Based Sea Level at Global and Regional Scales, Surv Geophys 38, 9-33. doi:10.1007/s10712-016-9389-8.

Andersen, O., Scharroo, R., 2011. Range and geophysical corrections in coastal regions and implications for mean sea surface determination. In: Vignudelli, S., Kostianoy, A., Cipollini, P., Benveniste, J. (Eds.), Coastal Altimetry. Springer-Verlag, Berlin Heidelberg, pp. 103–146.

Birol F., N.X Fuller, F. Lyard, M. Cancet, F. Niño, C. Delebecque, S. Fleury, F. Toublanc, A. Melet and M. Saraceno, F. Léger. 2017. Coastal applications from nadir altimetry: example of the X-TRACK regional products. Advances in Space Research, 10.1016/j.asr.2016.11.005.

Carrere, L.; Lyard, F.; Cancet, M.; Guillot, A.; Roblou, L., 2012, FES 2012: A New Global Tidal Model Taking Advantage of Nearly 20 Years of Altimetry. 20 Years of Progress in Radar Altimatry, held 24-29 September, 2013 in Venice, Italy. Edited by L. Ouwehand. ISBN: 978-92-9221-274-2, 2013, id.13. 2013ESASP.710E..13C

Garcia, E.S., Sandwell, D.T., Smith, W.H., 2014. Retracking Cryosat-2, Envisat and Jason-1 radar altimetry waveforms for improved gravity field recovery. Geophys. J. Int. ggt469.

Gaspar, P., Labroue, S., Ogor, F., Lafitte, G., Marchal, L., Rafanel, M., 2002. Improving nonparametric estimates of the sea state bias in radar altimeter measurements of sea level. J. Atmos. Ocean. Technol. 19, 1690–1707.

Labroue, S., Gaspar, P., Dorandeu, J., Zanife, O., Mertz, F., Vincent, P., Choquet, D., 2004. Nonparametric estimates of the sea state bias for the Jason-1 radar altimeter. Mar. Geod. 27, 453–481.

Lefèvre, F., F. H. Lyard, and C. Le Provost, E. J. O. Schrama, 2002. FES99: A Global Tide Finite Element Solution Assimilating Tide Gauge and Altimetric Information, https://doi.org/10.1175/1520-0426(2002)019<1345:FAGTFE>2.0.CO;2

Legeais, J.-F., Ablain, M., Zawadzki, L., et al., 2018. An accurate and homogeneous altimeter sea level record from the ESA climate change initiative. Earth Syst. Sci. Data Discuss., 1–35, https://doi.org/10.5194/essd-2017-116.

Marti F., Cazenave A., Birol F., Passaro, M. Leger F., Nino F., Almar R., Benveniste J. and Legeais J.F., 2019. Altimetry-based sea level trends along the coasts of western Africa, *Advances in Space Research*, https://doi.org/10.1016/J.asr.2019.05.033, published online 28 May 2019.

Passaro M., Cipollini P., Vignudelli S., Quartly G., Snaith H., 2014. ALES: A multi-mission subwaveform retracker for coastal and open ocean altimetry. Remote Sensing of Environment 145, 173-189, 10.1016/j.rse.2014.02.008.

Passaro M., Fenoglio-Marc L., Cipollini P., 2015. Validation of significant wave height from improved satellite altimetry in the German bight. IEEE Transactions on Geoscience and Remote Sensing 53(4): 2146-2156, 10.1109/TGRS.2014.2356331.

Passaro M., Rose S.K., Andersen O.B., Boergens E., Calafat F.M., Dettmering D., Benveniste J.: ALES+, 2018a. Adapting a homogenous ocean retracker for satellite altimetry to sea ice leads, coastal and inland waters. Remote Sensing of Environment, 211, 456-471, 10.1016/j.rse.2018.02.074.

Passaro M., Zulfikar Adlan N., Quartly G.D., 2018b. Improving the precision of sea level data from satellite altimetry with high-frequency and regional sea state bias corrections. Remote Sensing of Environment, 245-254, 10.1016/j.rse.2018.09.007.

Passaro M., Smith W., Schwatke C., Piccioni G., Dettmering D., 2018c. Validation of a global dataset based on subwaveform retracking: improving the precision of pulse-limited satellite altimetry. 11th Coastal Altimetry Workshop, Frascati (ESA-ESRIN), Italy, 2018-06-15.

Passaro M., Zulfikar Adlan N., Quartly G.D., 2018. Improving the precision of sea level data from satellite altimetry with high-frequency and regional sea state bias corrections. Remote Sensing of Environment, 245-254, 10.1016/j.rse.2018.09.007.

Piccioni G., Dettmering D., Passaro M., Schwatke C., Bosch W., Seitz F., 2018. Coastal Improvements for Tide Models: The Impact of ALES Retracker. Remote Sensing, 10(5), 10.3390/rs10050700.

Pires, N., Fernandes, M.J., Gommenginger, C., Scharroo, R., 2016. A conceptually simple modeling approach for Jason-1 sea state bias correction based on 3 parameters exclusively derived from altimetric information. Remote Sens. 8, 576.

Quartly, G. D.; Legeais, J.-F.; Ablain, M.; Zawadzki, L.; Fernandes, M. J.; Rudenko, S.; Carrère, L.; García, P. N.; Cipollini, P.; Andersen, O. B.; Poisson, J.-C.; Mbajon Njiche, S.; Cazenave, A.; Benveniste, J.. 2017 A new phase in the production of quality-controlled sea level data. *Earth System Science Data*, 9 (2). 557-572. https://doi.org/10.5194/essd-9-557-2017

Roblou L. et al. (2011) Post-processing Altimeter Data Towards Coastal Applications and Integration into Coastal Models. In: Vignudelli S., Kostianoy A., Cipollini P., Benveniste J. (eds) Coastal Altimetry. Springer, Berlin, Heidelberg.

Roscher R, Uebbing B, Kusche J (2017) STAR: Spatio-temporal altimeter waveform retracking using sparse representation and conditional random fields. Remote Sens Environ 201: 148–164. https://doi.org/10.1016/j.rse.2017.07.024

Tran, N., Labroue, S., Philipps, S., Bronner, E., Picot, N., 2010. Overview and update of the sea state bias corrections for the Jason-2, Jason-1 and TOPEX missions. Mar. Geod. 33, 348–362.

Vignudelli S, Cipollini P, Roblou L, Lyard F, Gasparini GP, Manzella G, Astraldi M (2005) Improved satellite altimetry in coastal systems: case study of the Corsica Channel (Mediterranean Sea). Geophys Res Lett. doi: 10.1029/2005GL022602

Xu X.Y., Birol F. and Cazenave A., 2018. Evaluation of Coastal Sea Level of Jason-2 Altimetry Offshore Hong Kong, , *Remote Sensing*, 10, 282, doi:10.3390/rs10020282.

Zaron, E.D., DeCarvalho, R., 2016. Identification and reduction of retracker-related noise in altimeter-derived sea surface height measurements. J. Atmos. Ocean. Technol. 33, 201–210.

WESTERN AFRICA

Annexes A to C

Figure 12

WESTERN AFRICA

ASCENDING TRACKS

Ranked from west to east

TRACK 035

TRACK 111

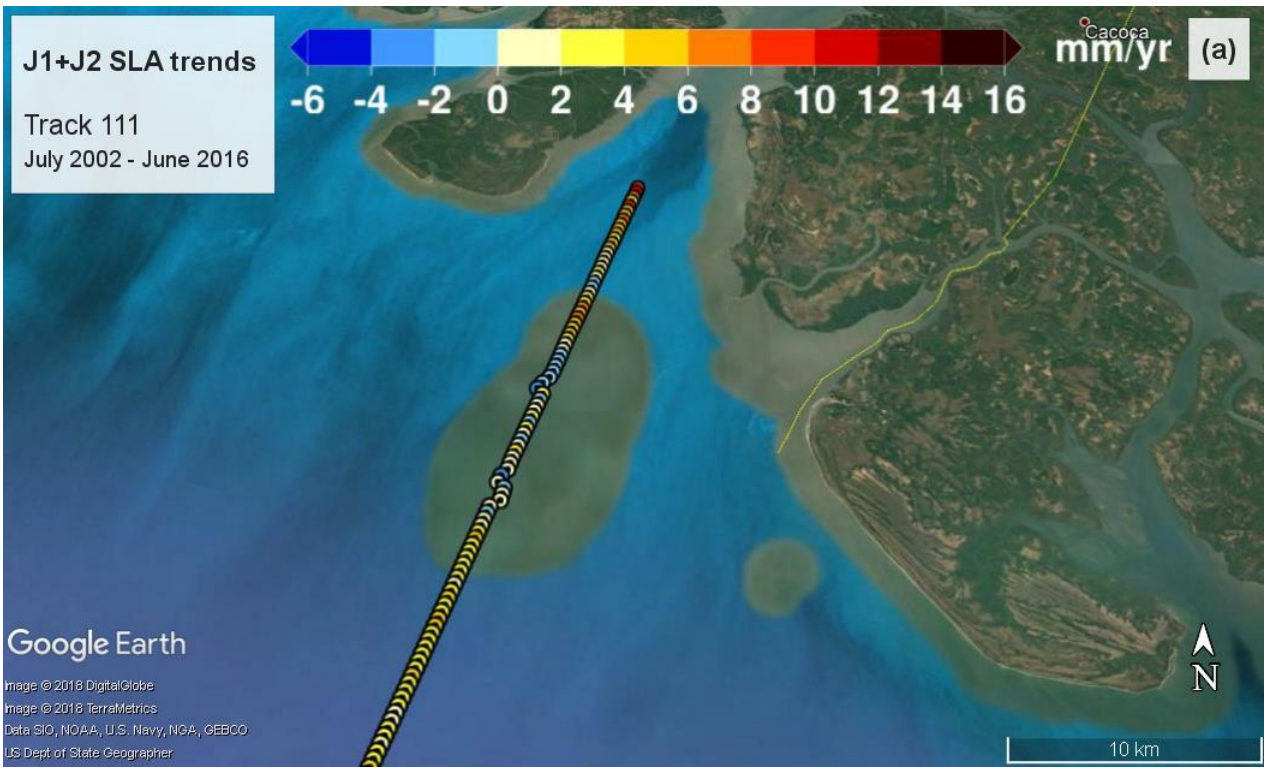

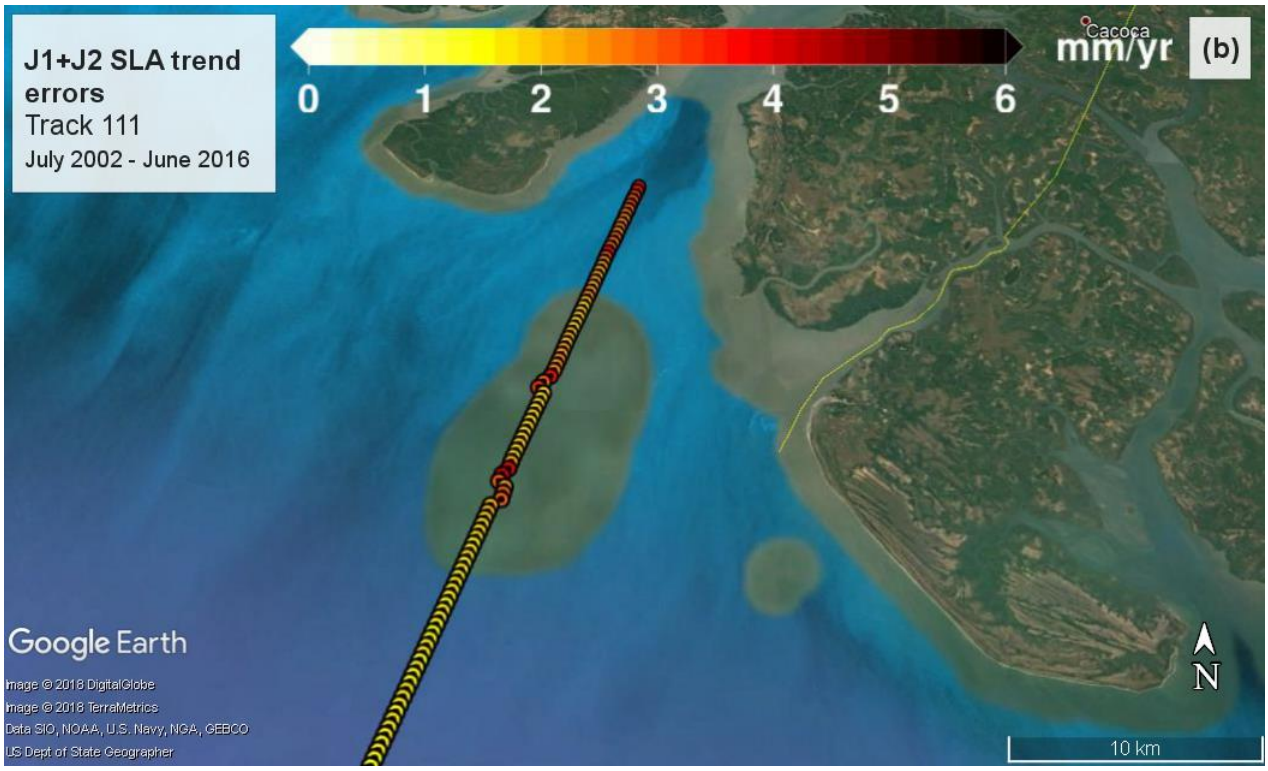

TRACK 187

TRACK 009

TRACK 085

TRACK 161

TRACK 237

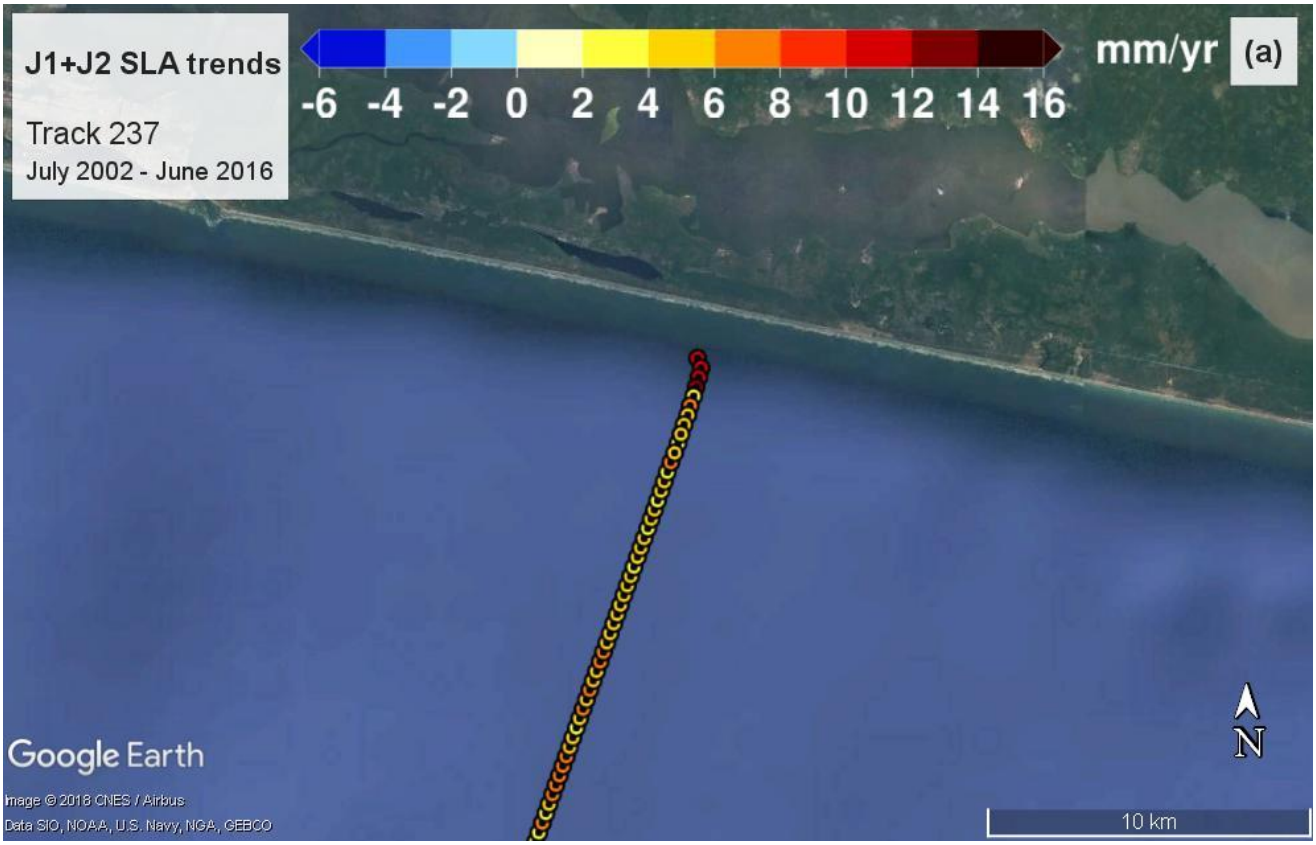

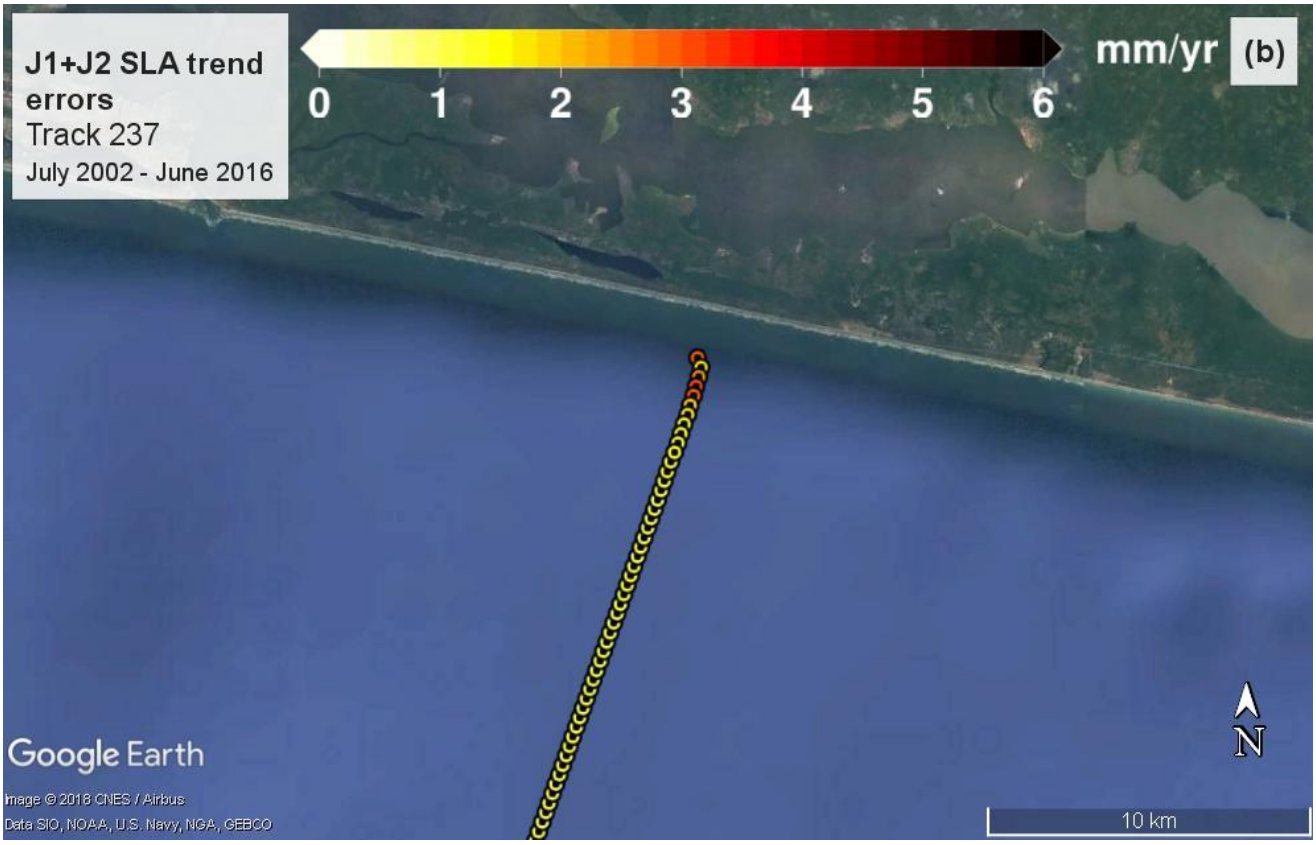

TRACK 059

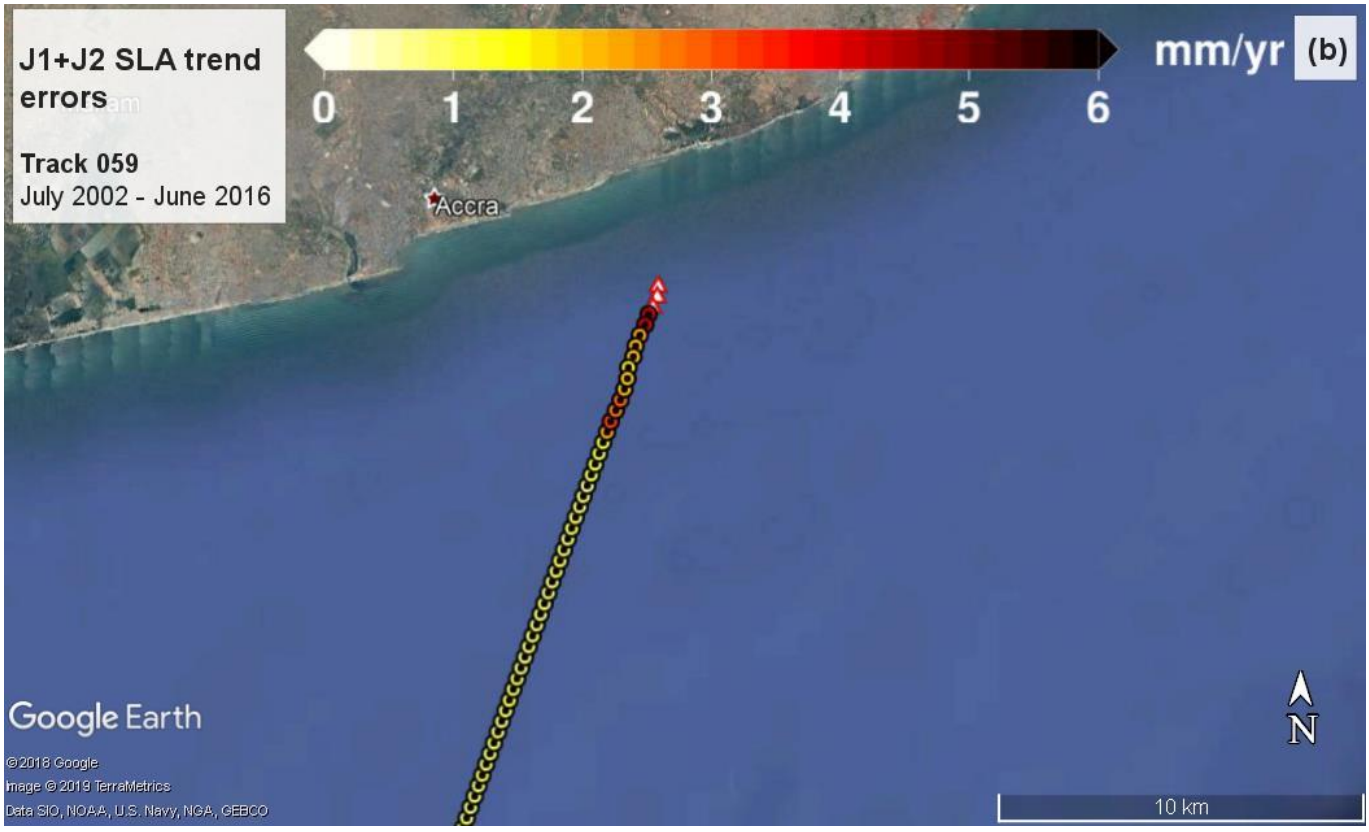

TRACK 135

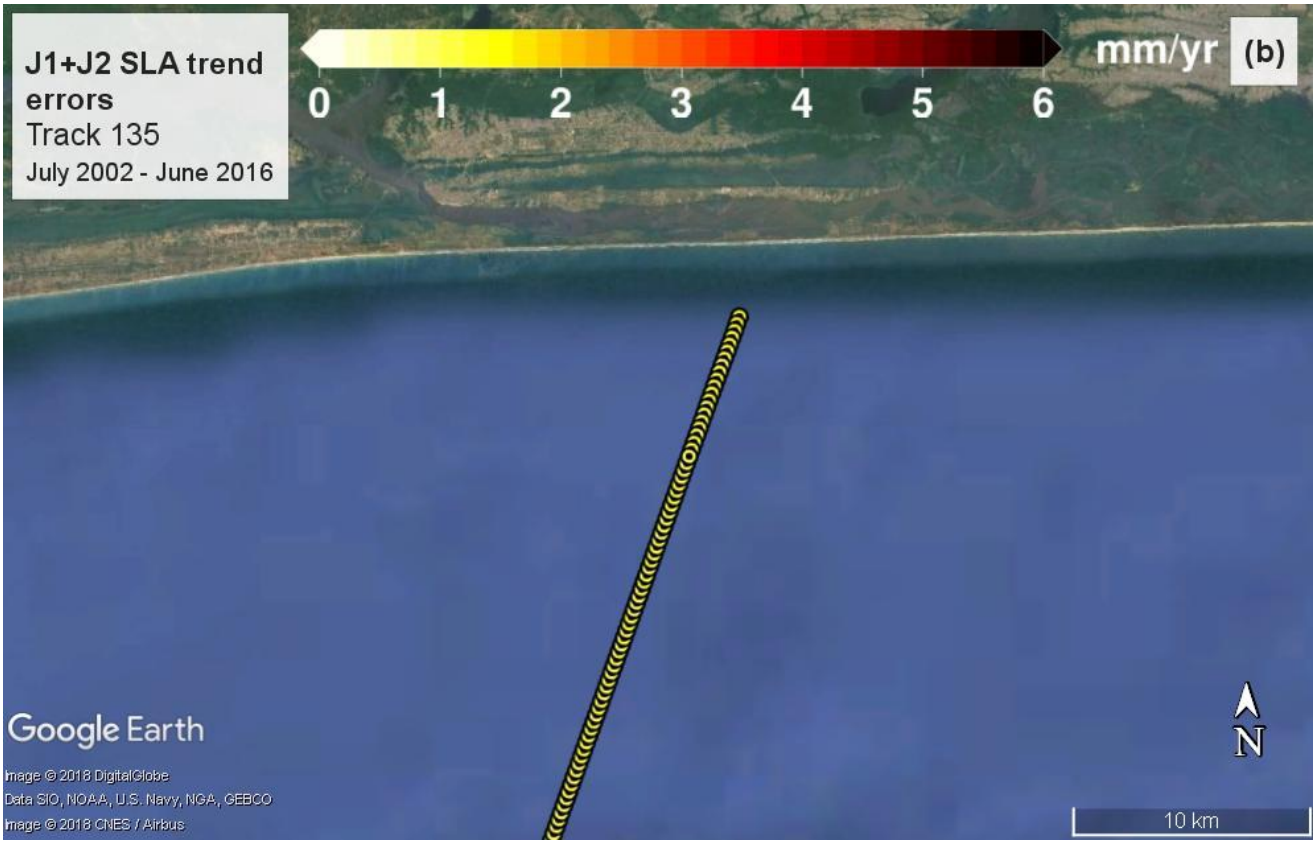

TRACK 211

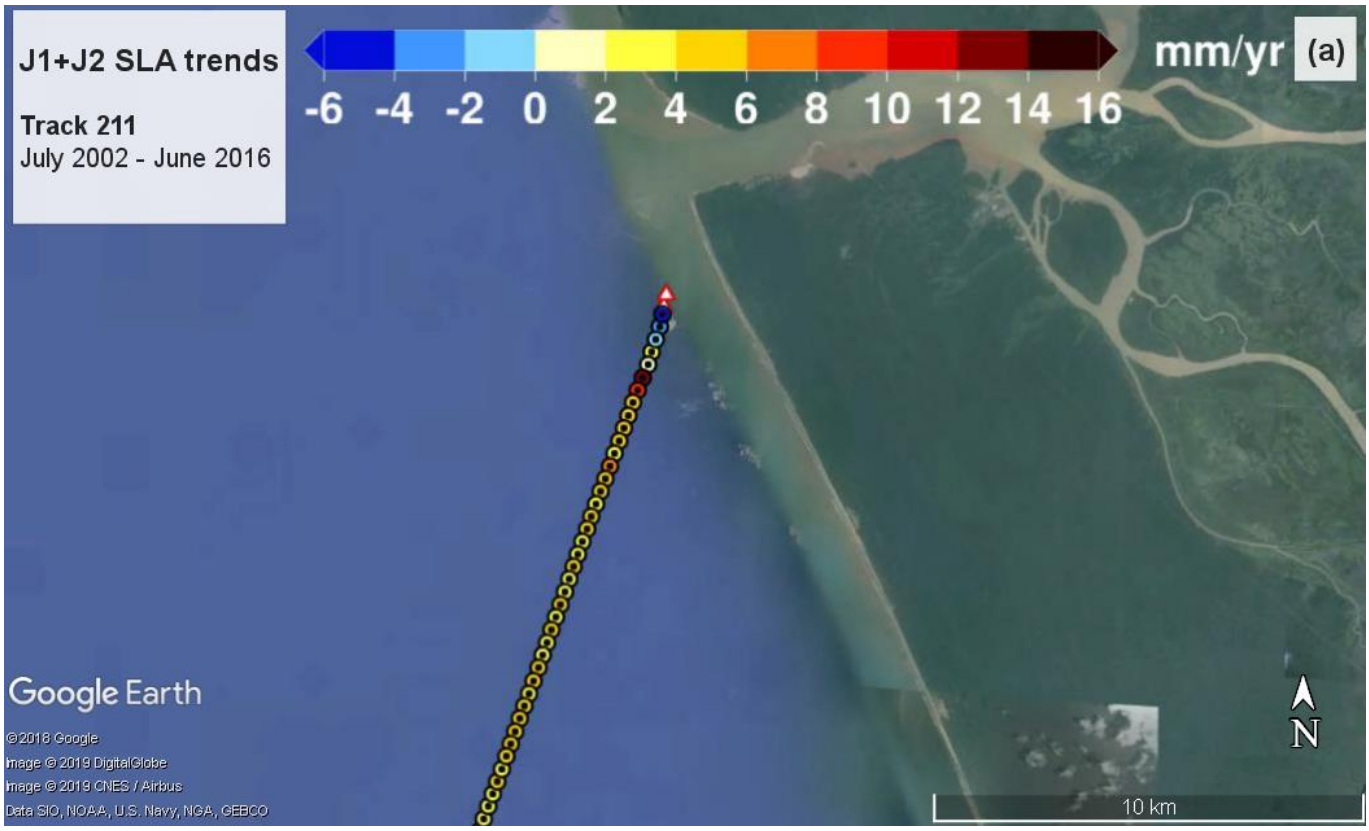

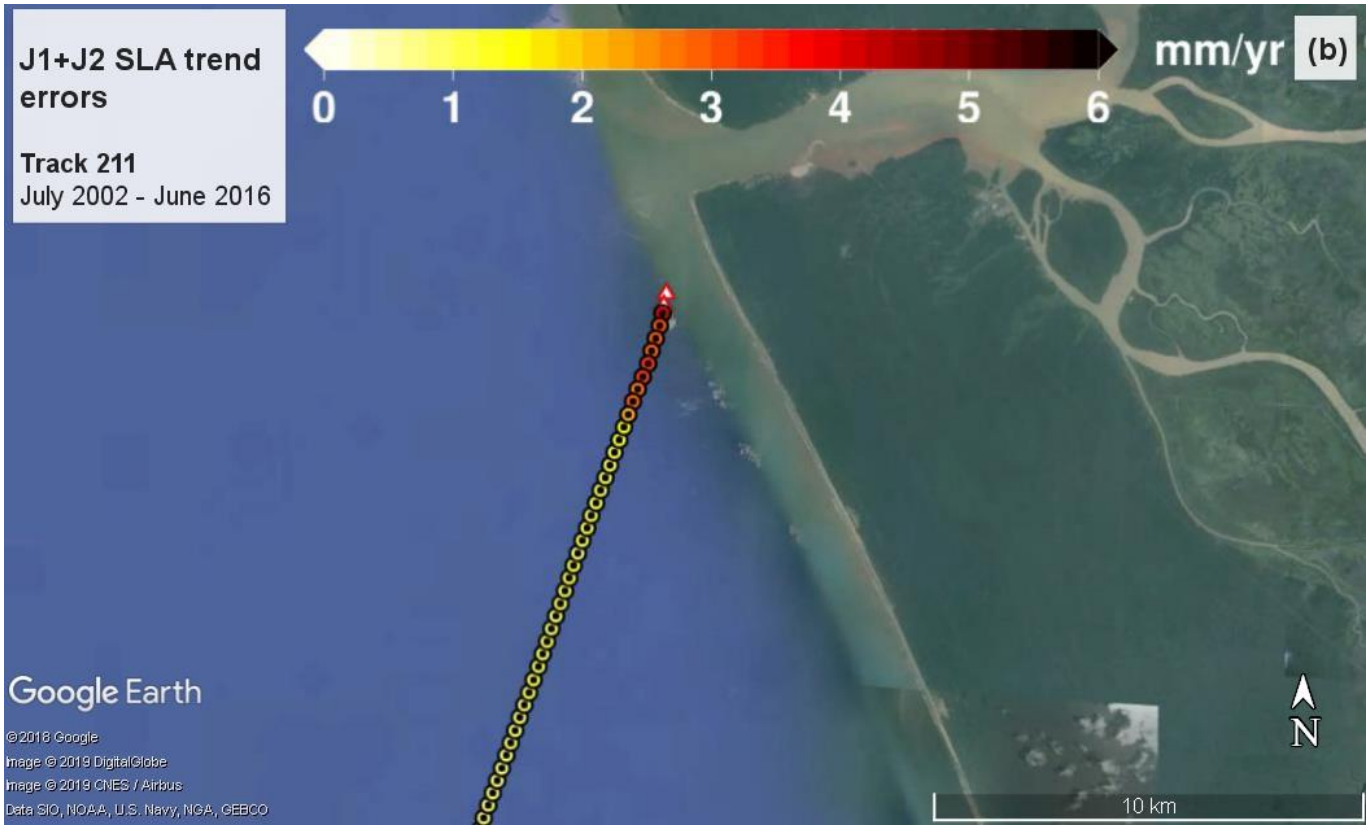

TRACK 033

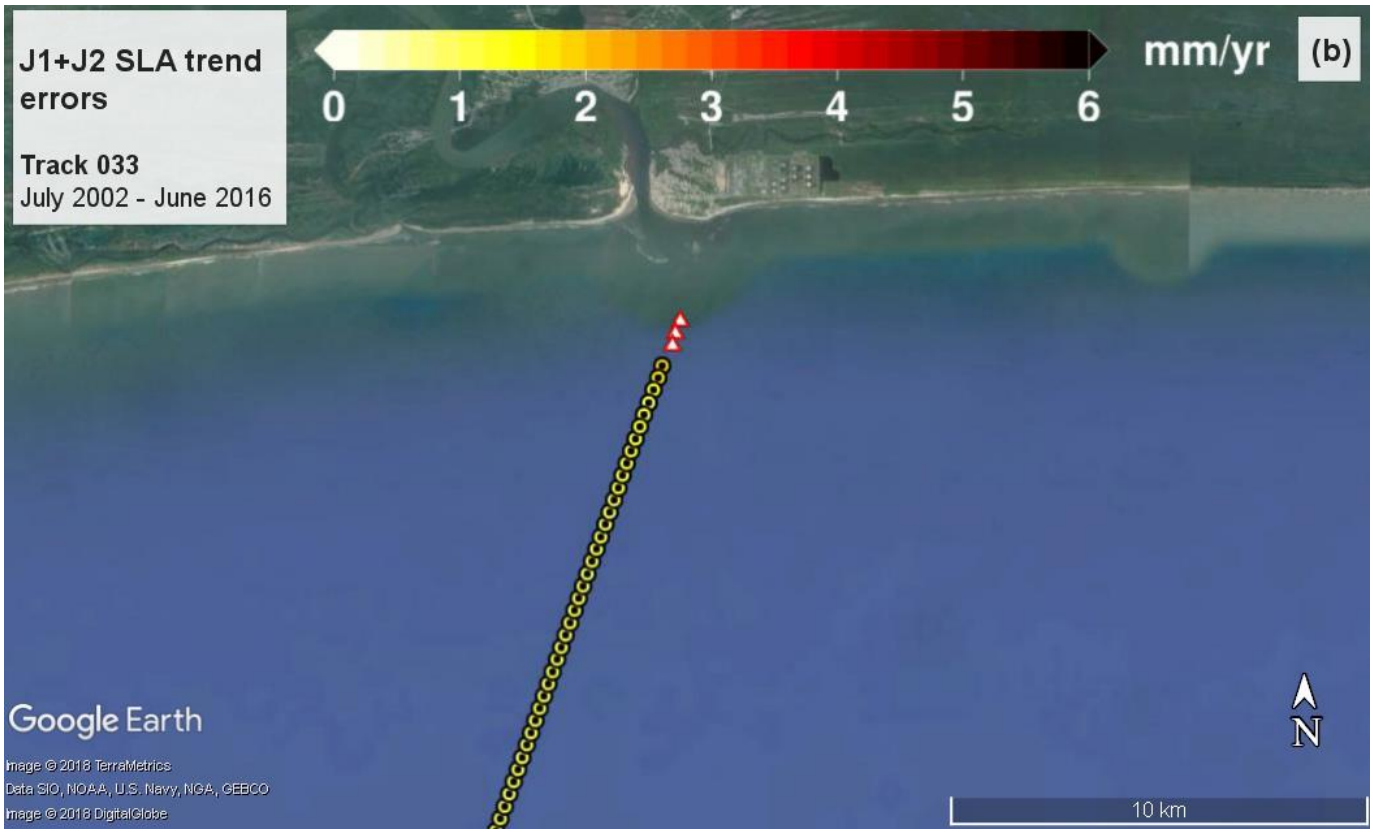

TRACK 109

TRACK 109 #2

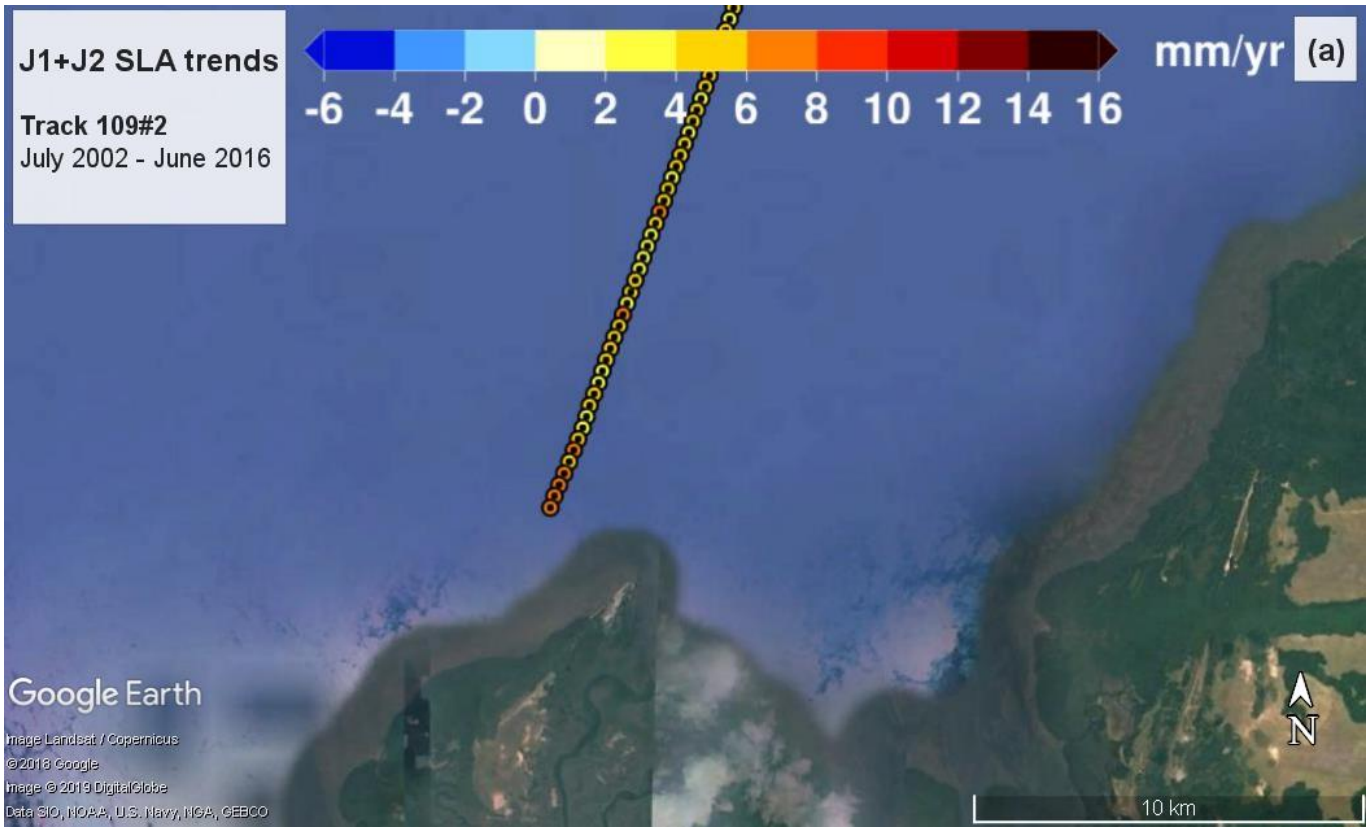

TRACK 185

TRACK 007

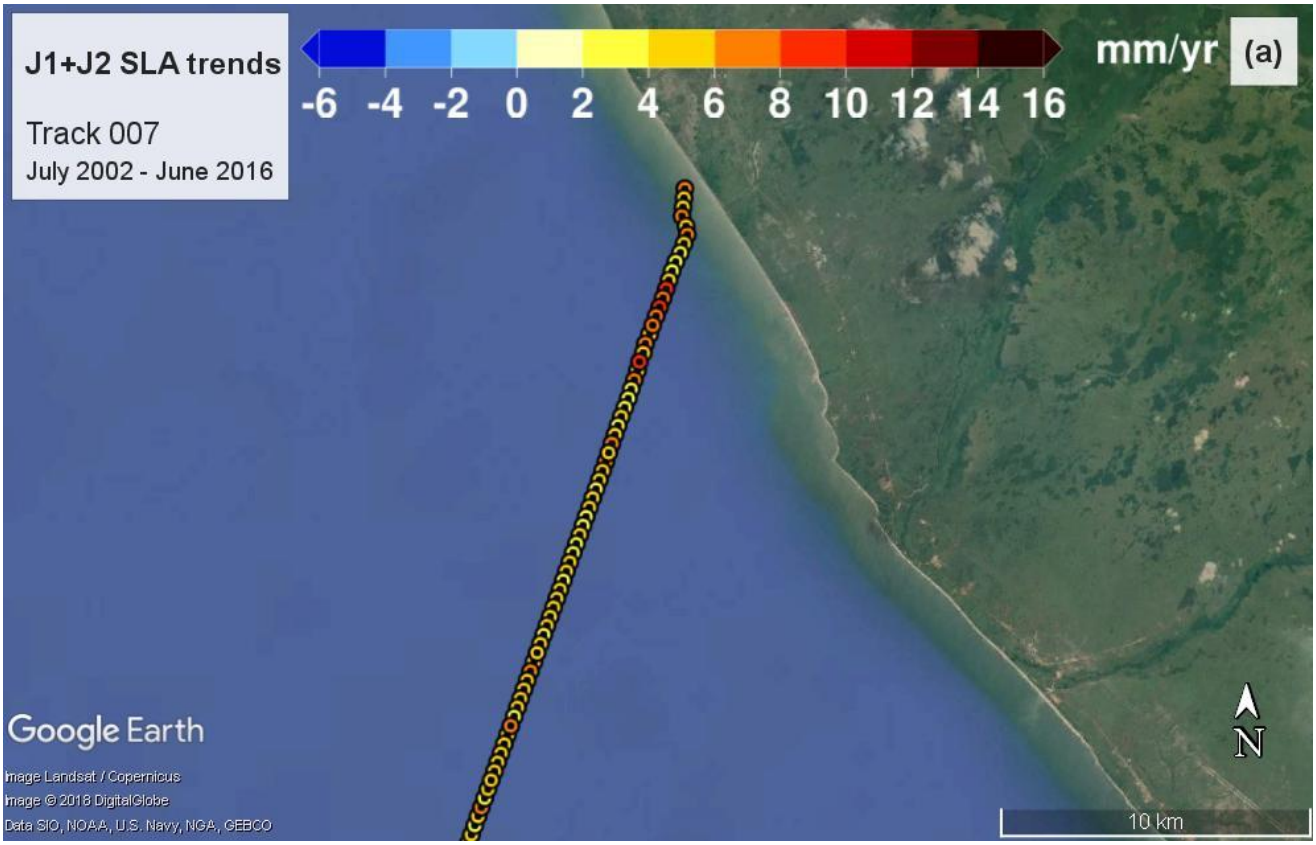

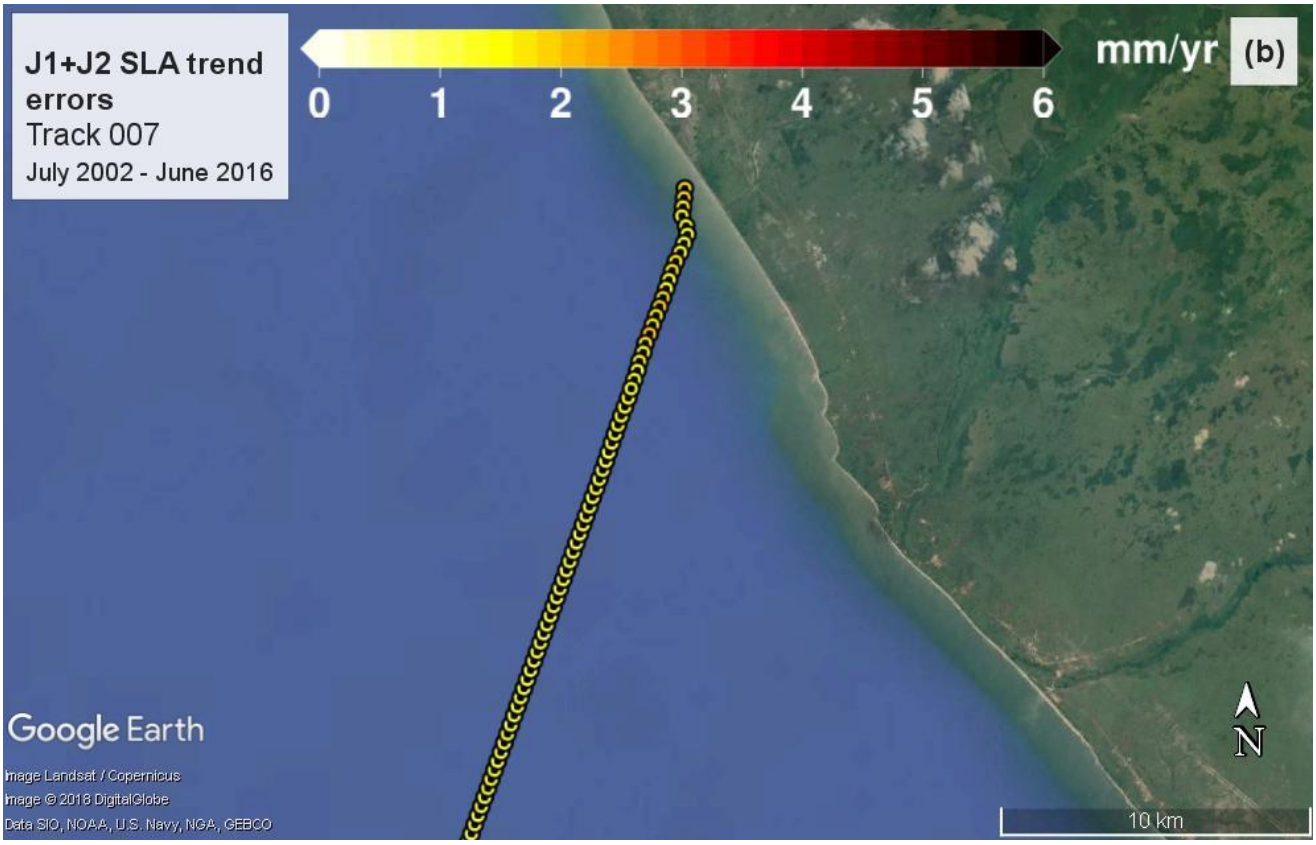

WESTERN AFRICA

DESCENDING TRACKS

Ranked from east to west

TRACK 020

TRACK 198

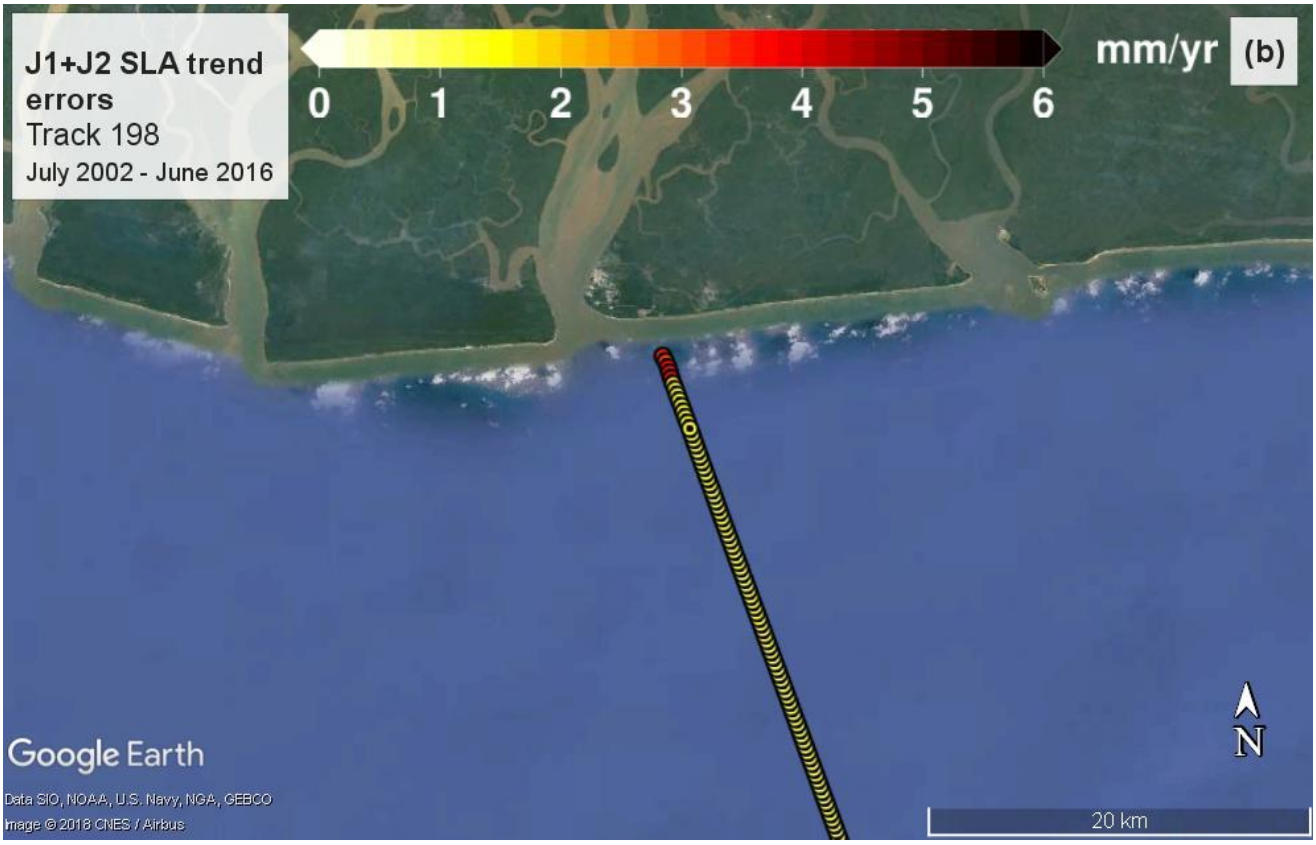

TRACK 122

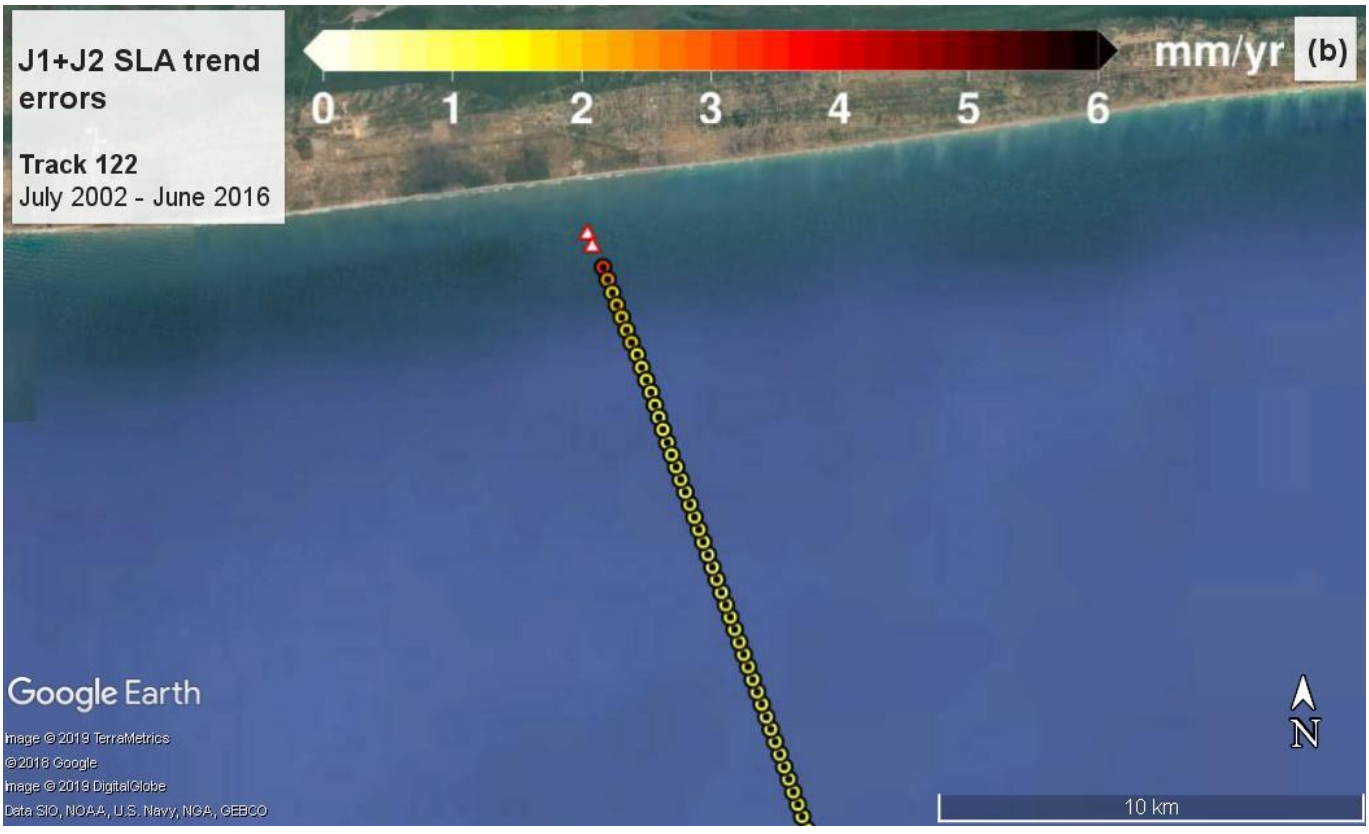

TRACK 046

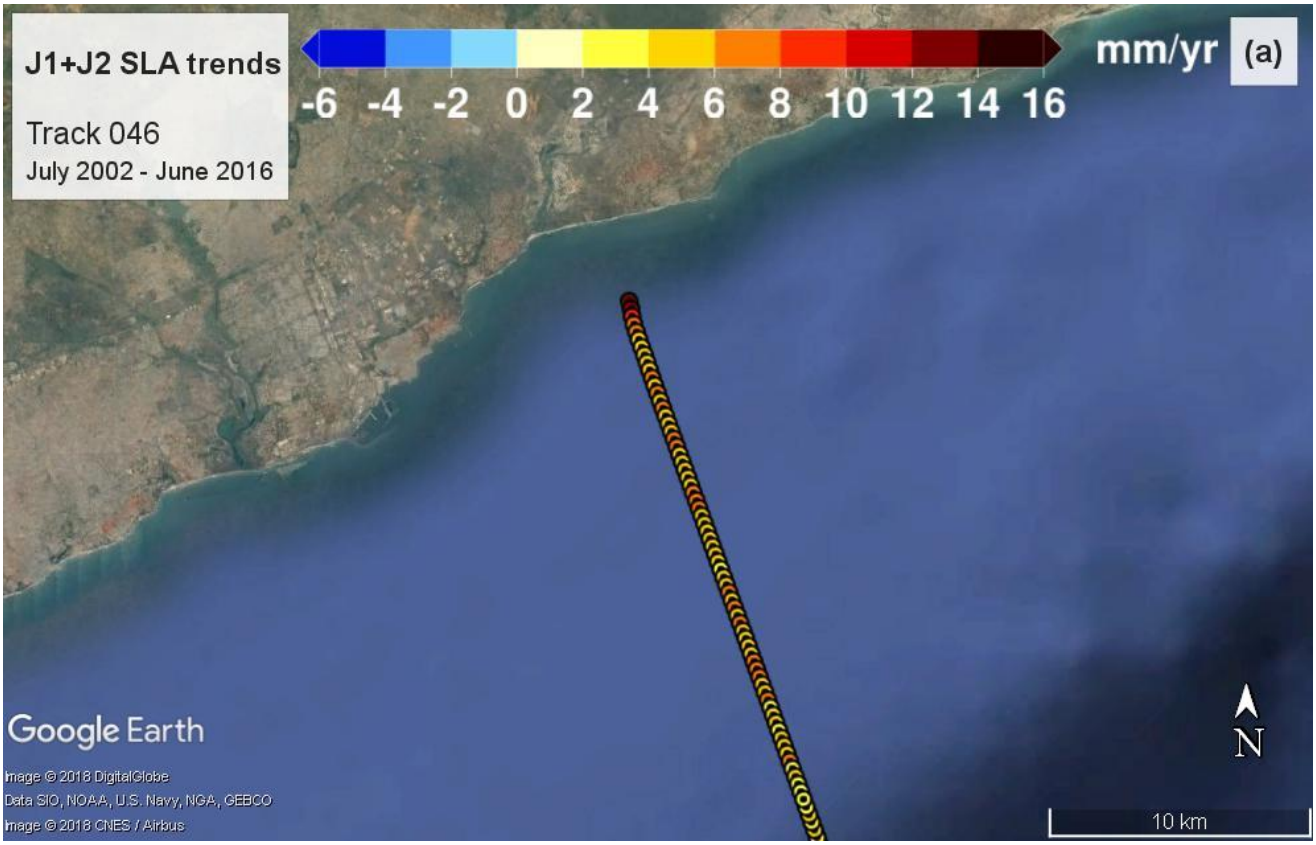

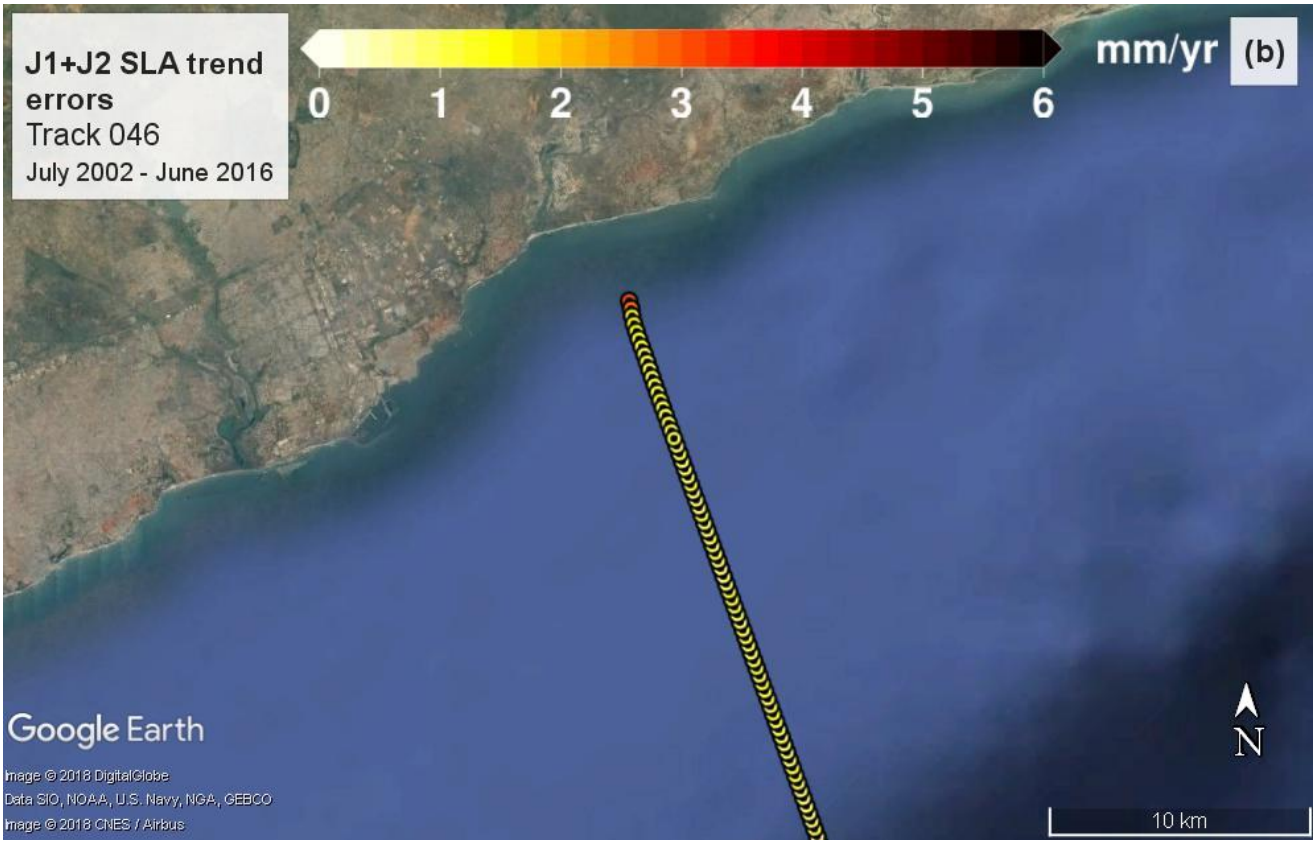

TRACK 224

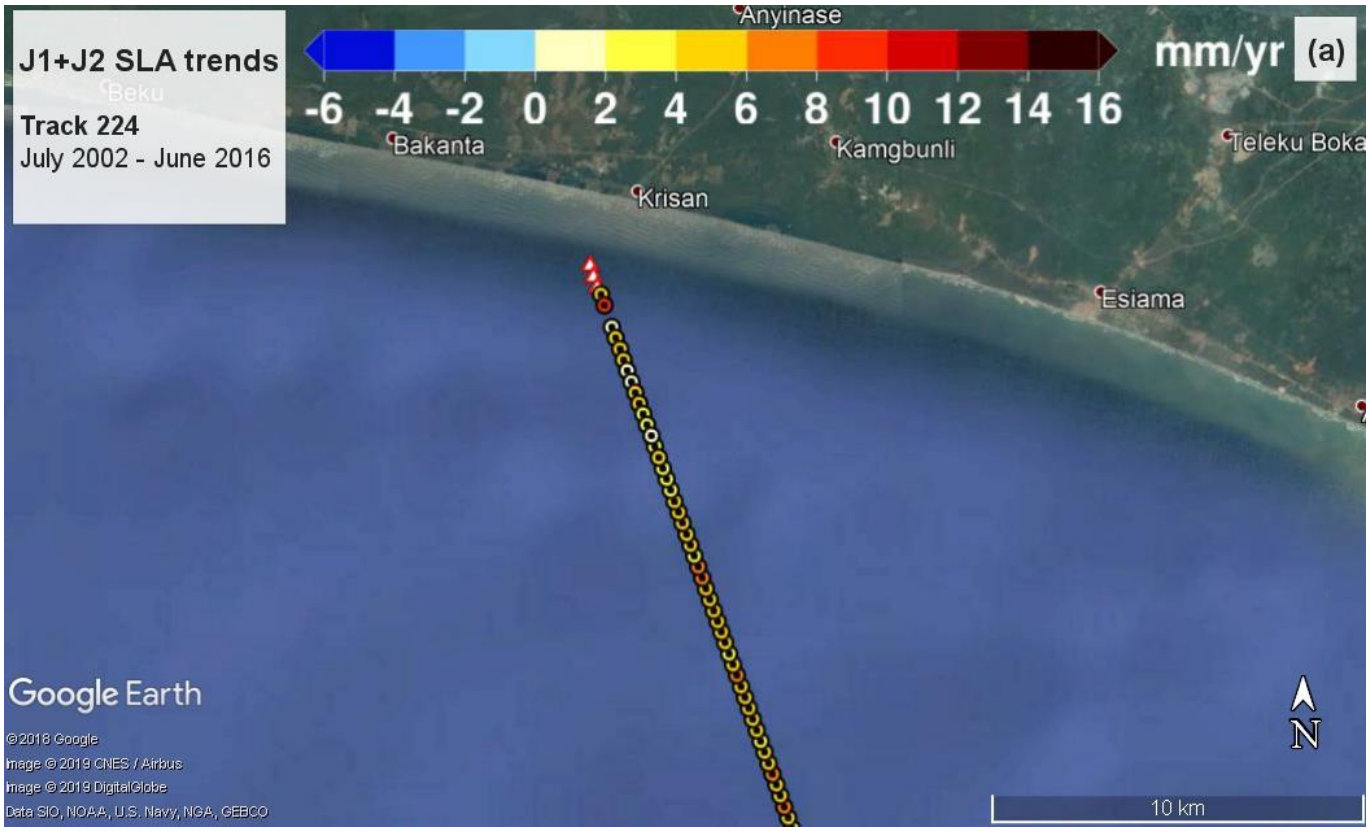

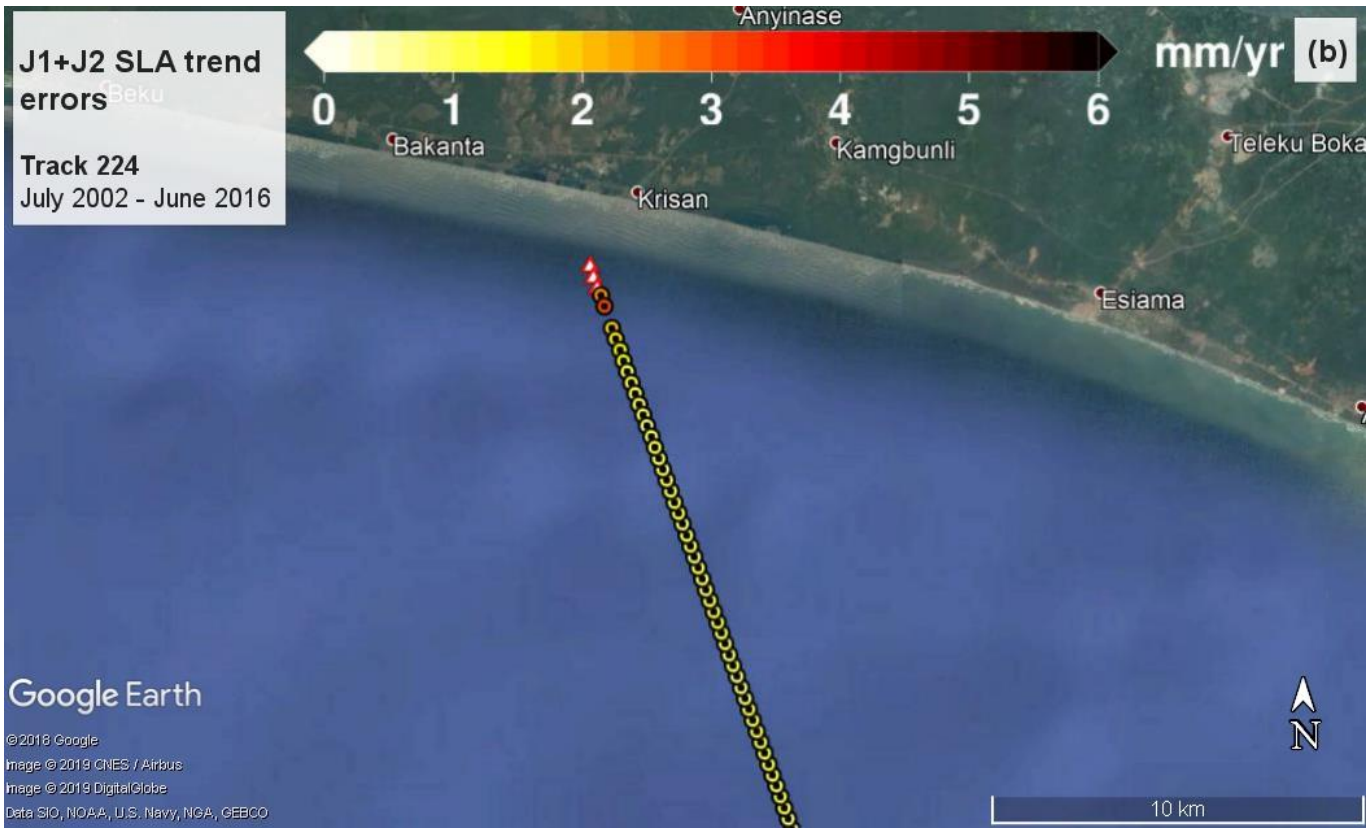

TRACK 148

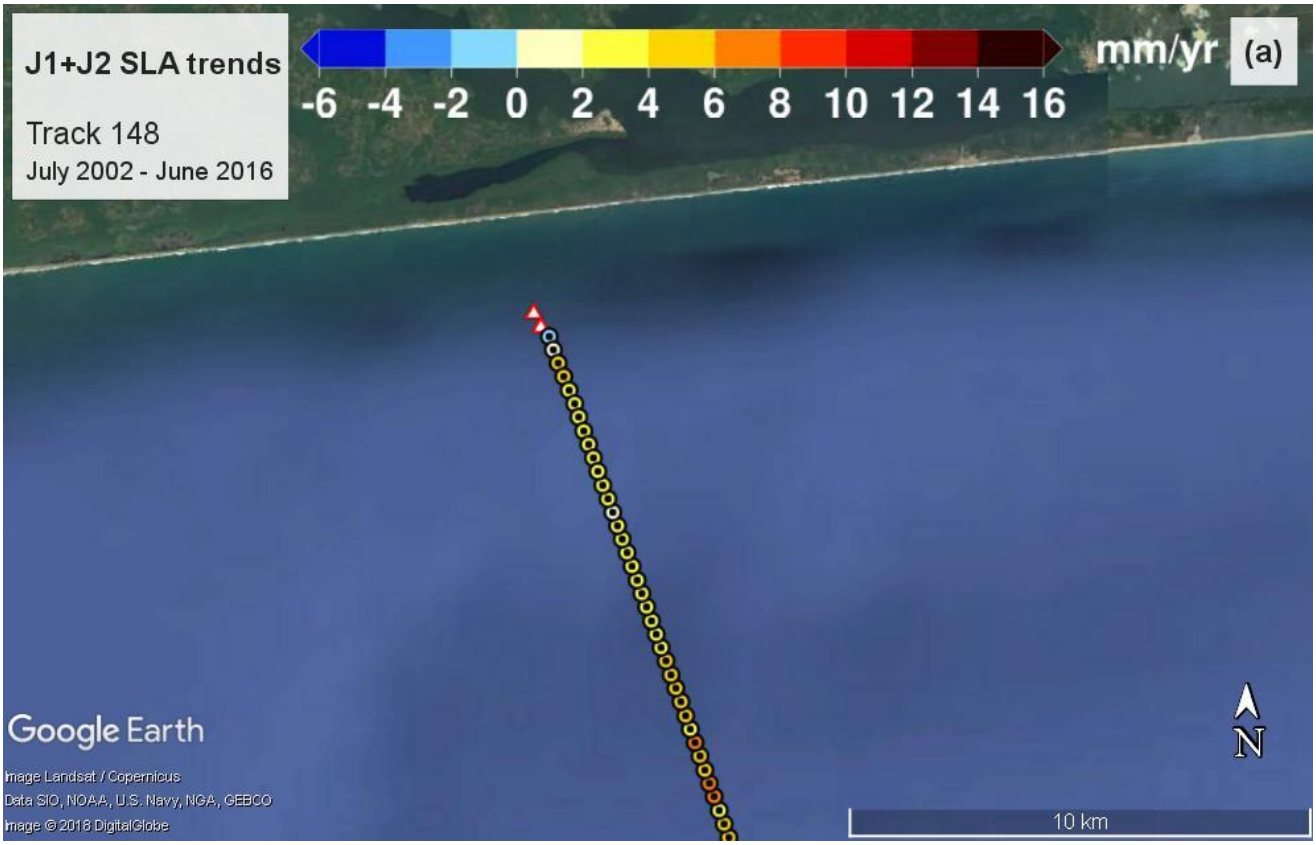

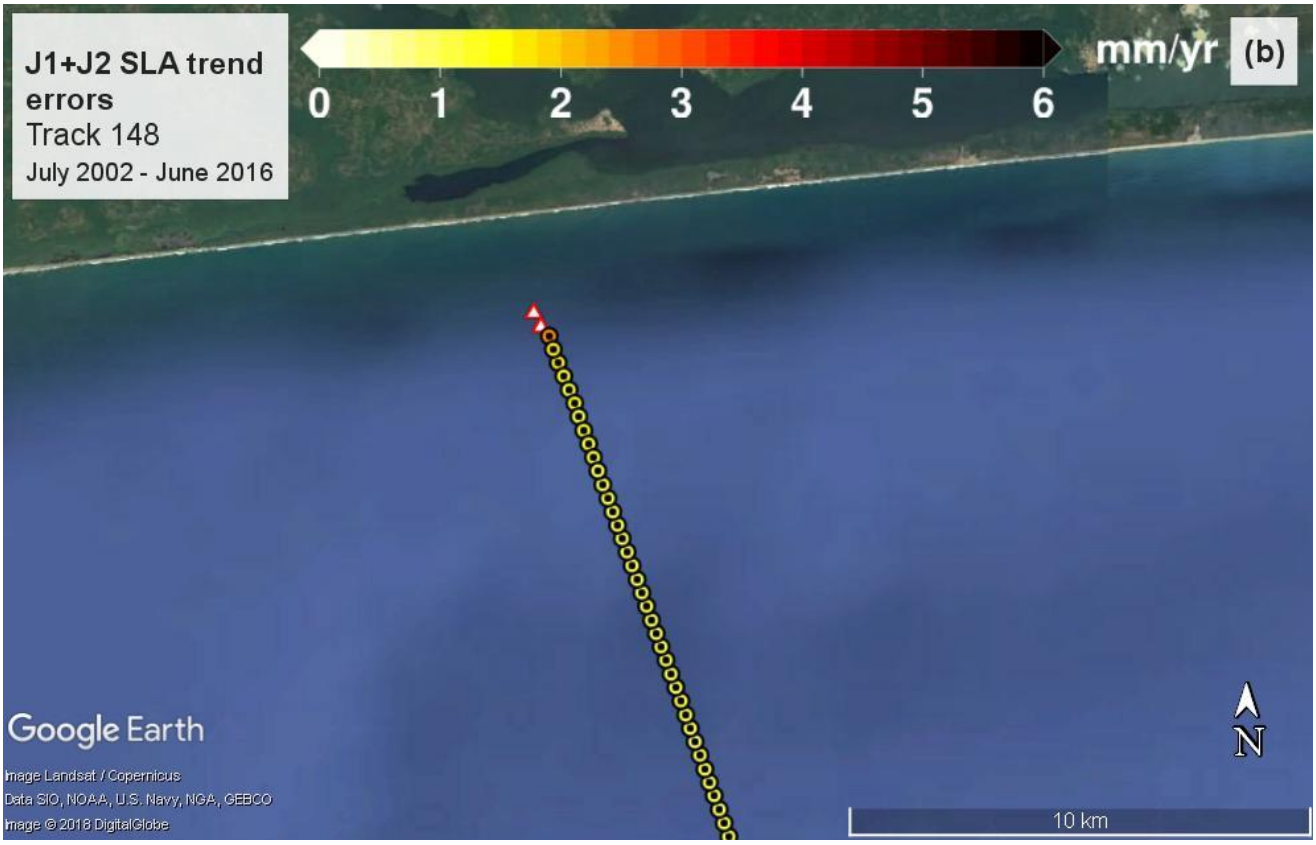

TRACK 072

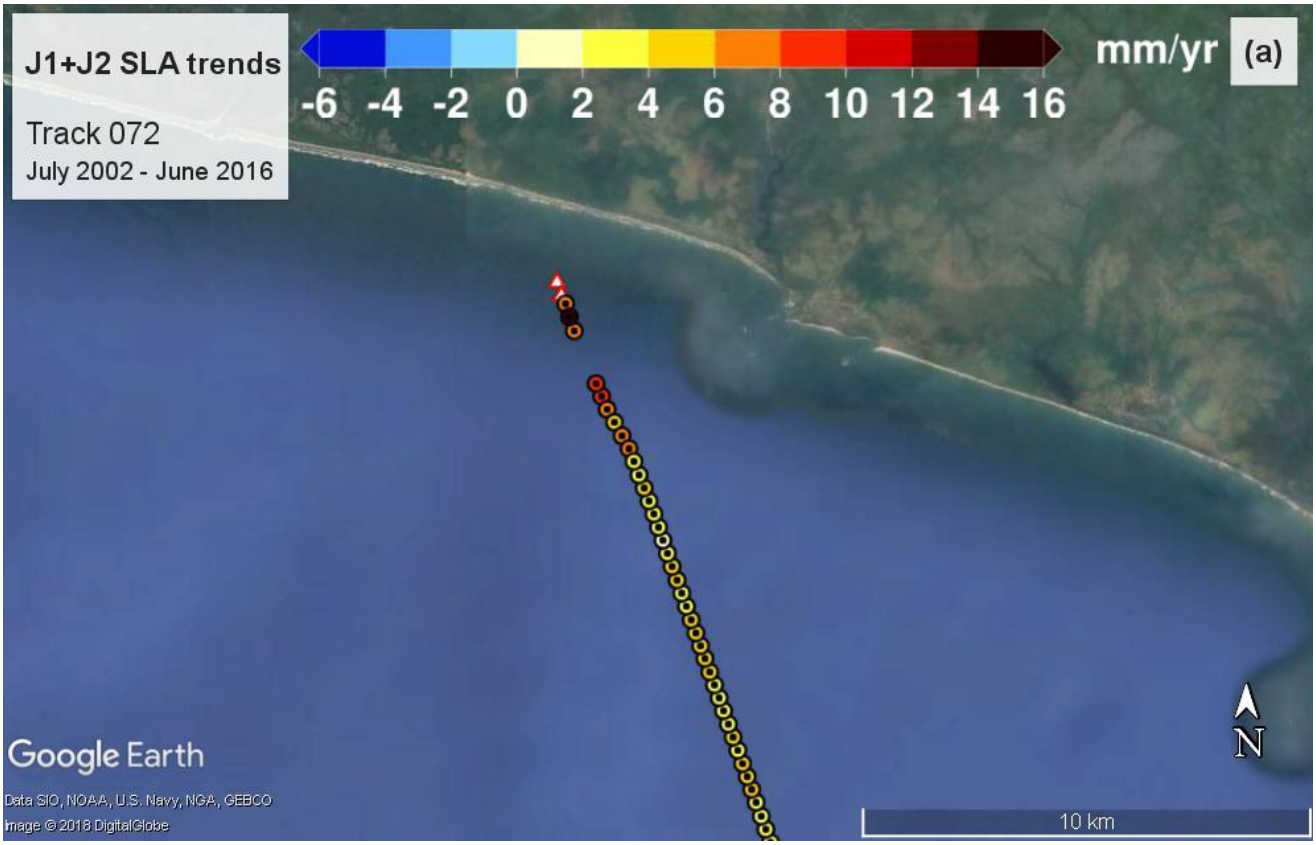

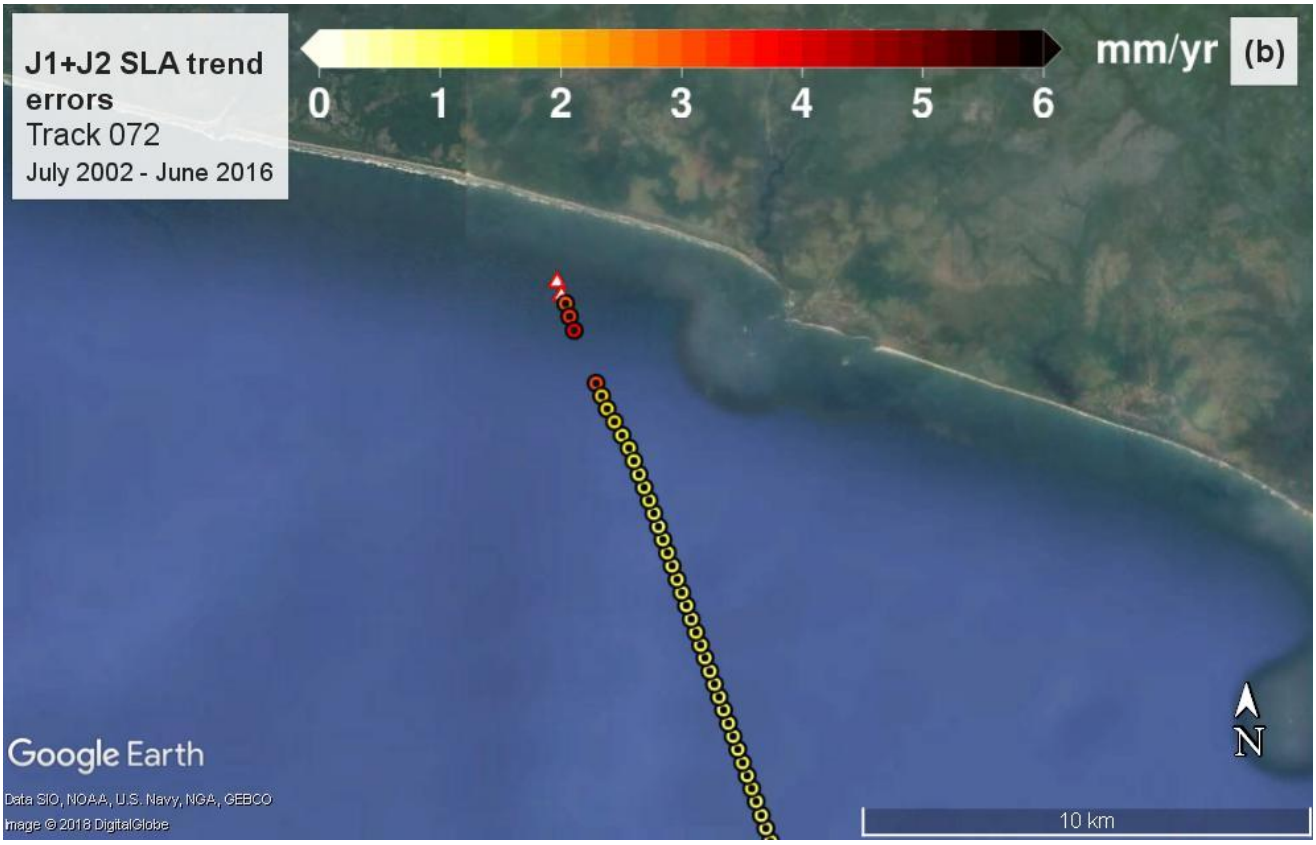

TRACK 250

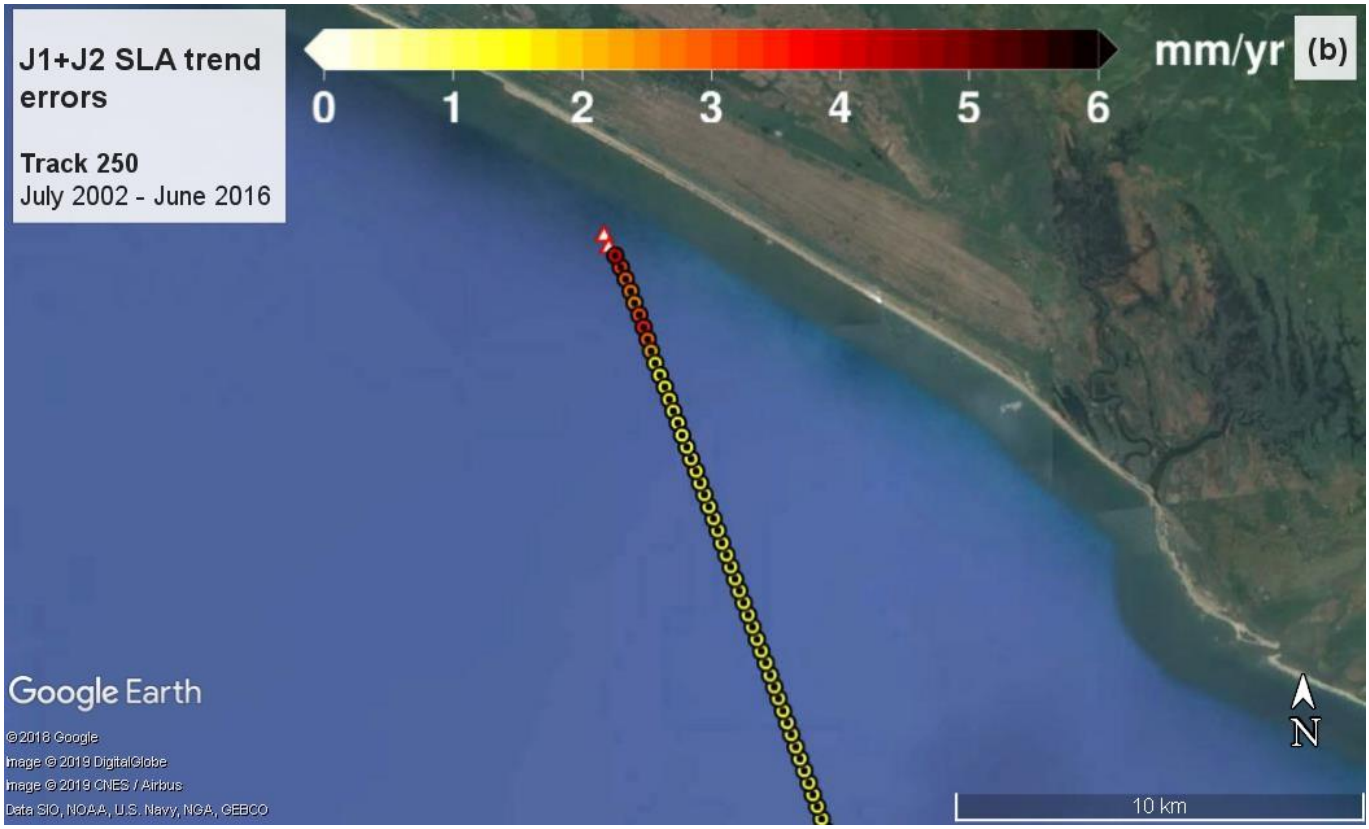

TRACK 174

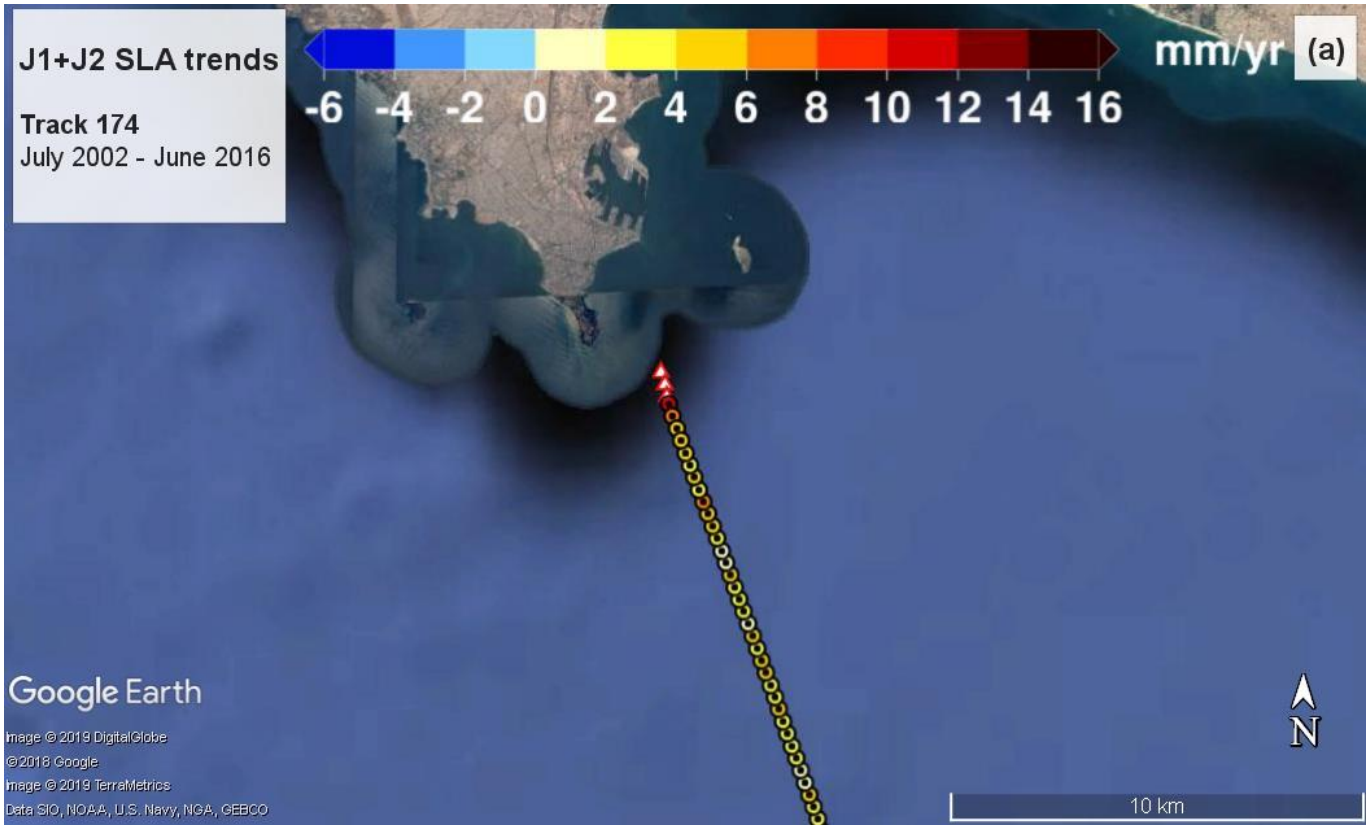

TRACK 174 #2

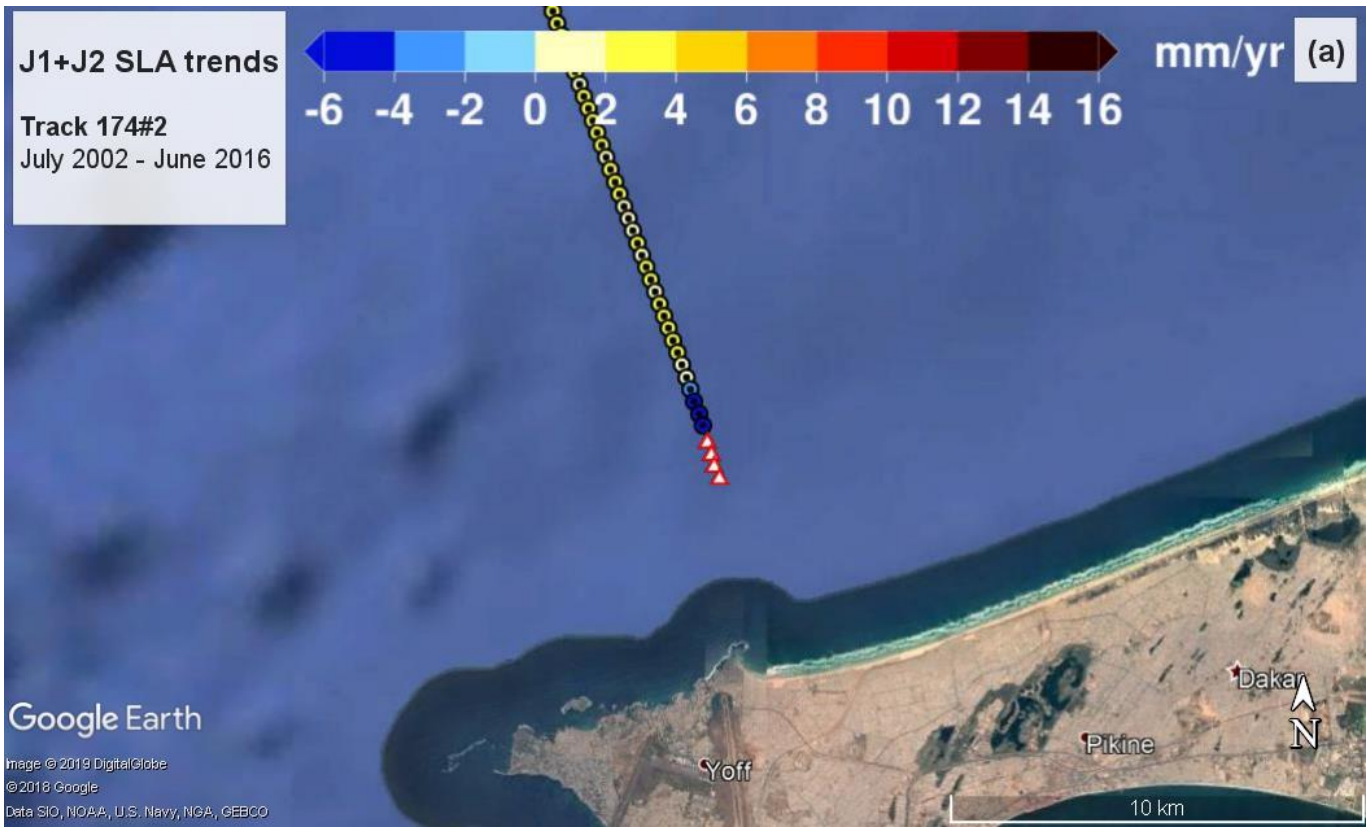

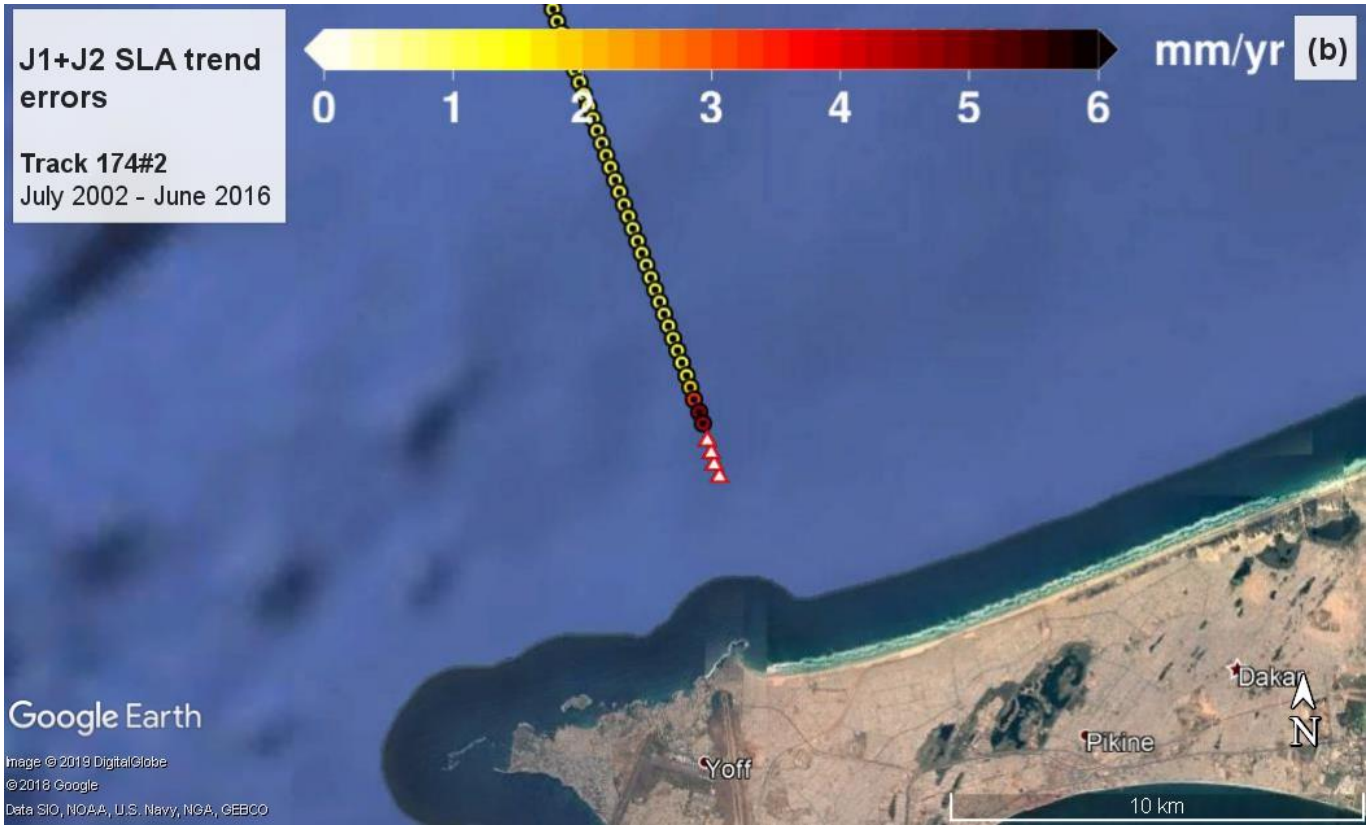

Figure 13

WESTERN AFRICA

ASCENDING TRACKS

Ranked from west to east

TRACK 035 X-TRACK/ALES 20Hz SLA – J1 + J2 – Jul2002 – Jun2016
(annual and semi-annual cycles removed)

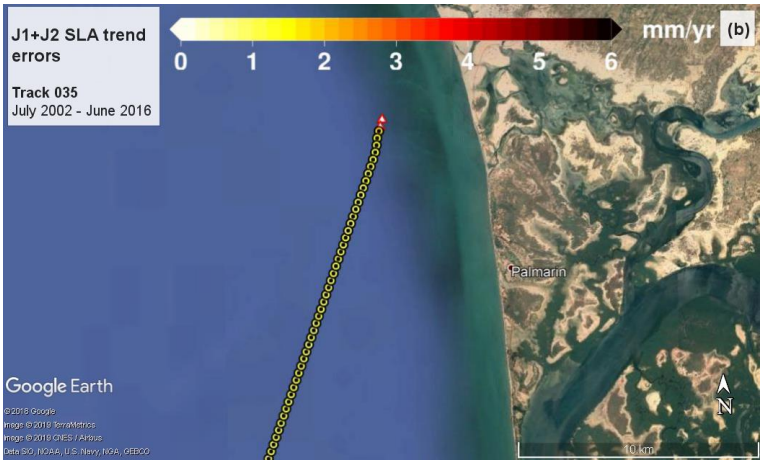

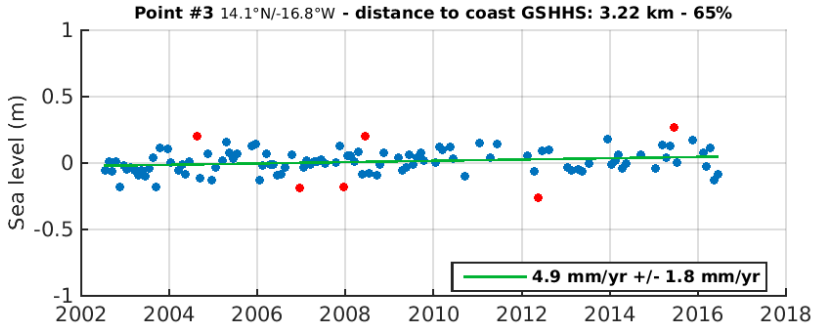

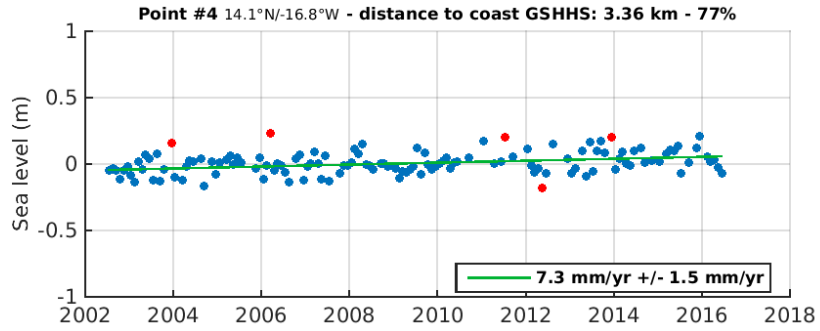

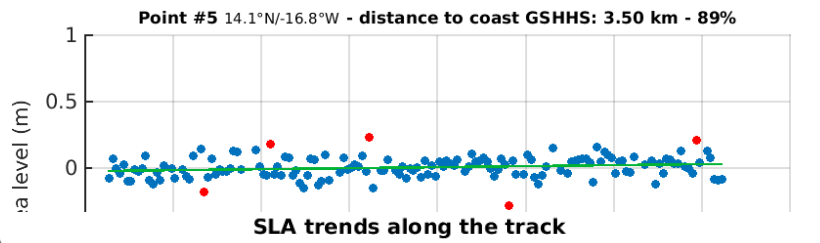

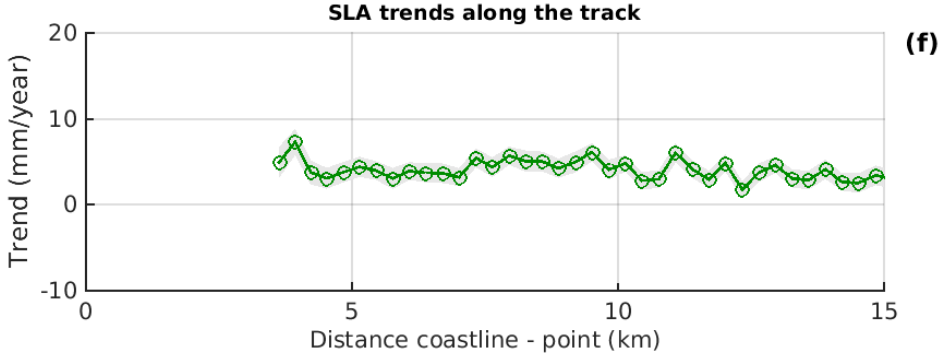

TRACK 111 X-TRACK/ALES 20Hz SLA – J1 + J2 – Jul2002 – Jun2016
(annual and semi-annual cycles removed)

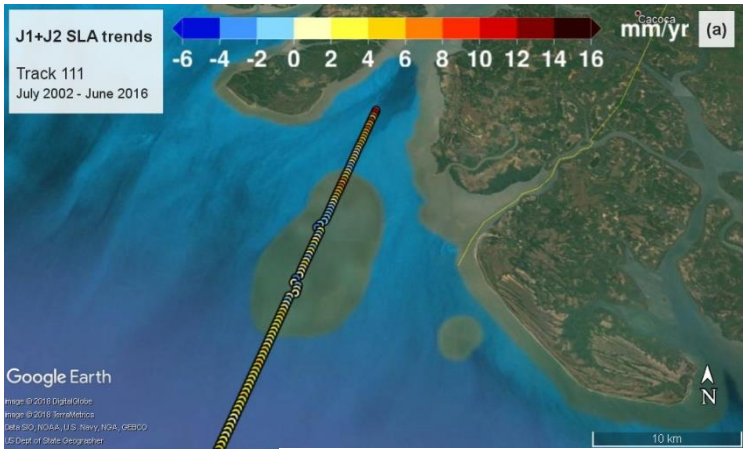

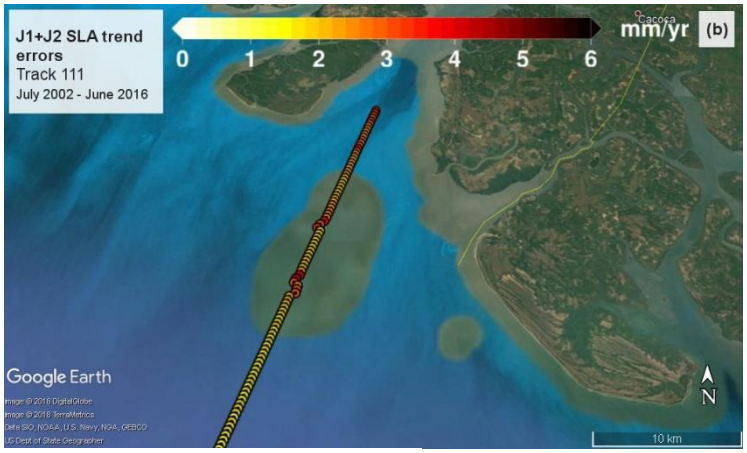

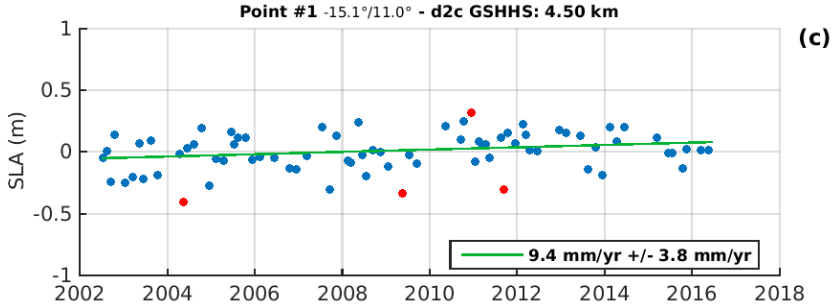

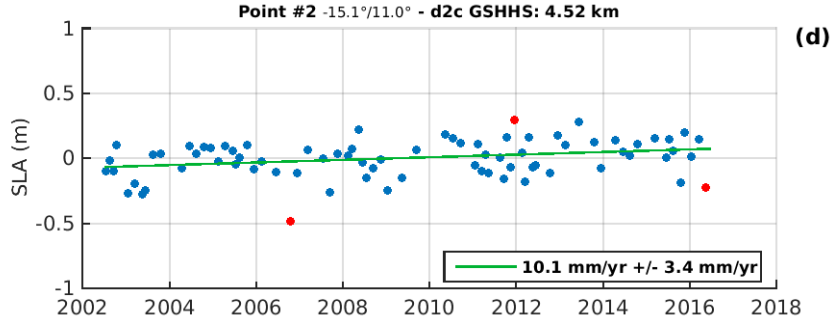

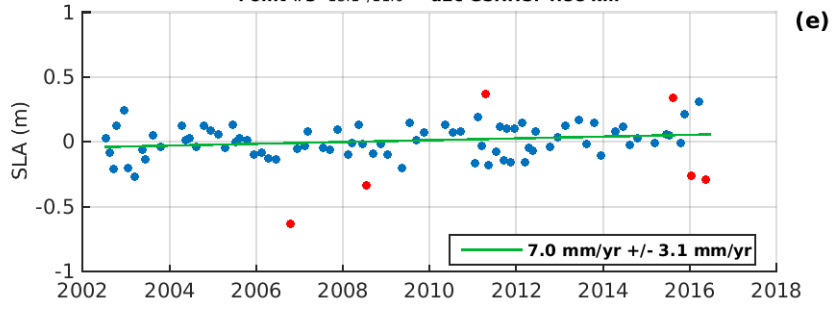

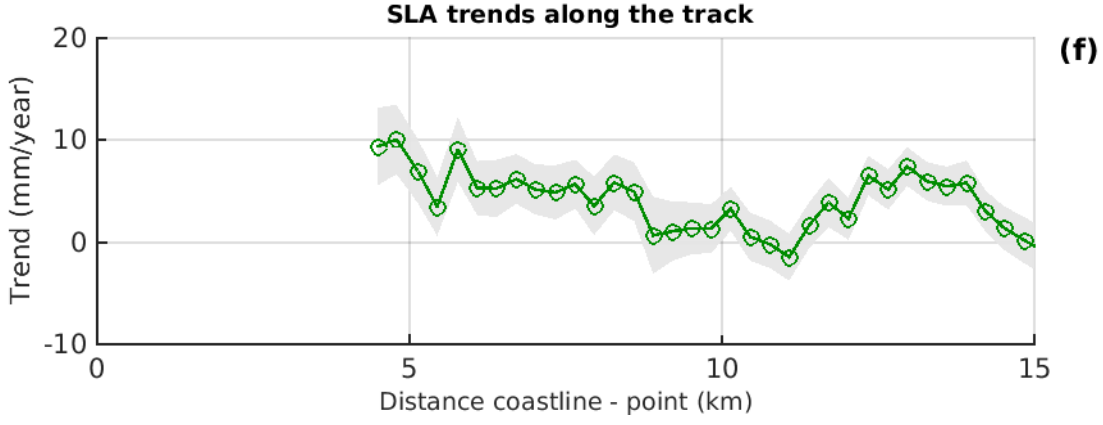

TRACK 187 X-TRACK/ALES 20Hz SLA – J1 + J2 – Jul2002 – Jun2016
(annual and semi-annual cycles removed)

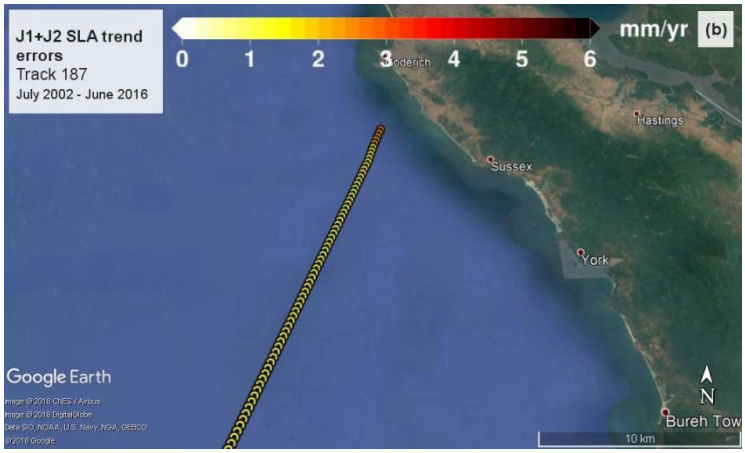

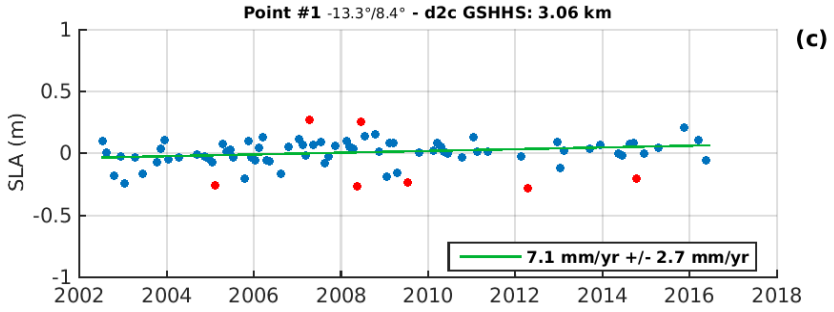

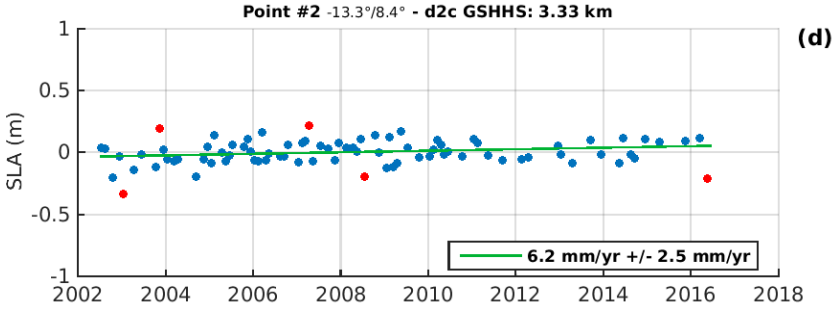

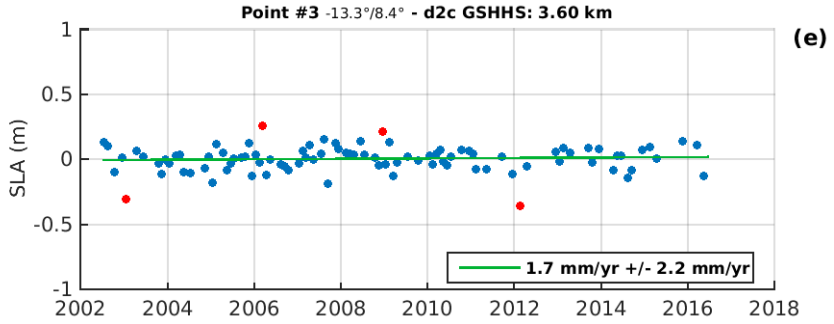

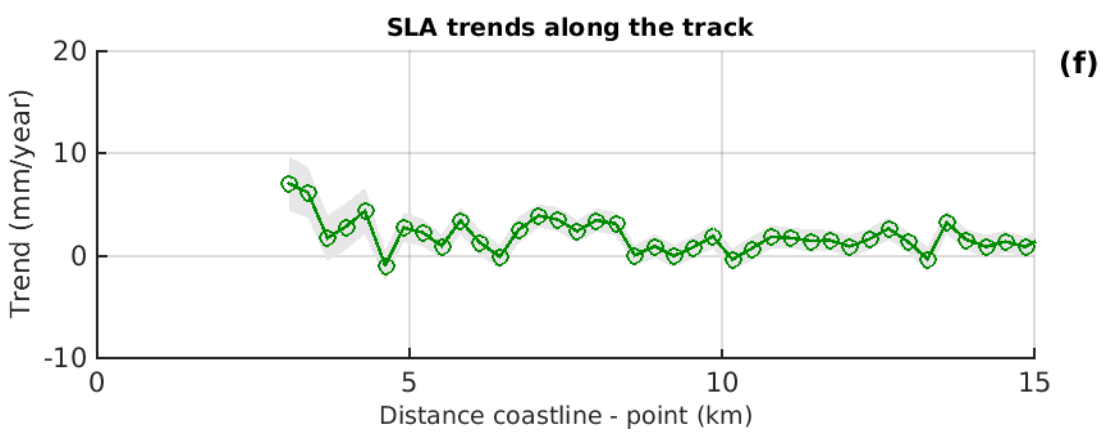

TRACK 009 X-TRACK/ALES 20Hz SLA – J1 + J2 – Jul2002 – Jun2016 (annual and semi-annual cycles removed)

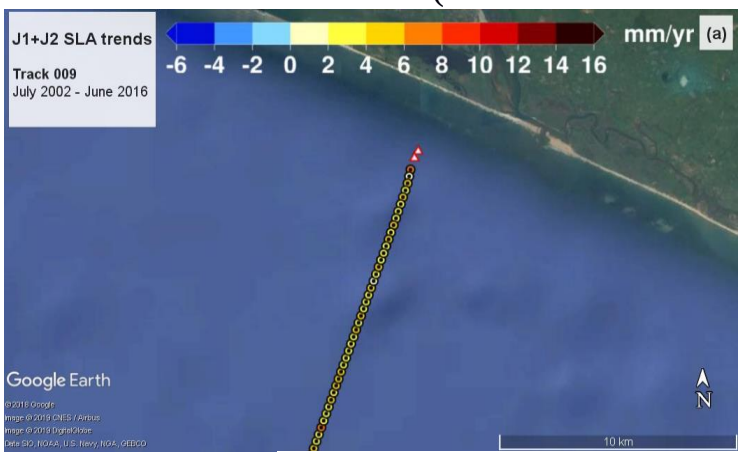

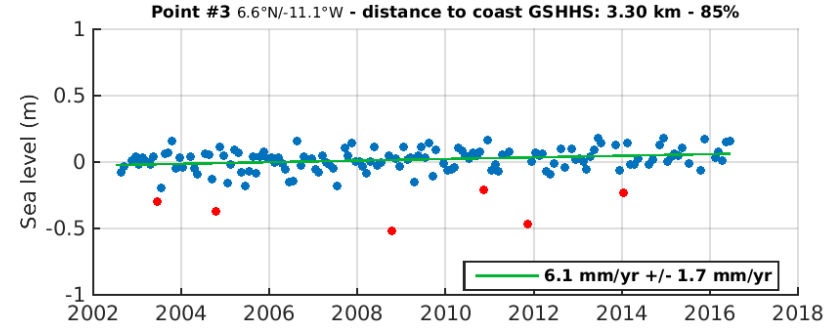

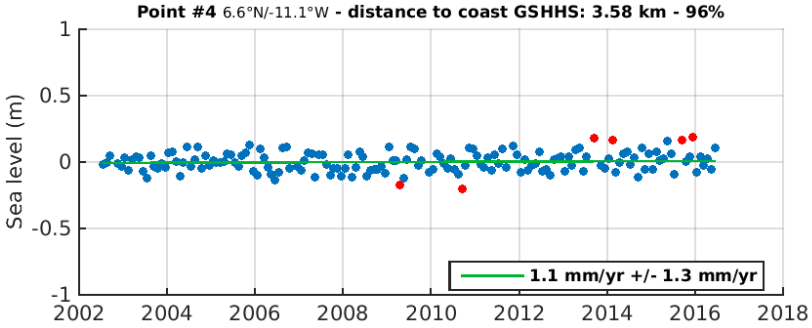

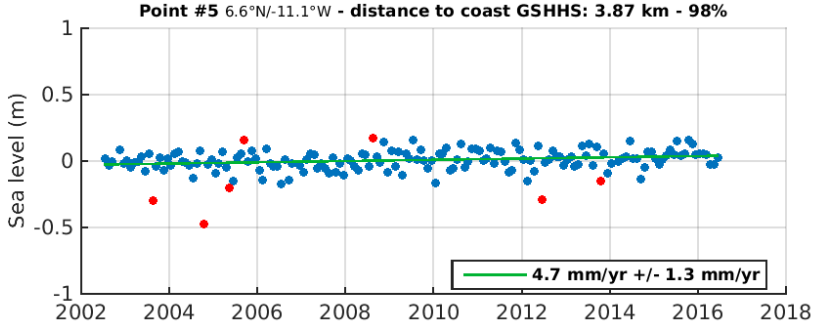

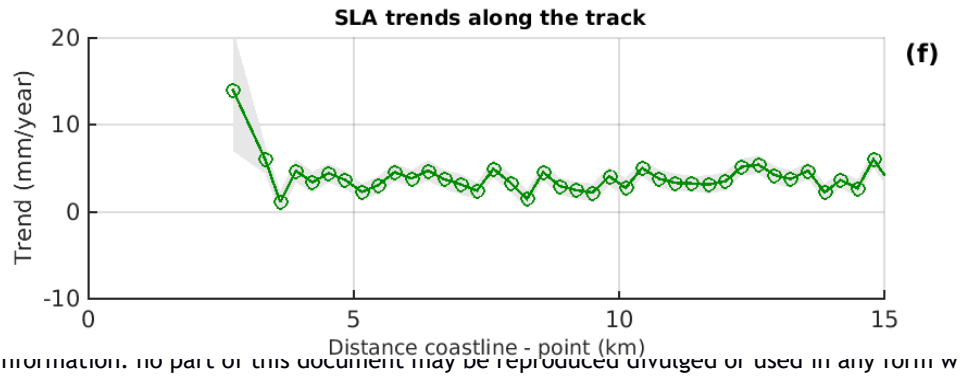

TRACK 085 X-TRACK/ALES 20Hz SLA – J1 + J2 – Jul2002 – Jun2016
(annual and semi-annual cycles removed)

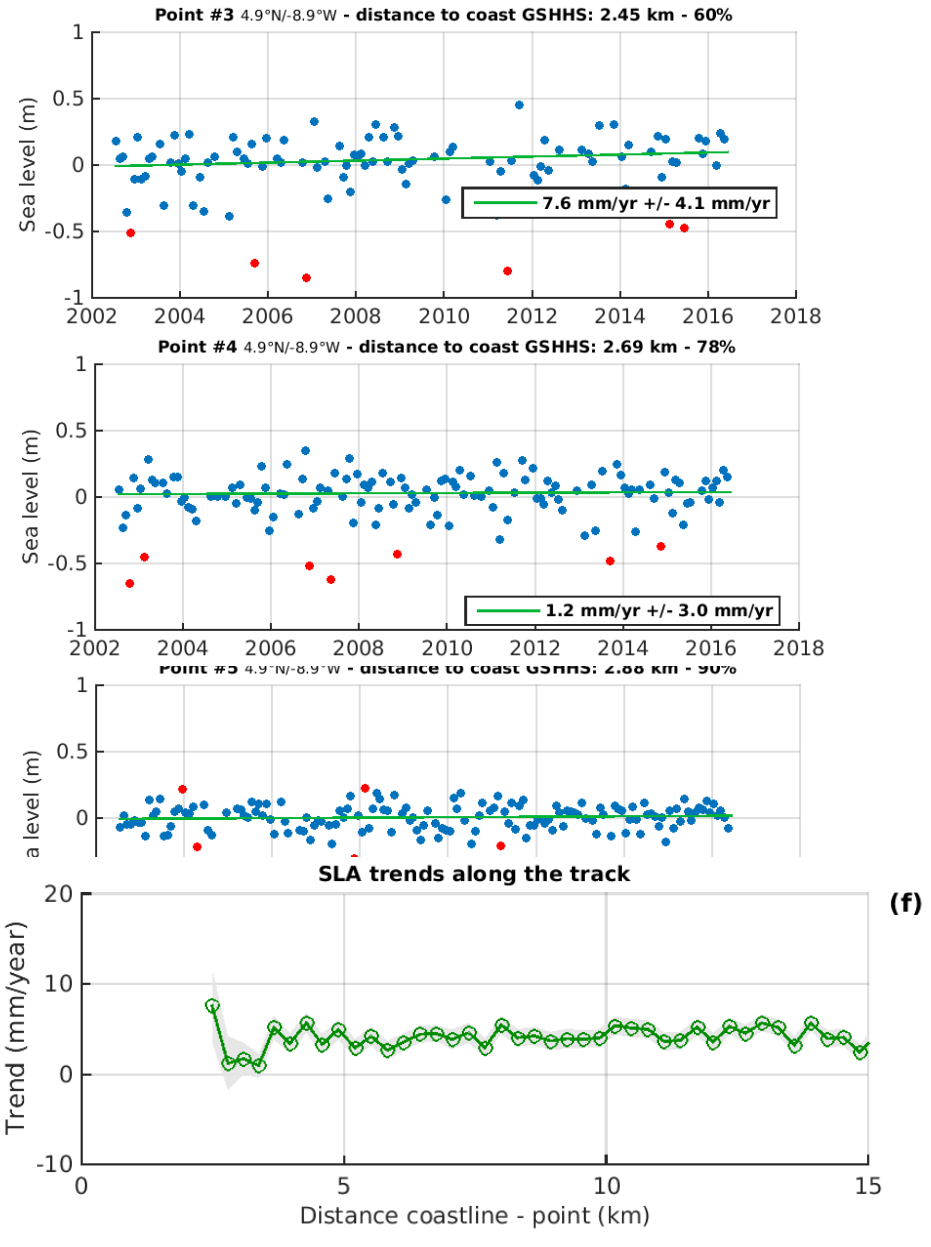

TRACK 161 X-TRACK/ALES 20Hz SLA – J1 + J2 – Jul2002 – Jun2016
(annual and semi-annual cycles removed)

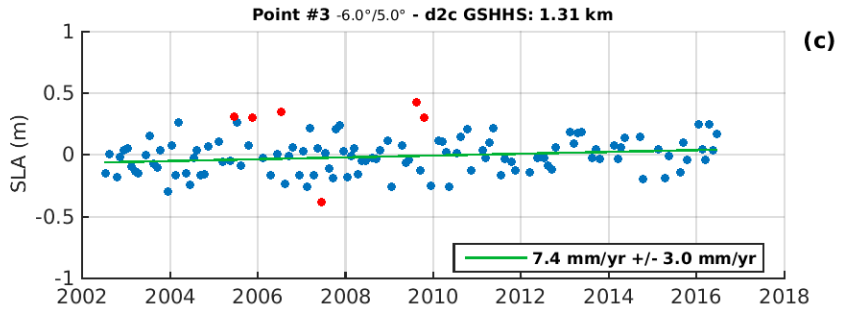

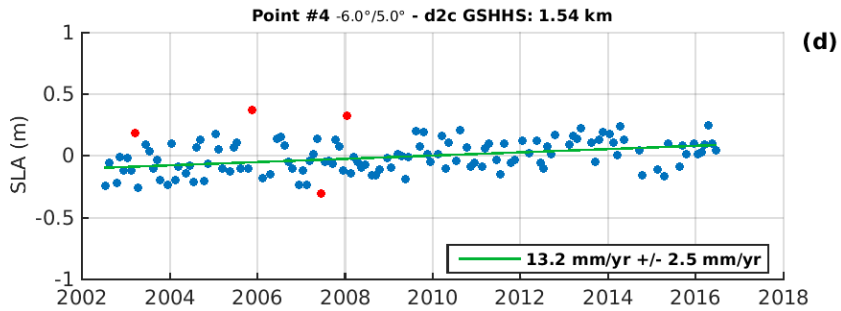

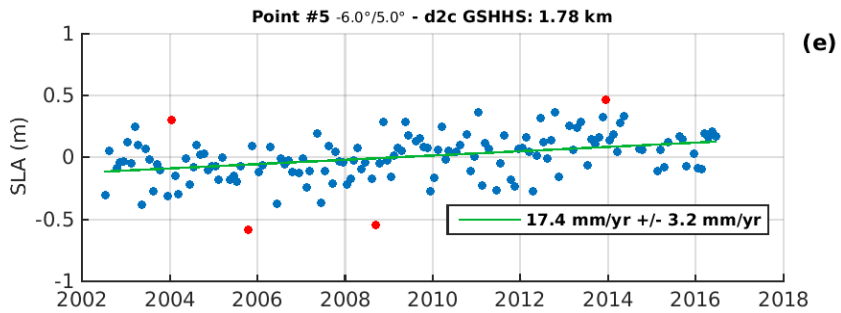

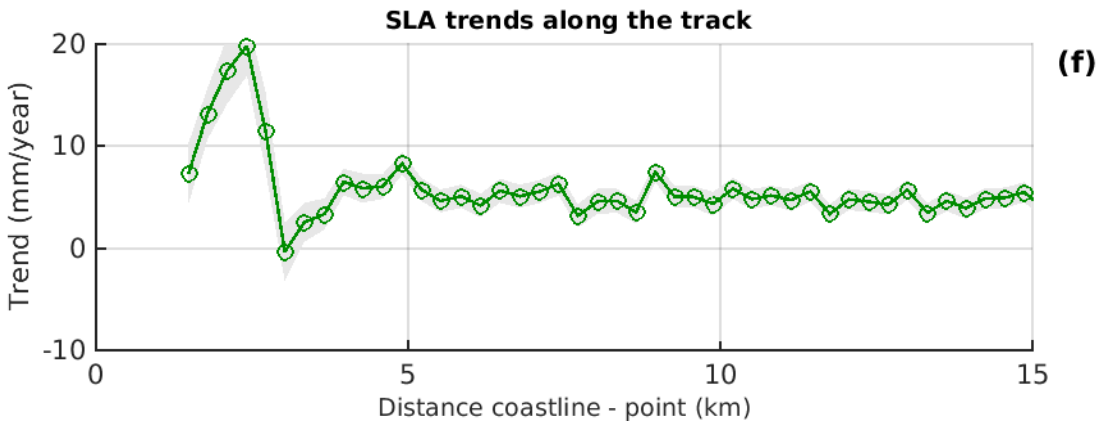

TRACK 237 X-TRACK/ALES 20Hz SLA – J1 + J2 – Jul2002 – Jun2016
(annual and semi-annual cycles removed)

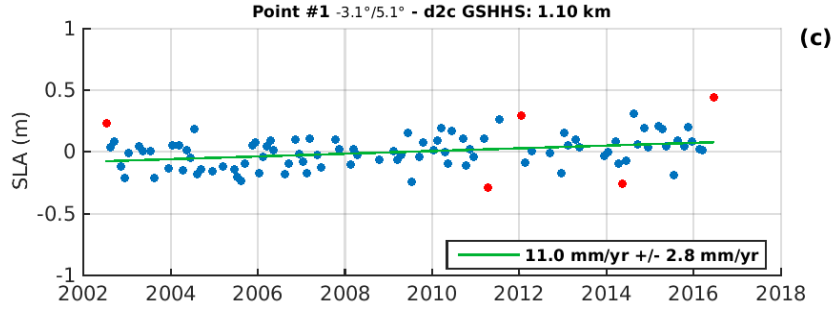

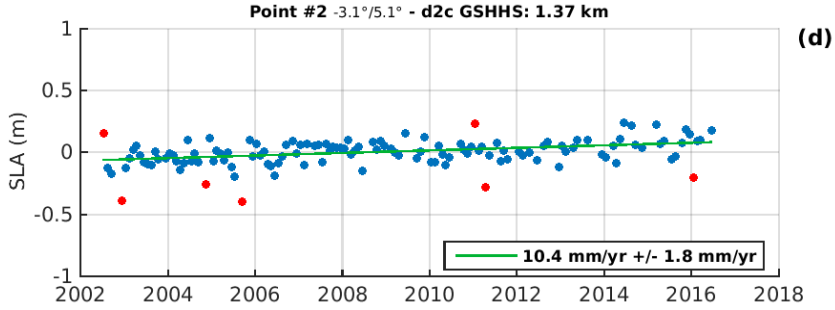

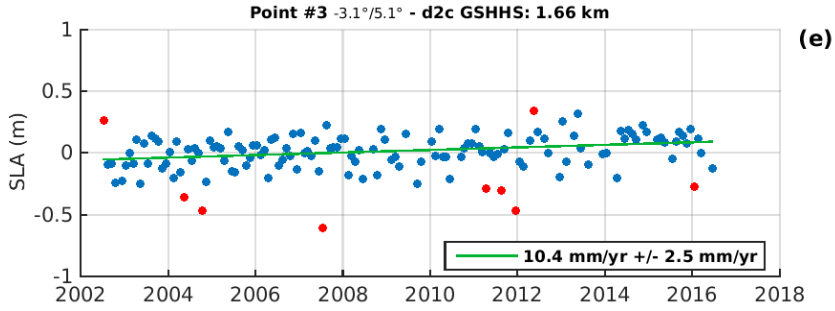

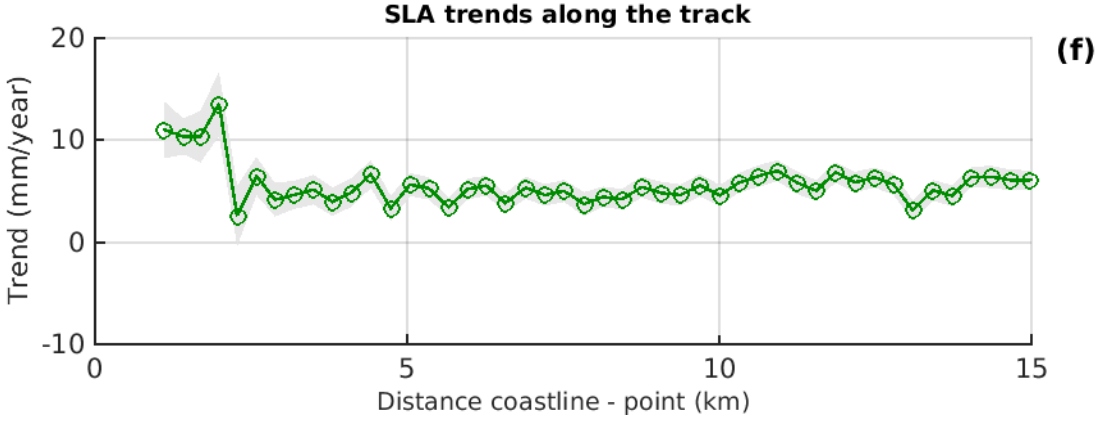

TRACK 059 X-TRACK/ALES 20Hz SLA – J1 + J2 – Jul2002 – Jun2016
(annual and semi-annual cycles removed)

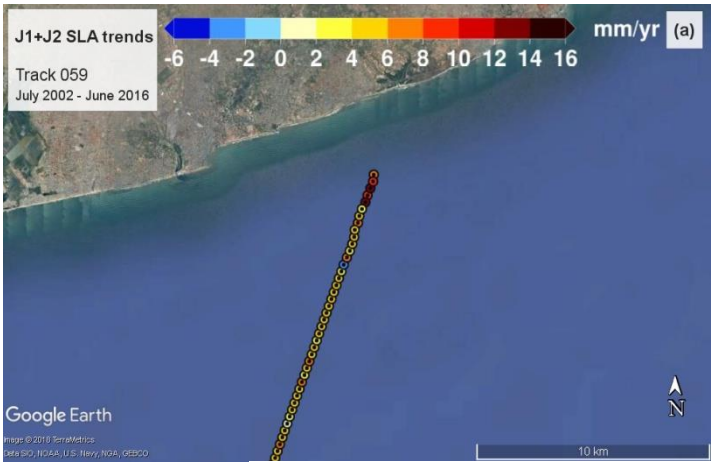

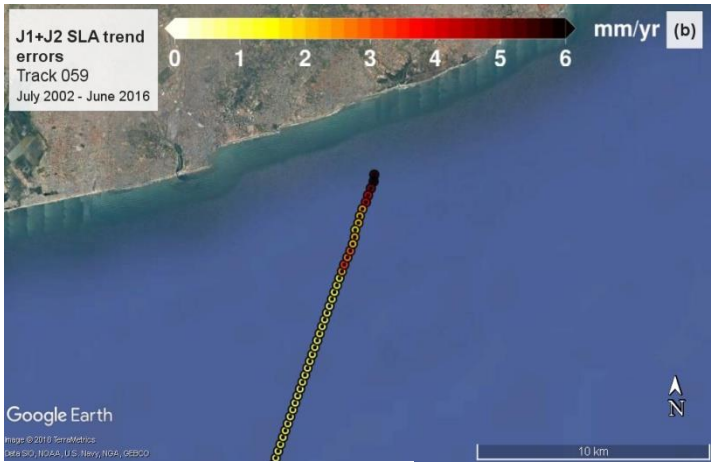

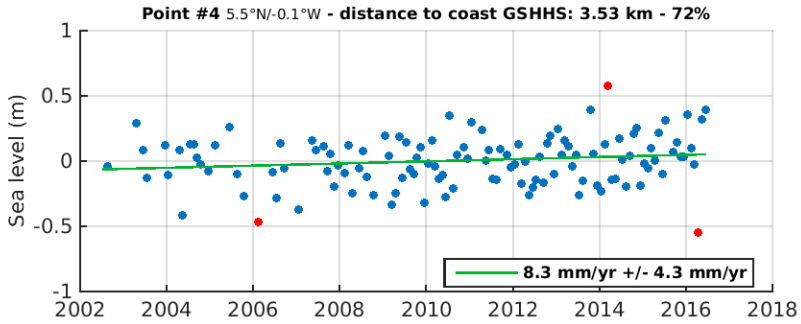

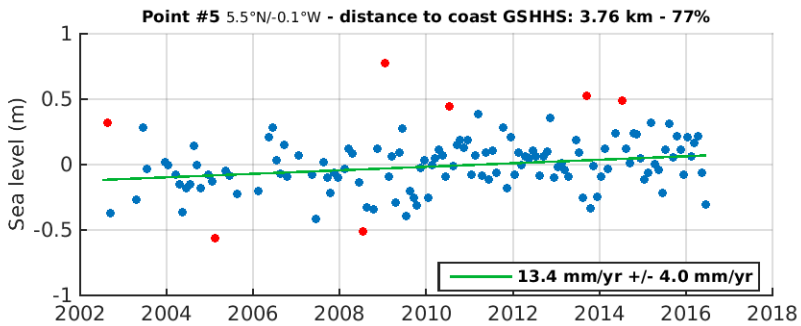

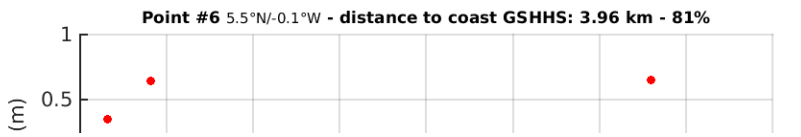

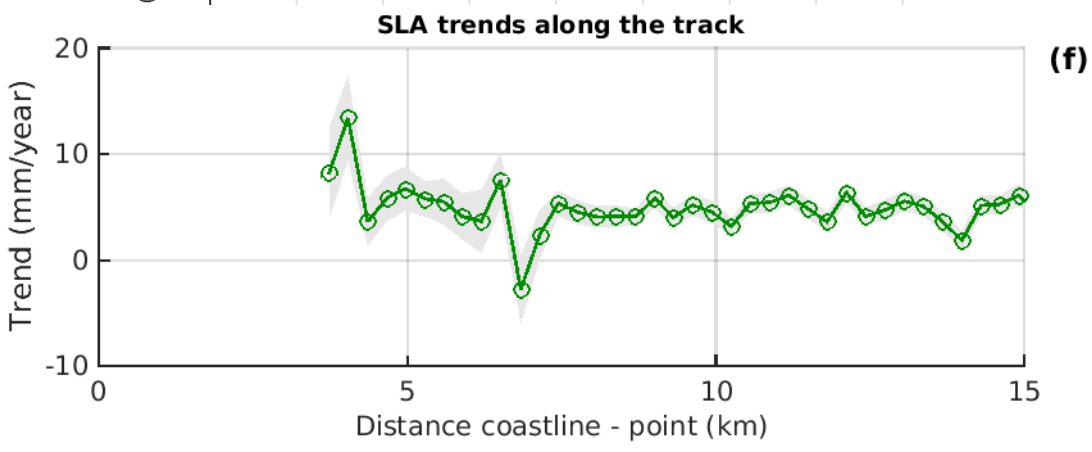

TRACK 135 X-TRACK/ALES 20Hz SLA – J1 + J2 – Jul2002 – Jun2016
(annual and semi-annual cycles removed)

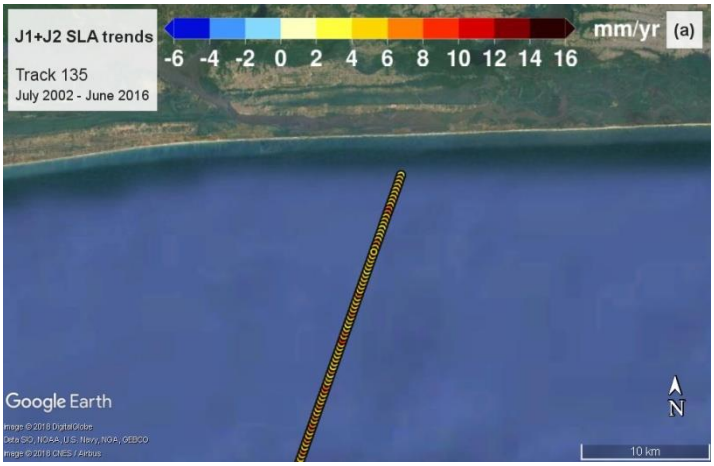

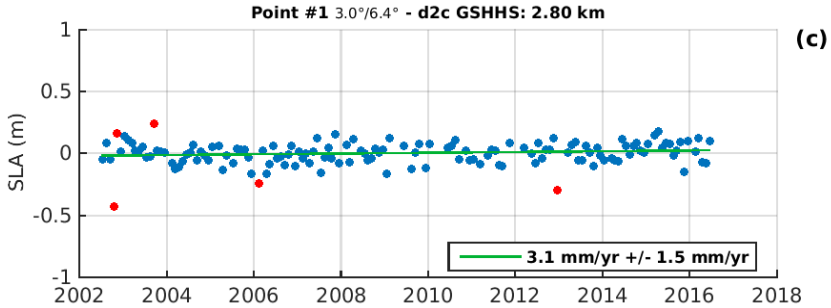

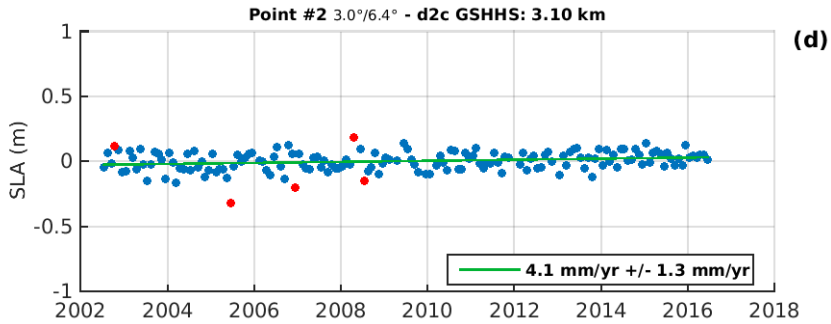

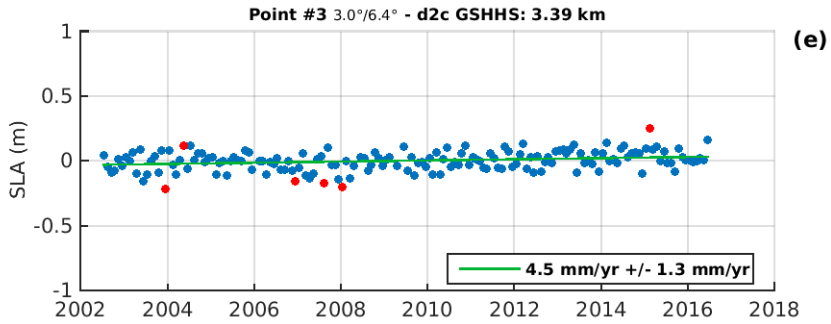

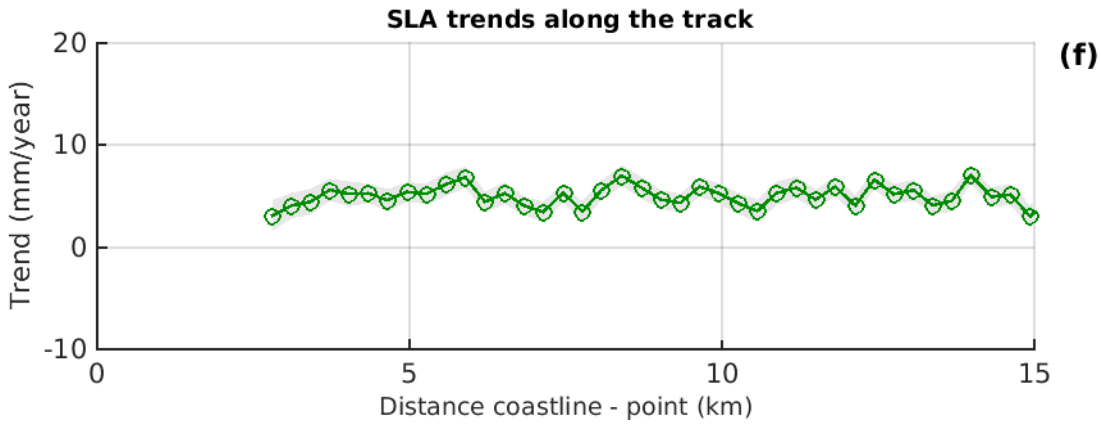

TRACK 211 X-TRACK/ALES 20Hz SLA – J1 + J2 – Jul2002 – Jun2016
(annual and semi-annual cycles removed)

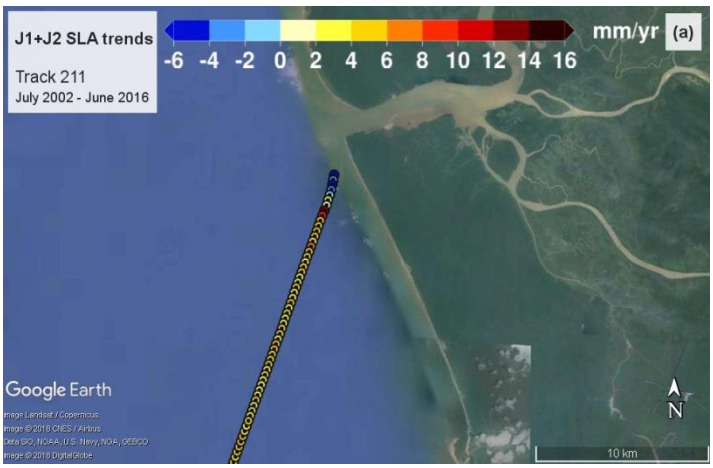

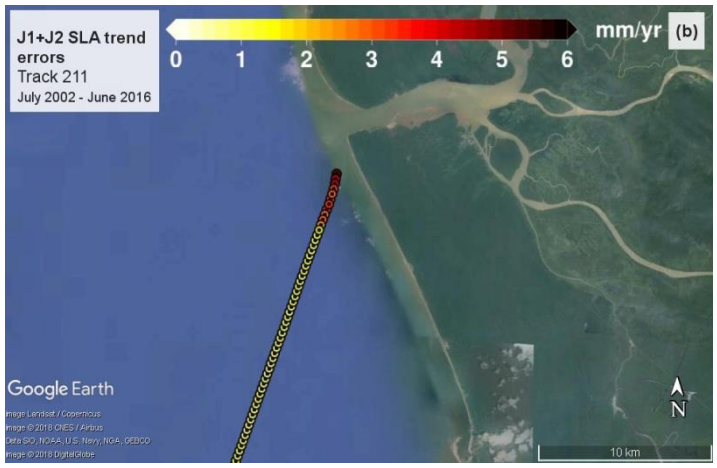

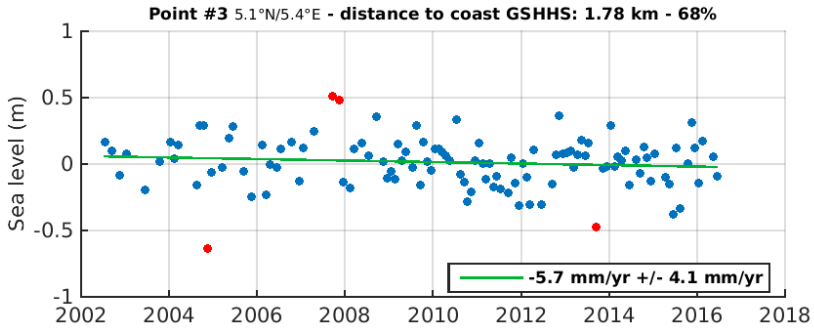

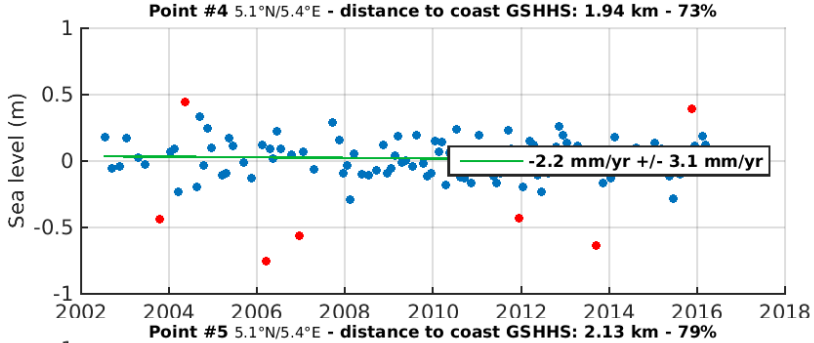

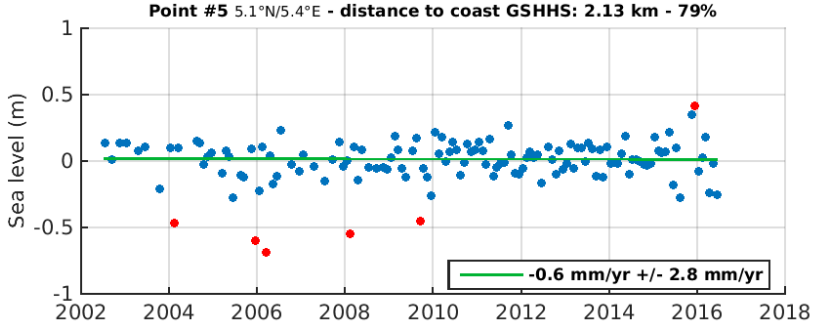

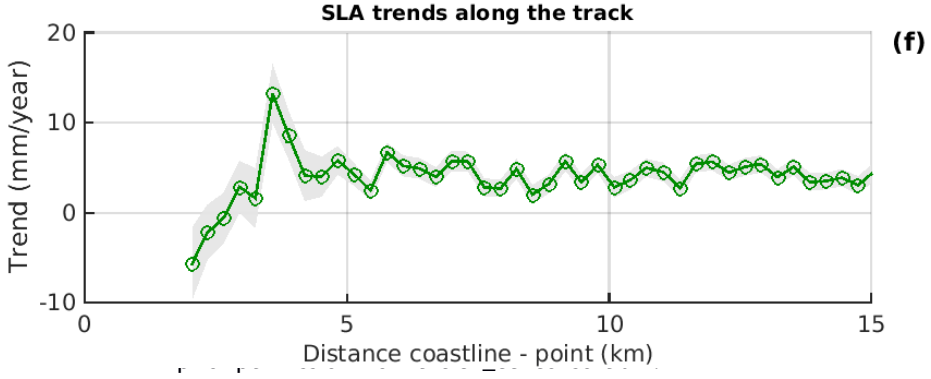

TRACK 033 X-TRACK/ALES 20Hz SLA – J1 + J2 – Jul2002 – Jun2016
(annual and semi-annual cycles removed)

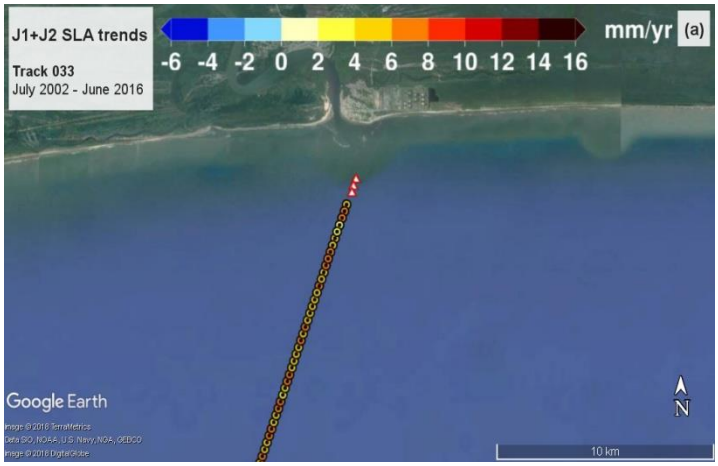

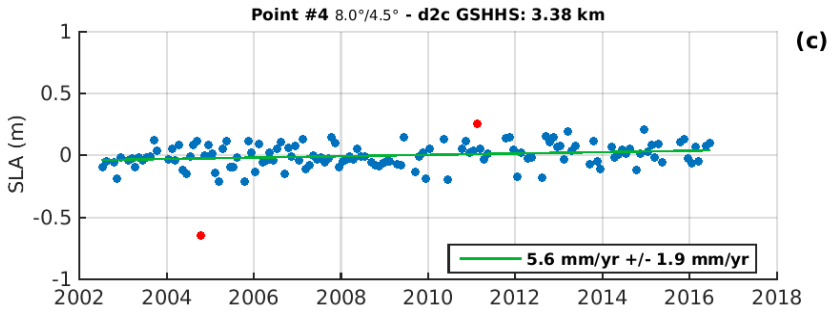

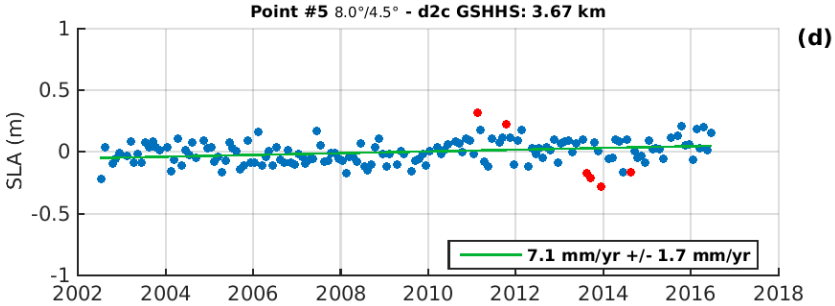

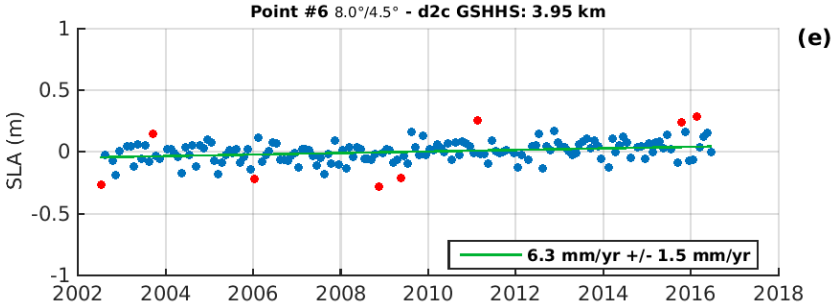

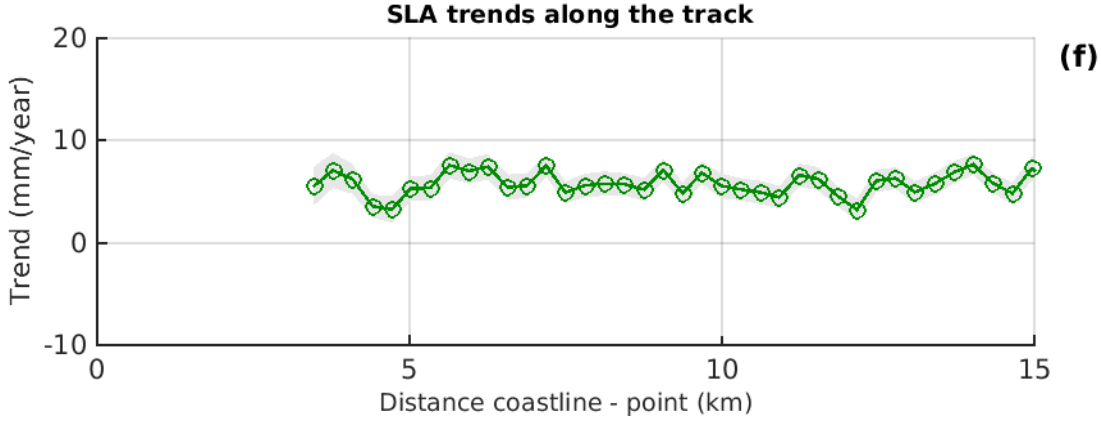

TRACK 109 X-TRACK/ALES 20Hz SLA – J1 + J2 – Jul2002 – Jun2016
(annual and semi-annual cycles removed)

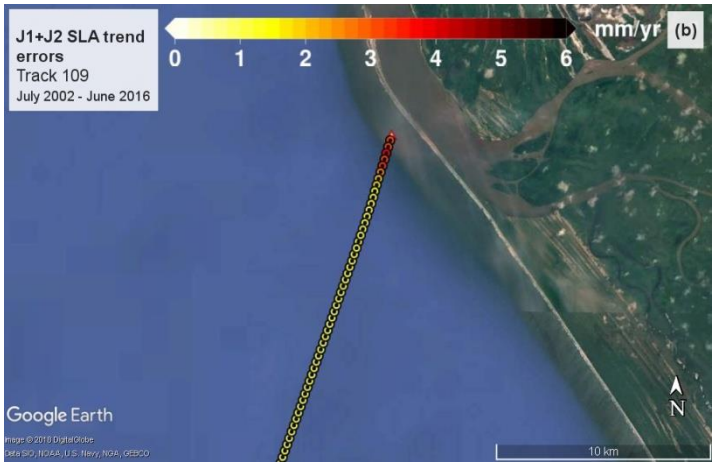

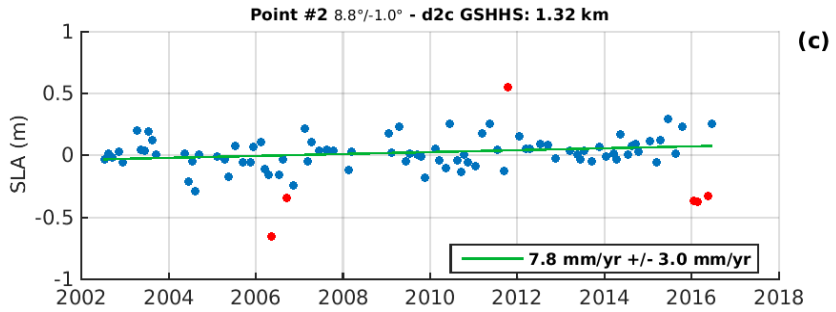

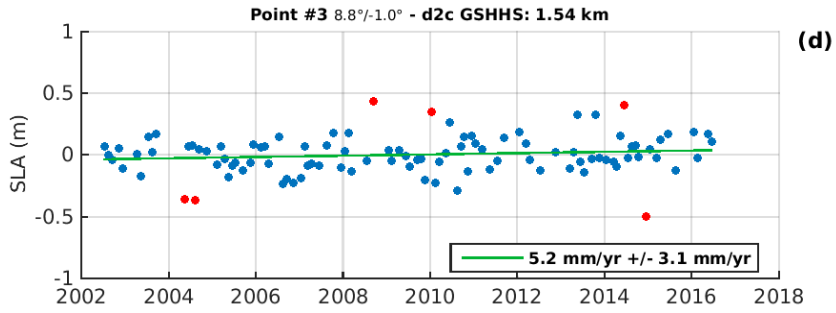

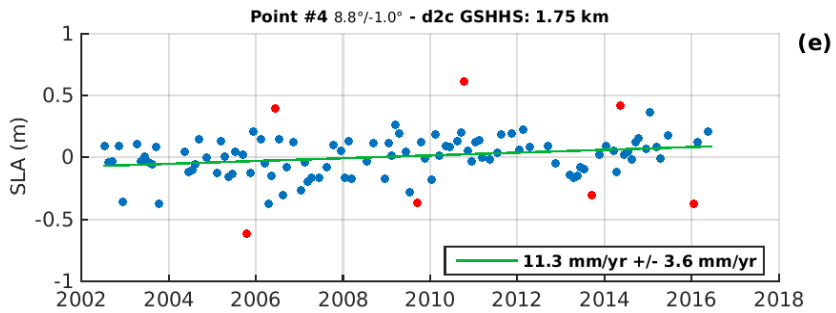

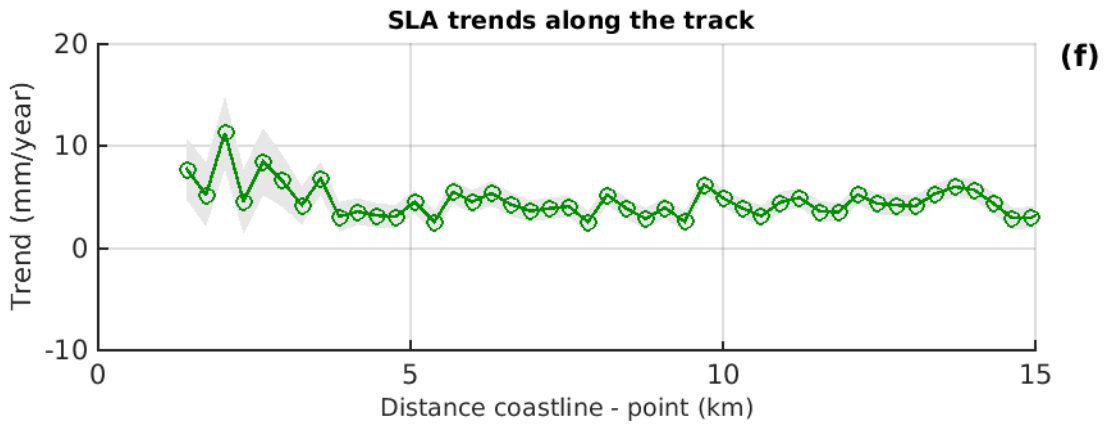

TRACK 185 X-TRACK/ALES 20Hz SLA – J1 + J2 – Jul2002 – Jun2016
(annual and semi-annual cycles removed)

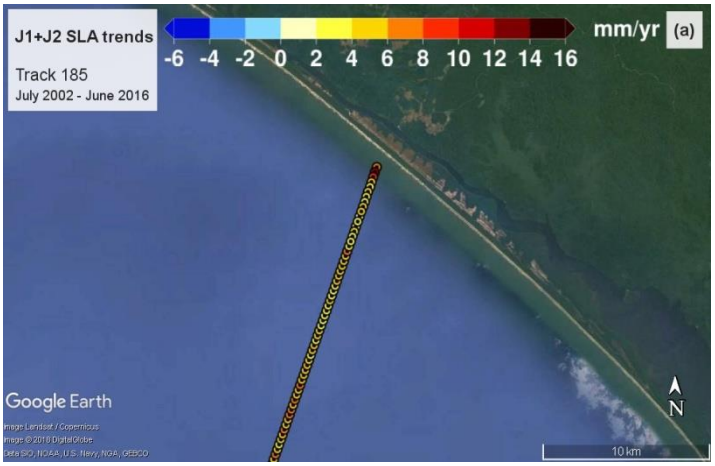

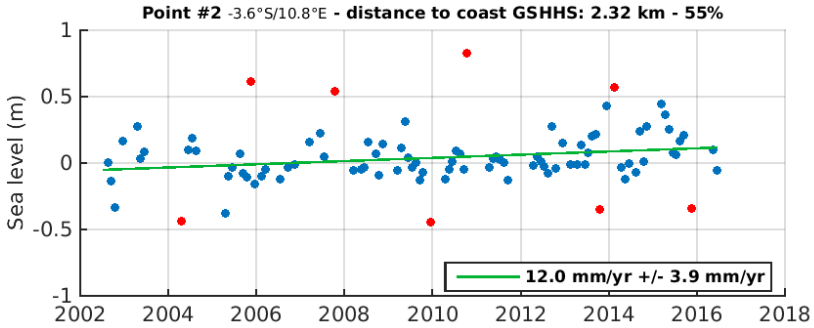

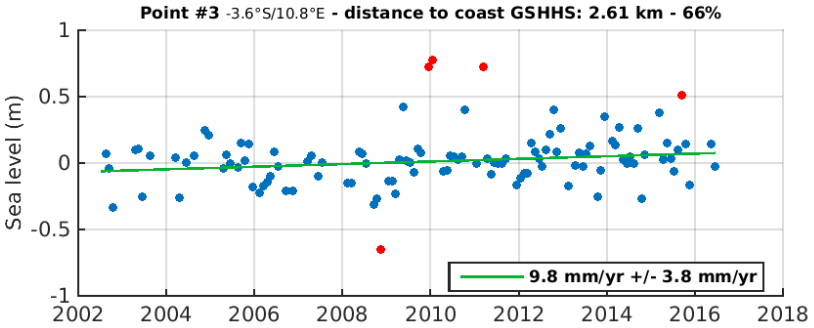

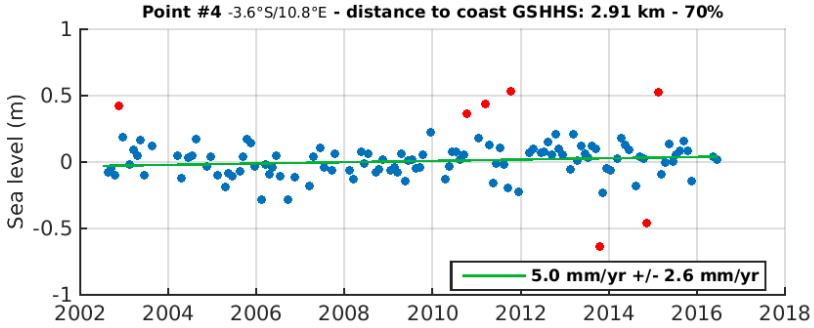

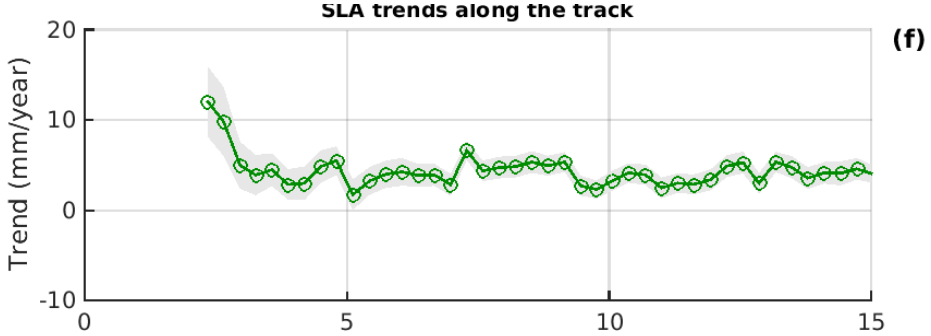

TRACK 007 X-TRACK/ALES 20Hz SLA – J1 + J2 – Jul2002 – Jun2016
(annual and semi-annual cycles removed)

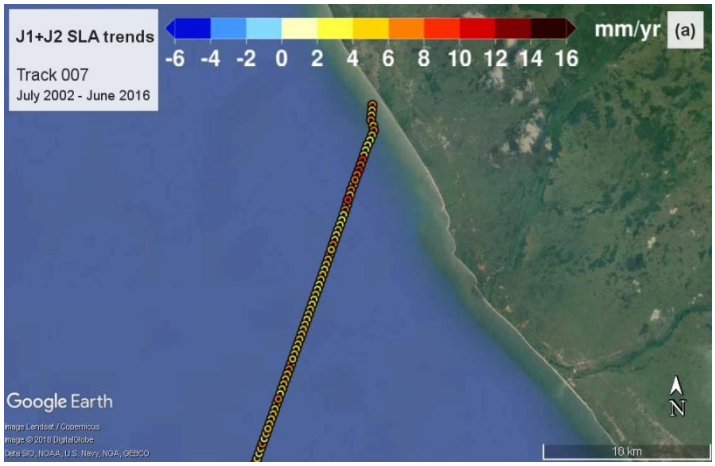

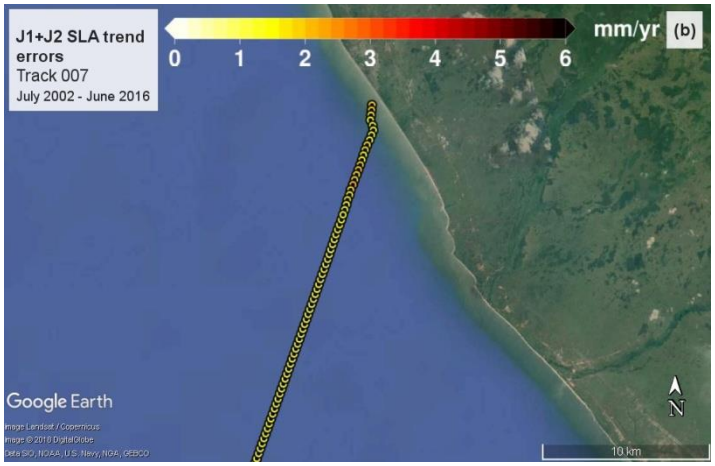

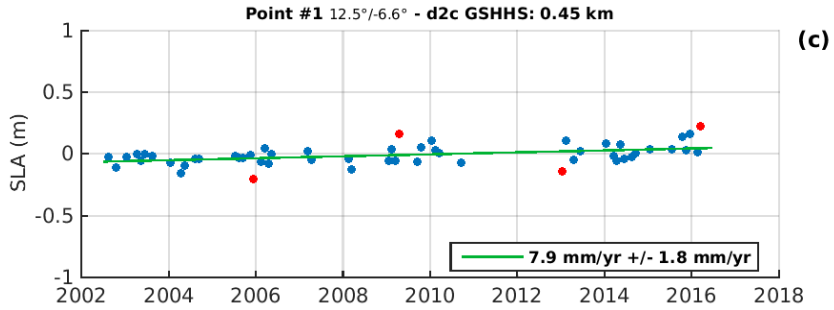

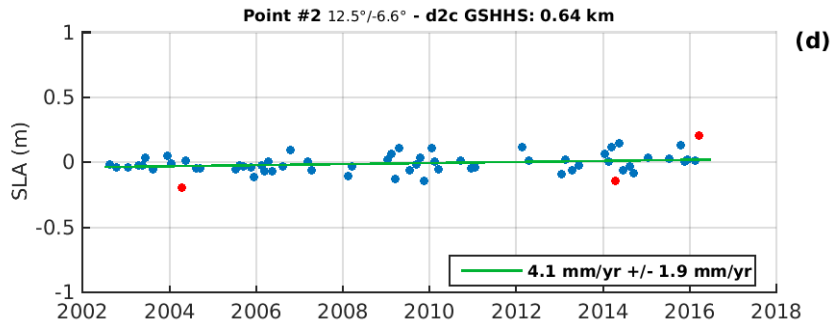

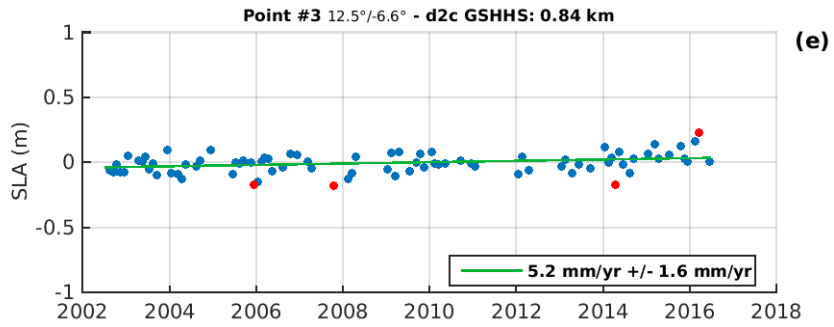

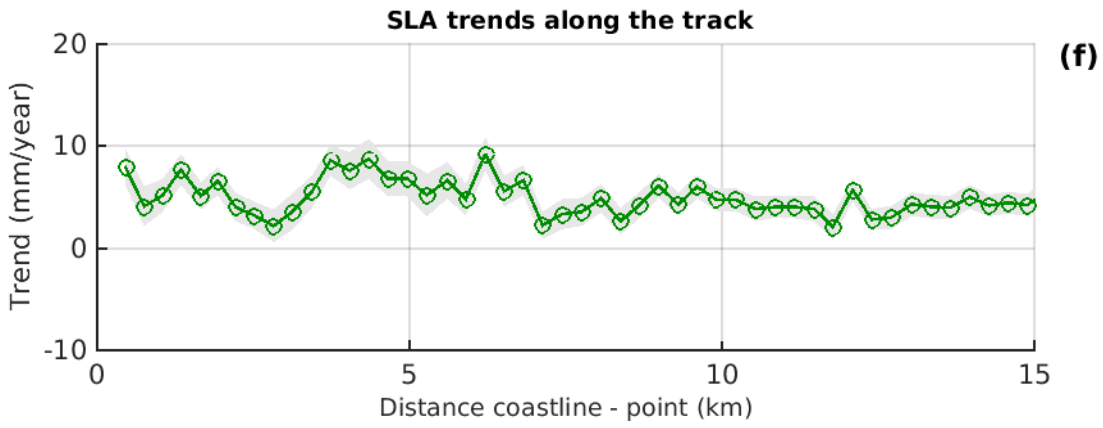

WESTERN AFRICA

DESCENDING TRACKS

Ranked from east to west

TRACK 020 X-TRACK/ALES 20Hz SLA – J1 + J2 – Jul2002 – Jun2016
(annual and semi-annual cycles removed)

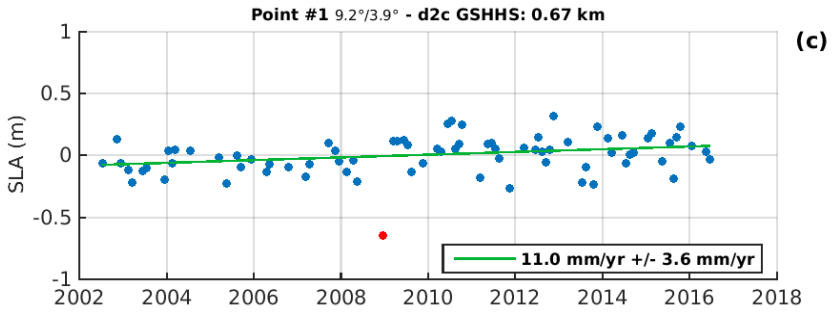

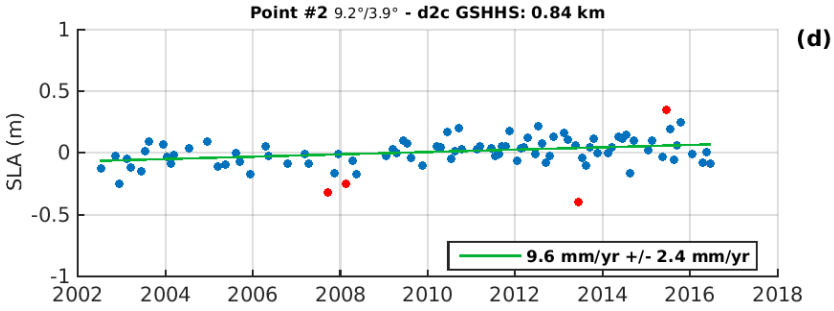

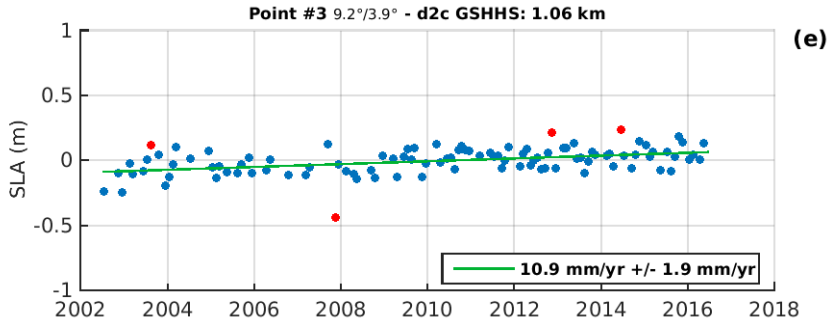

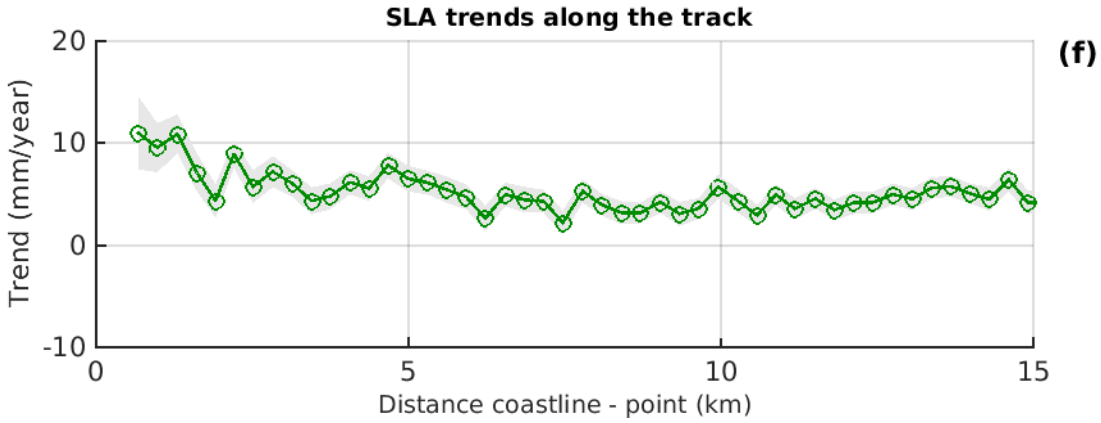

TRACK 198 X-TRACK/ALES 20Hz SLA – J1 + J2 – Jul2002 – Jun2016
(annual and semi-annual cycles removed)

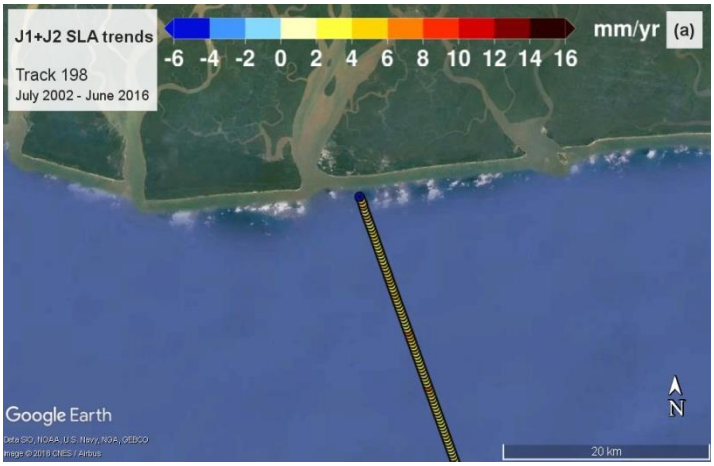

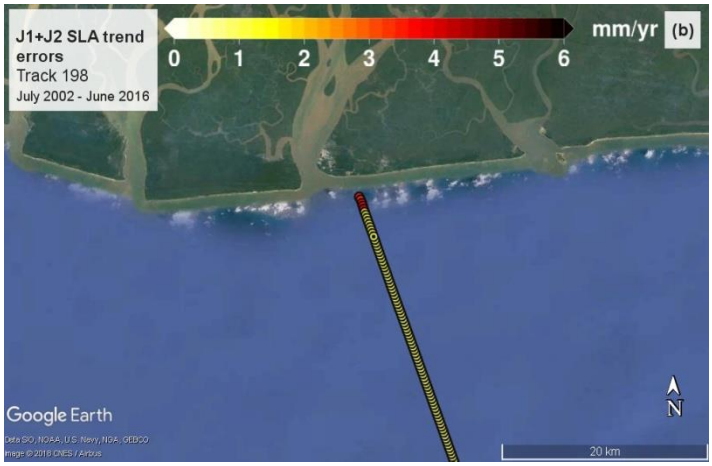

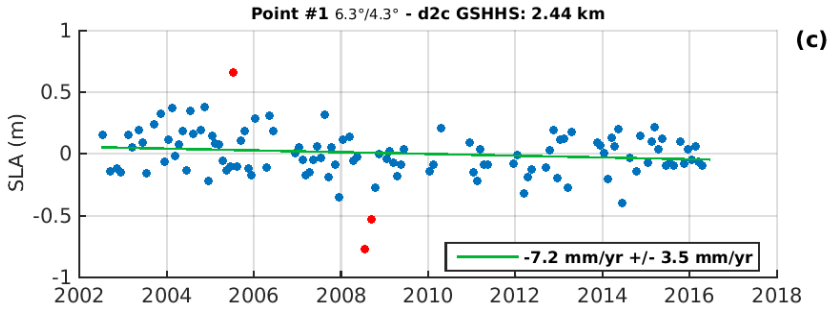

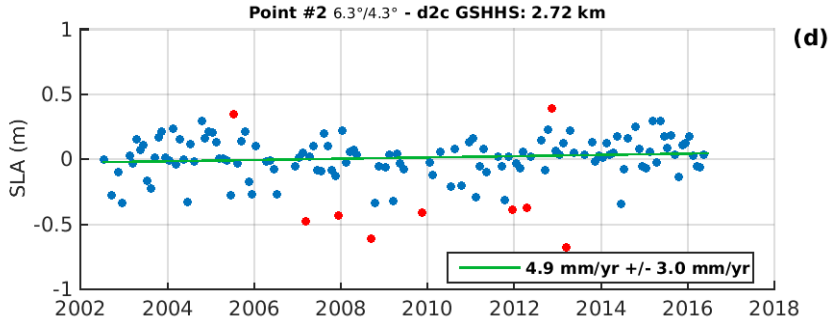

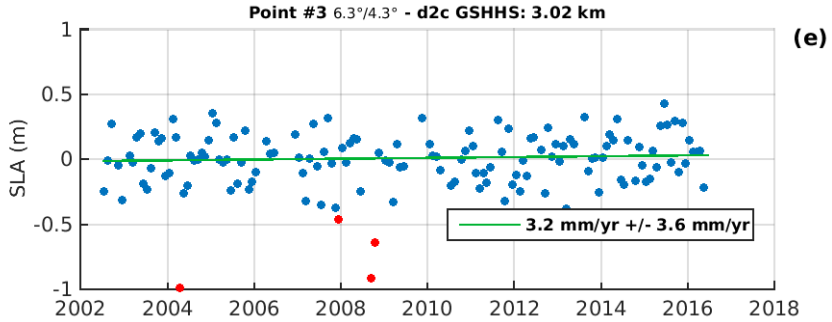

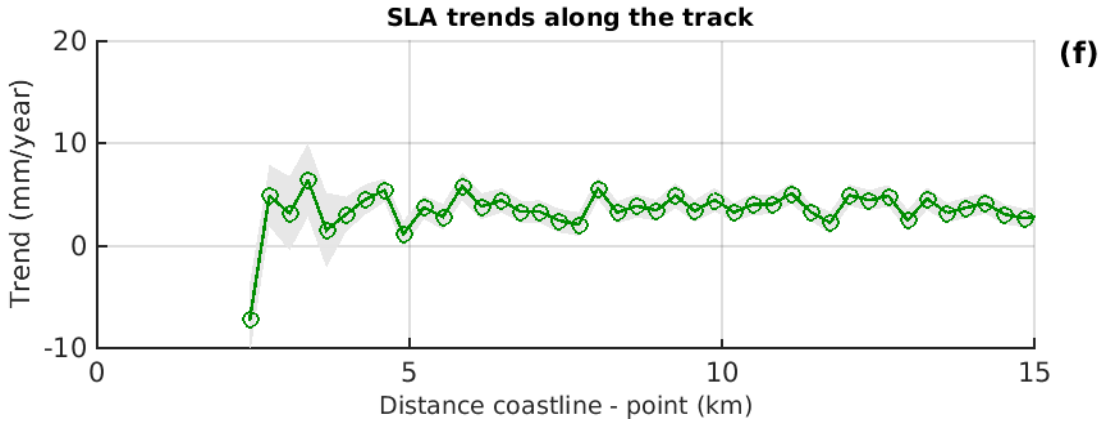

TRACK 122 X-TRACK/ALES 20Hz SLA – J1 + J2 – Jul2002 – Jun2016
(annual and semi-annual cycles removed)

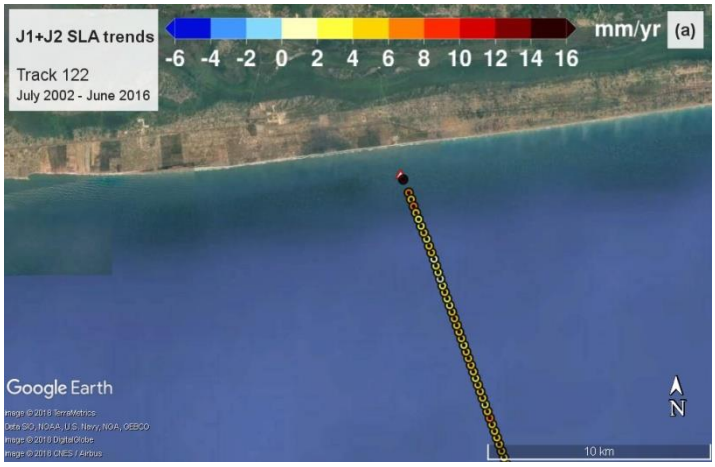

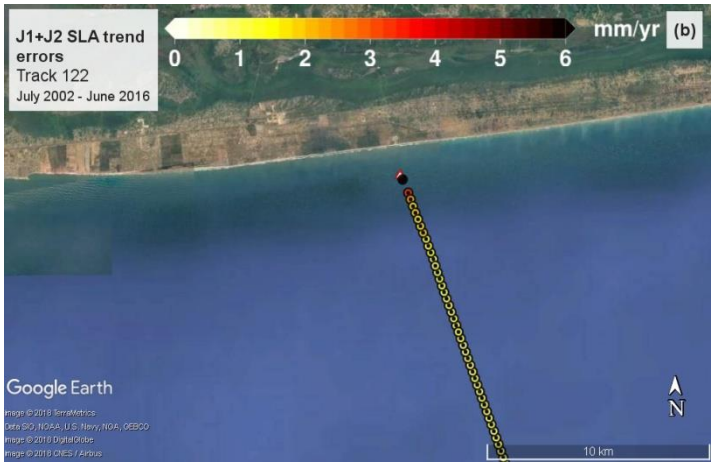

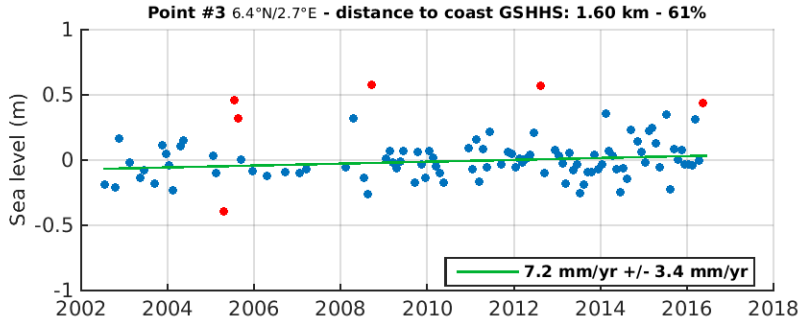

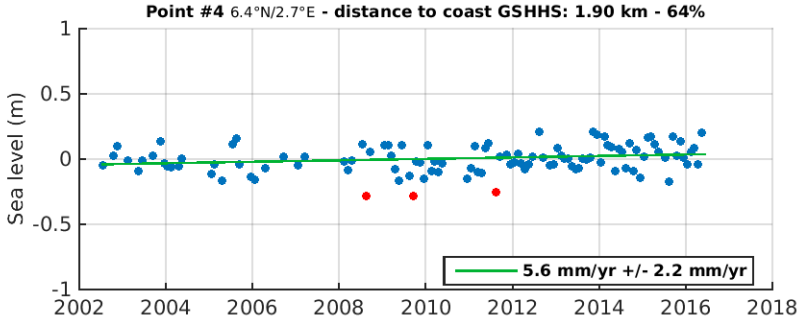

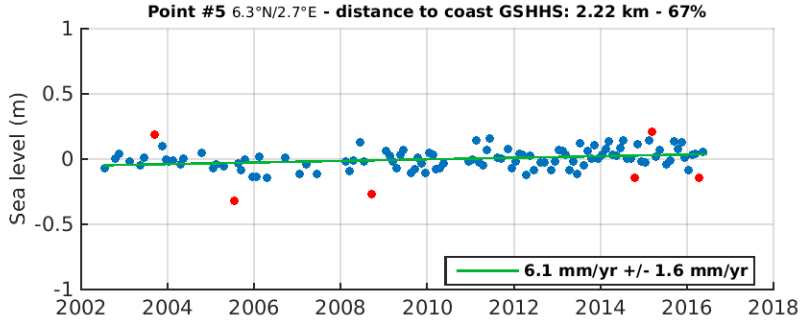

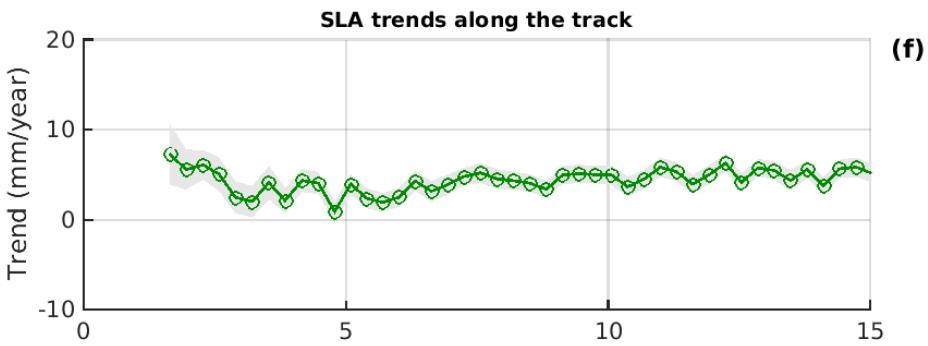

TRACK 046 X-TRACK/ALES 20Hz SLA – J1 + J2 – Jul2002 – Jun2016
(annual and semi-annual cycles removed)

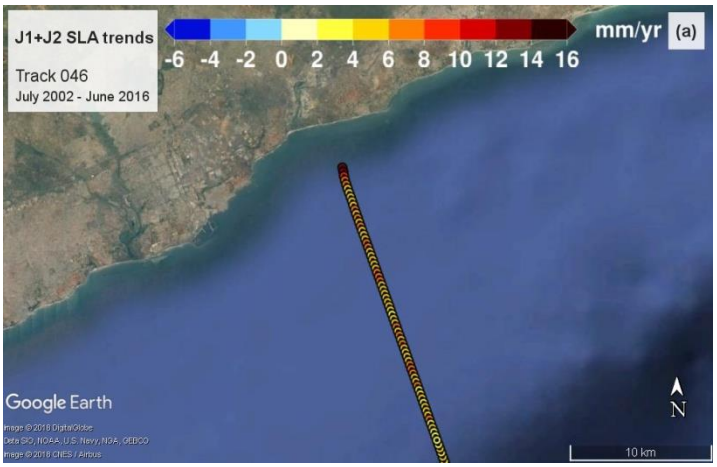

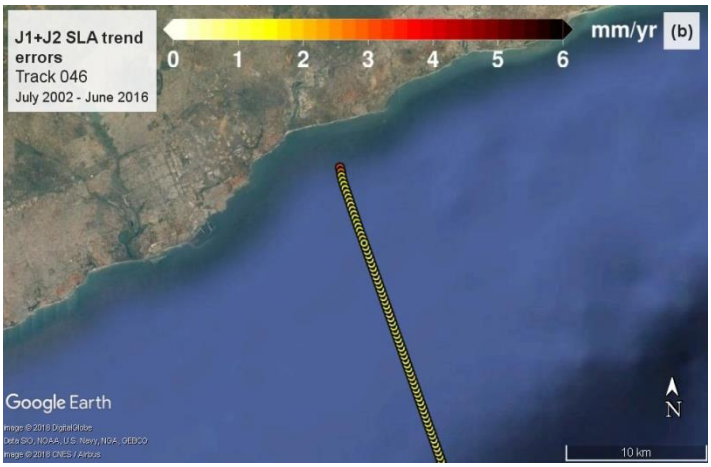

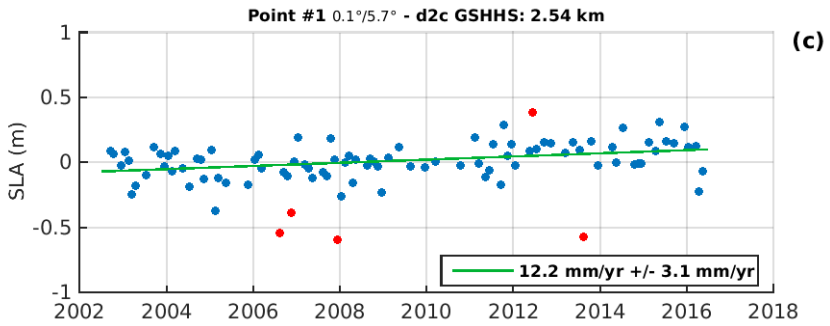

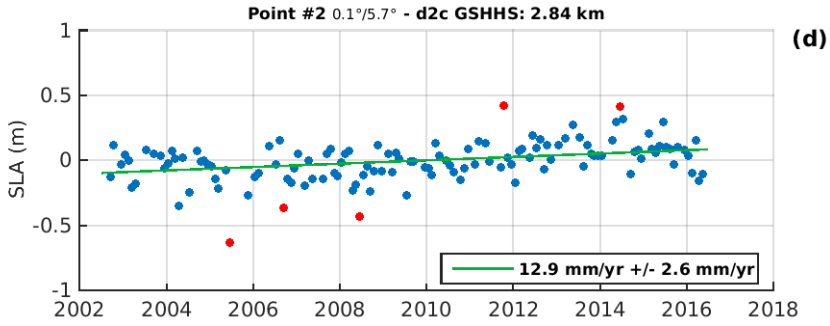

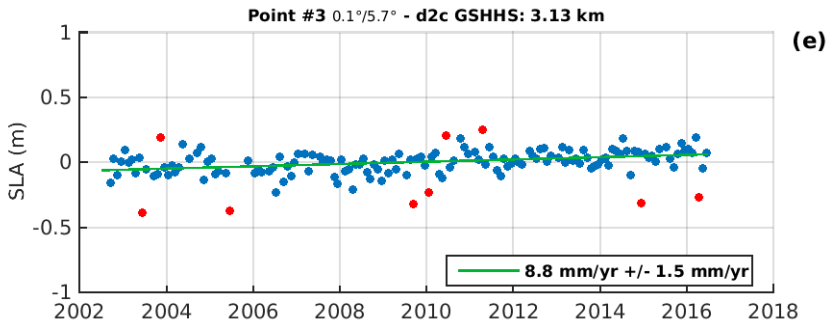

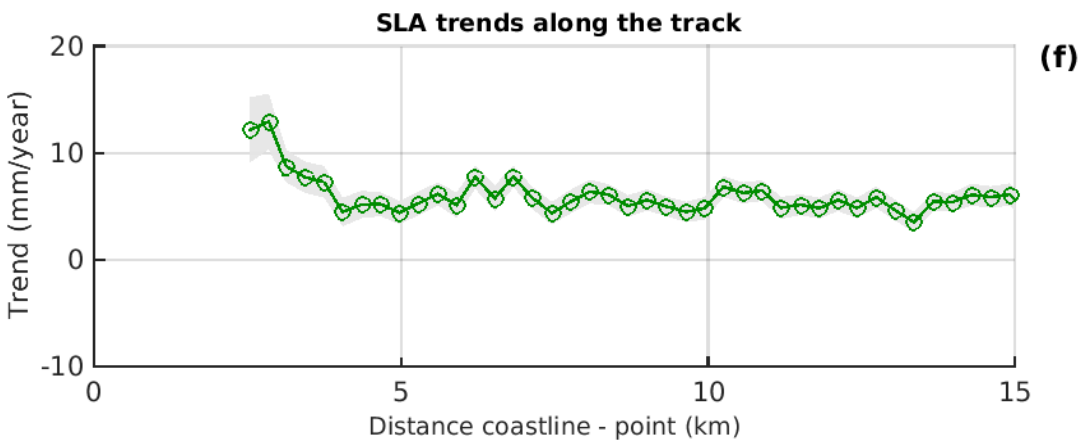

TRACK 224 X-TRACK/ALES 20Hz SLA – J1 + J2 – Jul2002 – Jun2016
(annual and semi-annual cycles removed)

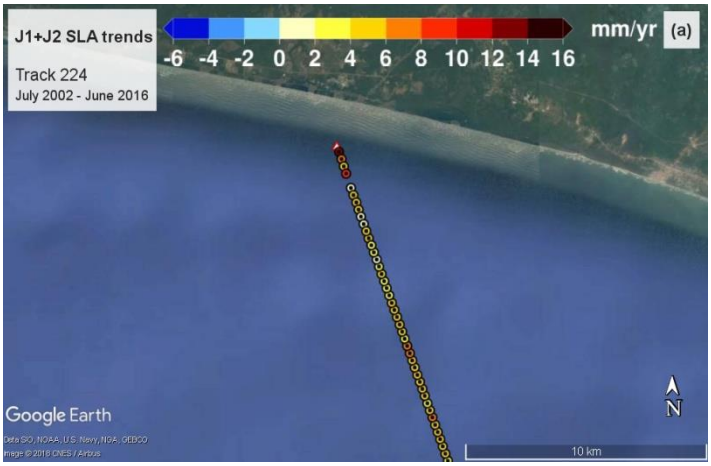

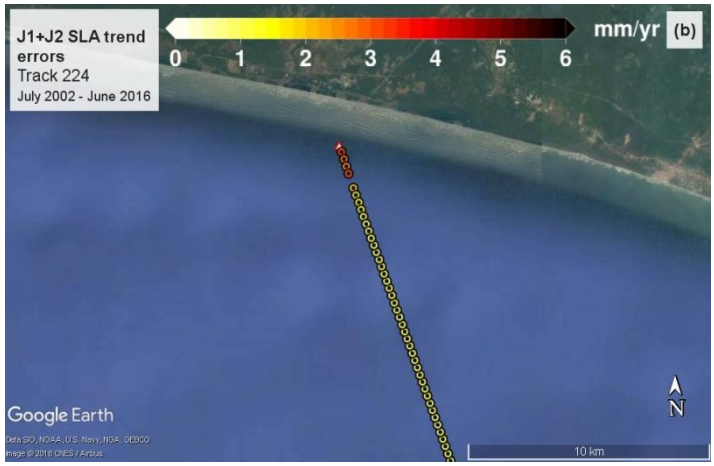

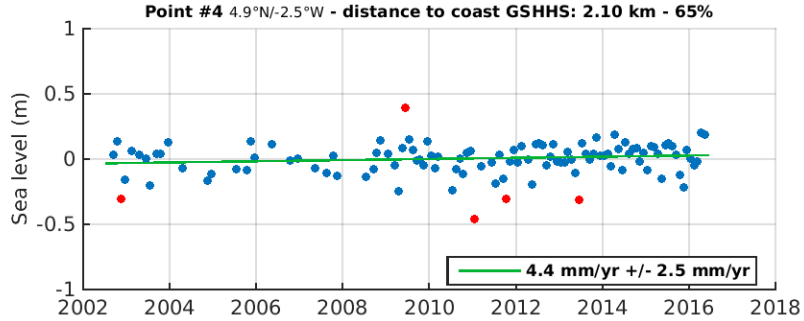

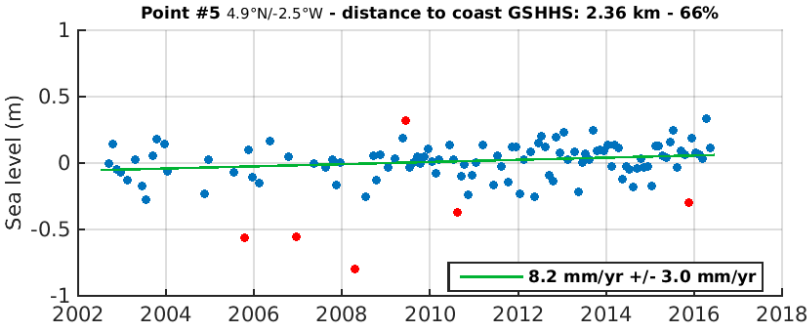

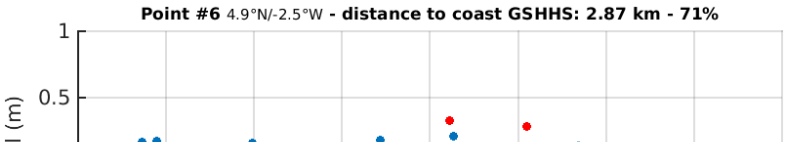

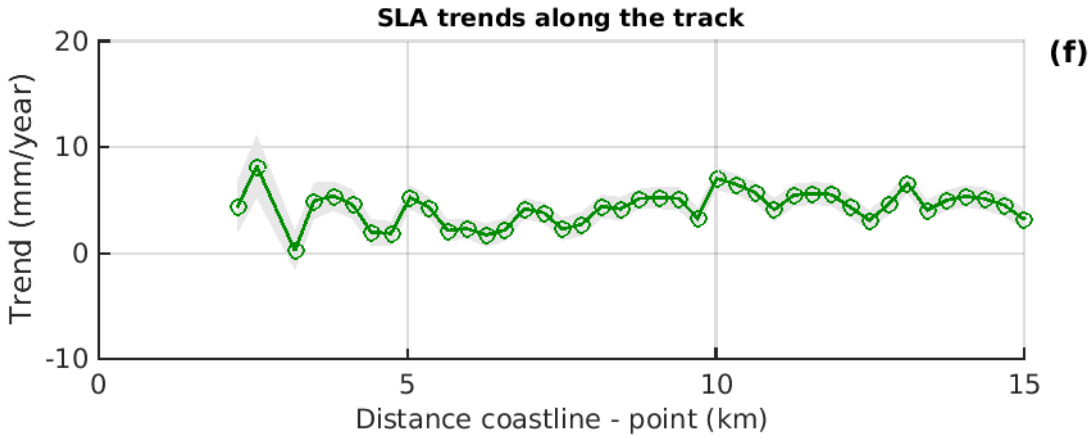

TRACK 148 X-TRACK/ALES 20Hz SLA – J1 + J2 – Jul2002 – Jun2016
(annual and semi-annual cycles removed)

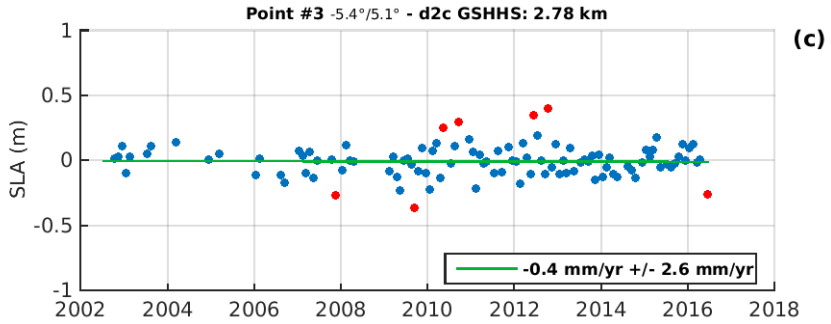

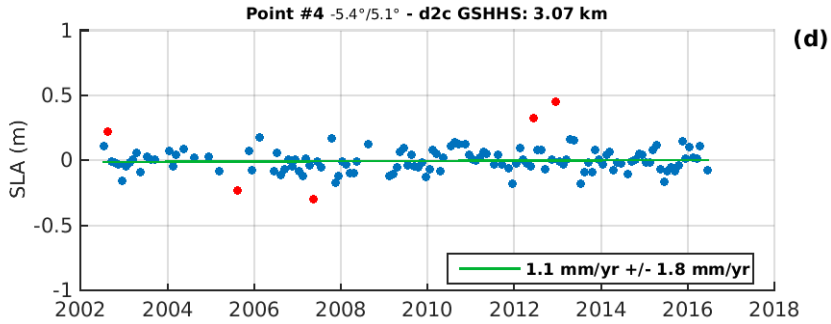

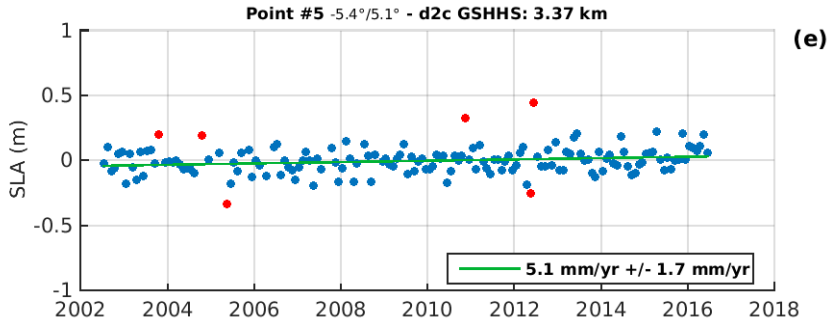

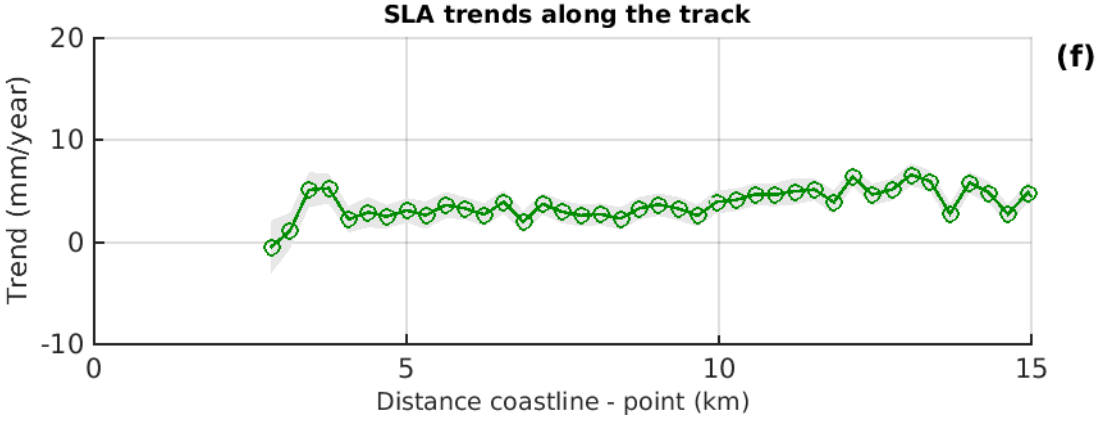

TRACK 072 X-TRACK/ALES 20Hz SLA – J1 + J2 – Jul2002 – Jun2016
(annual and semi-annual cycles removed)

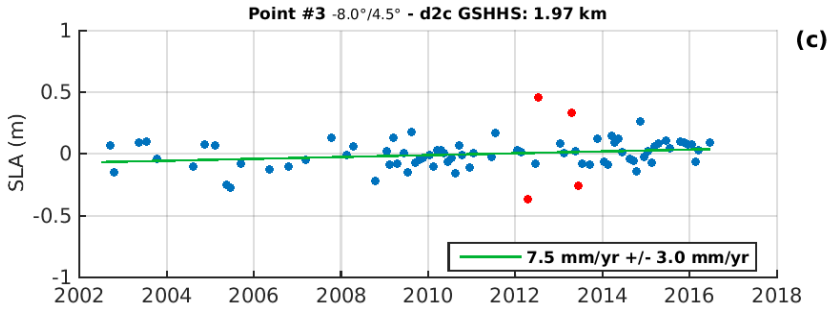

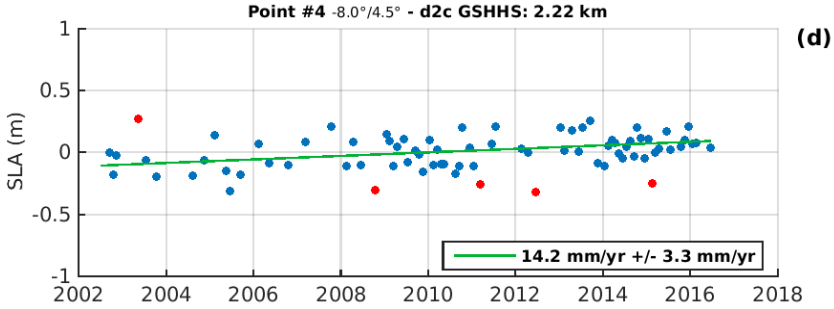

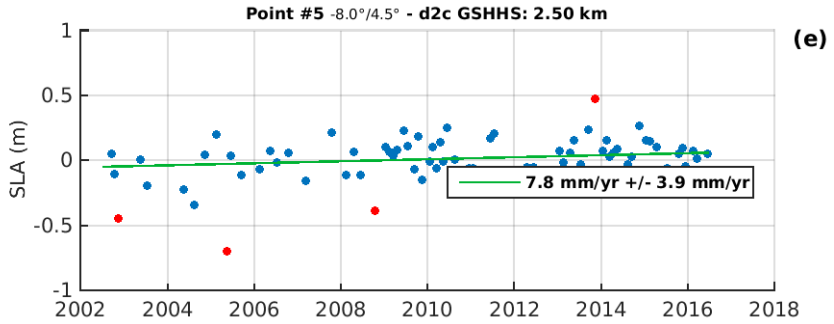

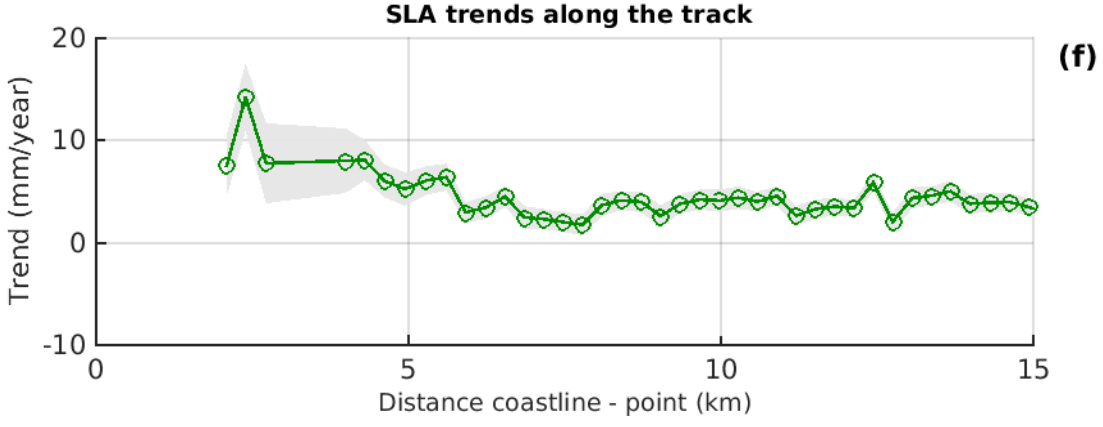

TRACK 250 X-TRACK/ALES 20Hz SLA – J1 + J2 – Jul2002 – Jun2016
(annual and semi-annual cycles removed)

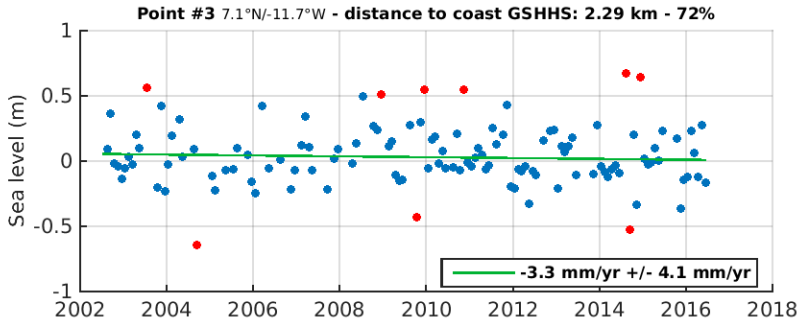

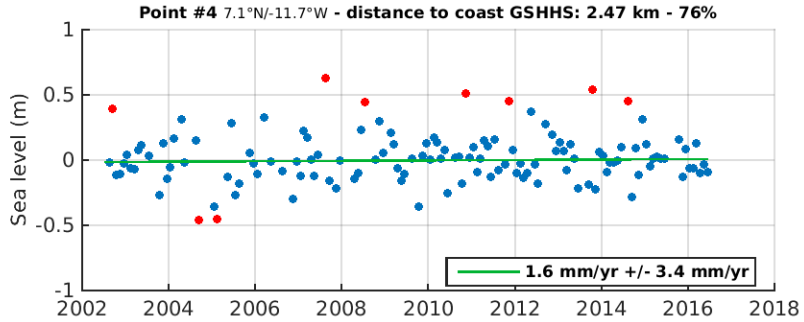

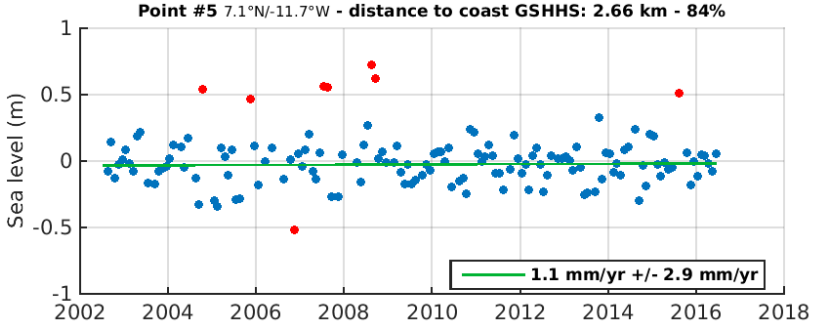

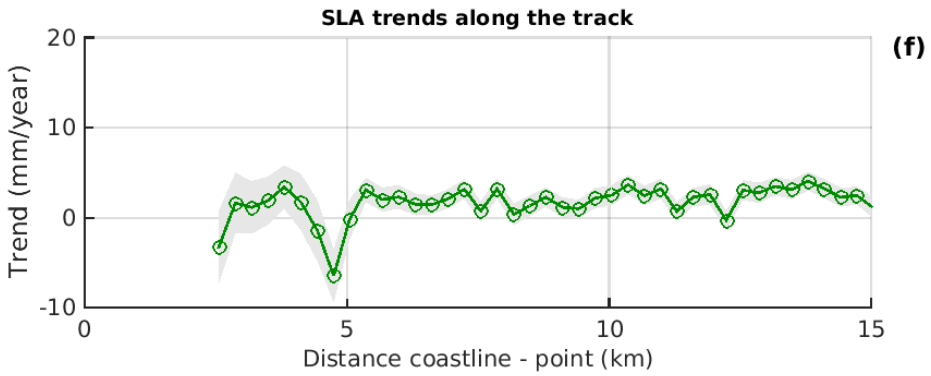

TRACK 174 X-TRACK/ALES 20Hz SLA – J1 + J2 – Jul2002 – Jun2016
(annual and semi-annual cycles removed)

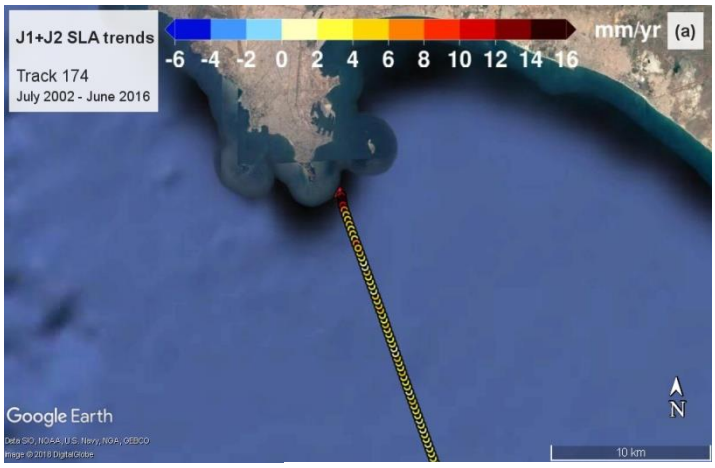

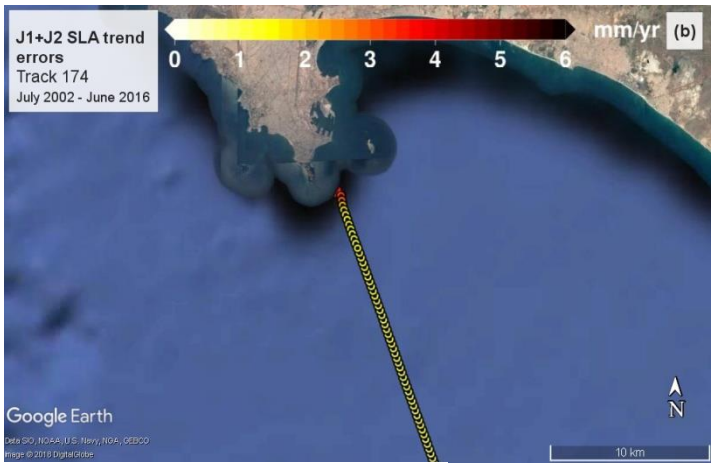

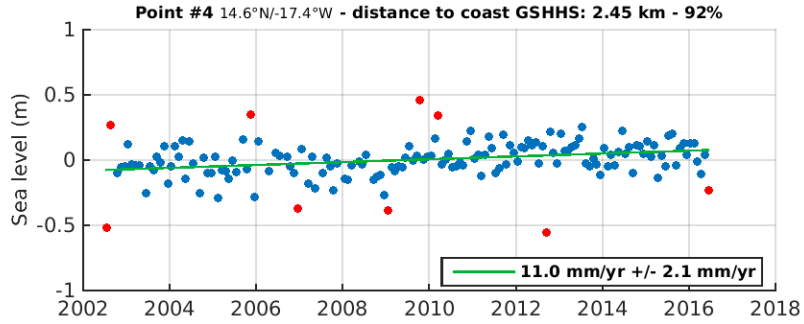

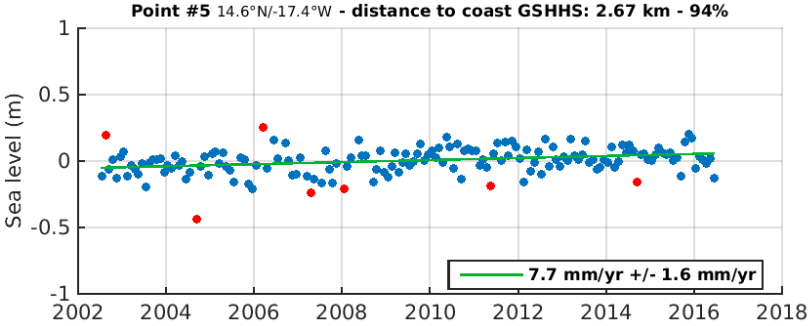

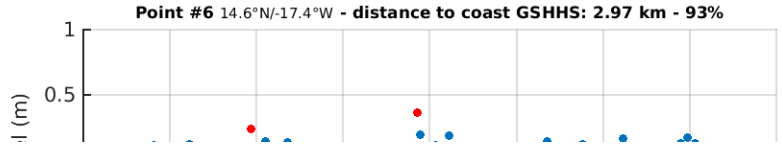

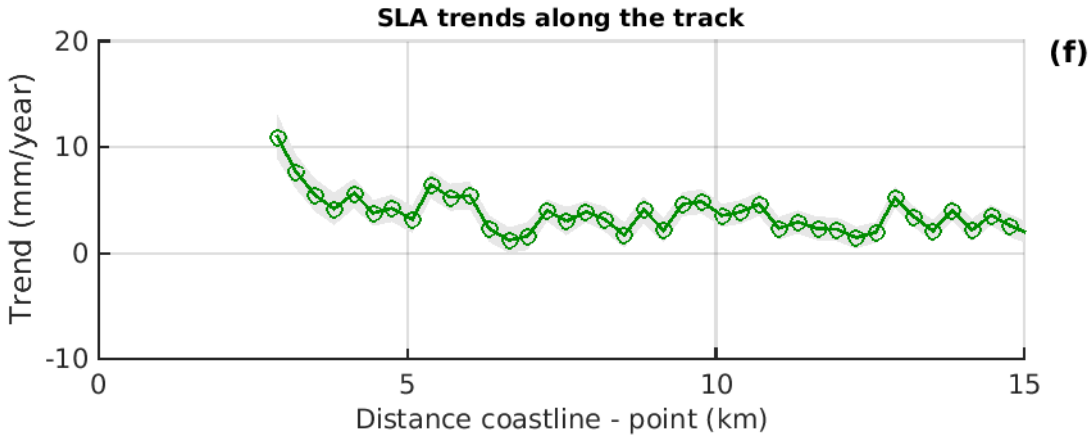

TRACK 174 #2 X-TRACK/ALES 20Hz SLA – J1 + J2 – Jul2002 – Jun2016
(annual and semi-annual cycles removed)

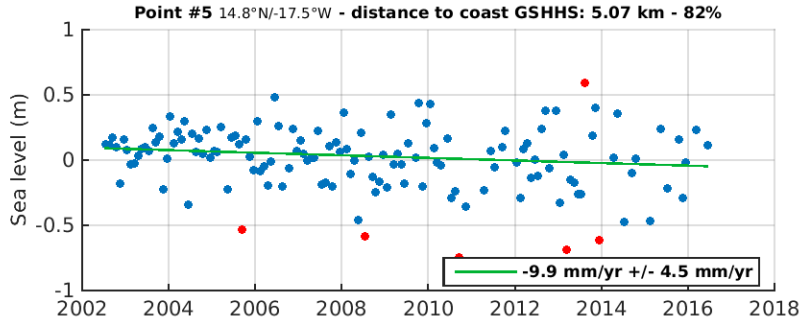

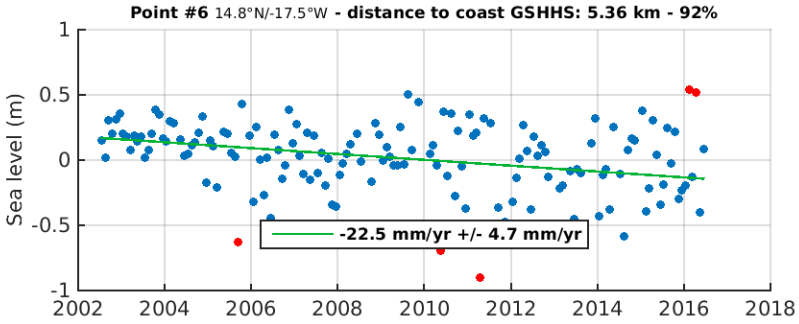

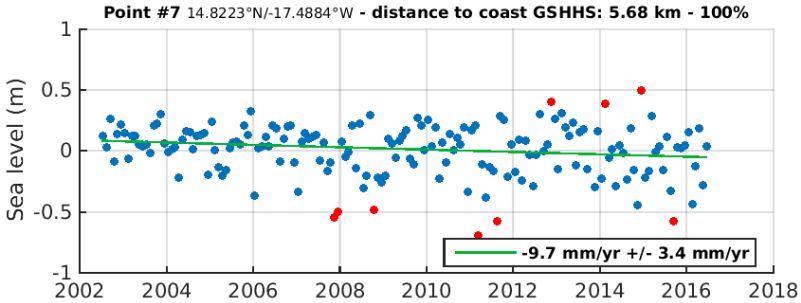

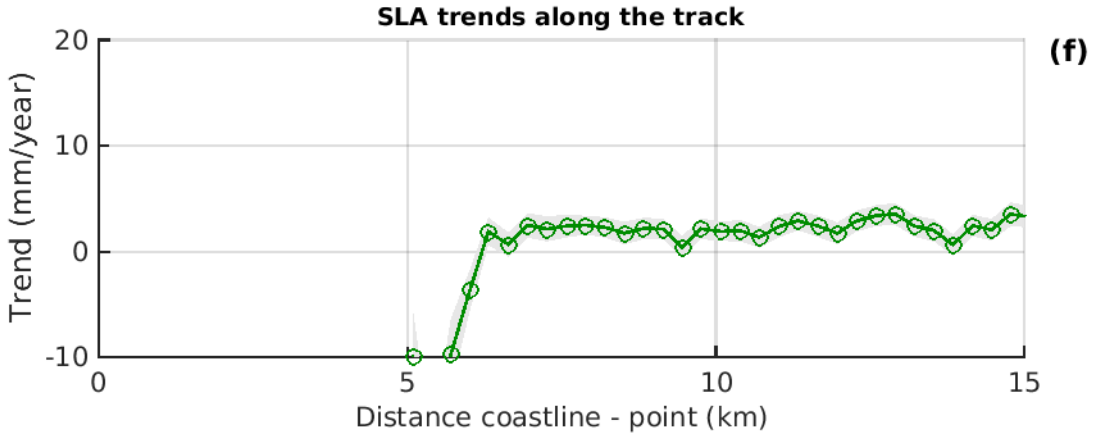

Annex C

Figure 14

WESTERN AFRICA: ASCENDING TRACKS – Ranked from west to east

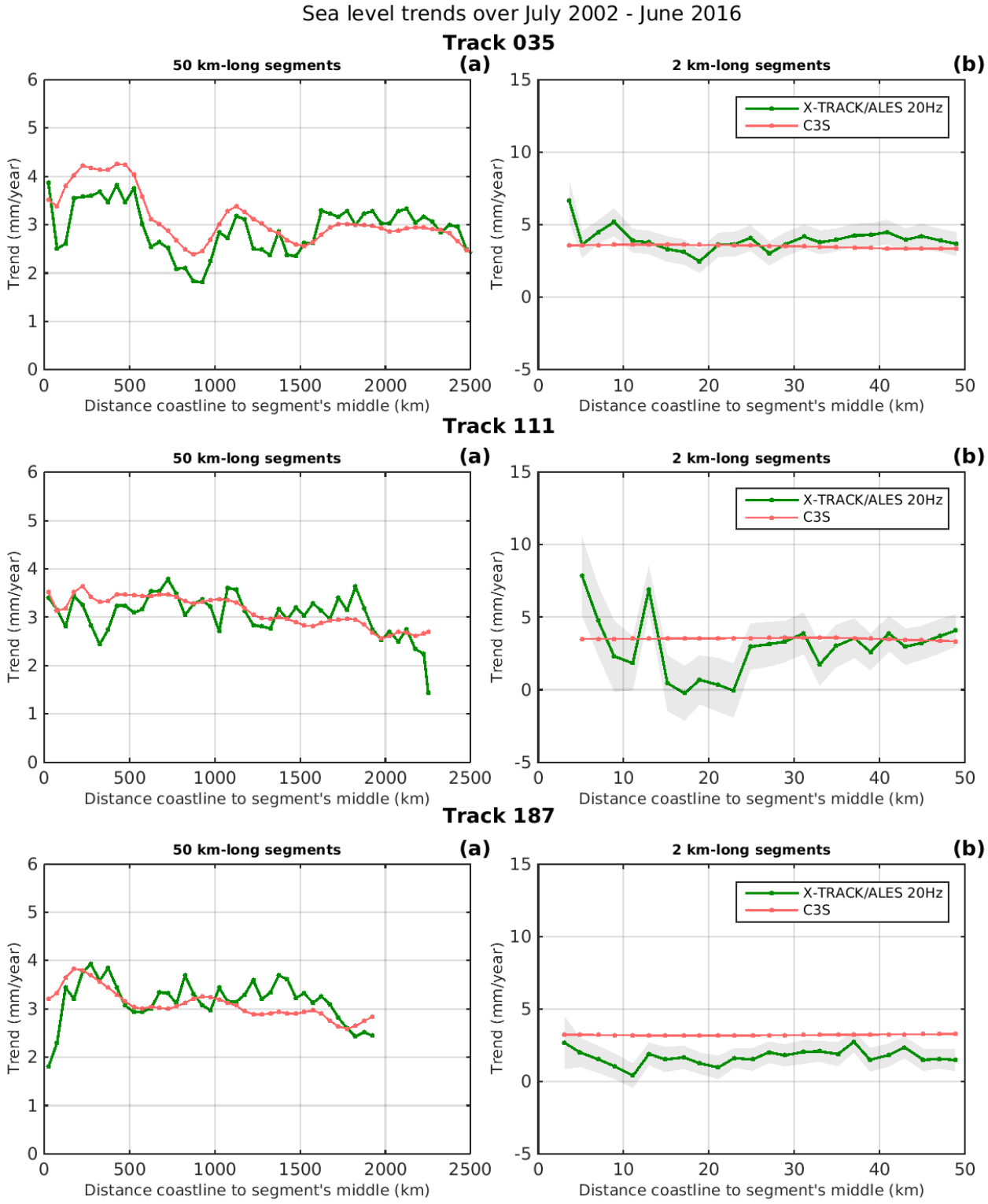

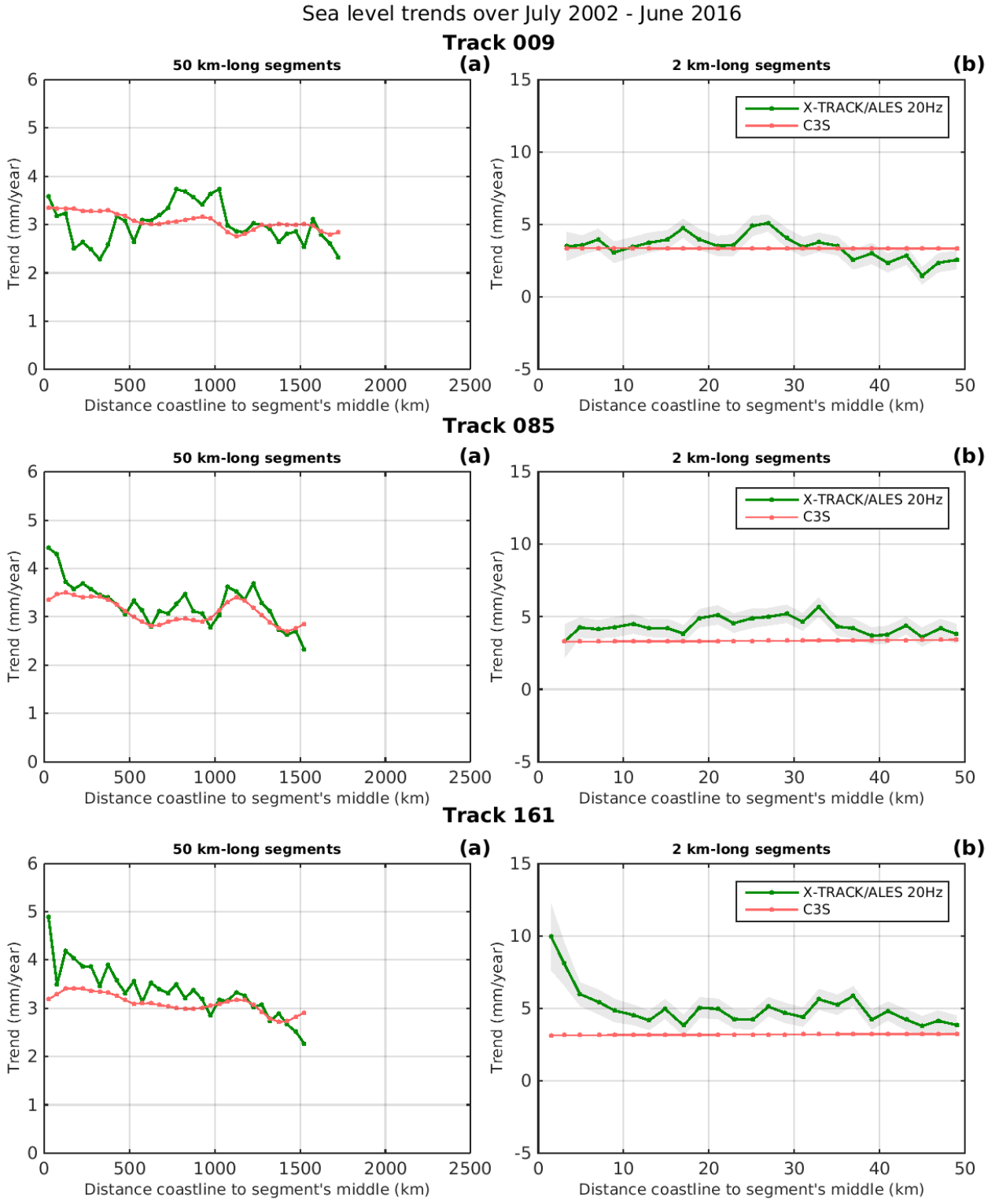

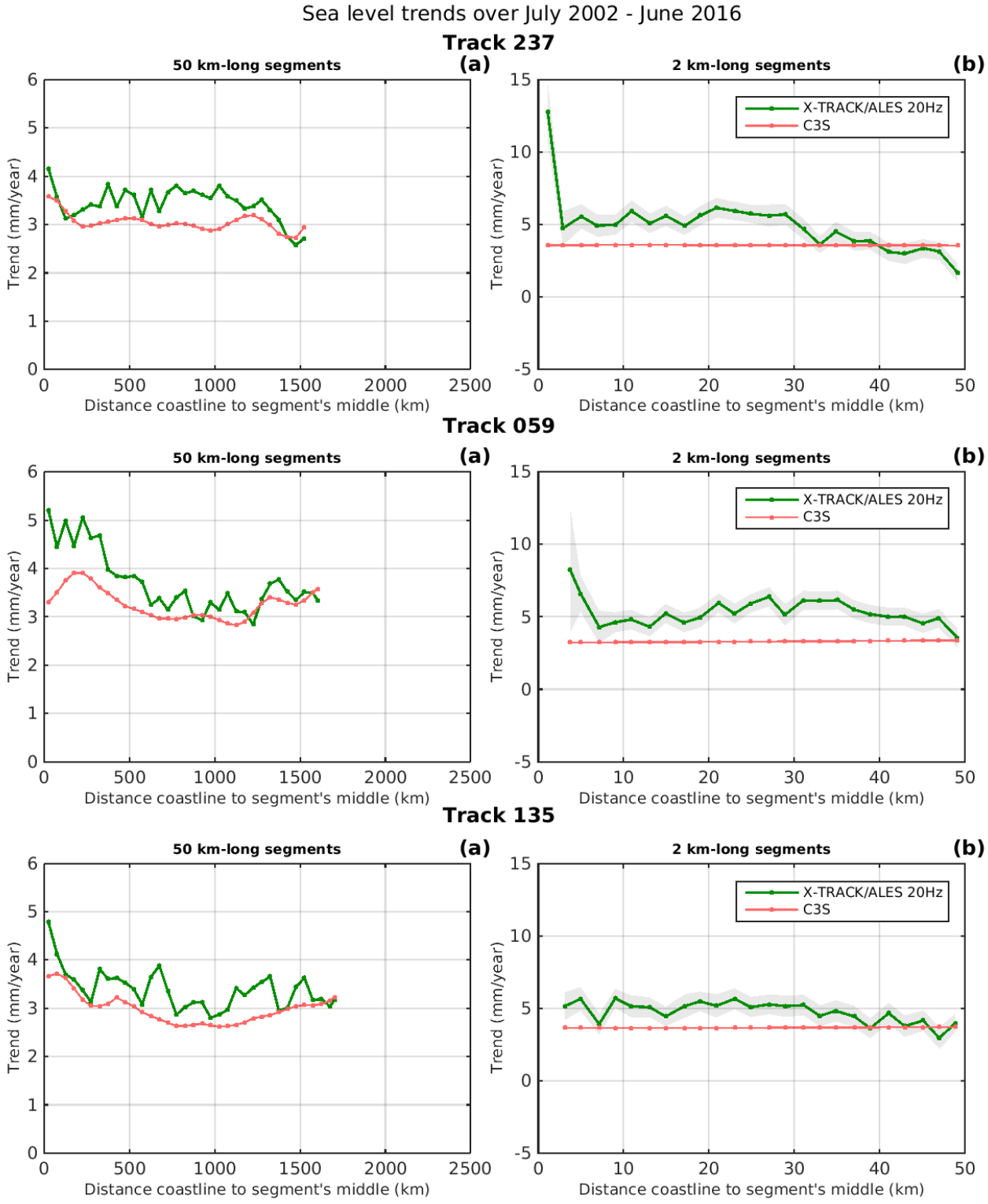

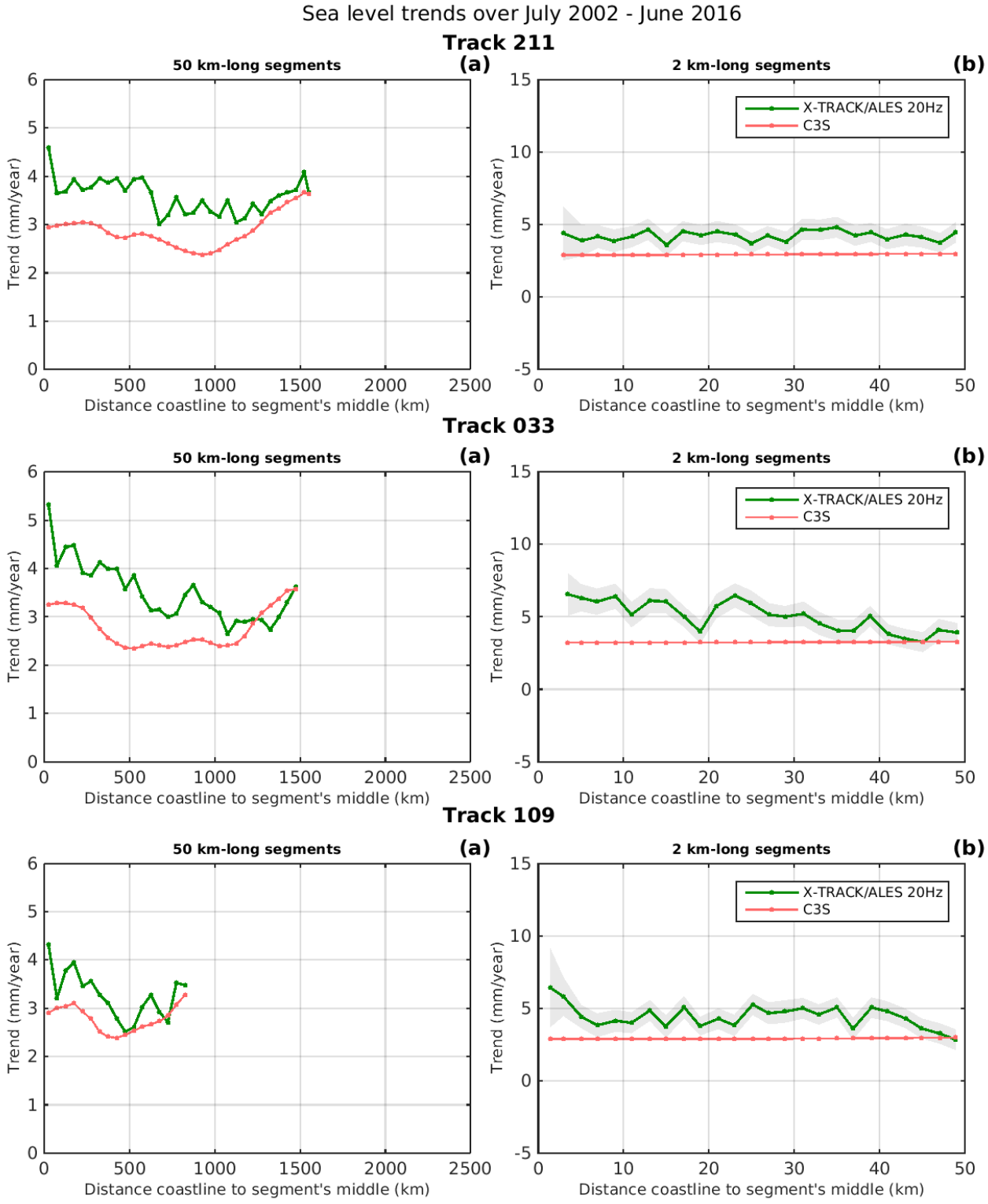

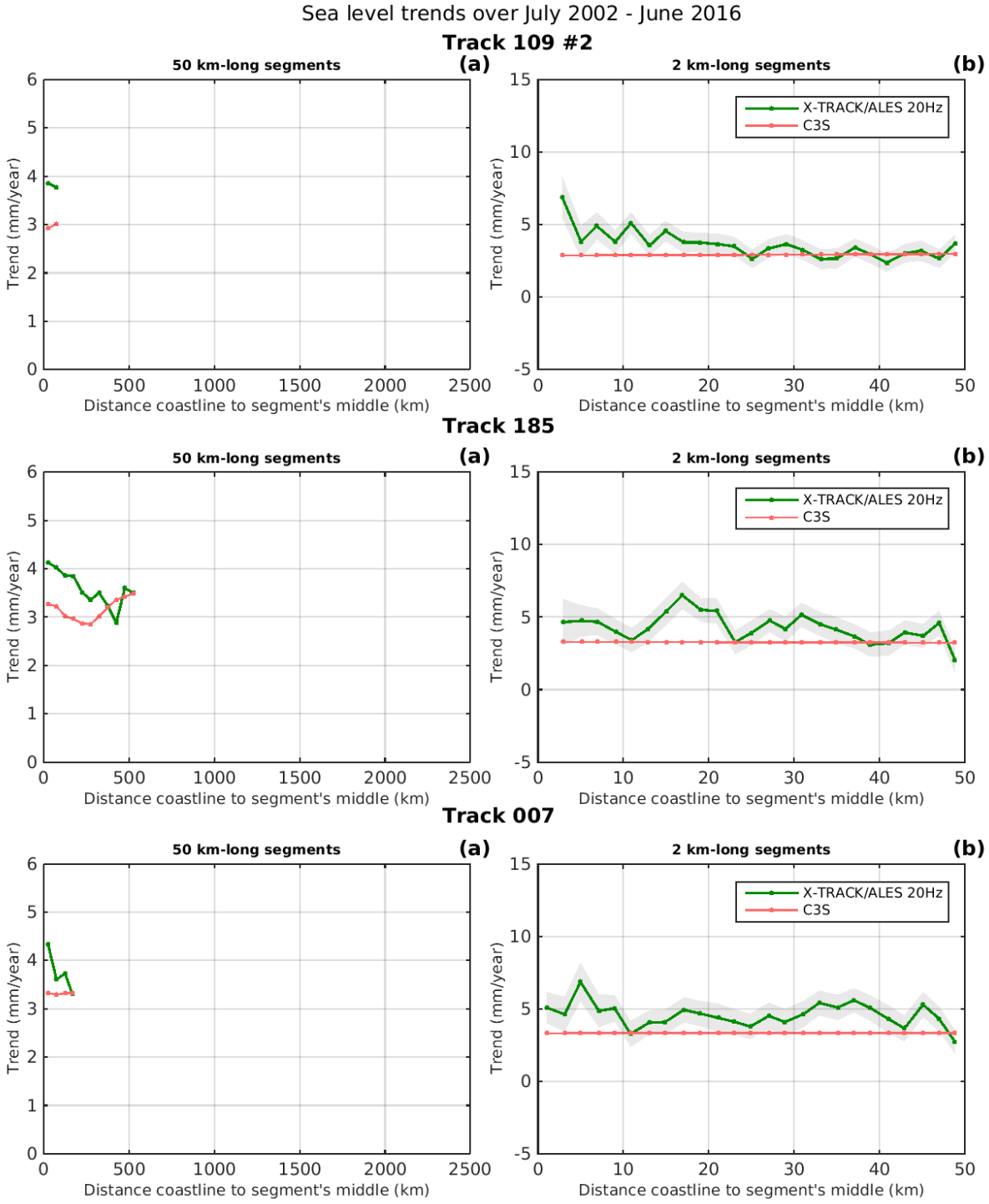

WESTERN AFRICA: DESCENDING TRACKS – Ranked from east to west

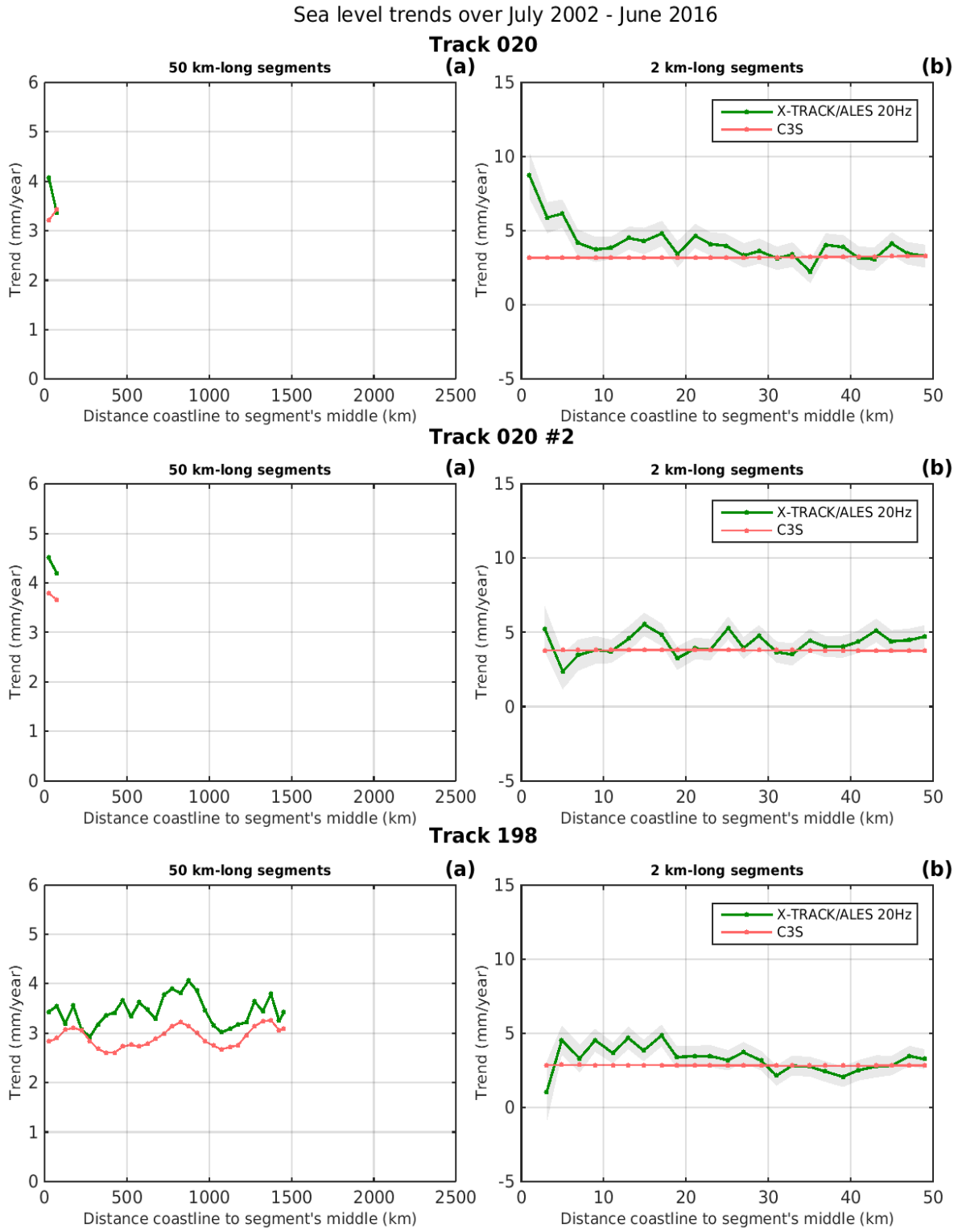

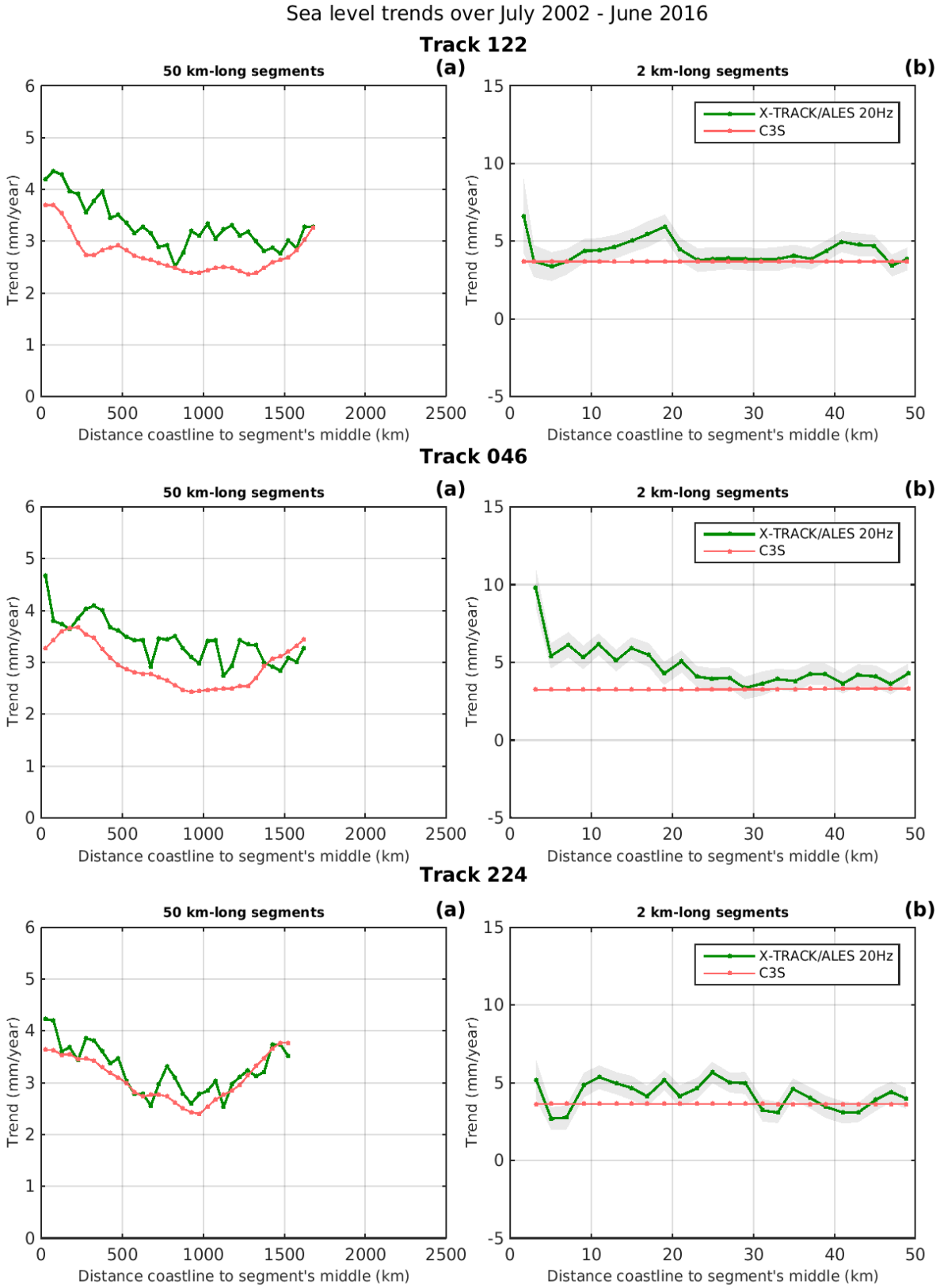

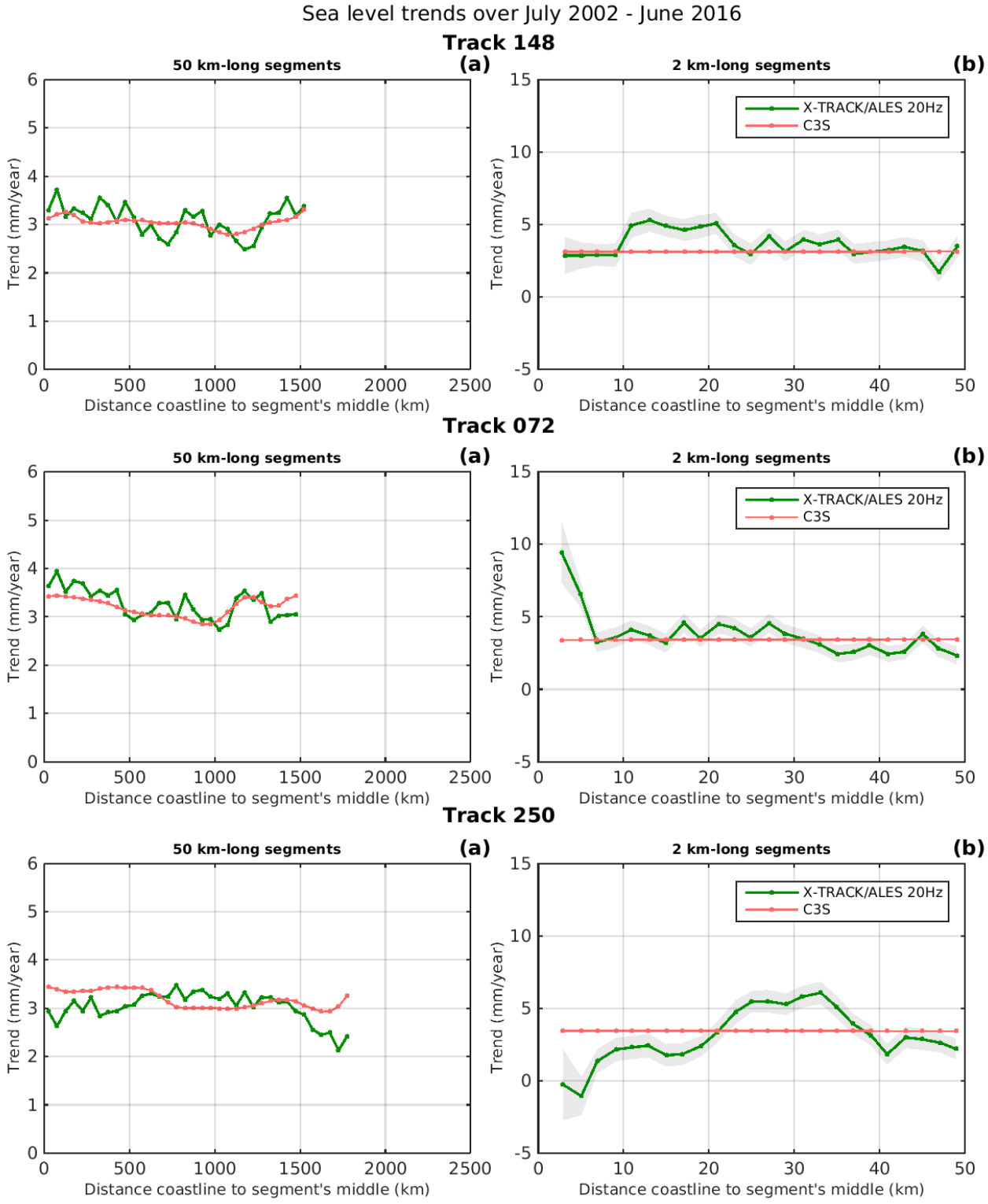

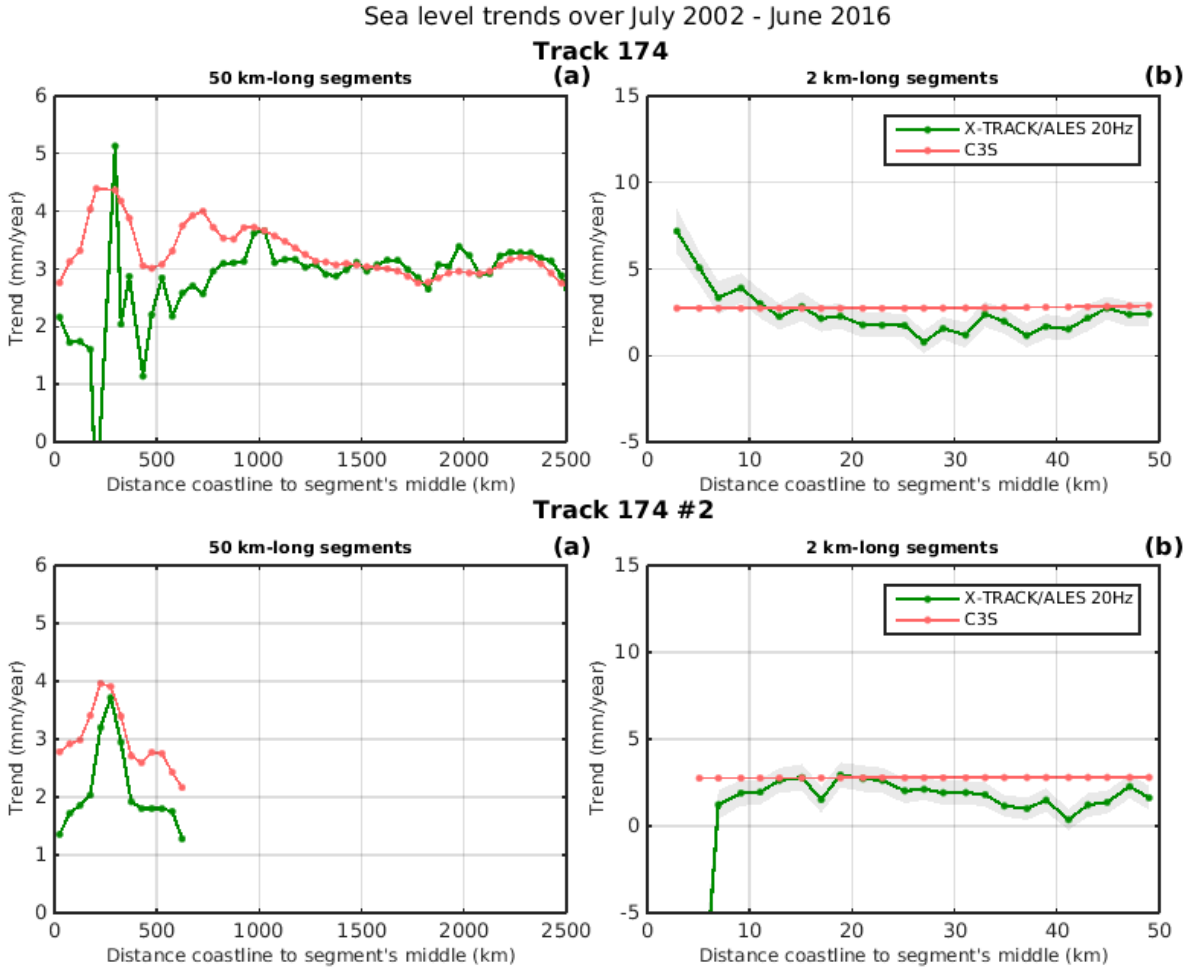

NORTHERN EUROPE

Annexes D and E

Annex D

Figure 17

NORTHERN EUROPE

ASCENDING TRACKS

Ranked from west to east

TRACK 239 “#1”

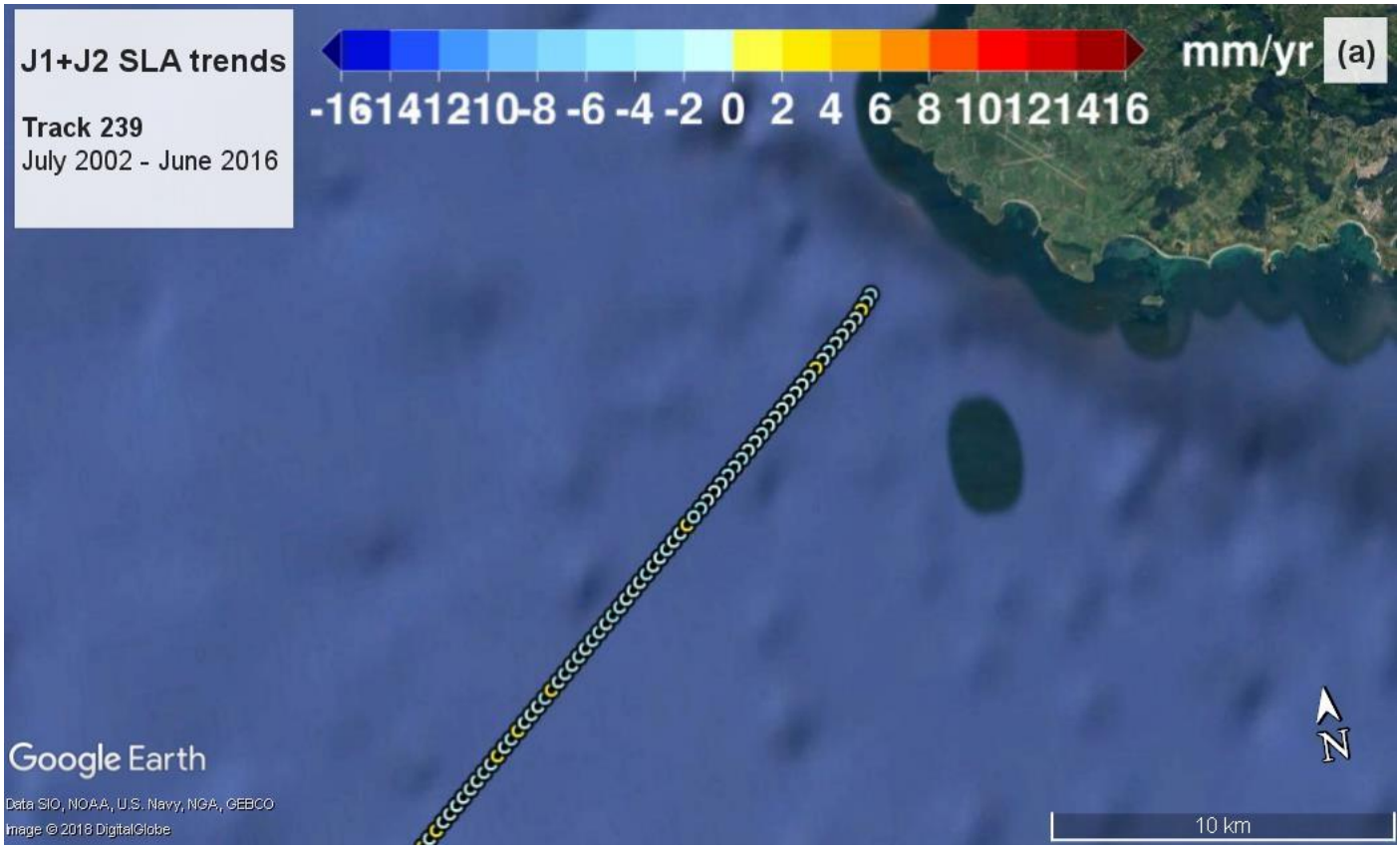

TRACK 239 “#2”

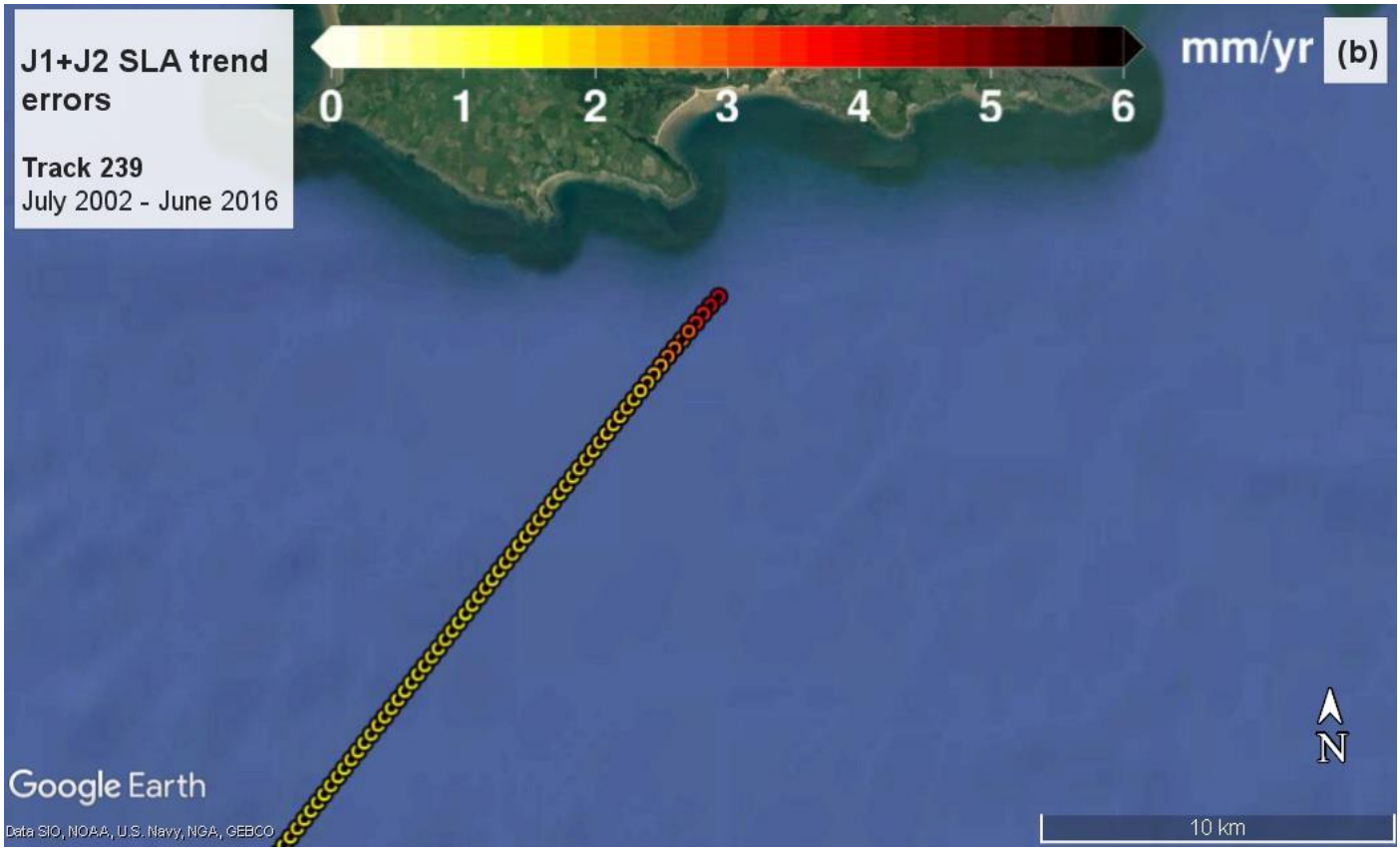

TRACK 061

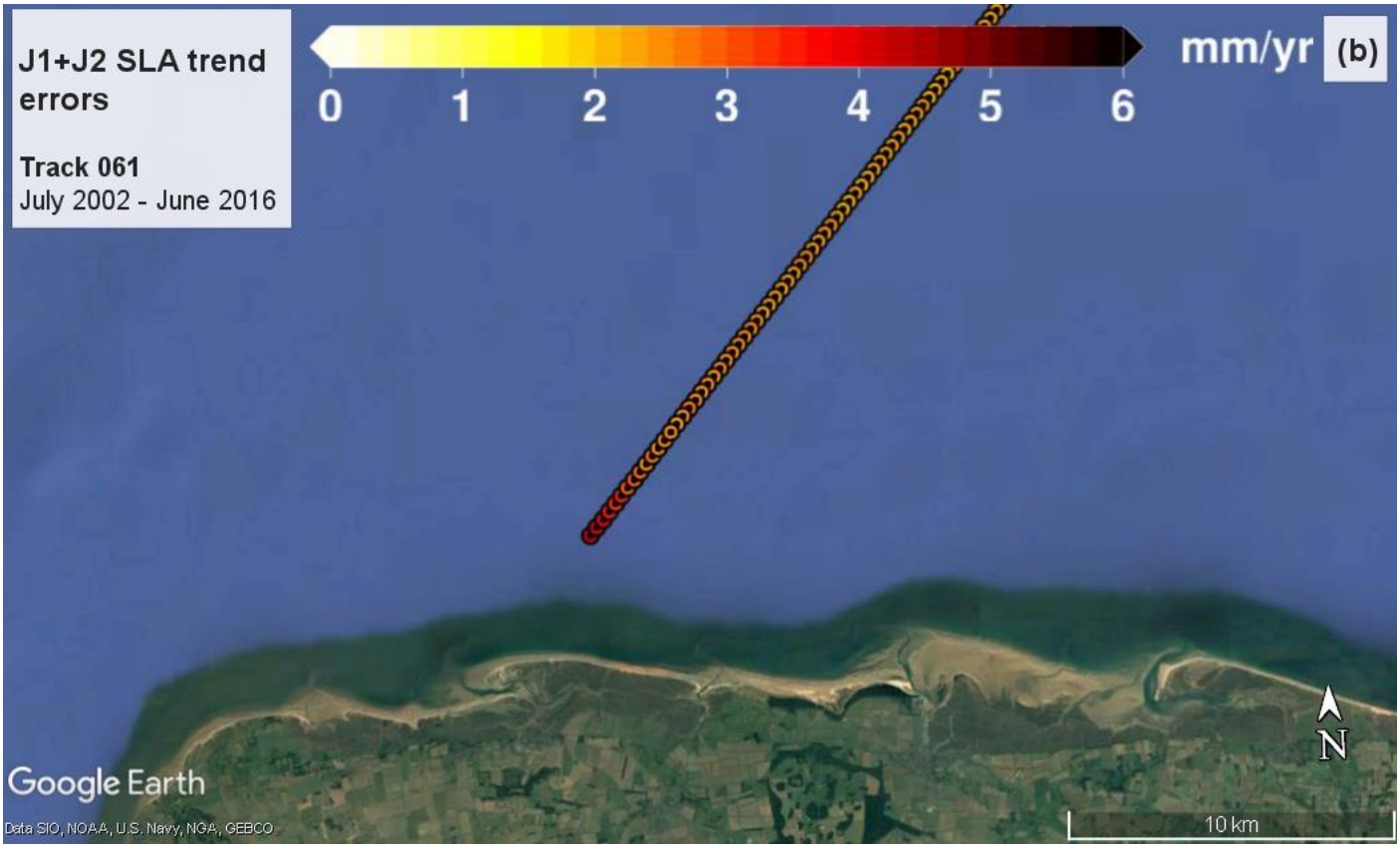

TRACK 137 “#1”

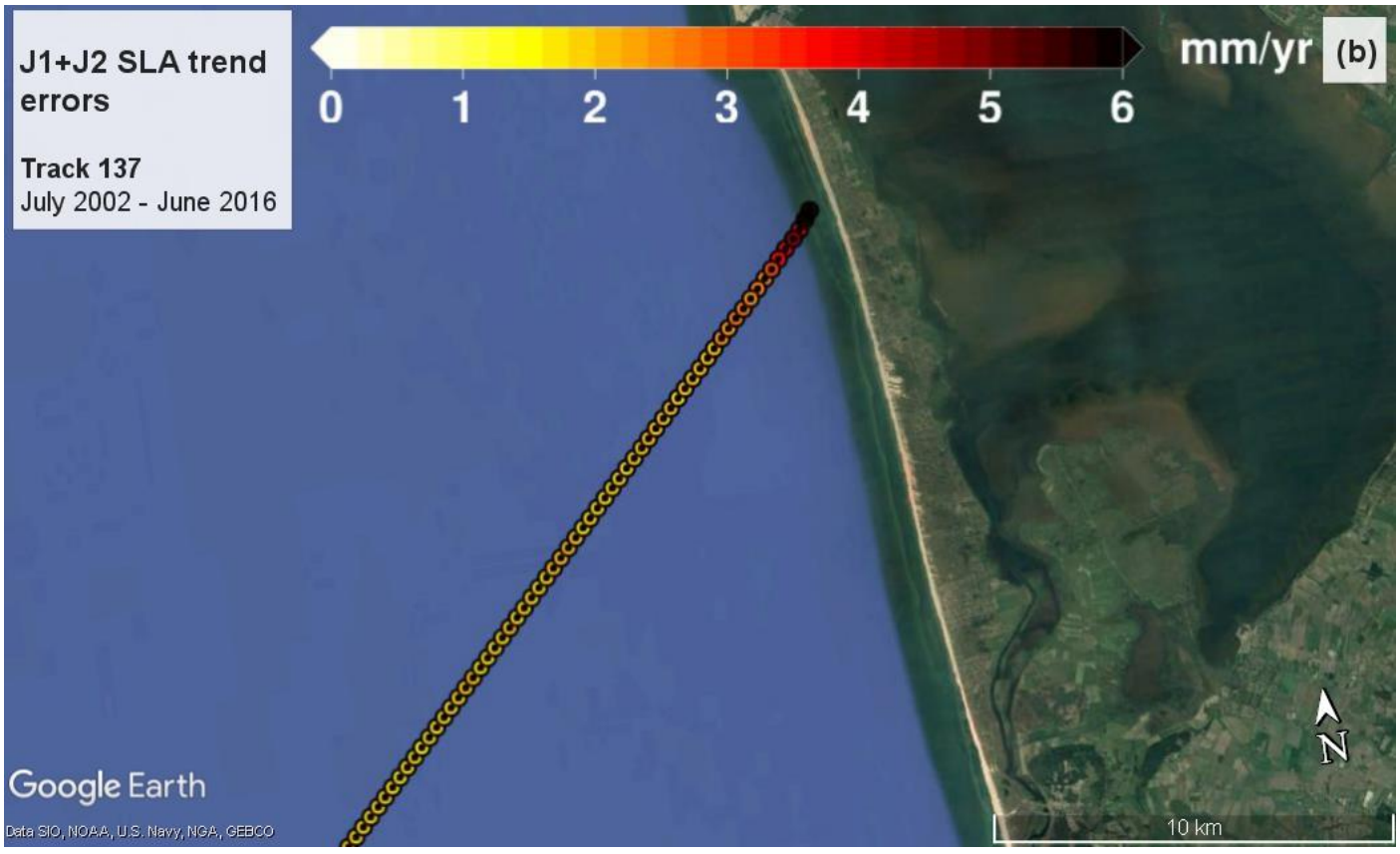

TRACK 137 “#2”

TRACK 213 “#1”

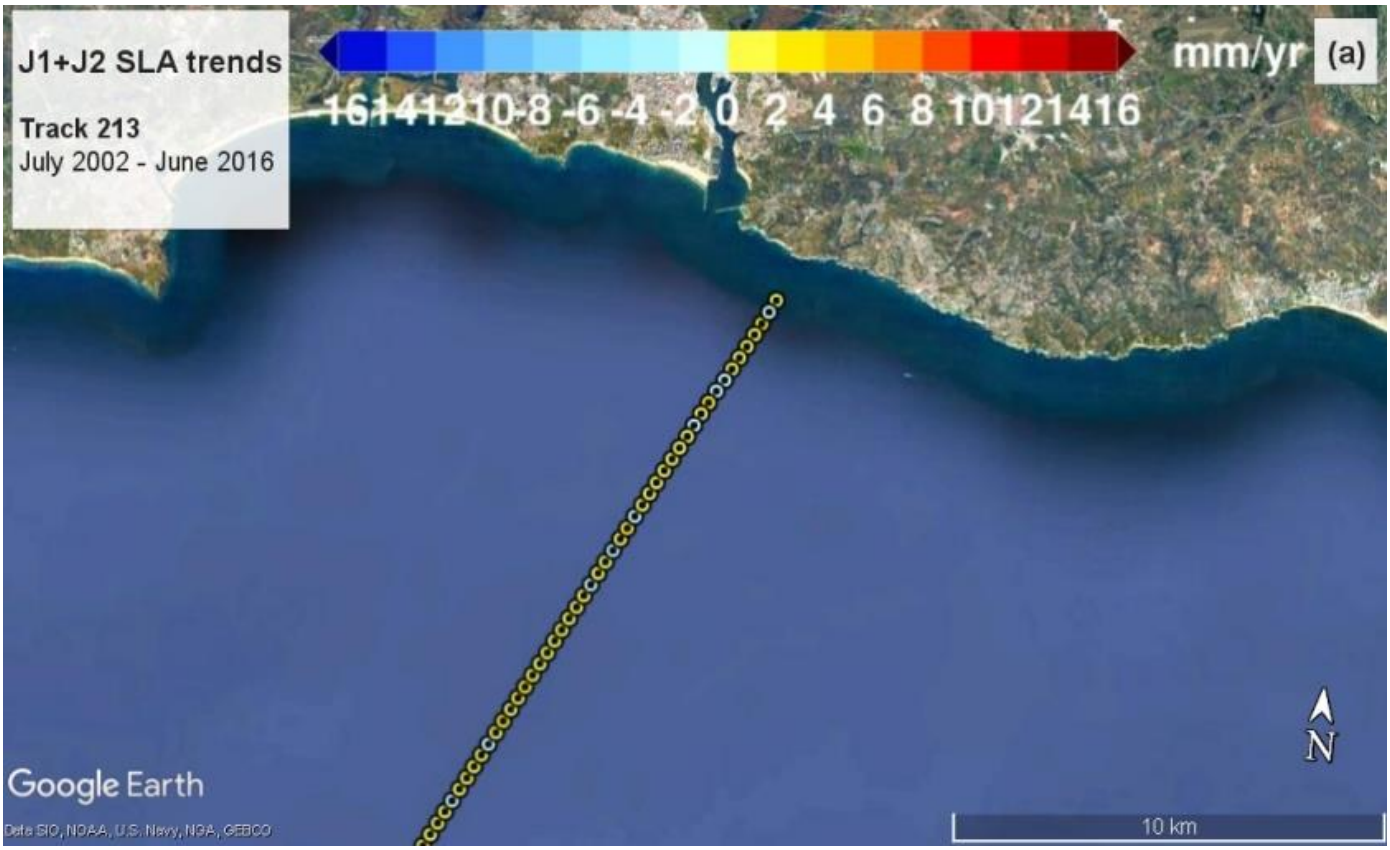

TRACK 213 “#2”

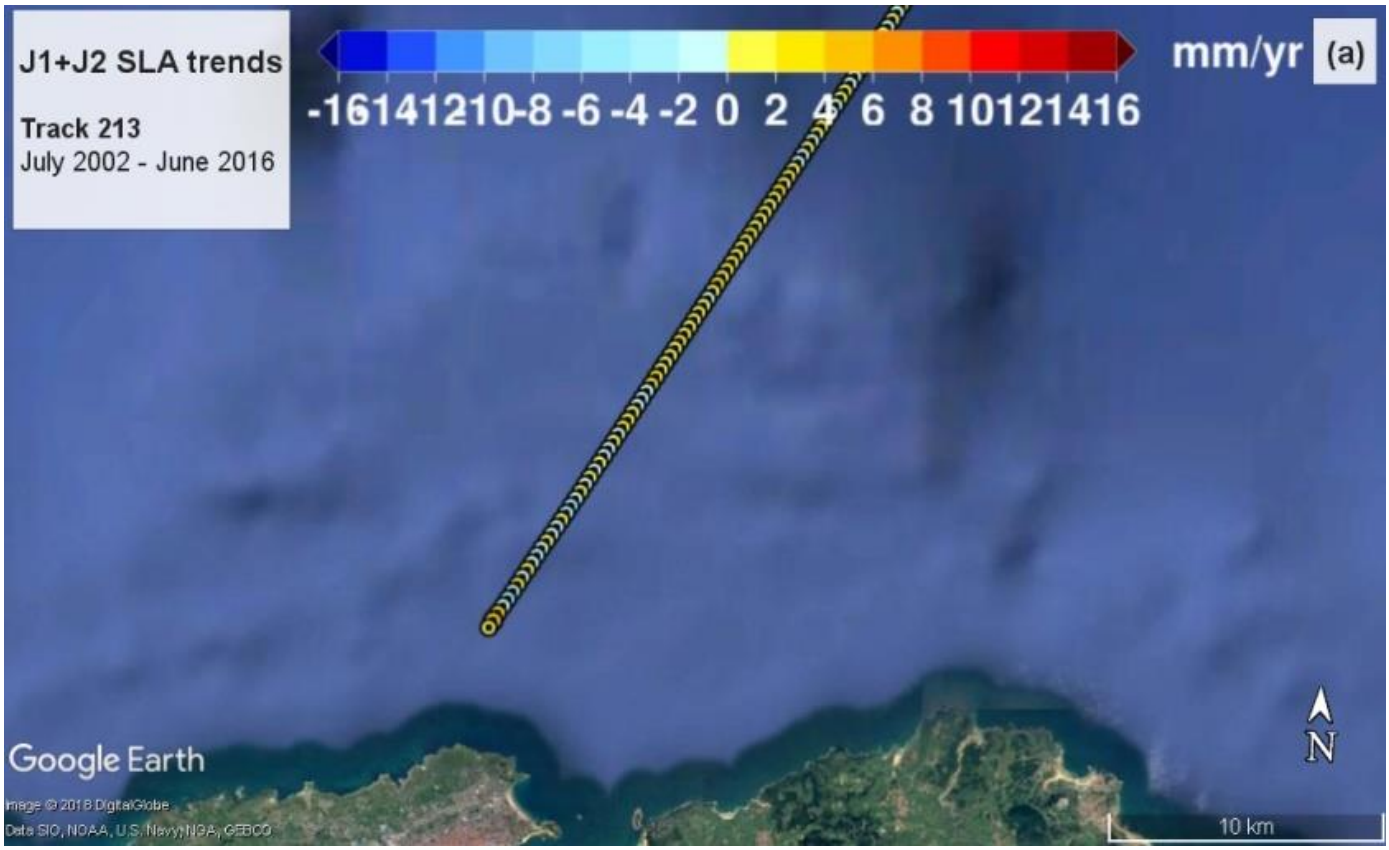

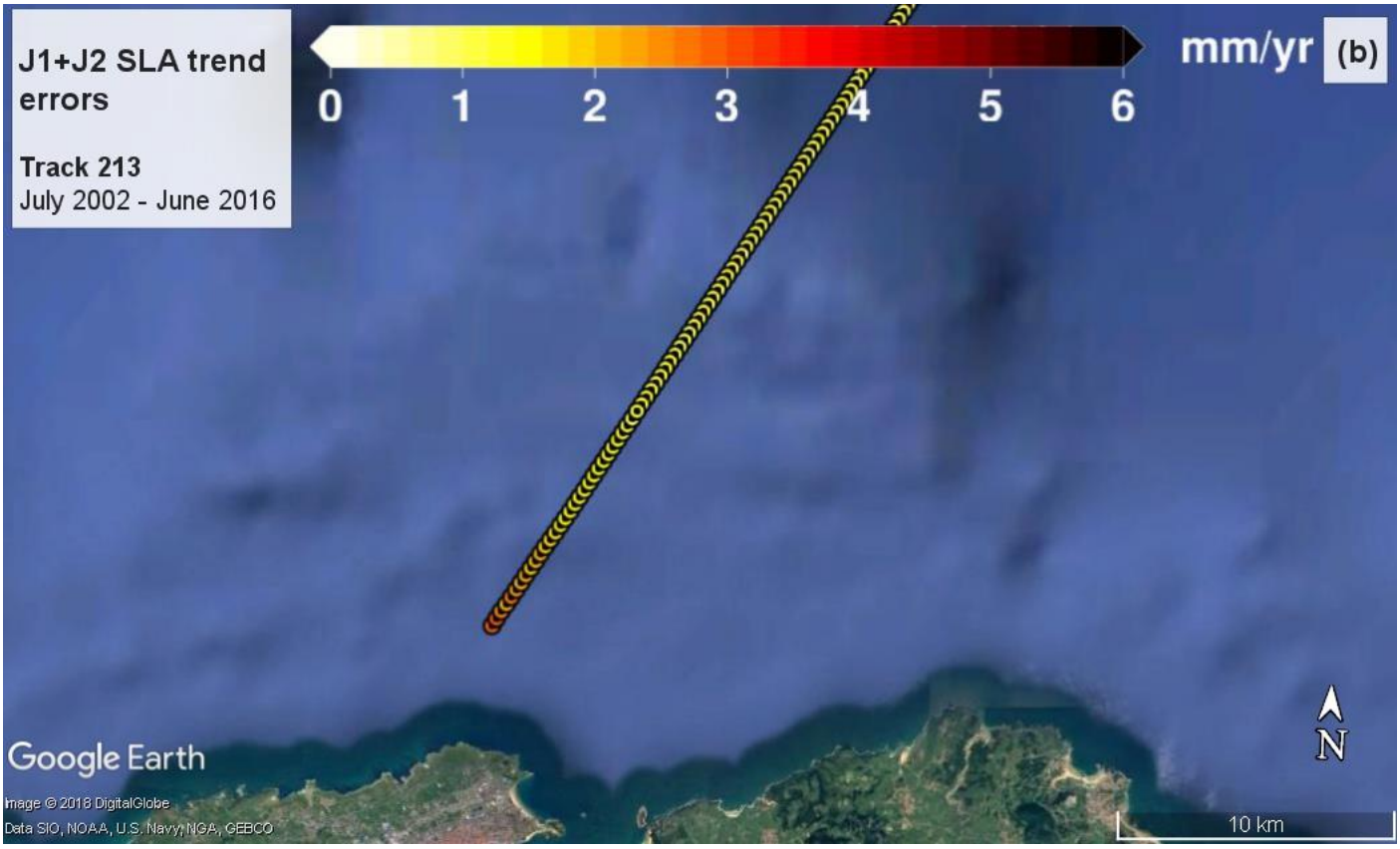

TRACK 035

NORTHERN EUROPE

DESCENDING TRACKS

Ranked from east to west

TRACK 120

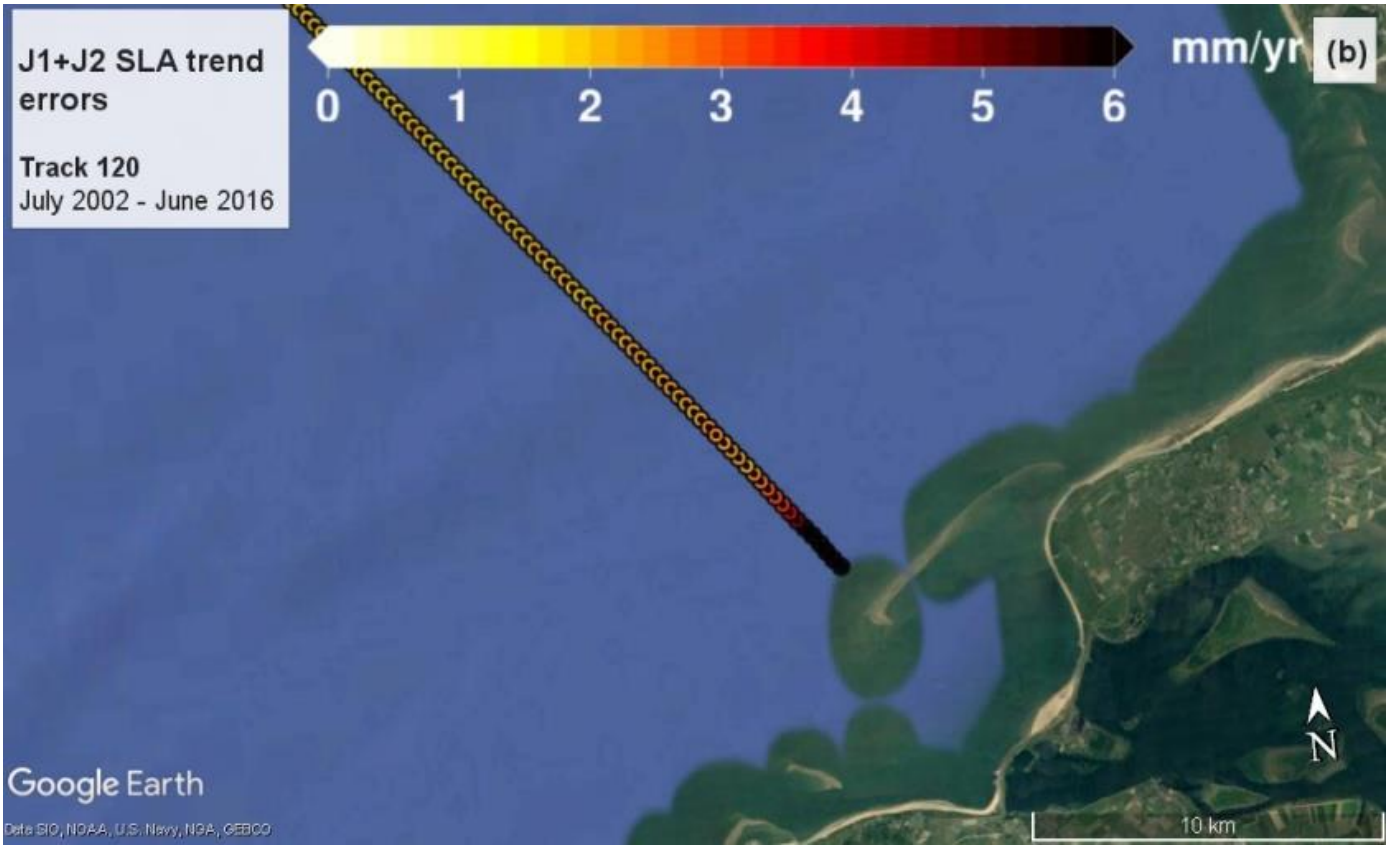

TRACK 248

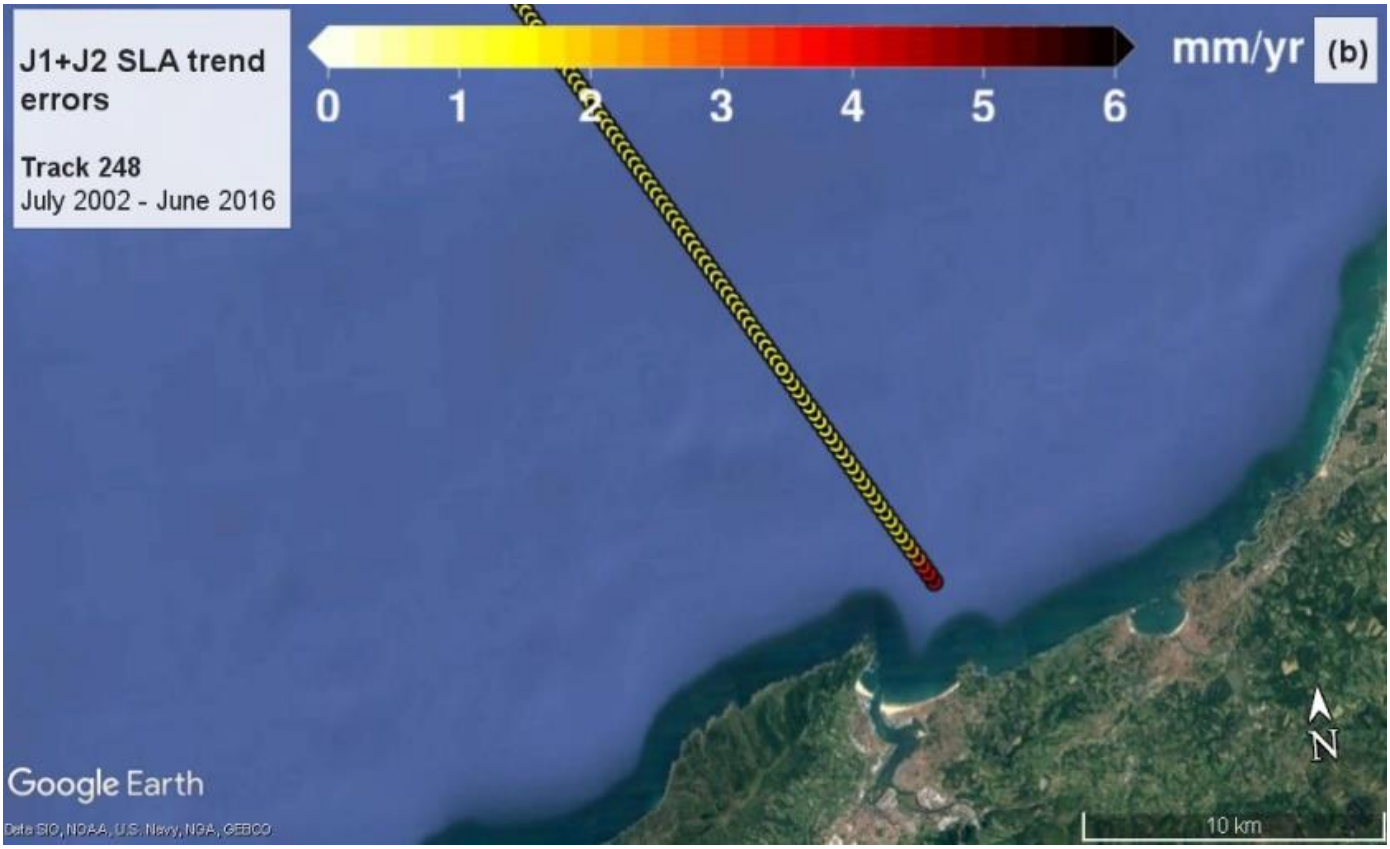

TRACK 172

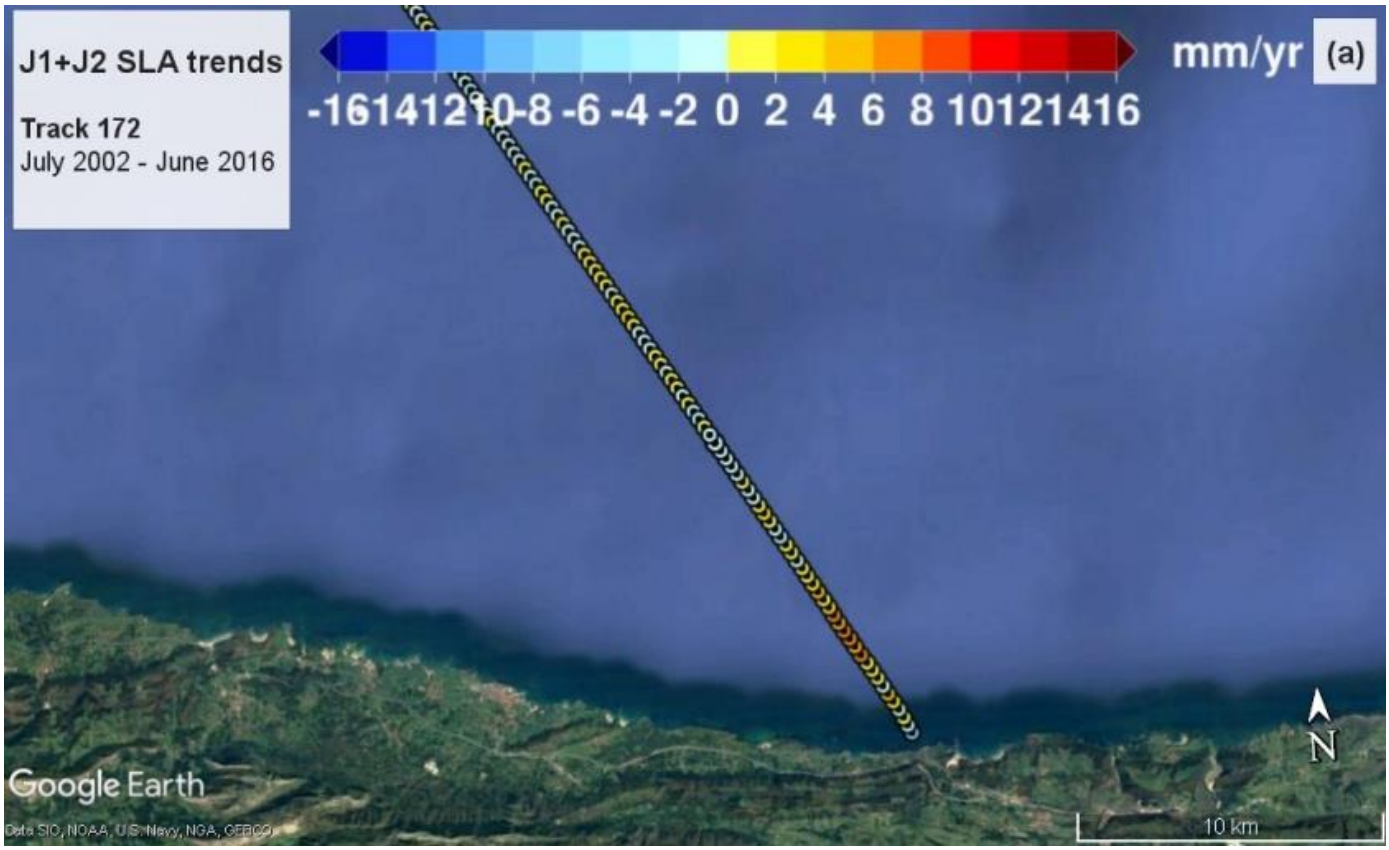

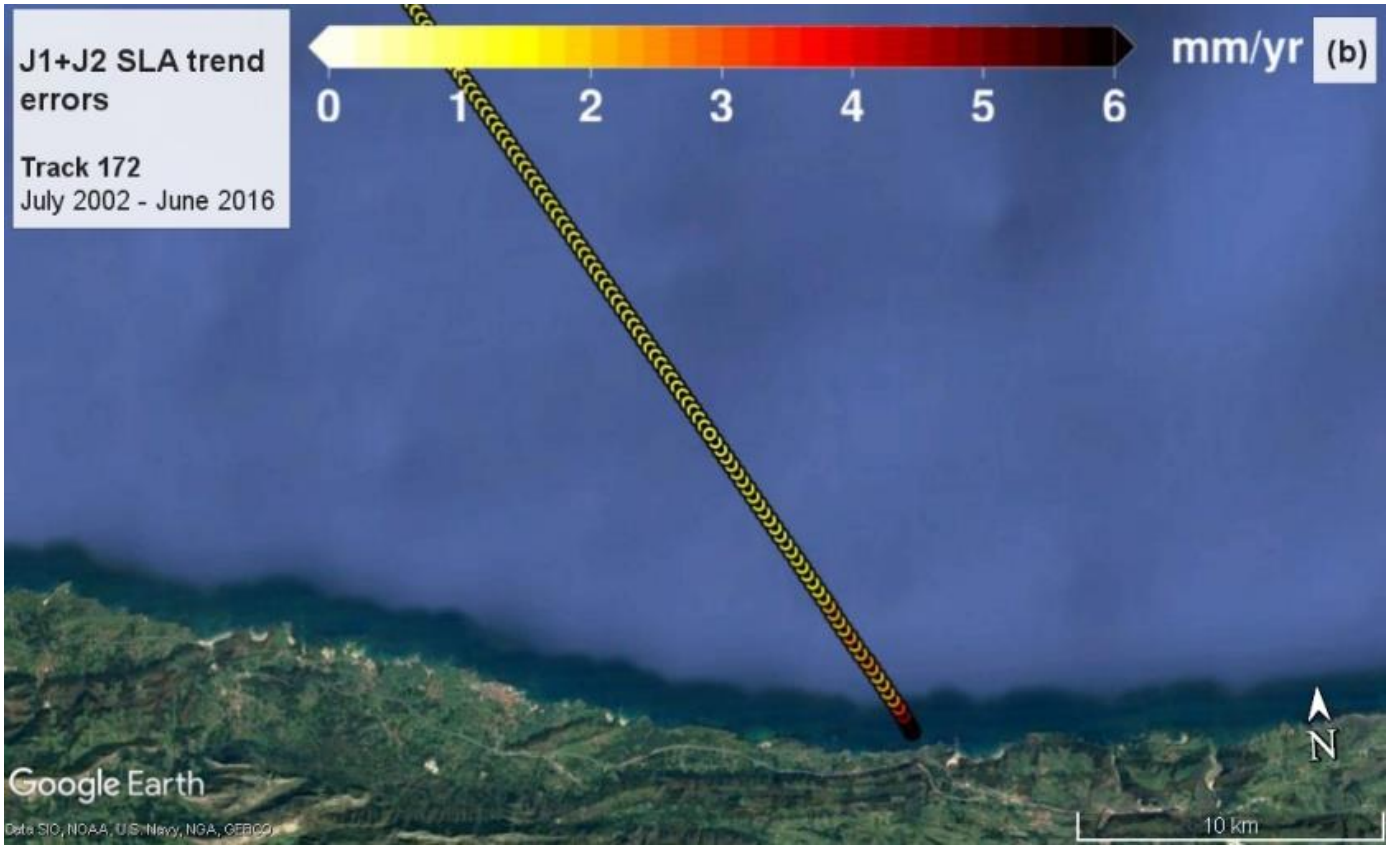

TRACK 096

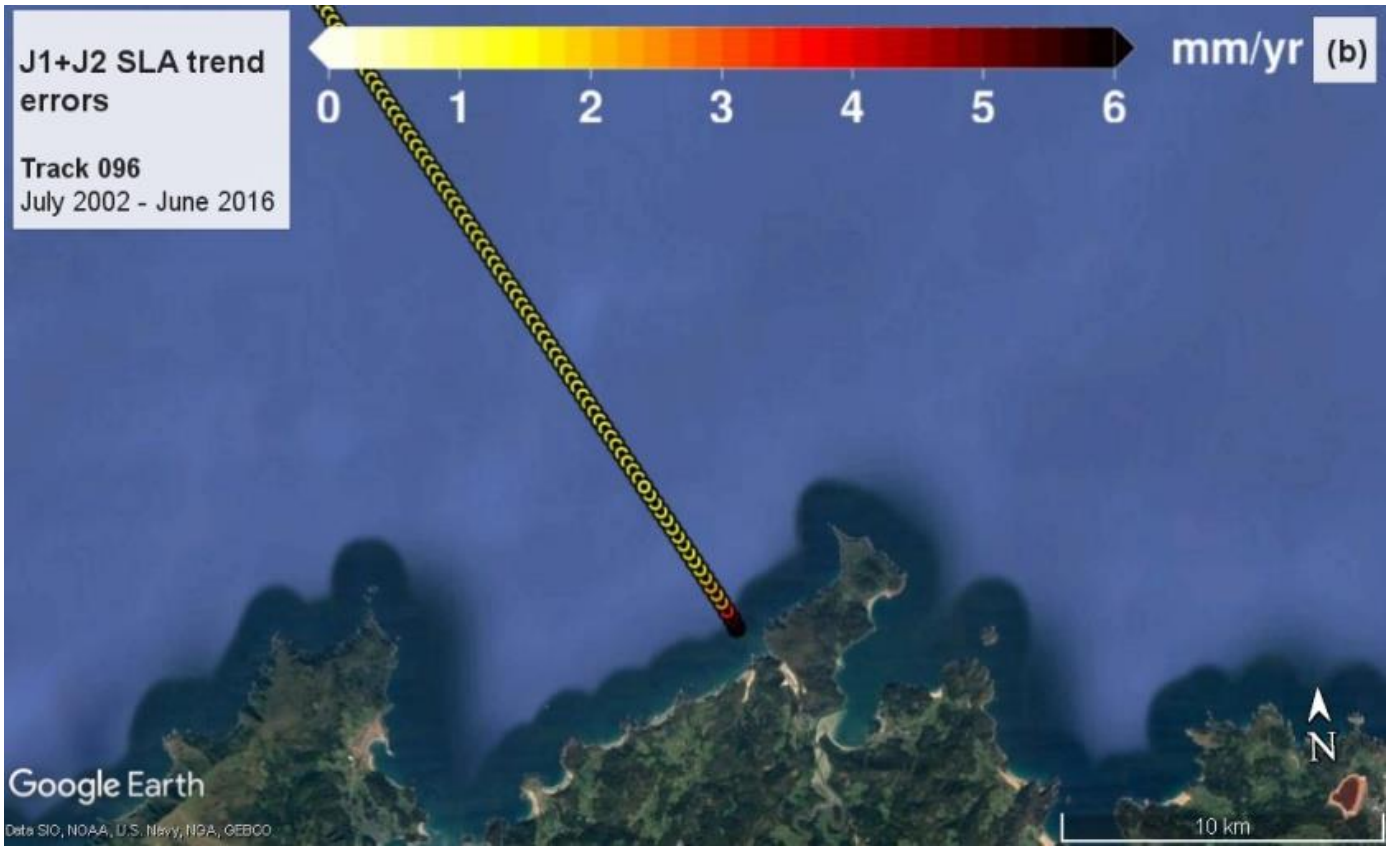

TRACK 198

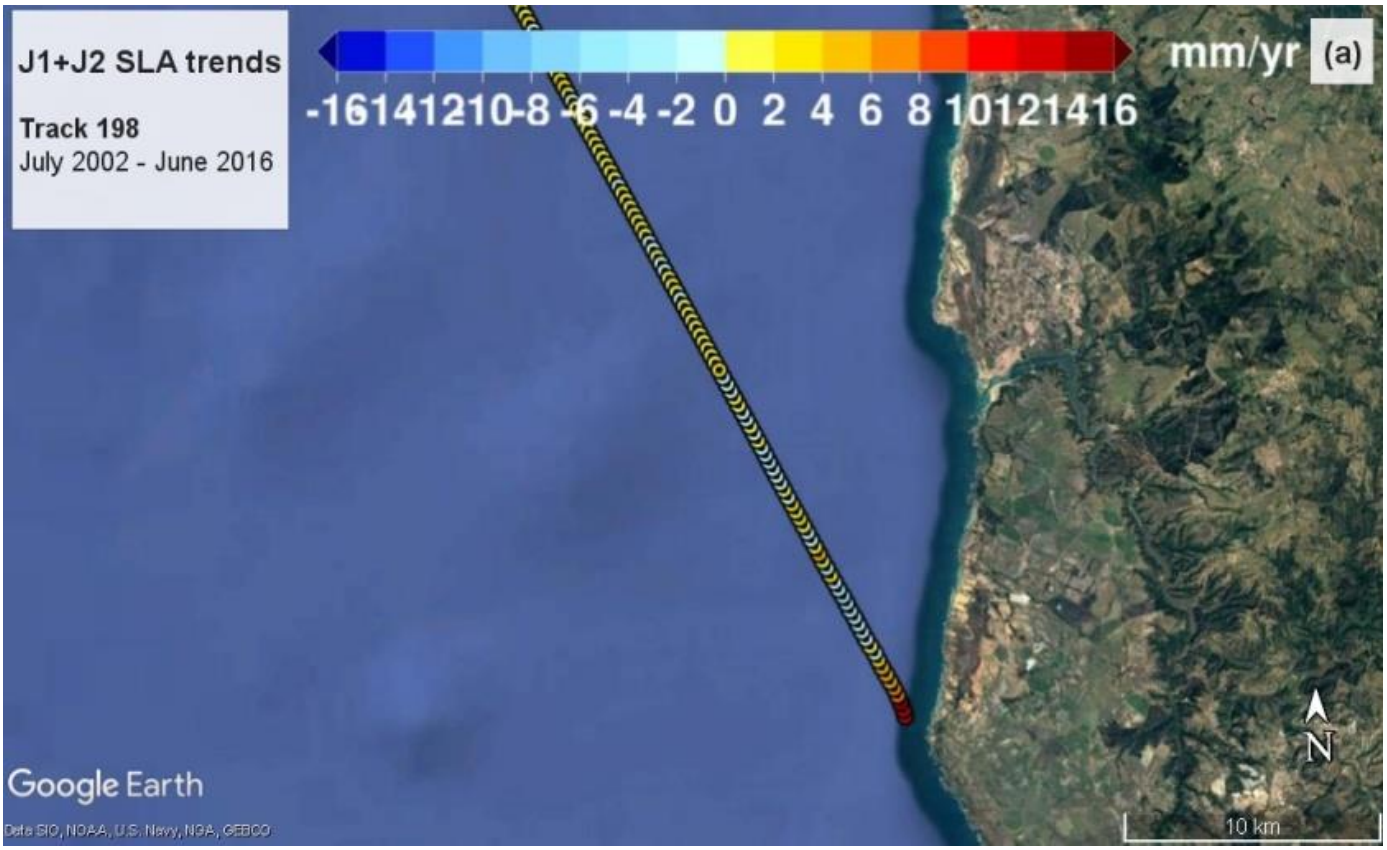

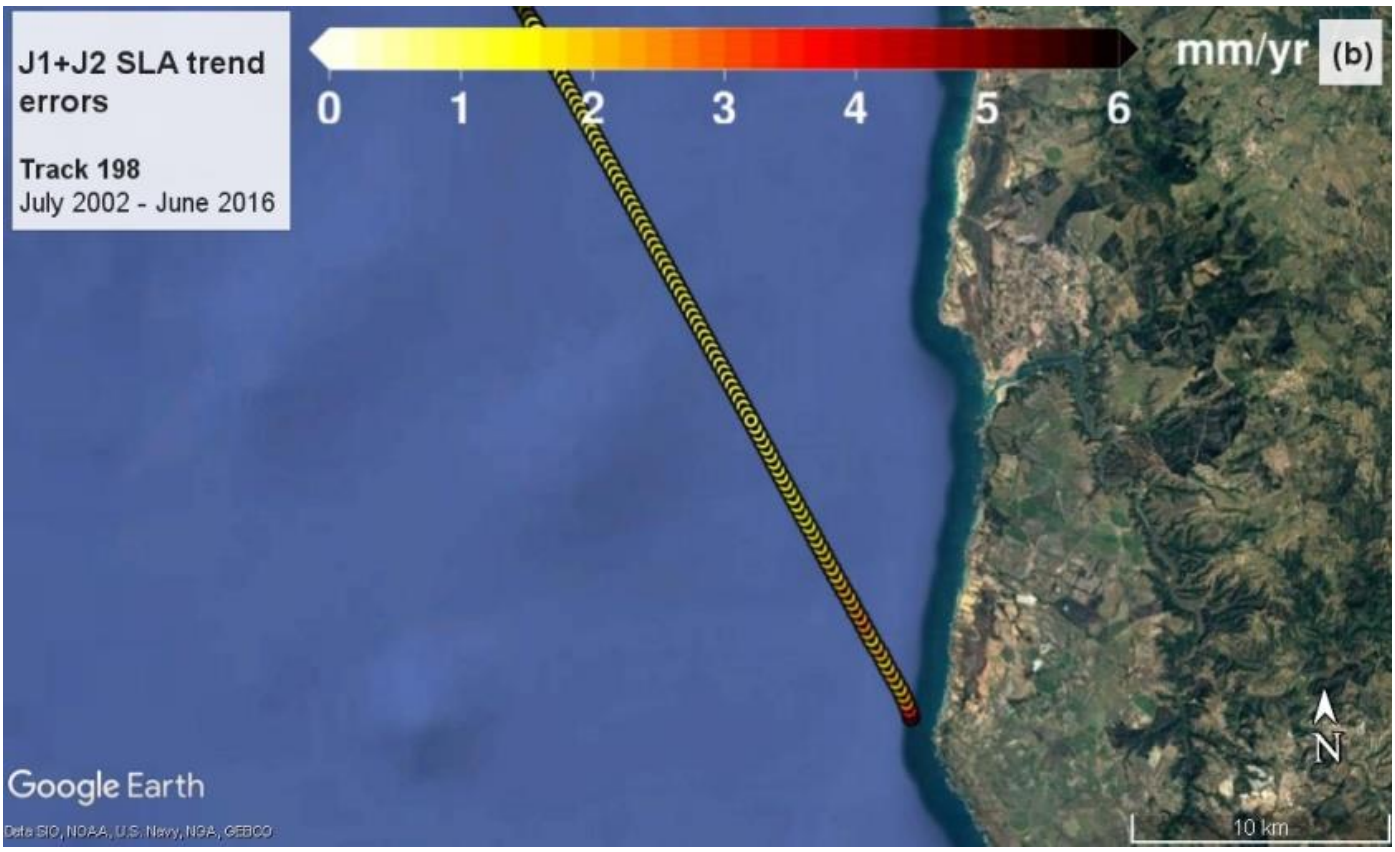

Annex E

Figure 17

NORTHERN EUROPE

ASCENDING TRACKS

Ranked from west to east

TRACK 239 "#1" X-TRACK/ALES 20Hz SLA – J1 + J2 – Jul2002 – Jun2016 (annual and semi-annual cycles removed)

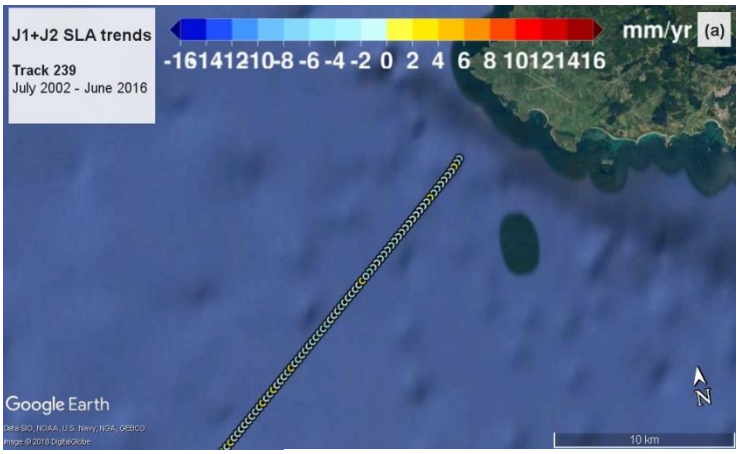

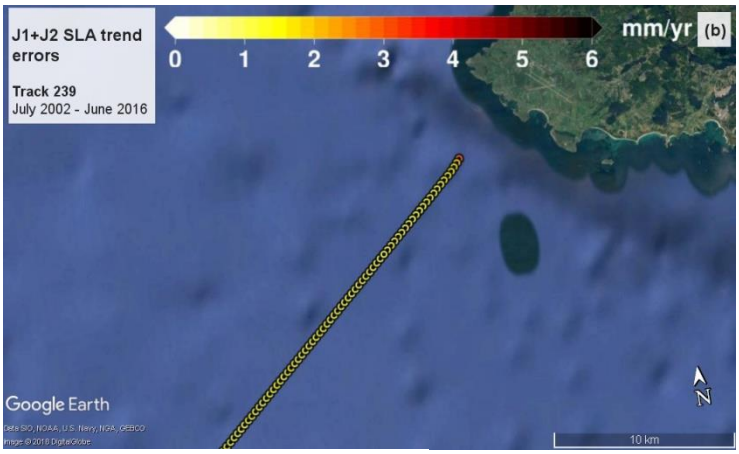

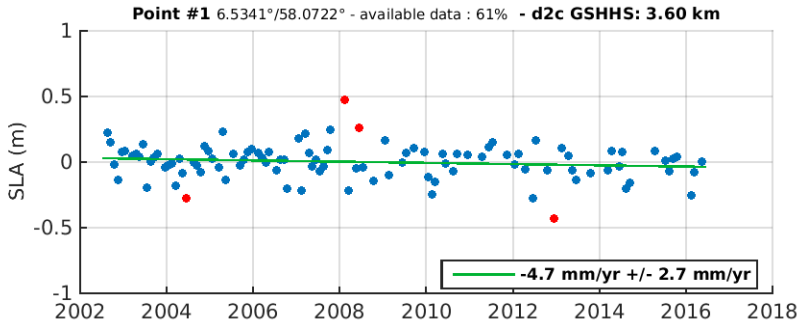

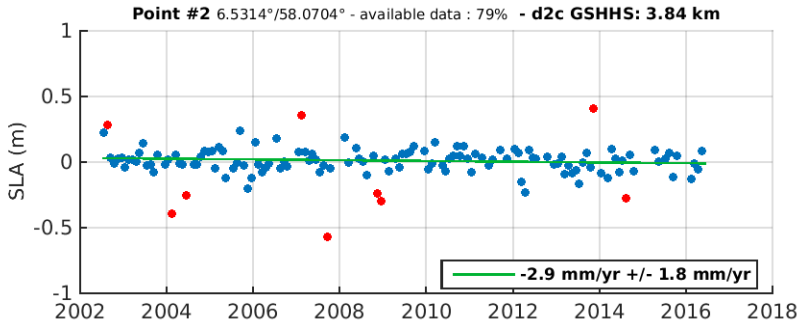

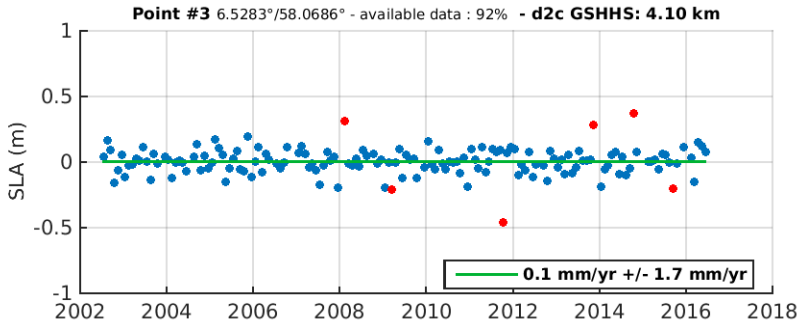

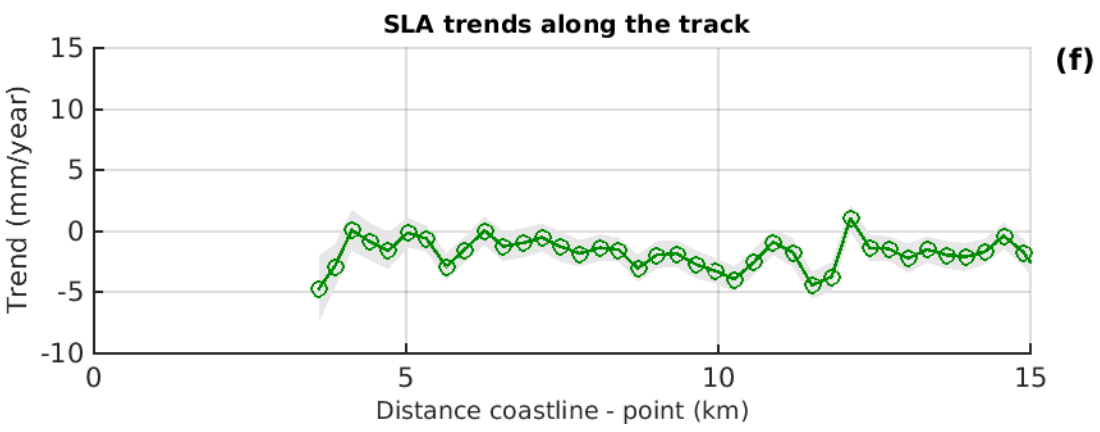

TRACK 239 "#2" X-TRACK/ALES 20Hz SLA – J1 + J2 – Jul2002 – Jun2016
(annual and semi-annual cycles removed)

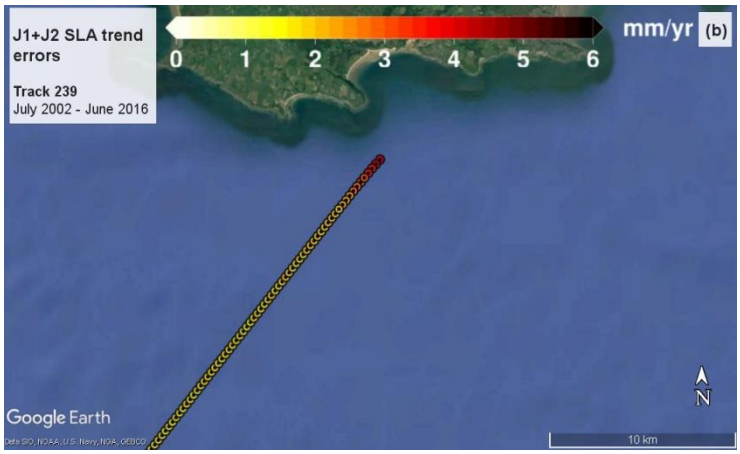

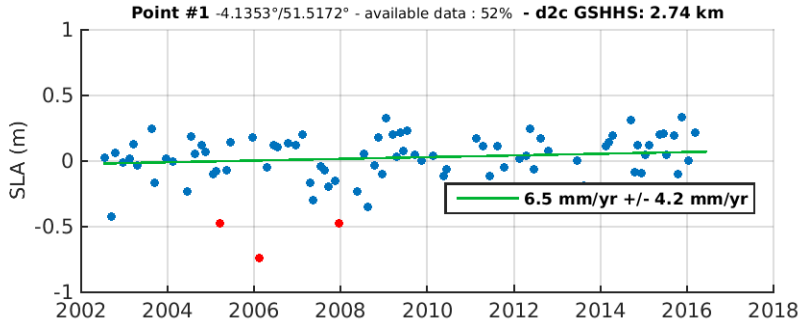

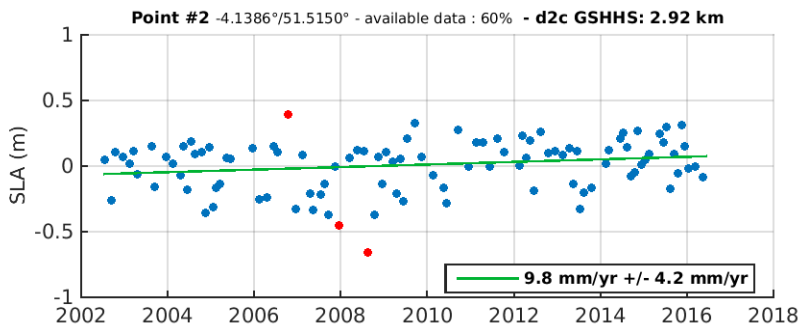

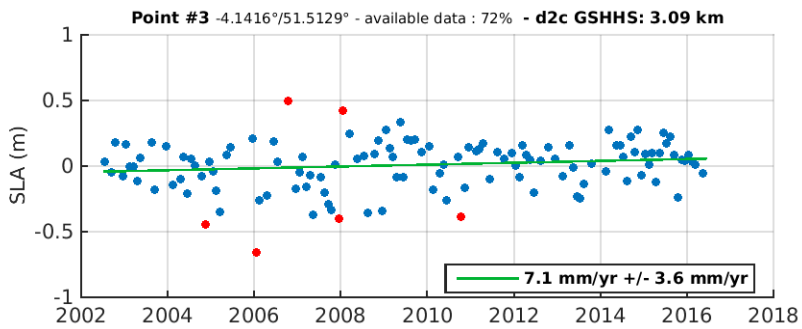

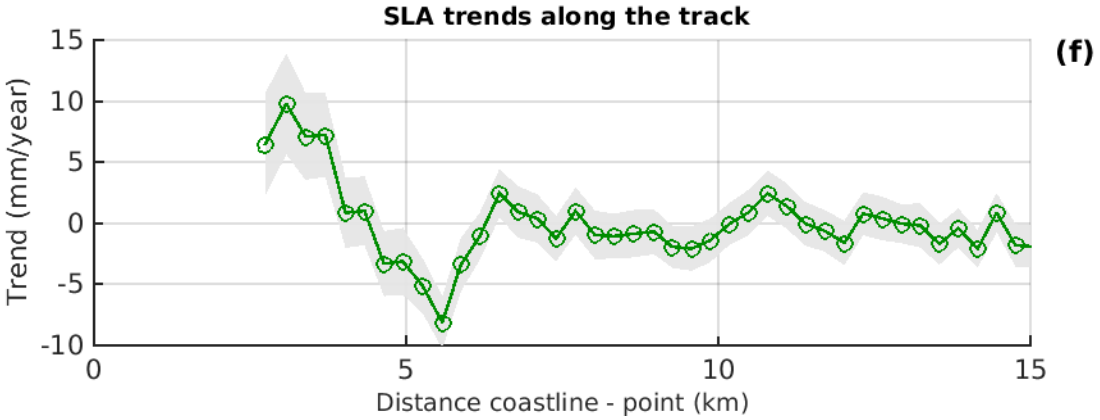

TRACK 061 X-TRACK/ALES 20Hz SLA – J1 + J2 – Jul2002 – Jun2016
(annual and semi-annual cycles removed)

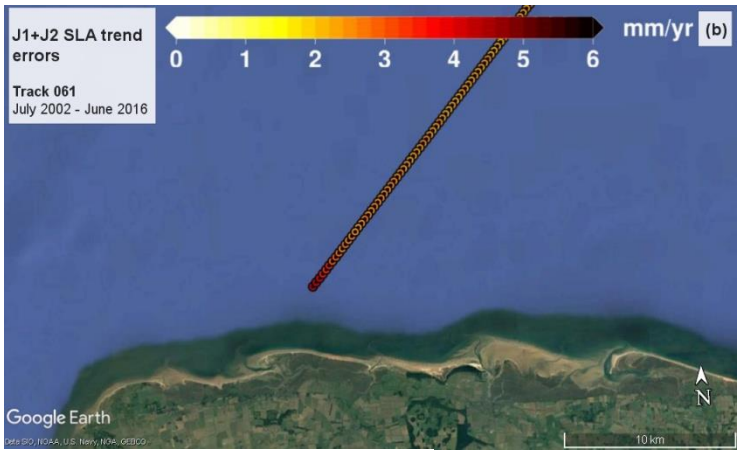

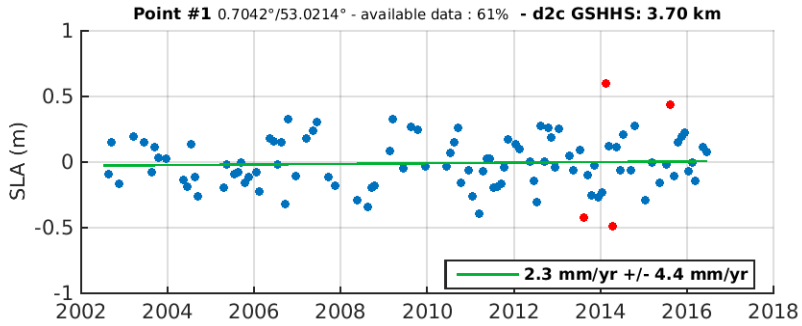

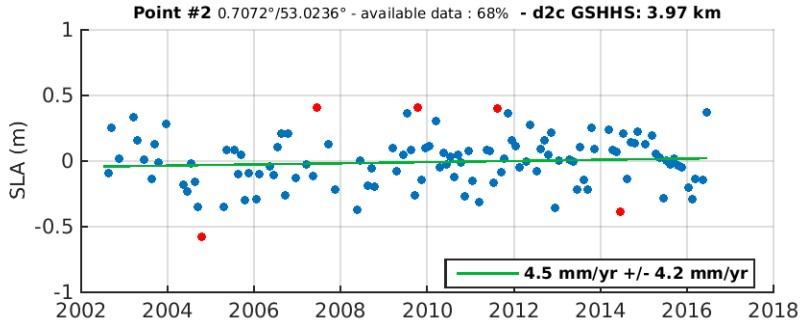

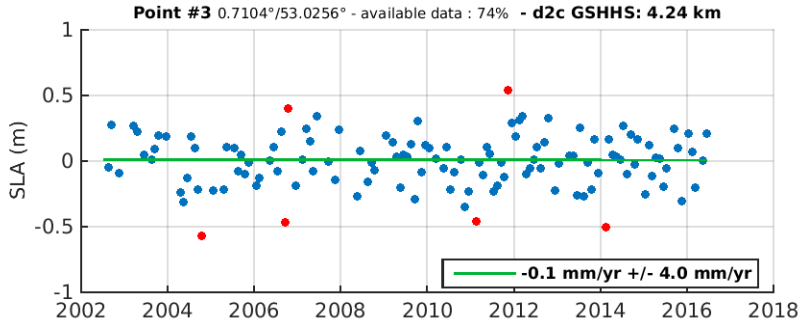

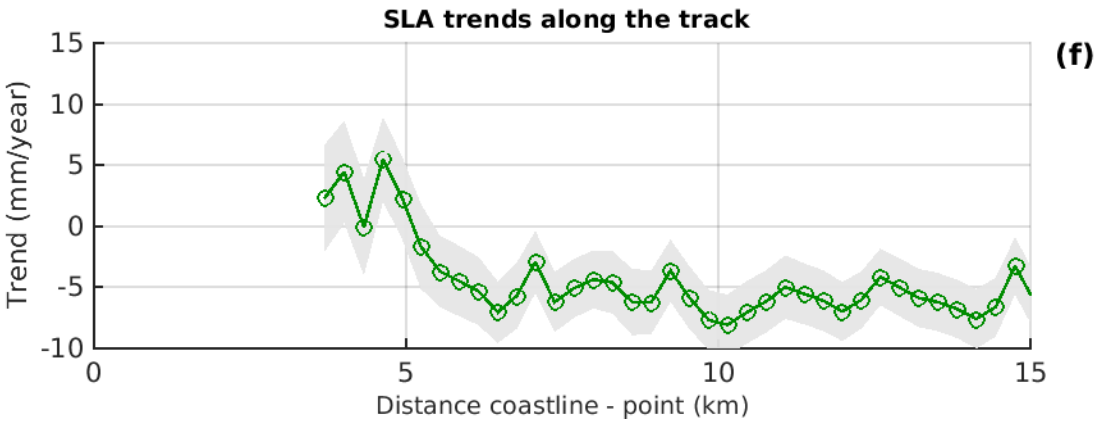

TRACK 137 "#1" X-TRACK/ALES 20Hz SLA – J1 + J2 – Jul2002 – Jun2016
(annual and semi-annual cycles removed)

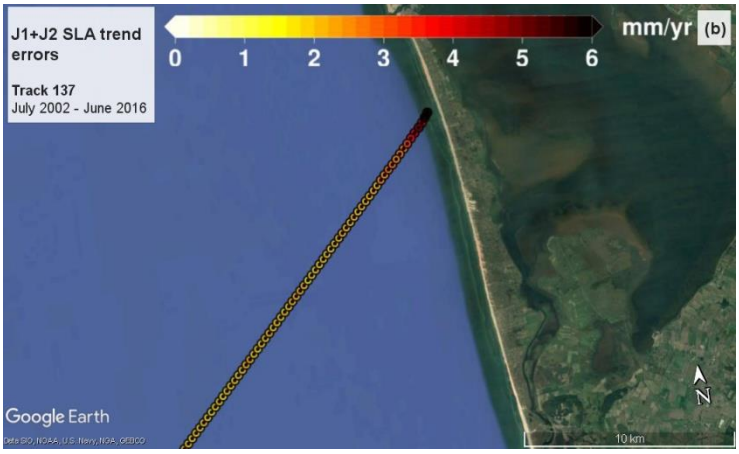

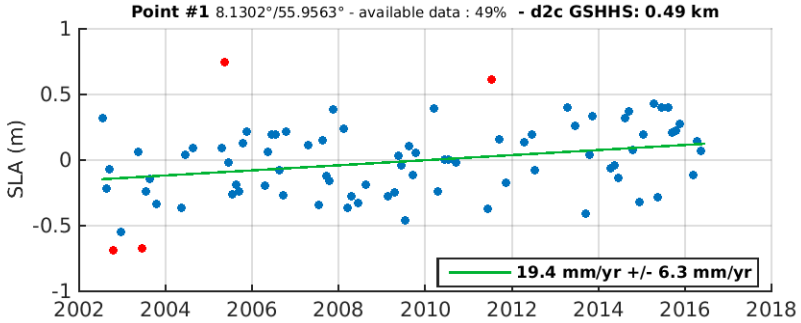

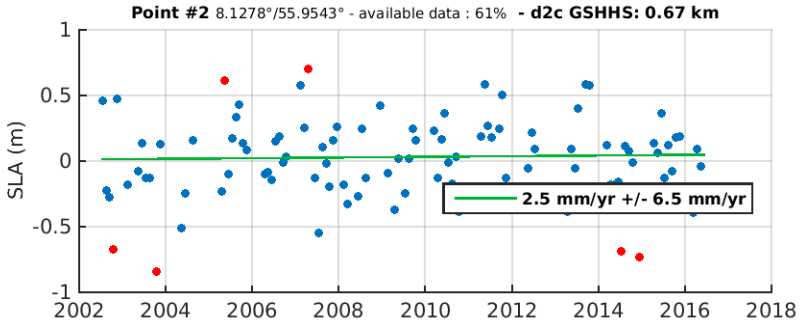

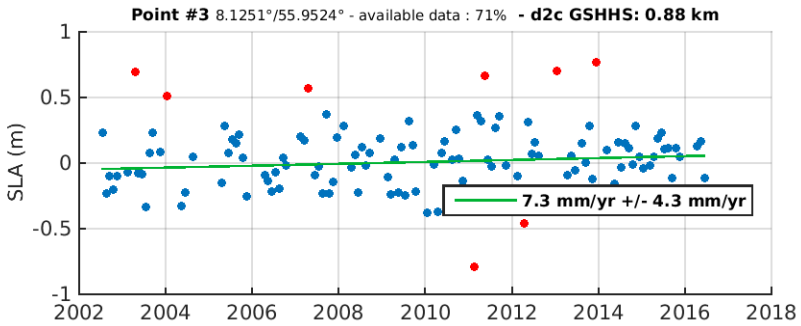

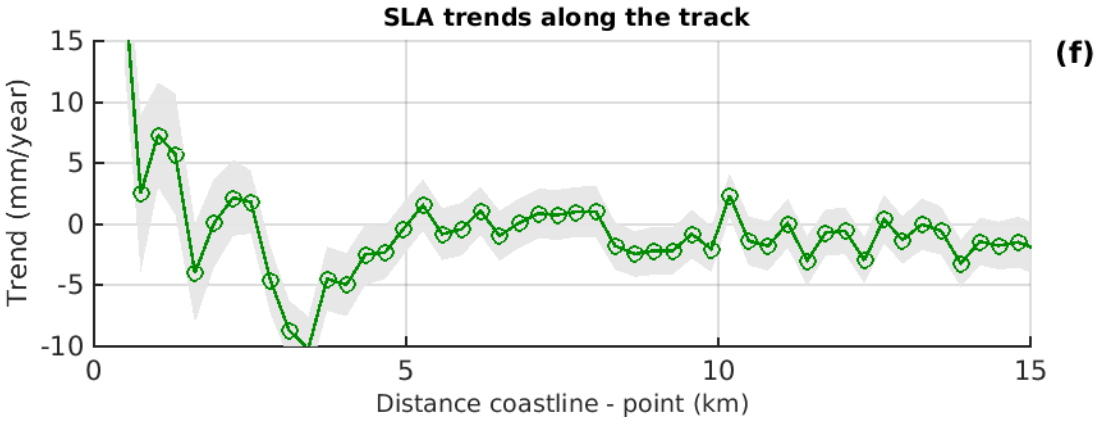

TRACK 137 "#2" X-TRACK/ALES 20Hz SLA – J1 + J2 – Jul2002 – Jun2016
(annual and semi-annual cycles removed)

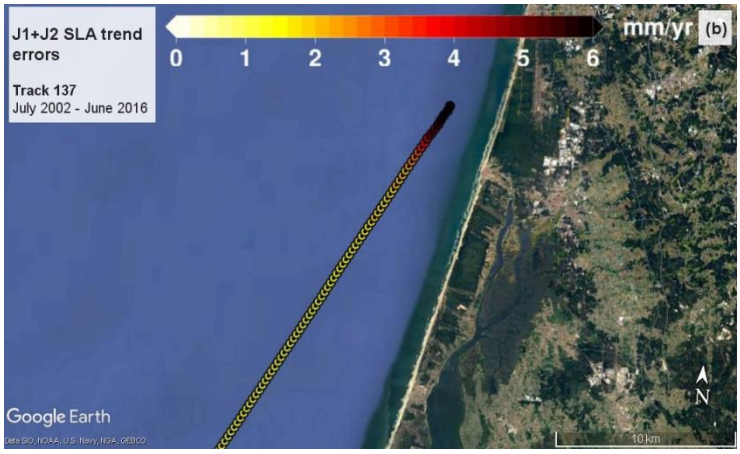

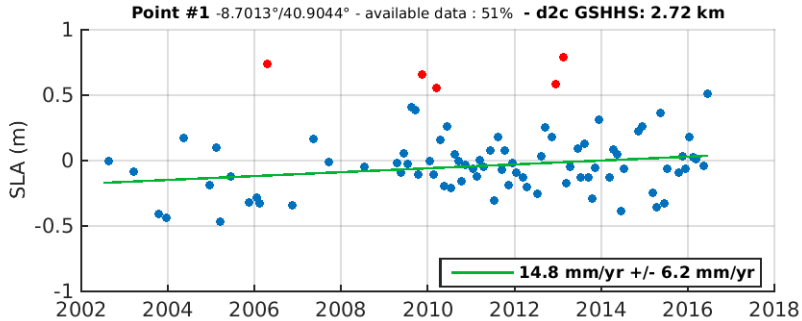

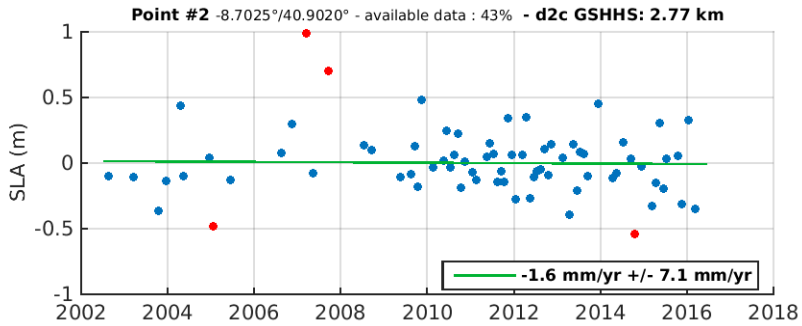

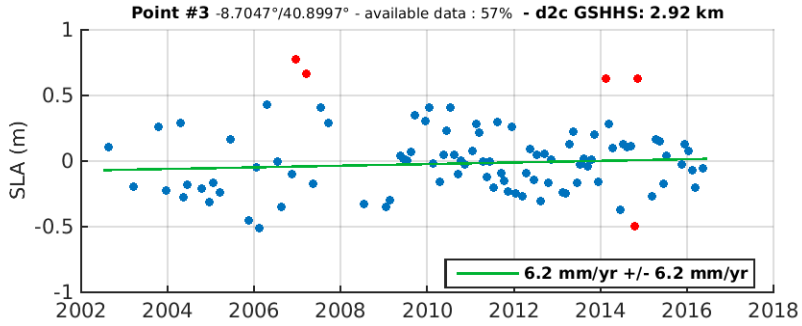

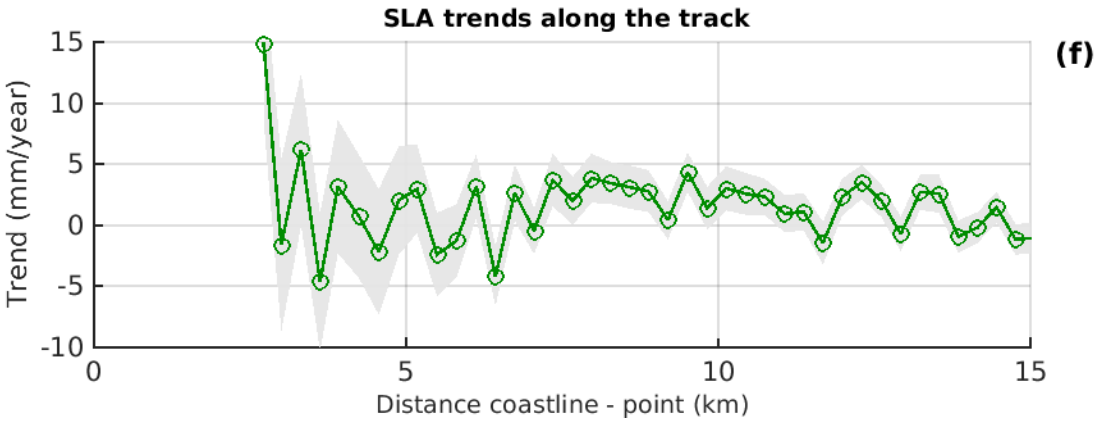

TRACK 213 "#1" X-TRACK/ALES 20Hz SLA – J1 + J2 – Jul2002 – Jun2016
(annual and semi-annual cycles removed)

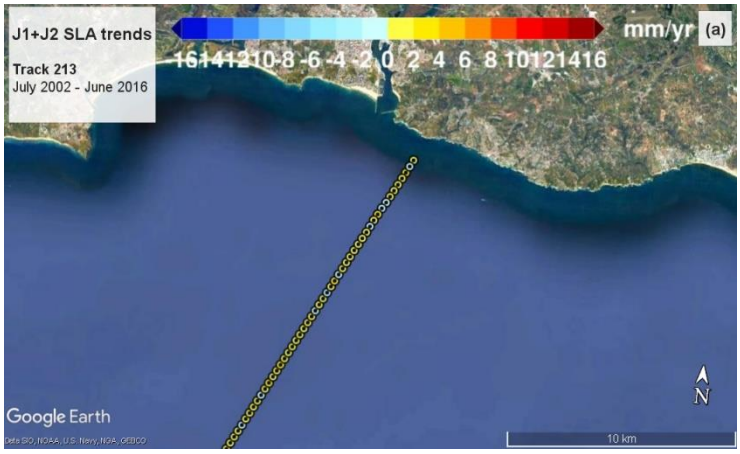

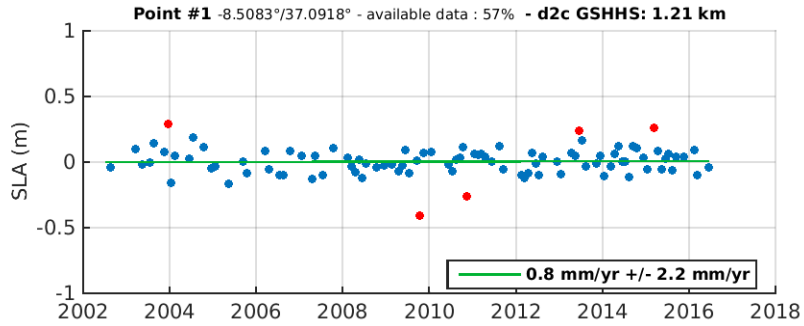

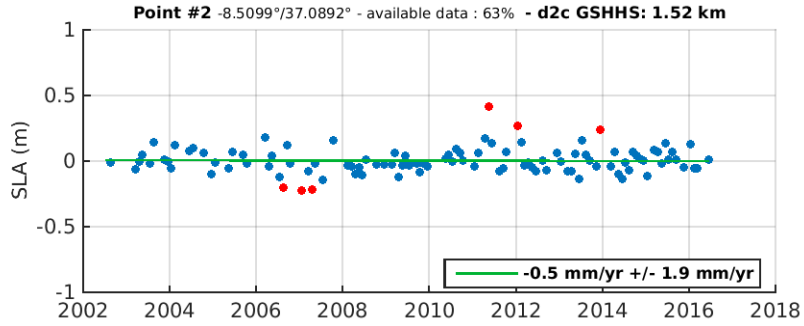

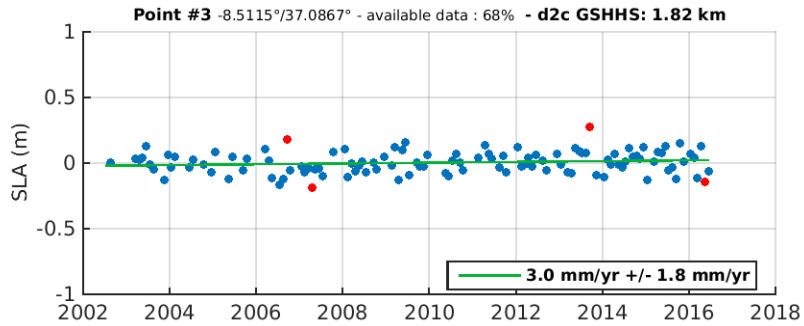

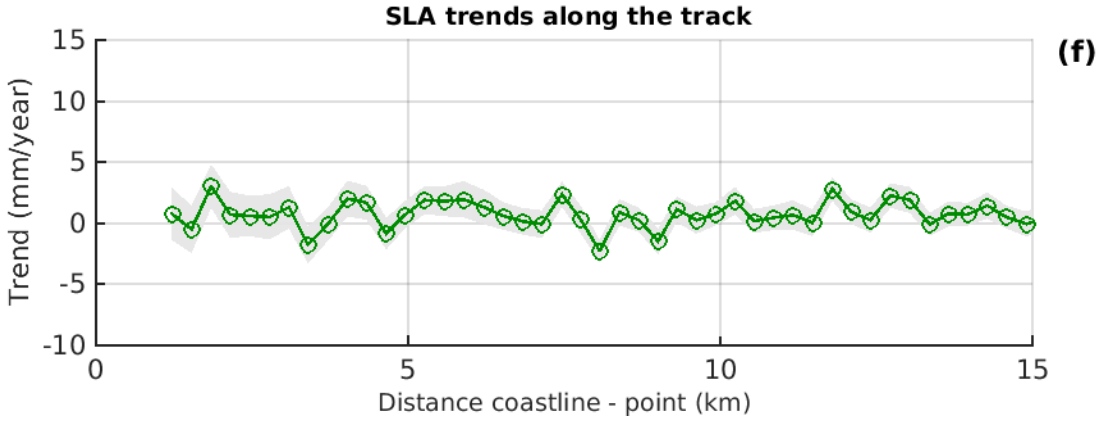

TRACK 213 "#2" X-TRACK/ALES 20Hz SLA – J1 + J2 – Jul2002 – Jun2016
(annual and semi-annual cycles removed)

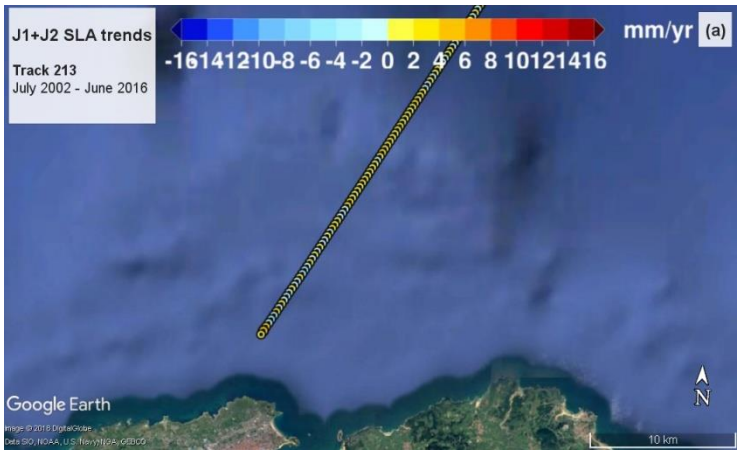

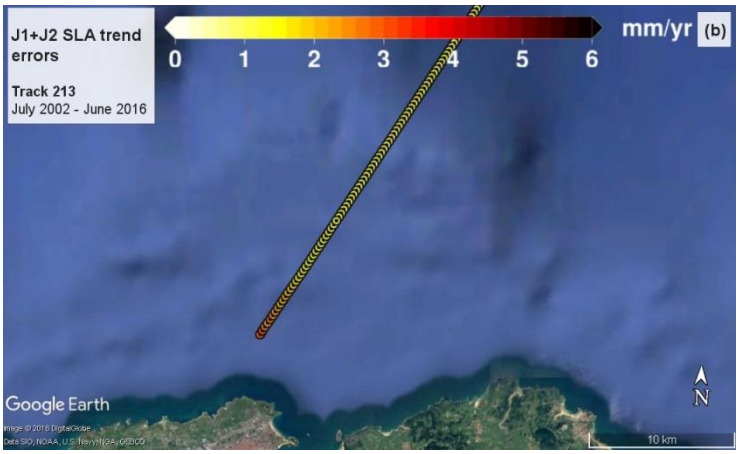

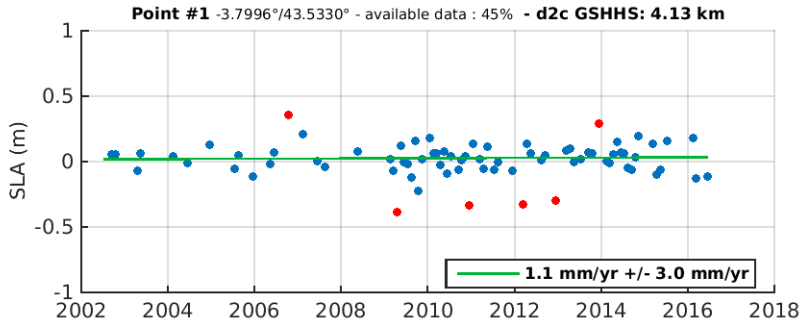

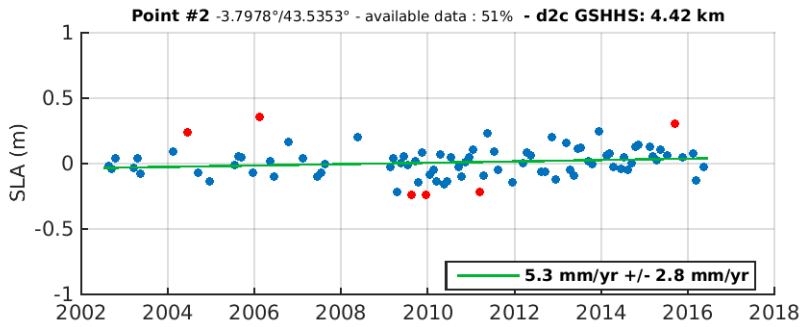

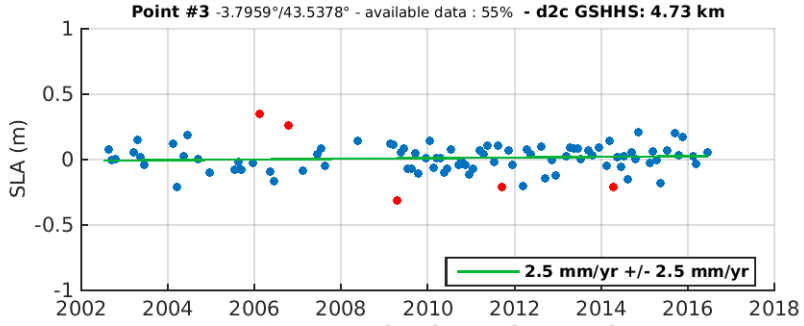

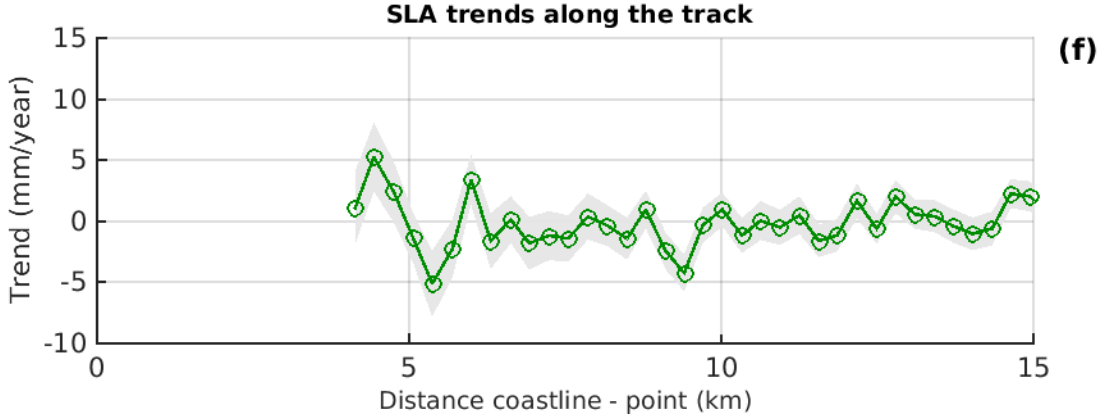

TRACK 035 X-TRACK/ALES 20Hz SLA – J1 + J2 – Jul2002 – Jun2016
(annual and semi-annual cycles removed)

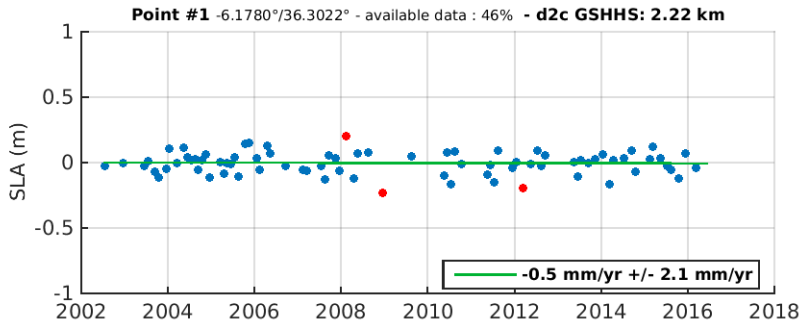

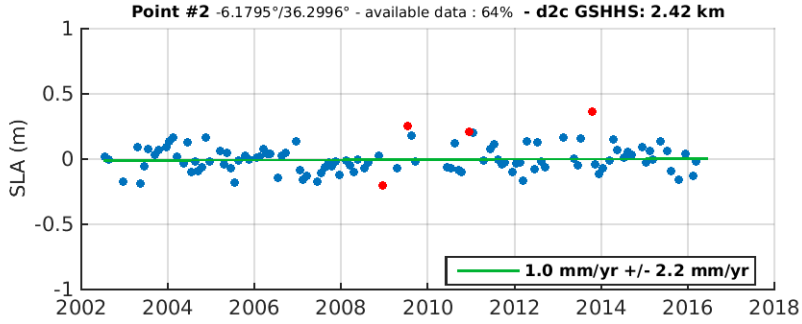

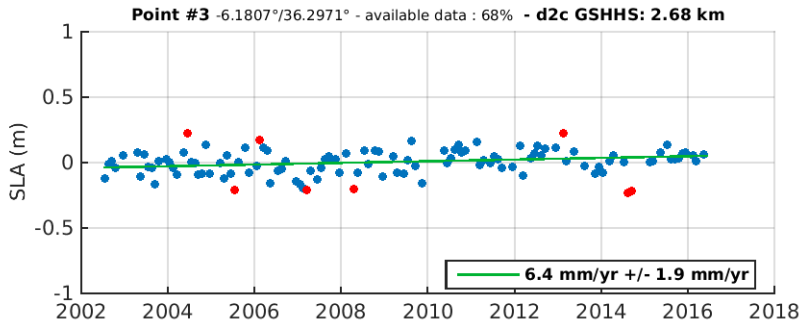

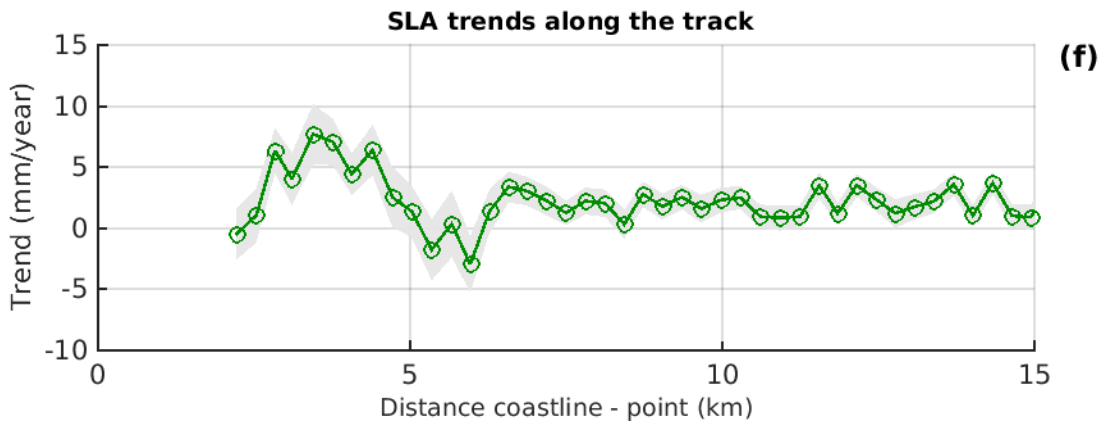

F

NORTHERN EUROPE

DESCENDING TRACKS

Ranked from east to west

TRACK 120 X-TRACK/ALES 20Hz SLA – J1 + J2 – Jul2002 – Jun2016
(annual and semi-annual cycles removed)

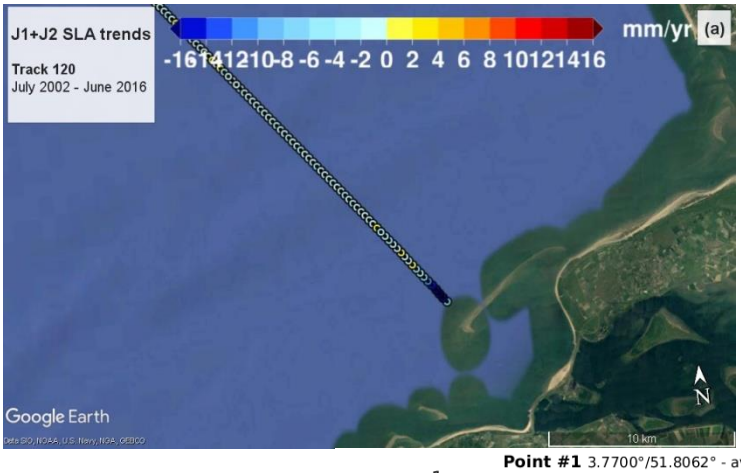

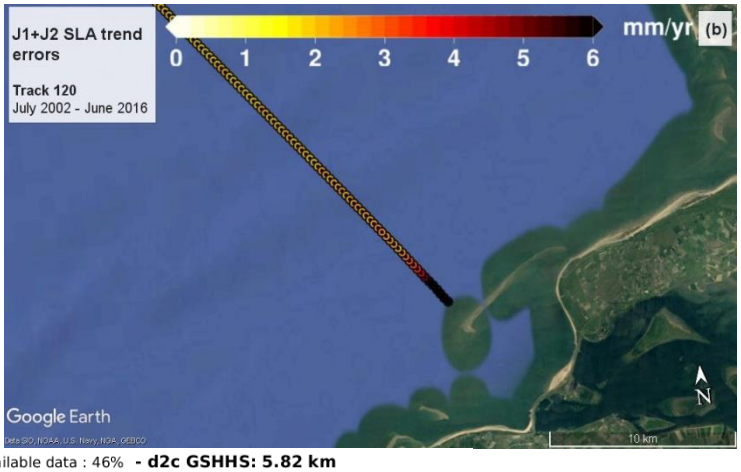

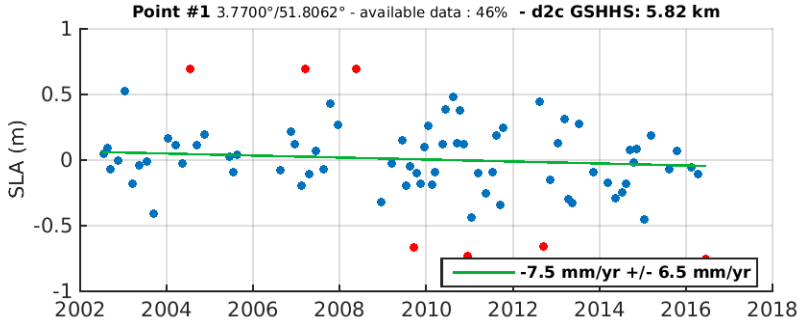

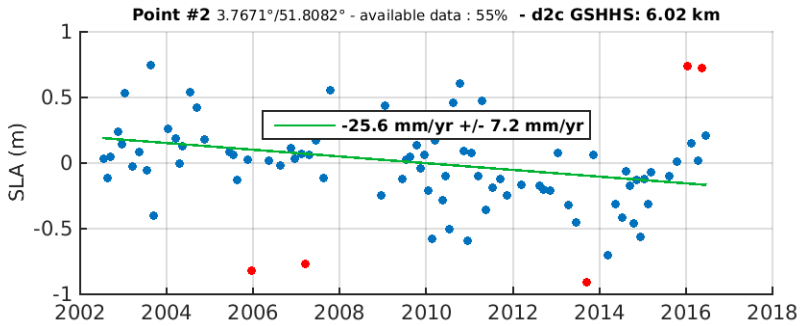

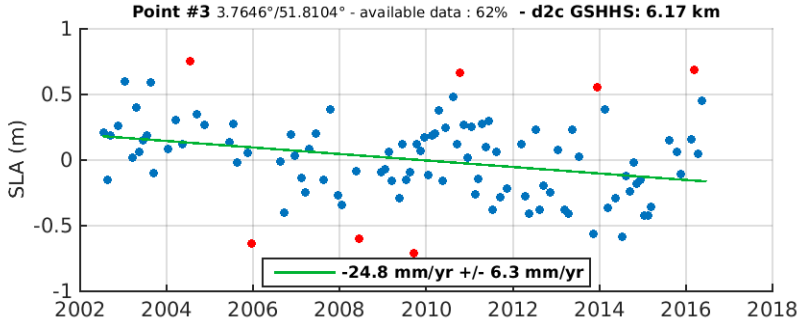

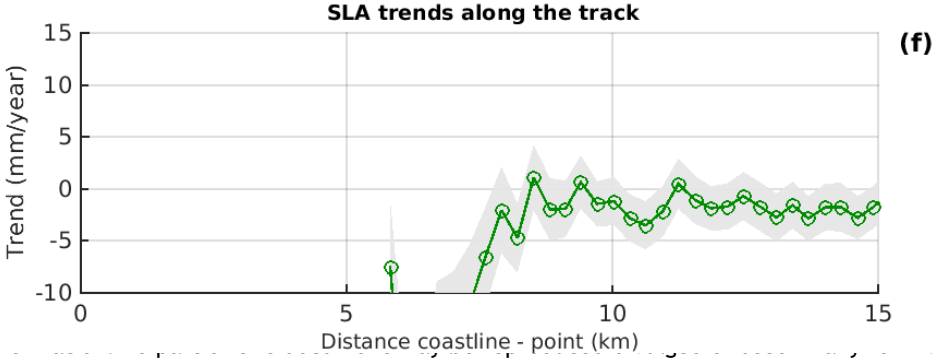

TRACK 248 X-TRACK/ALES 20Hz SLA – J1 + J2 – Jul2002 – Jun2016
(annual and semi-annual cycles removed)

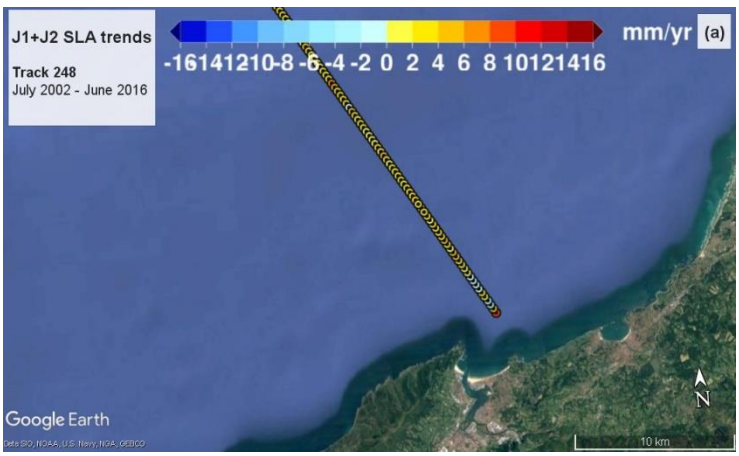

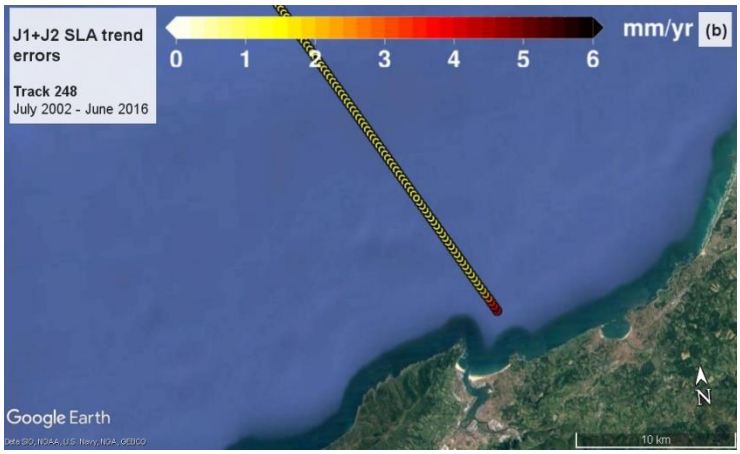

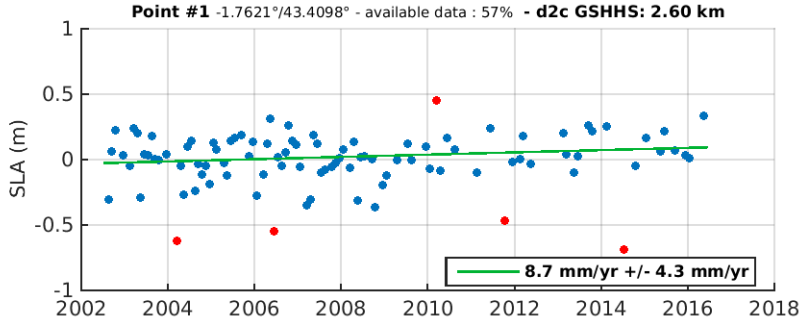

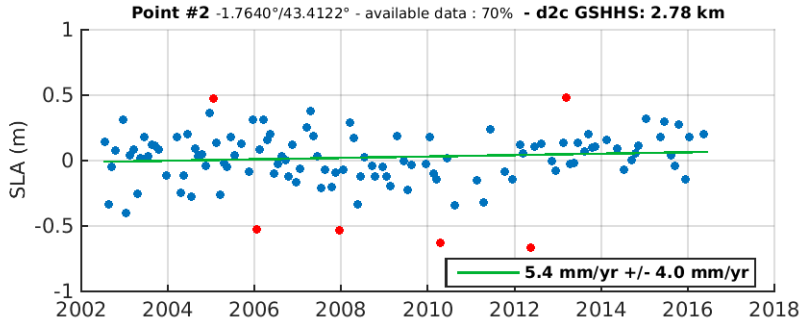

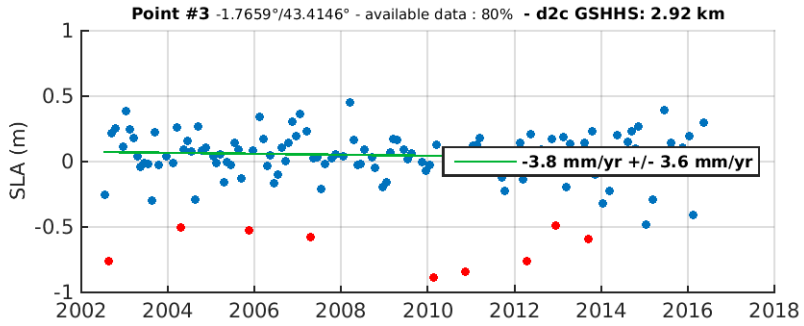

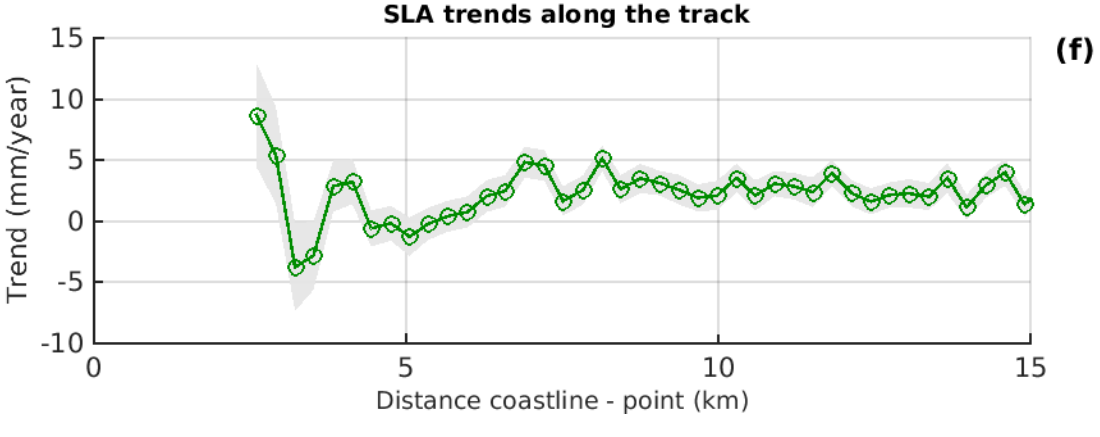

TRACK 172 X-TRACK/ALES 20Hz SLA – J1 + J2 – Jul2002 – Jun2016
(annual and semi-annual cycles removed)

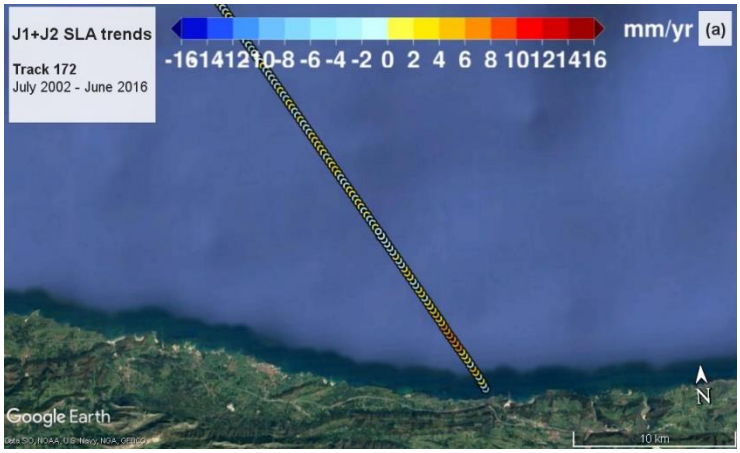

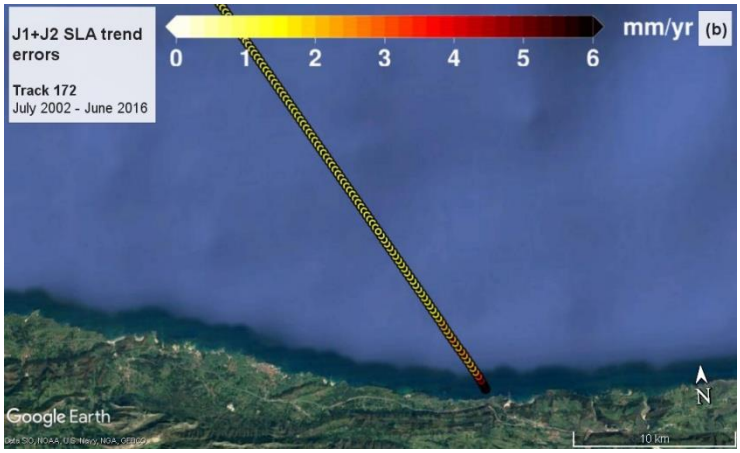

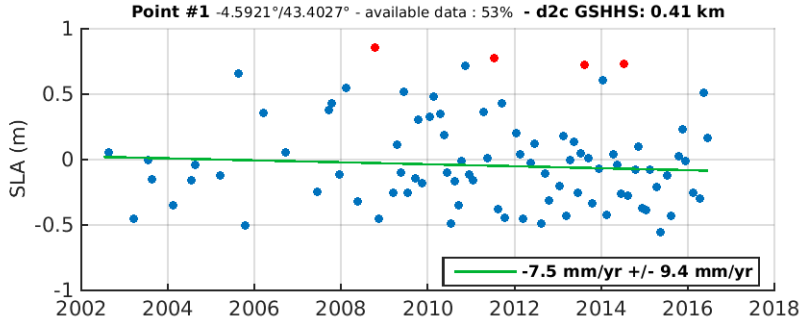

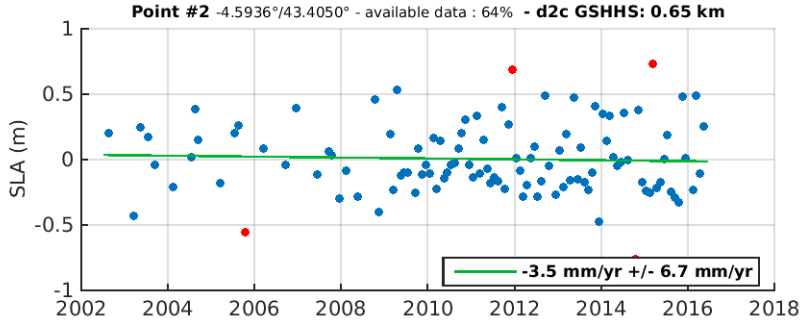

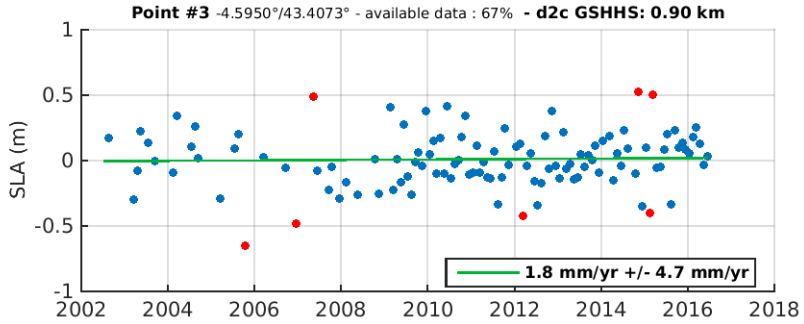

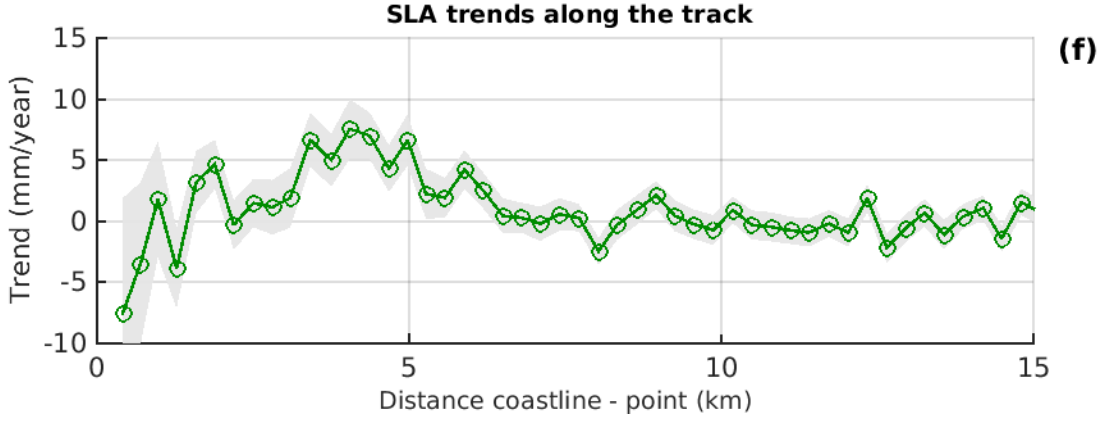

TRACK 096 X-TRACK/ALES 20Hz SLA – J1 + J2 – Jul2002 – Jun2016
(annual and semi-annual cycles removed)

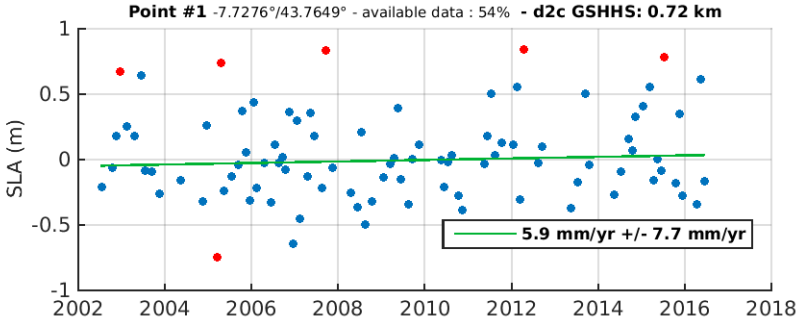

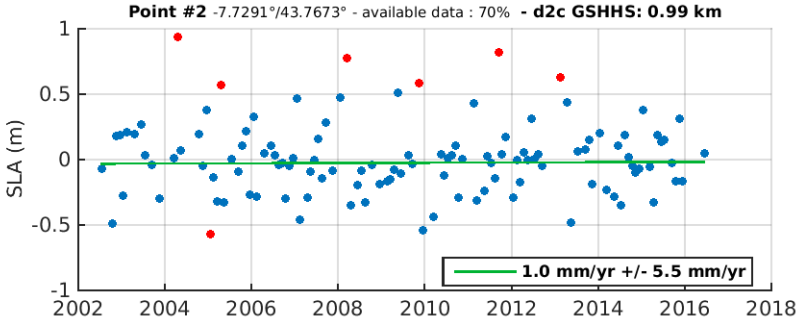

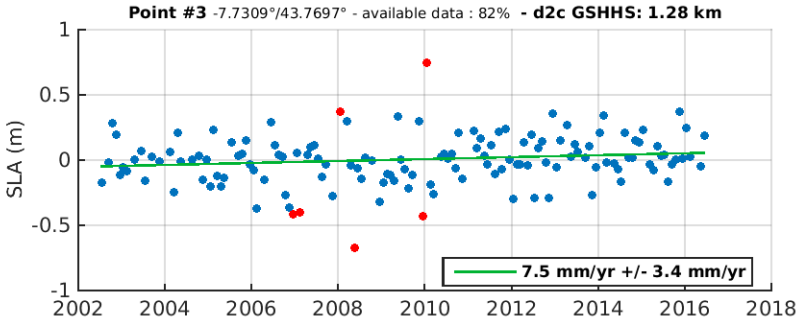

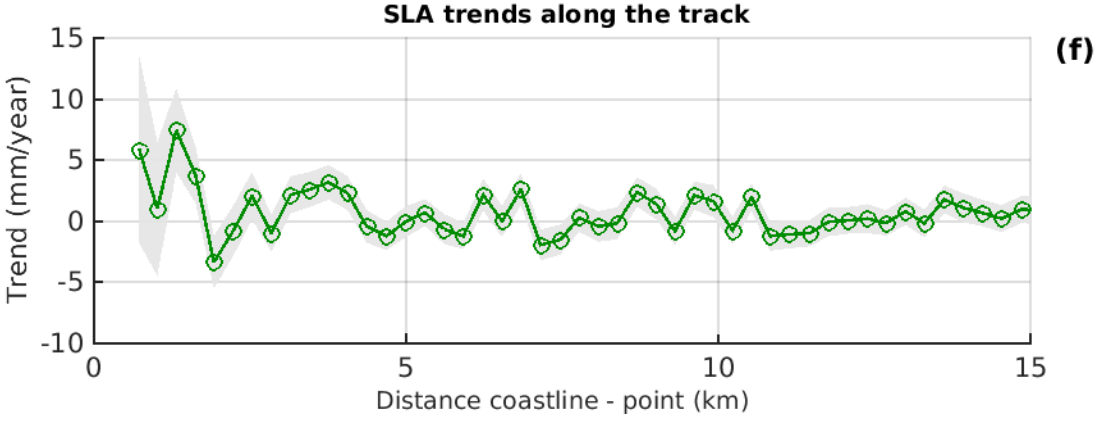

TRACK 198 X-TRACK/ALES 20Hz SLA – J1 + J2 – Jul2002 – Jun2016
(annual and semi-annual cycles removed)

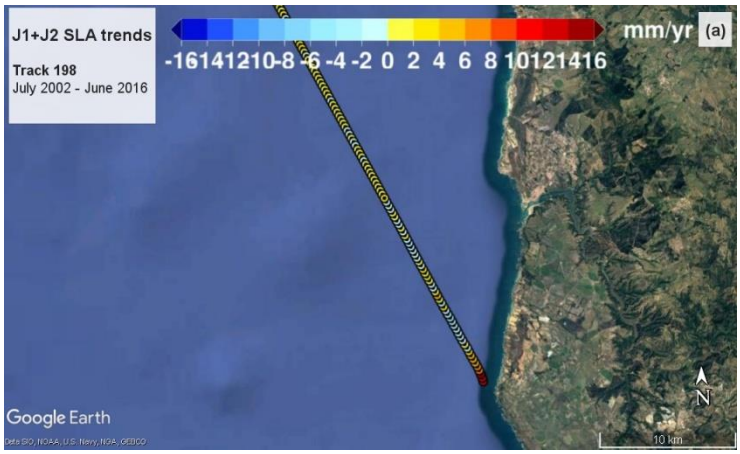

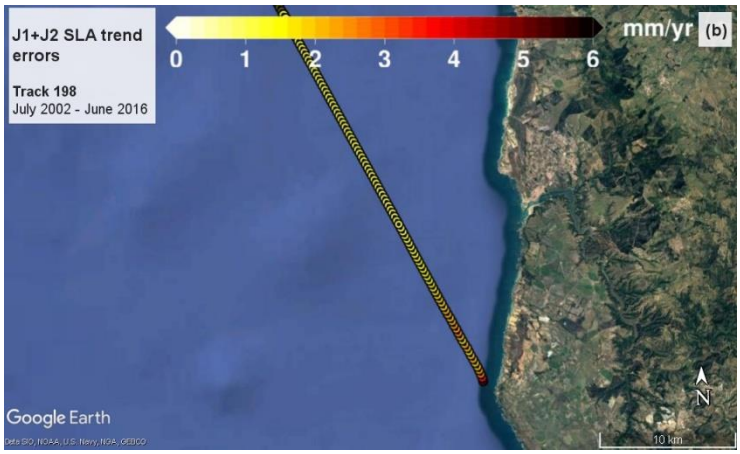

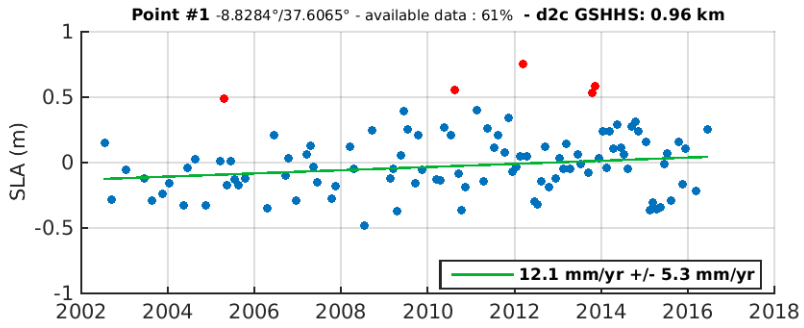

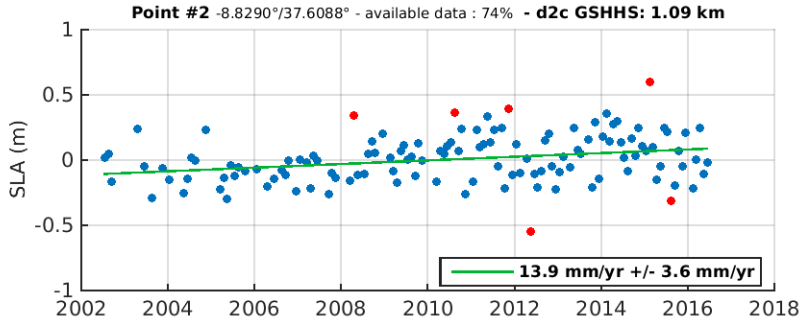

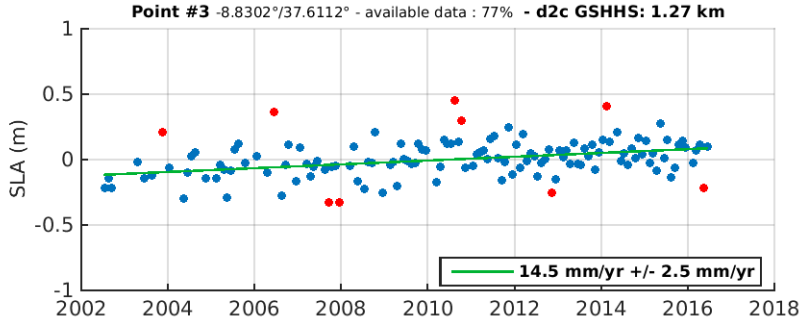

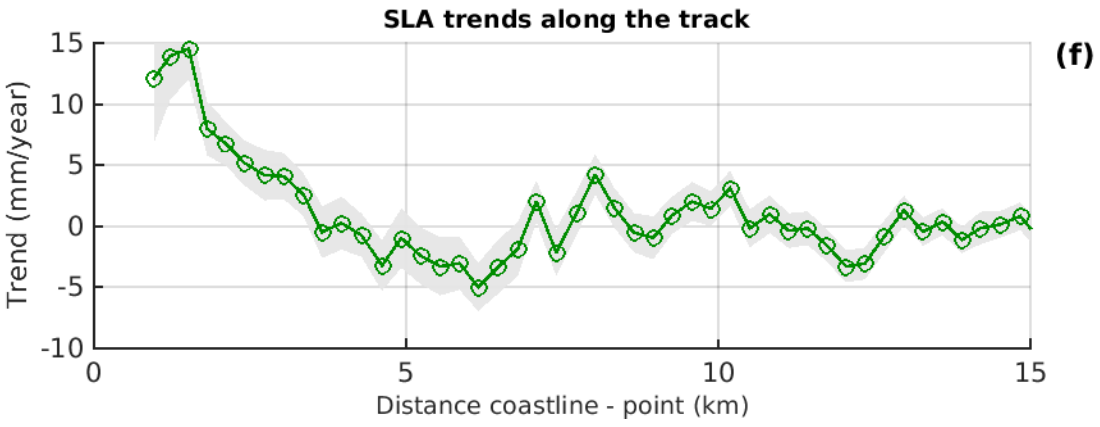

MEDITERRANEAN SEA

Annexes F and G

Annex F (MEDITERRANEAN SEA)

Figure 18

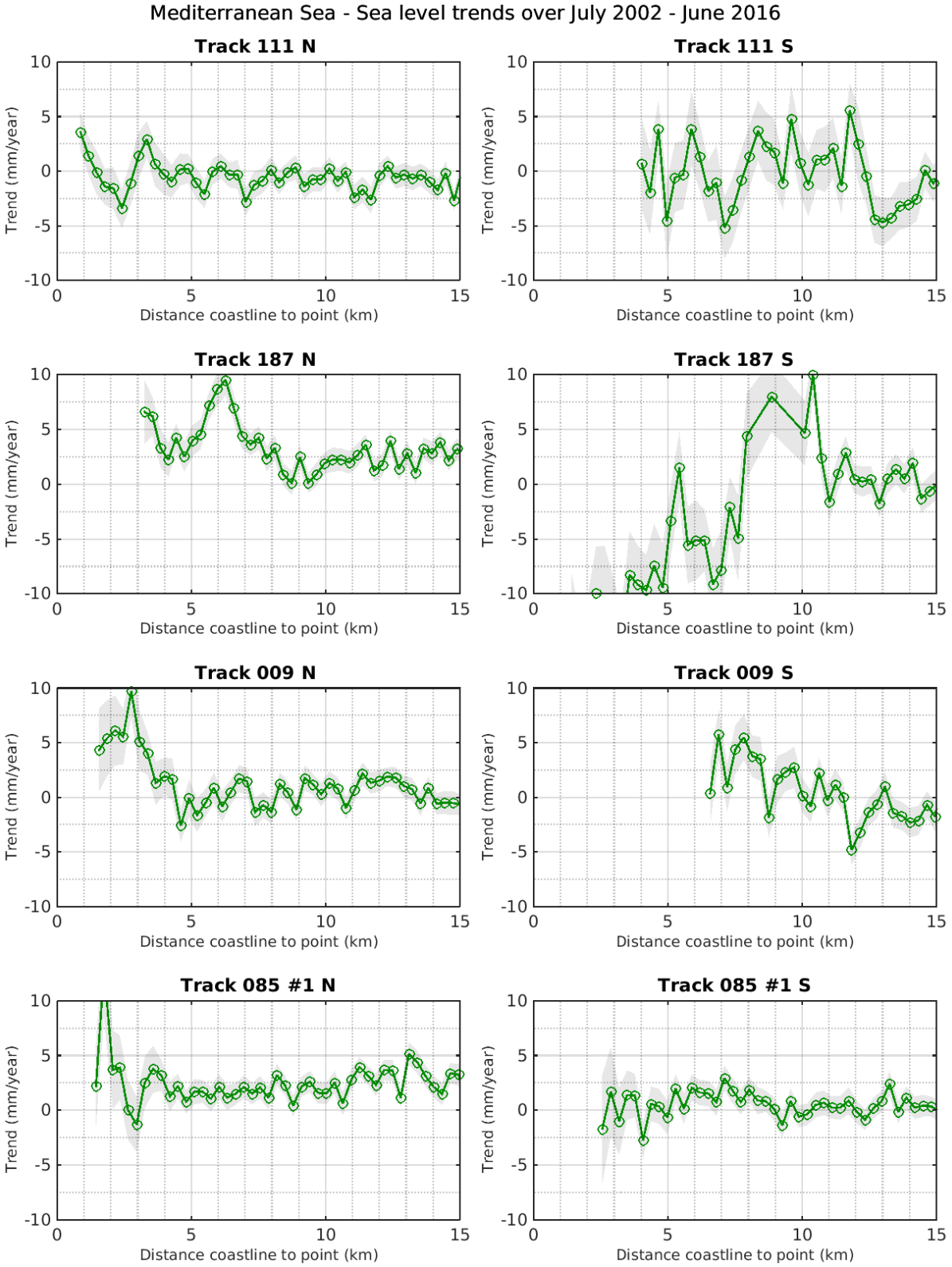

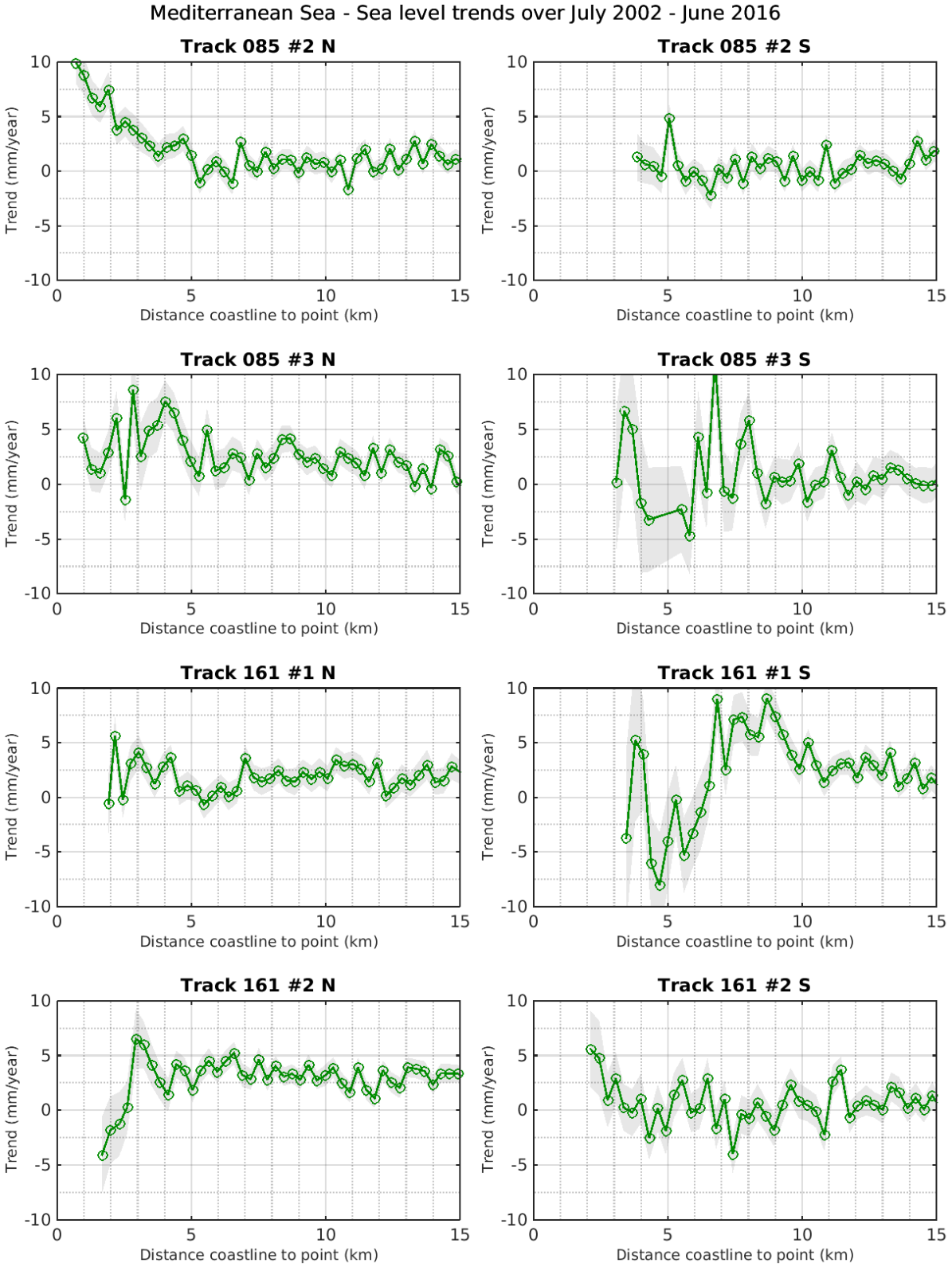

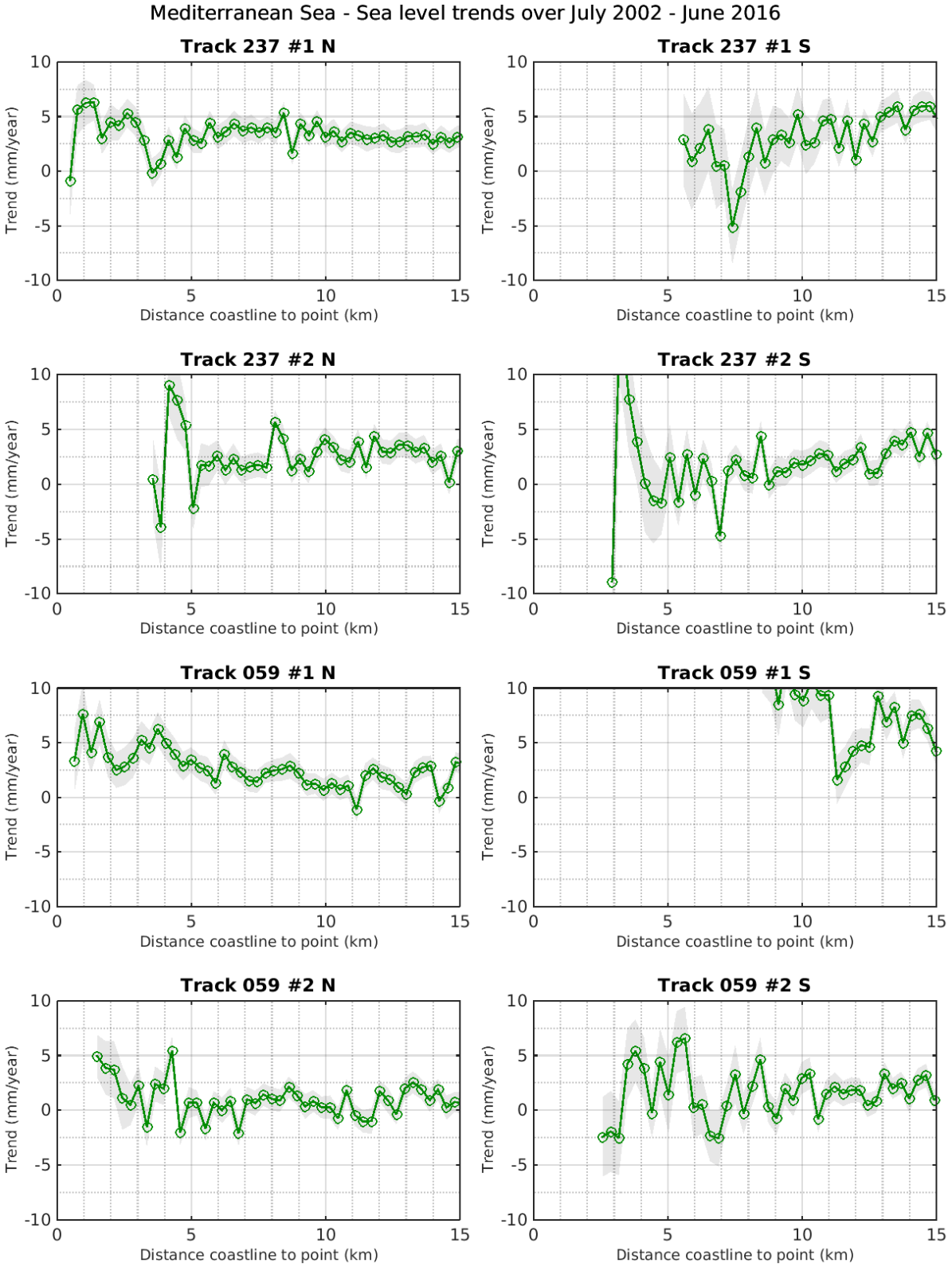

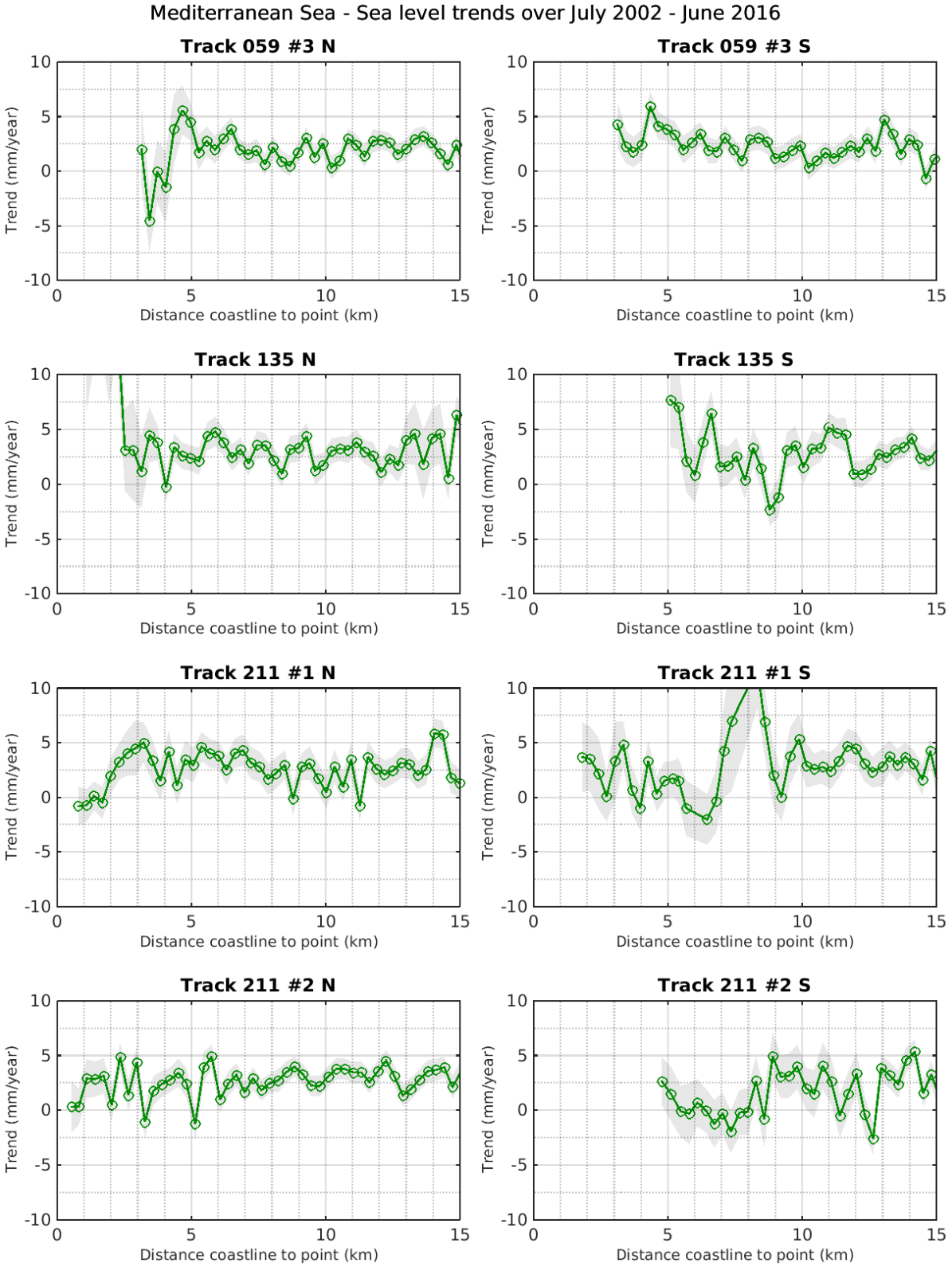

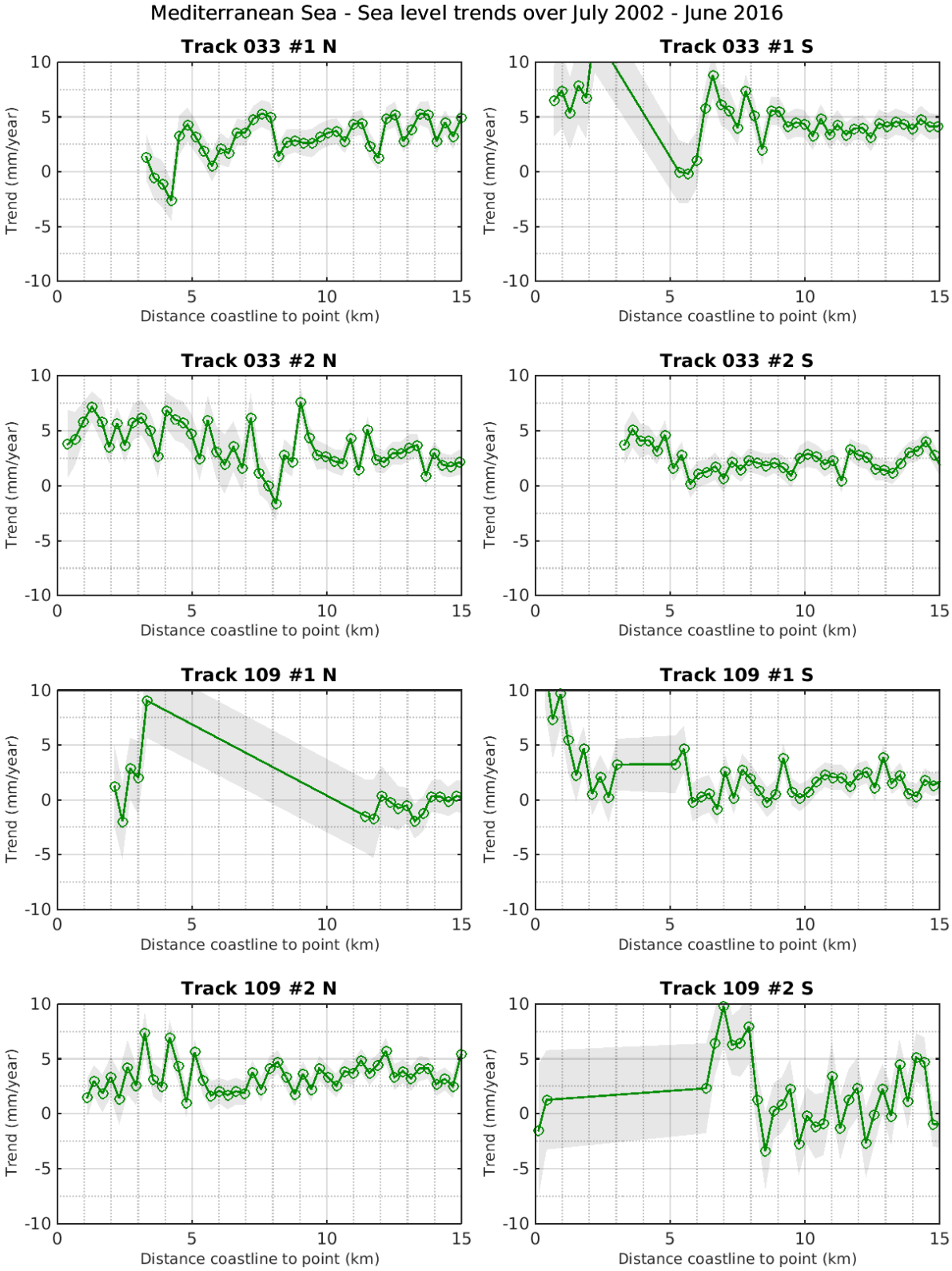

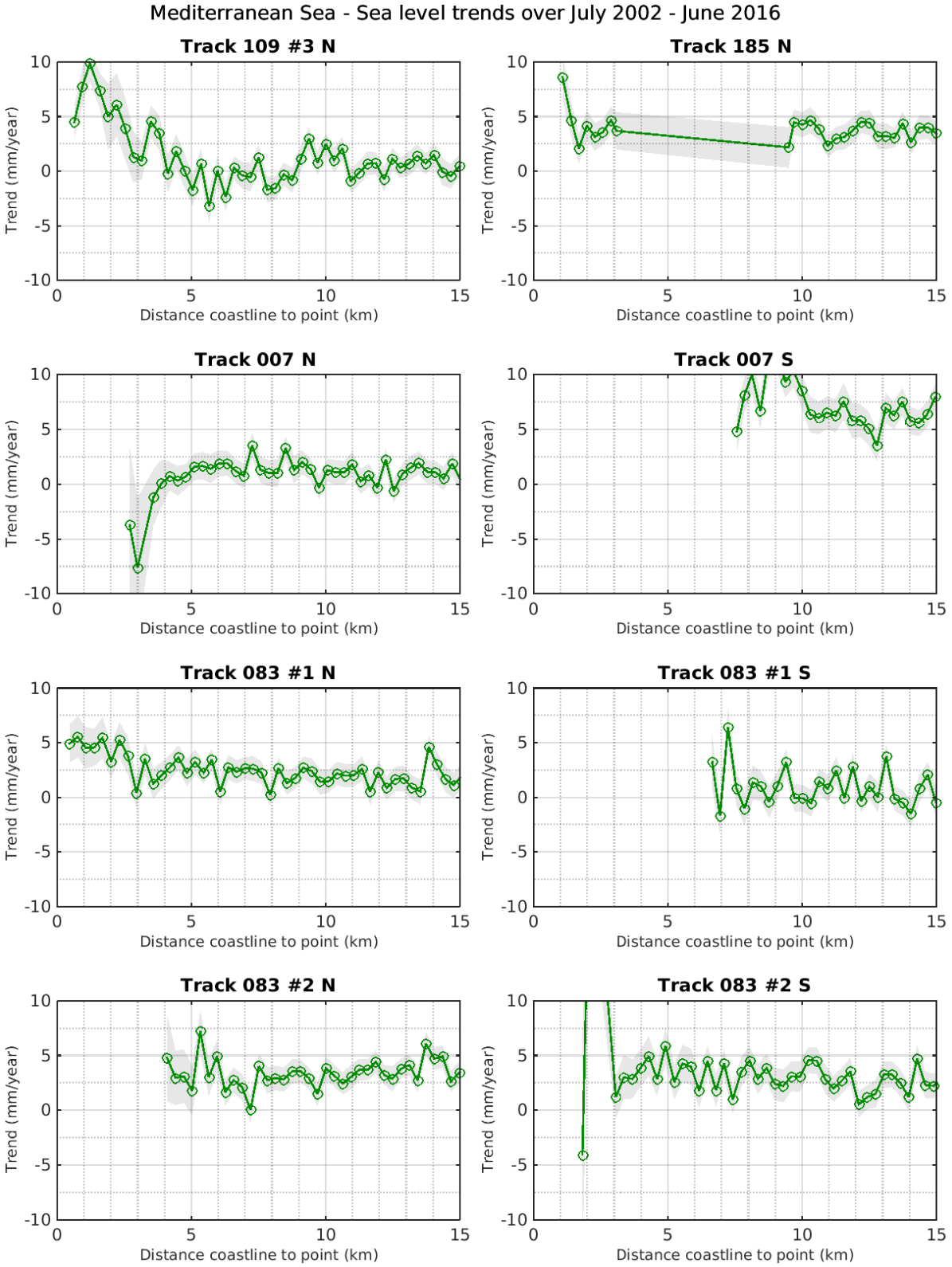

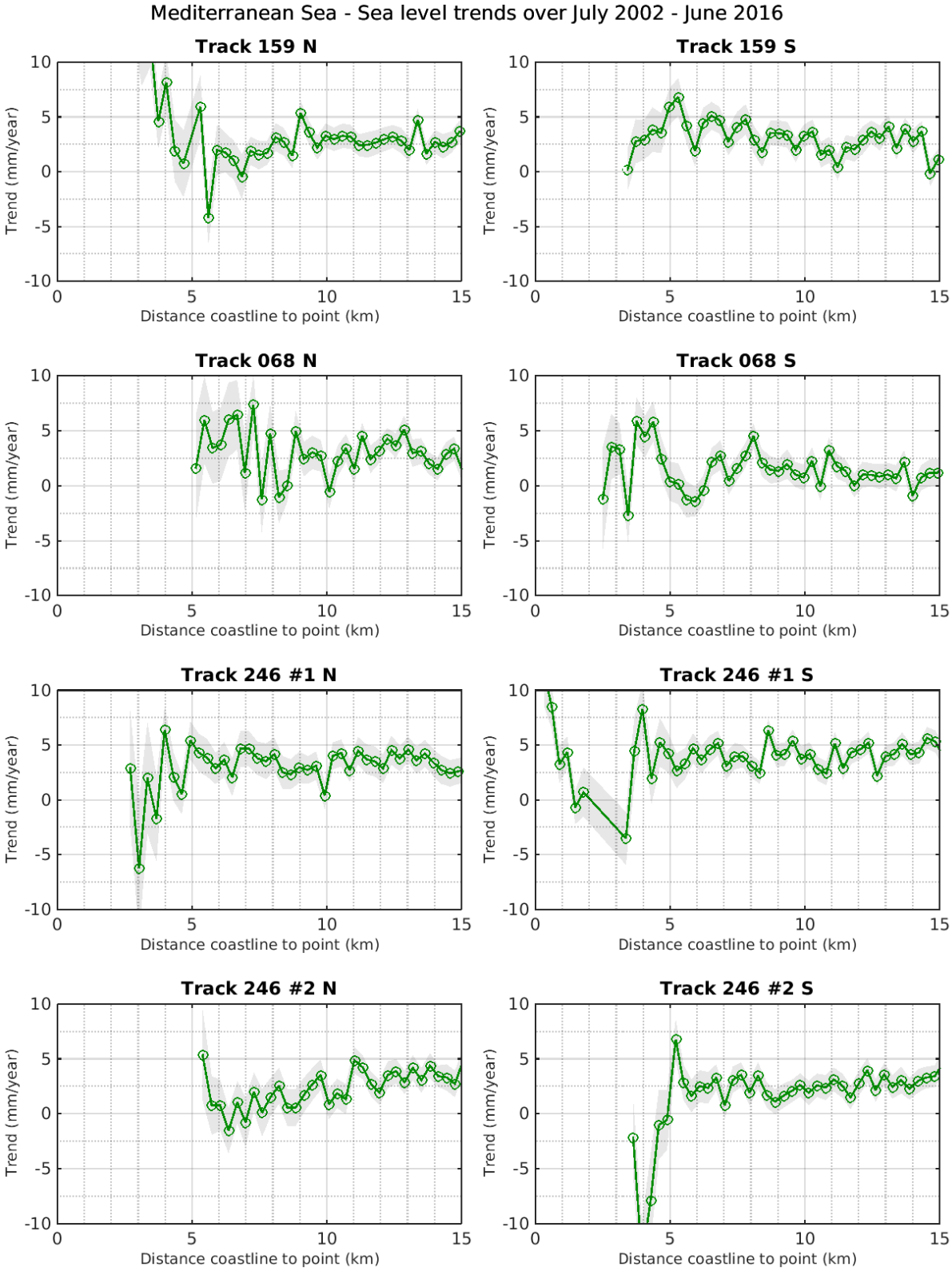

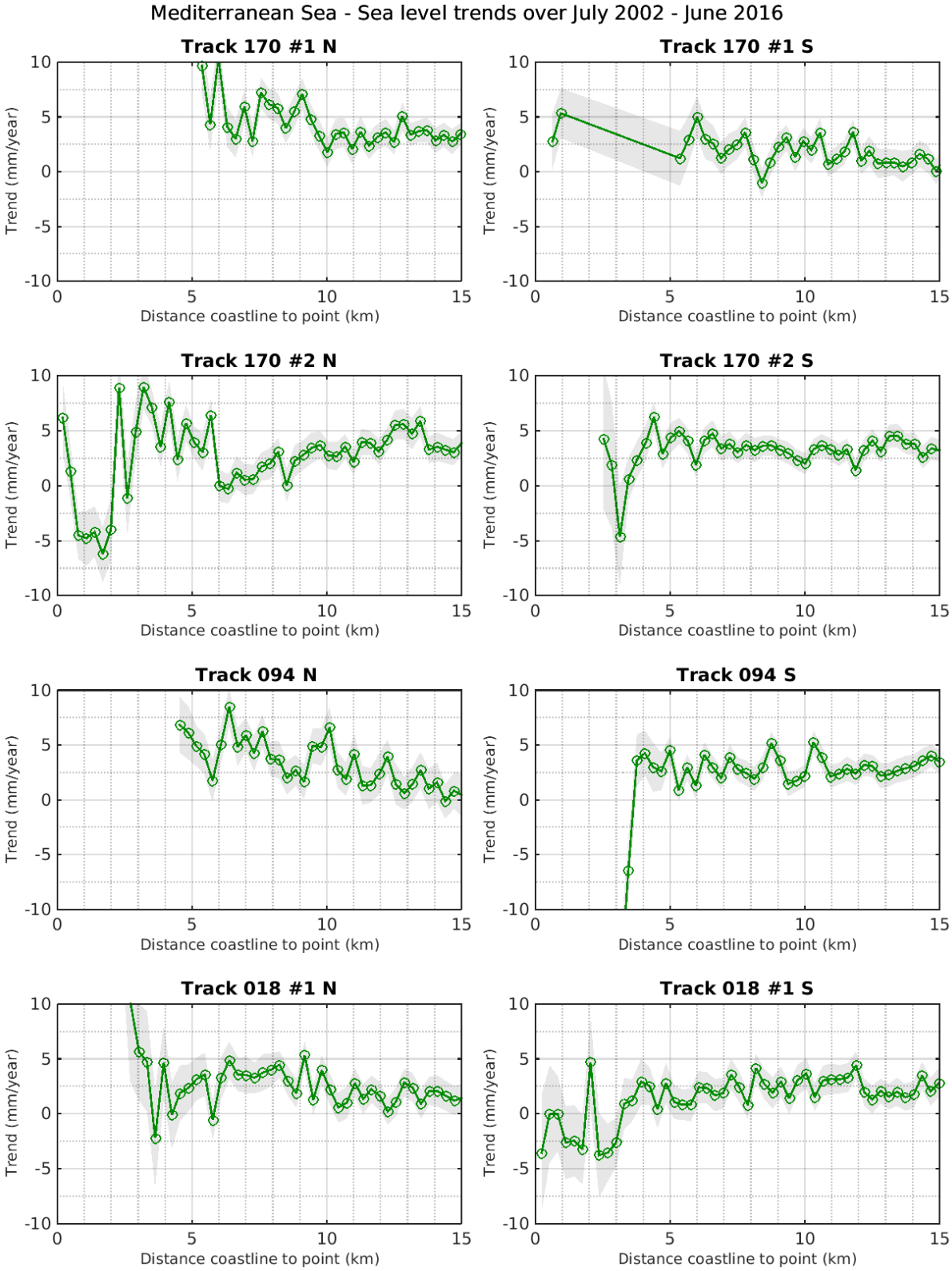

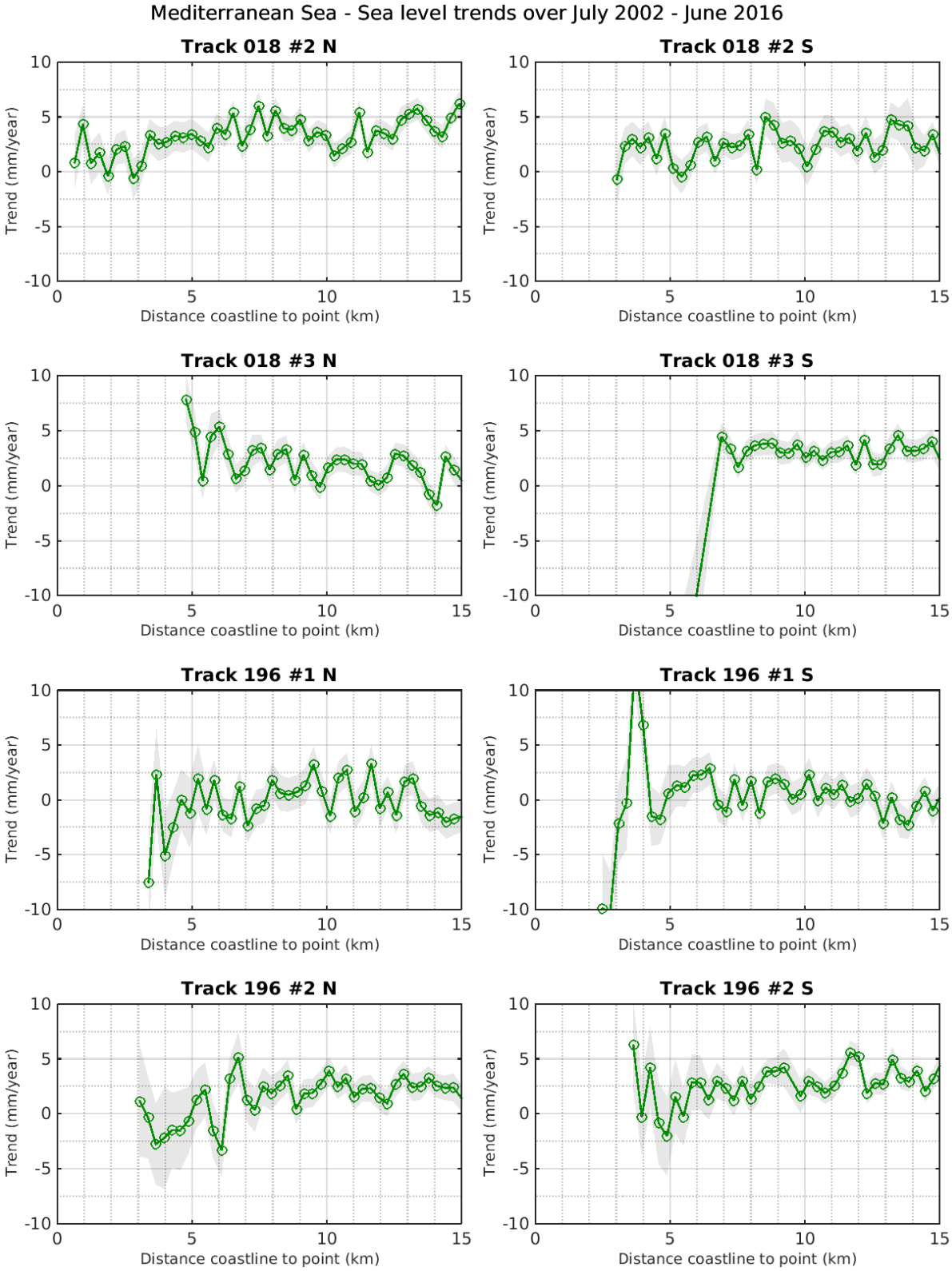

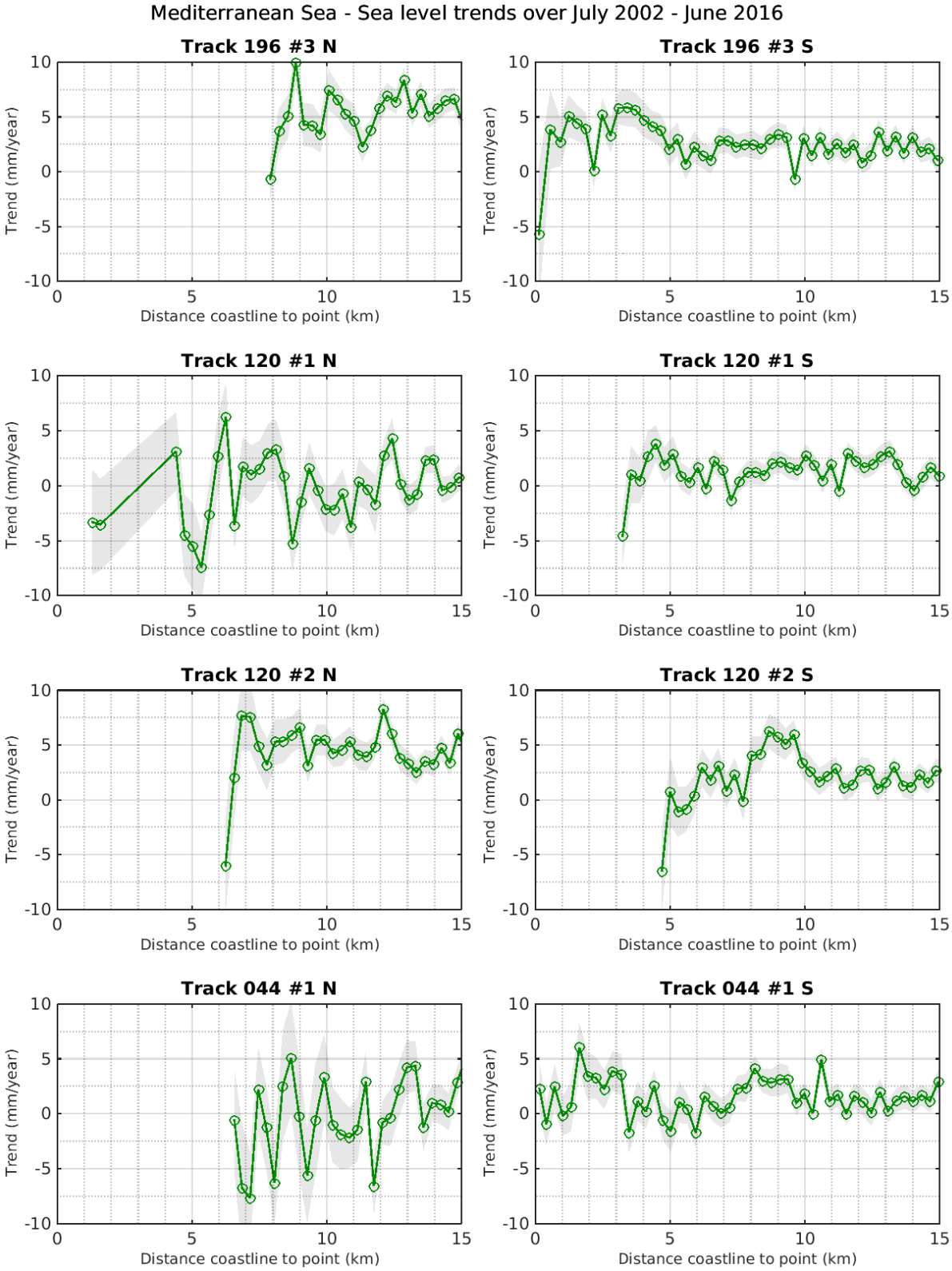

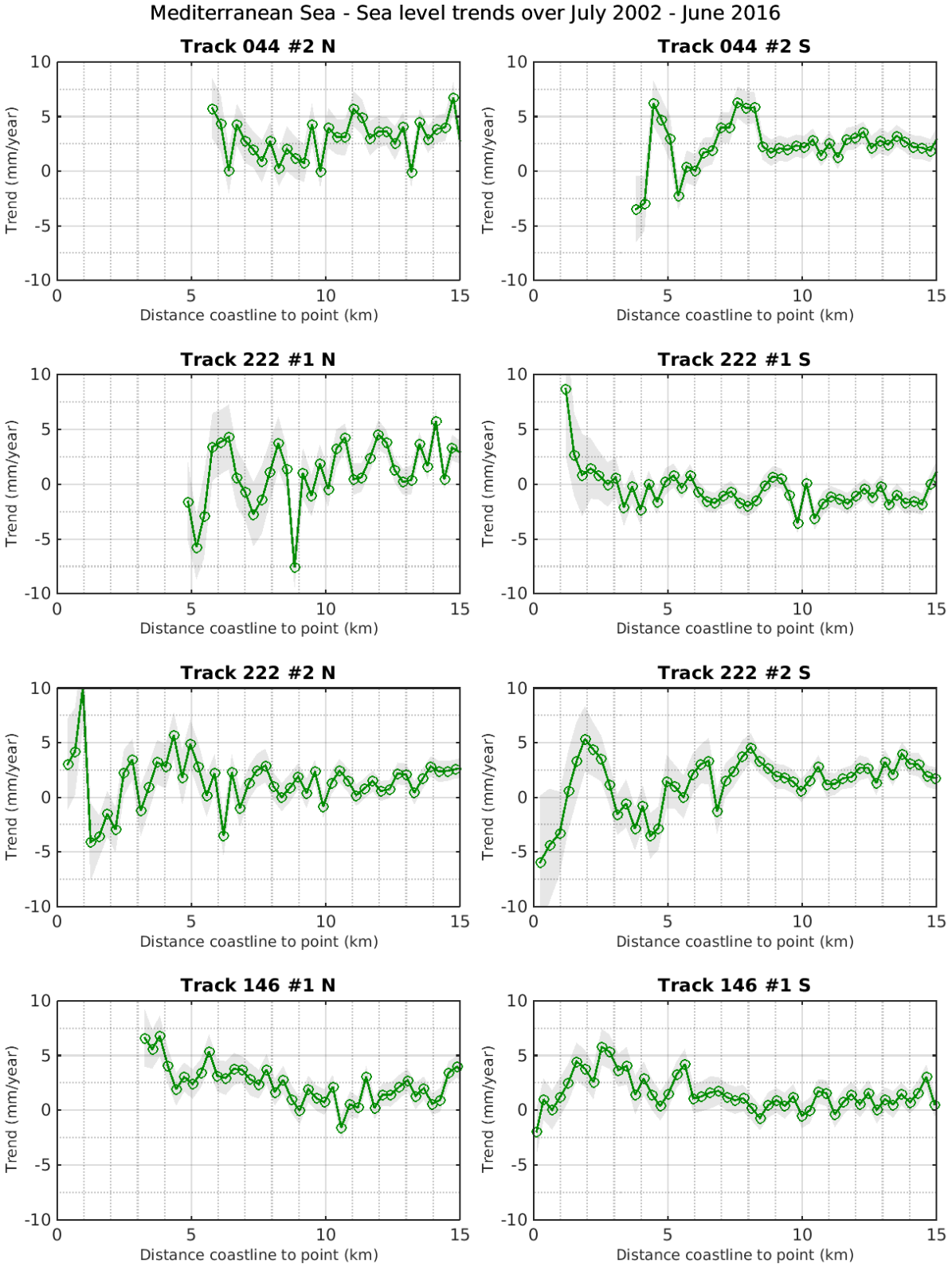

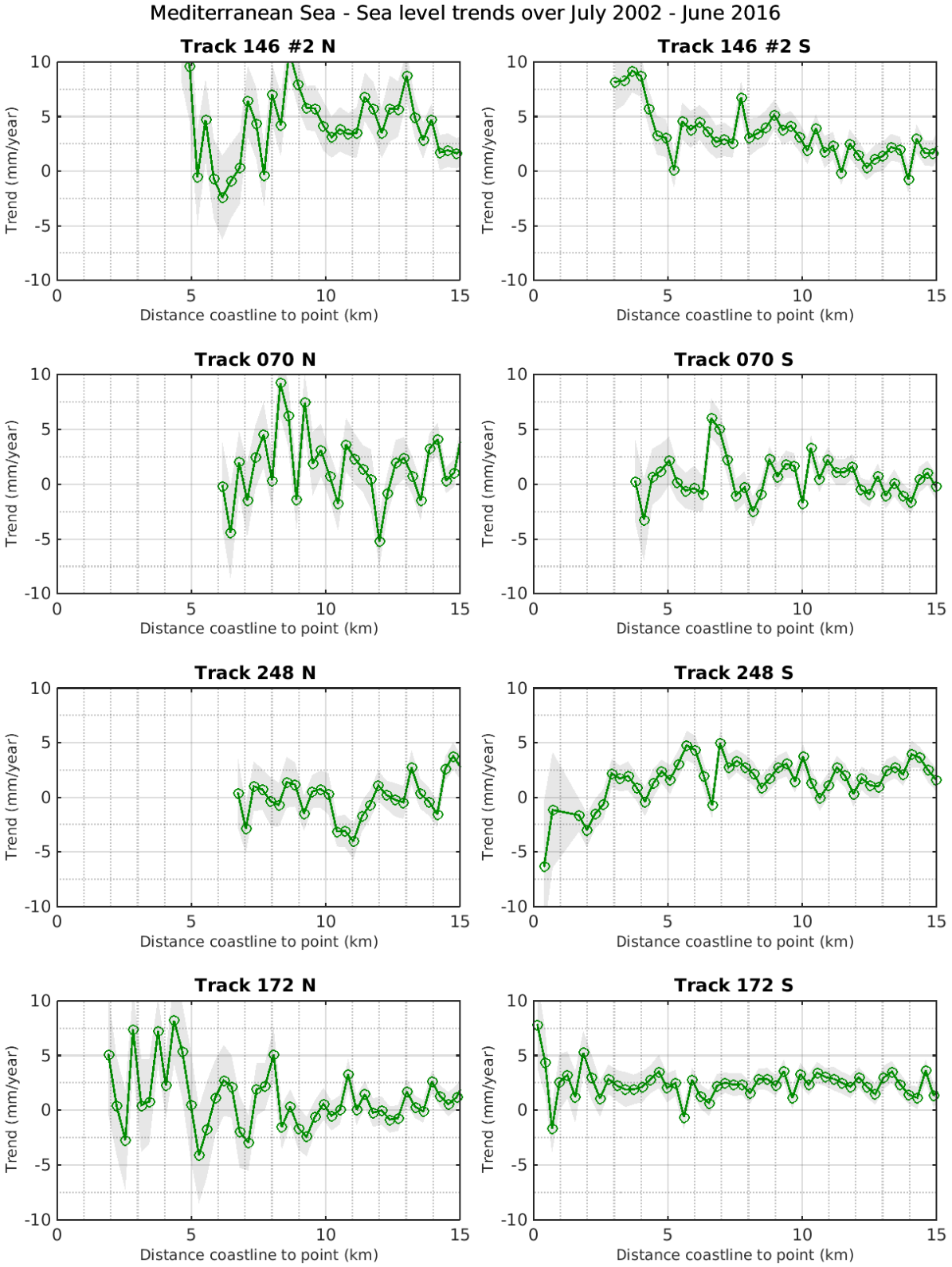

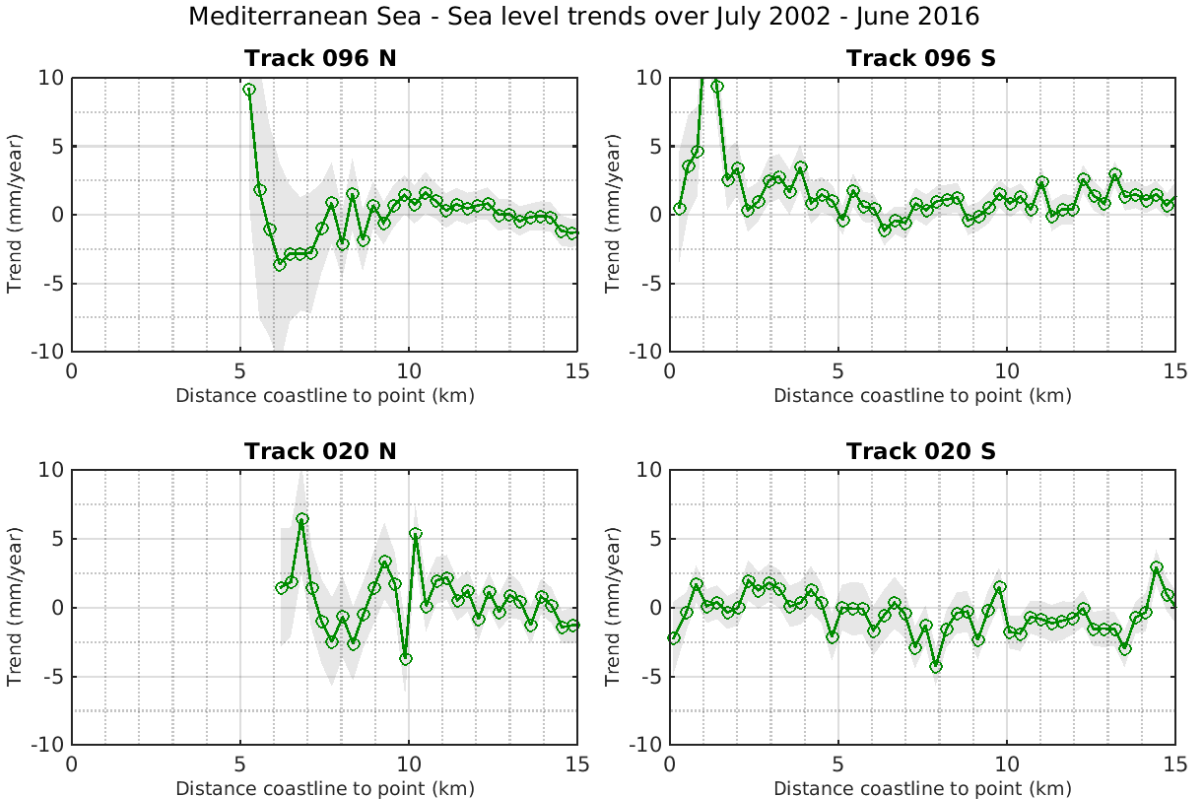

Annex G (MEDITERRANEAN SEA)

Figure 21

Track 020 S (Morocco)

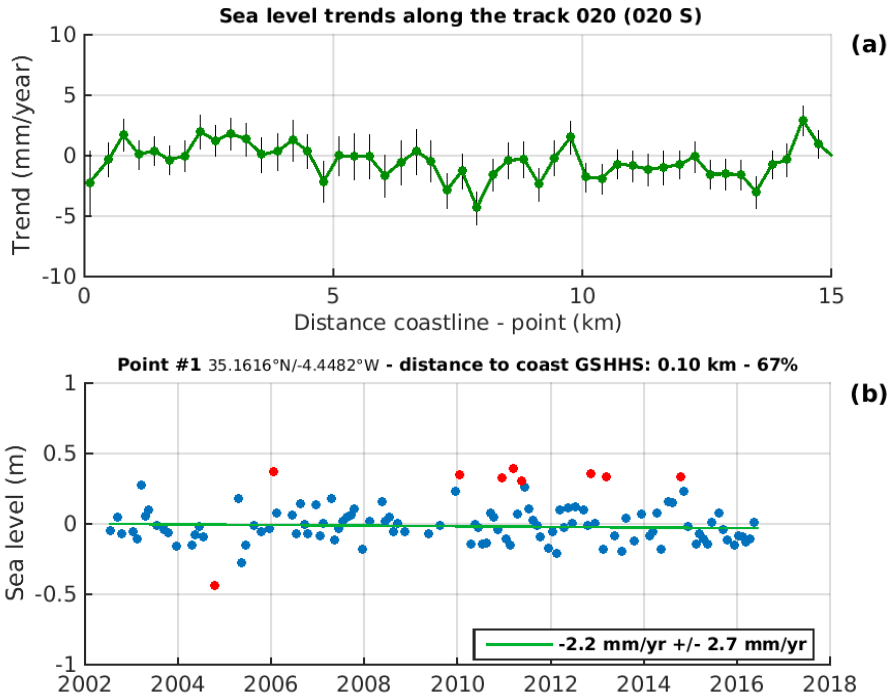

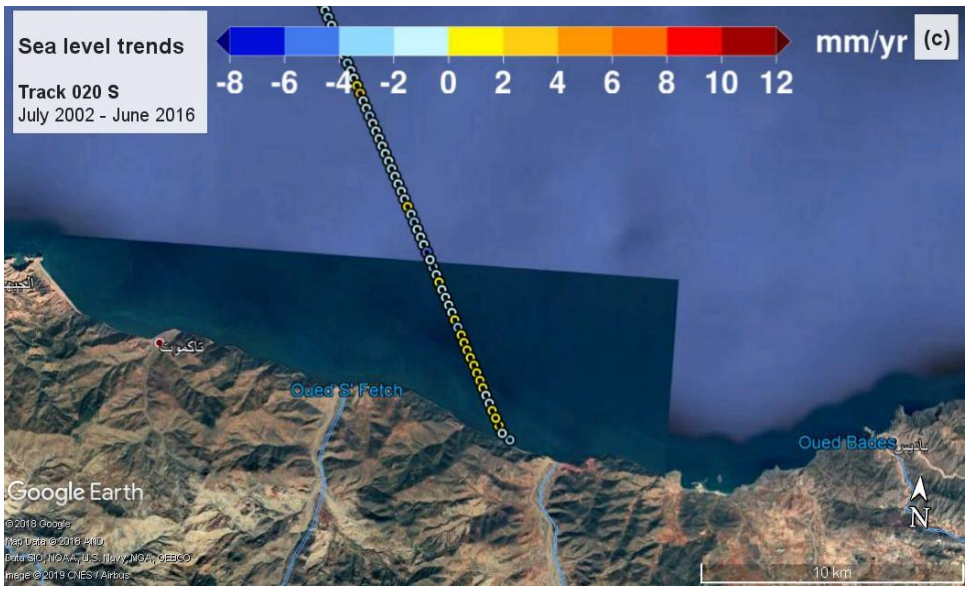

Track 111 N (Spain, Andalousia)

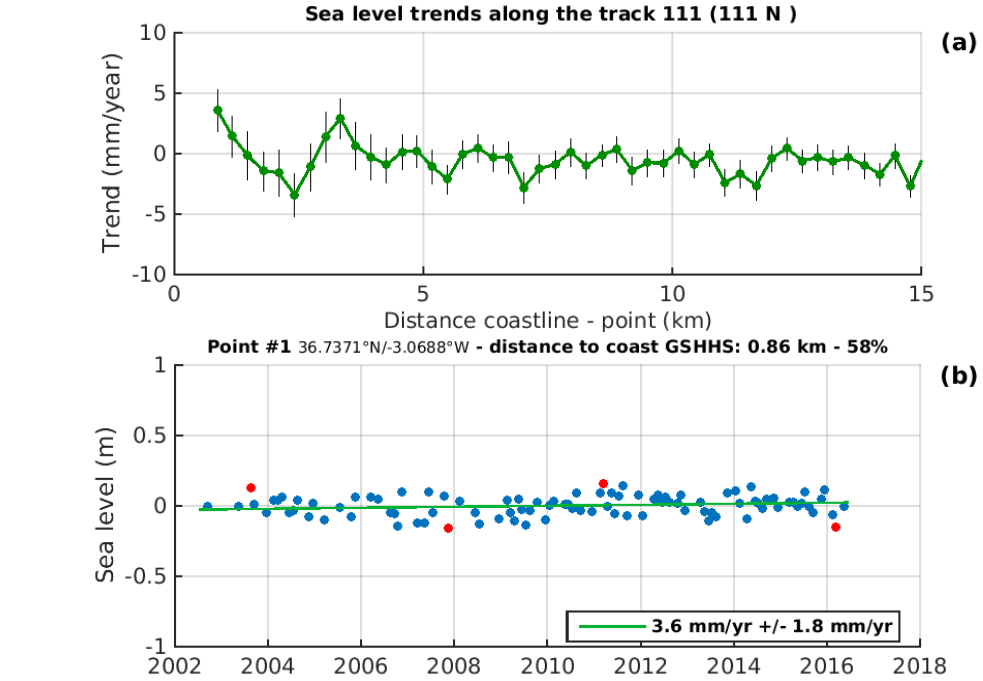

Track 248 S (Algeria, near Algiers)

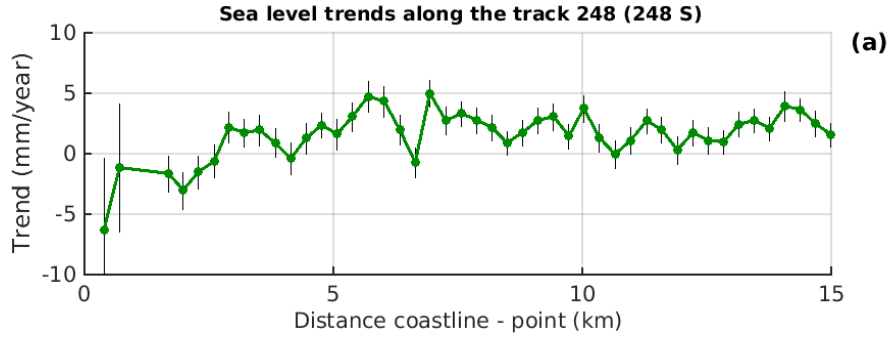

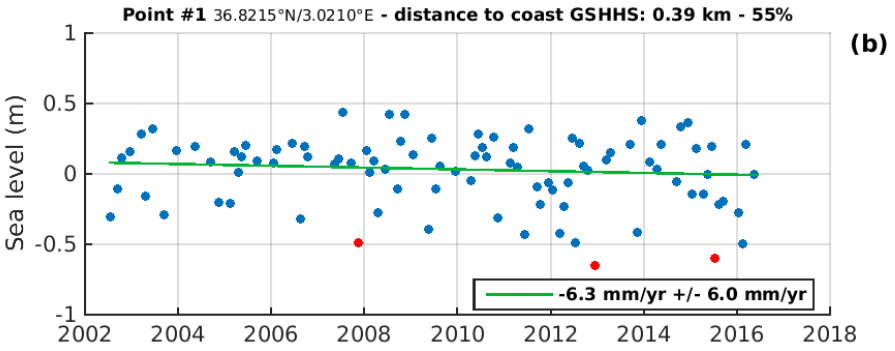

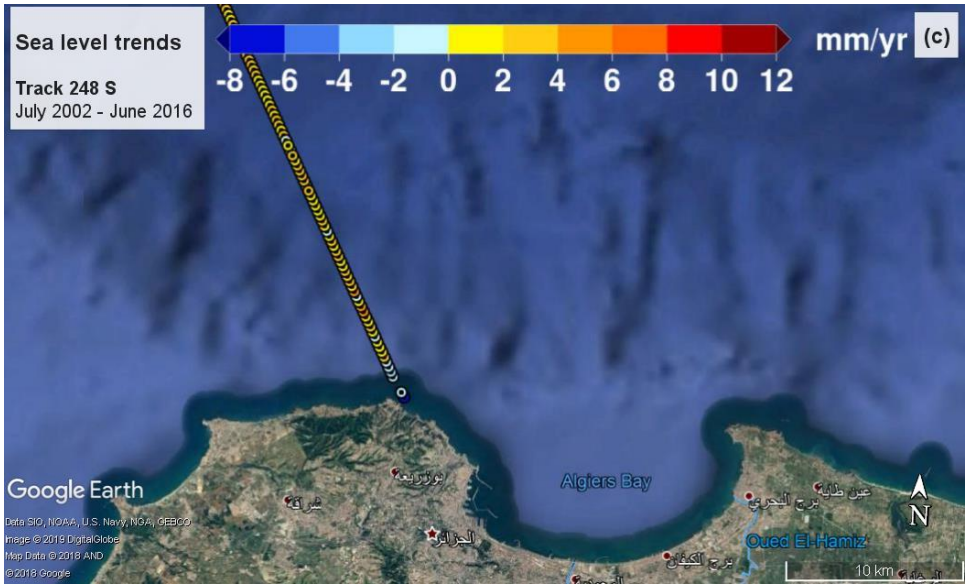

Track 085 #2 N (France, southwest of Corsica)

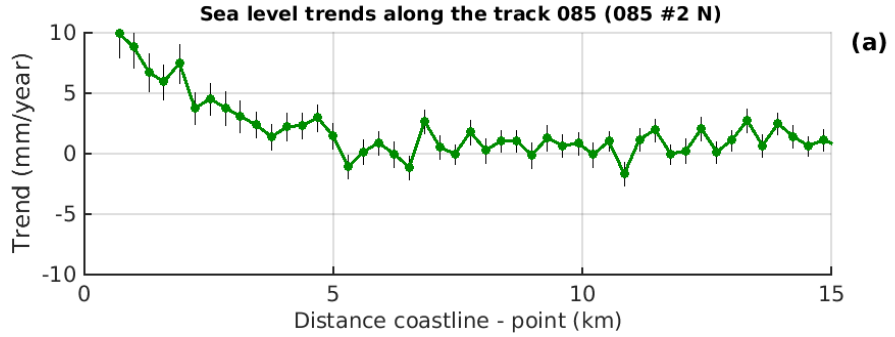

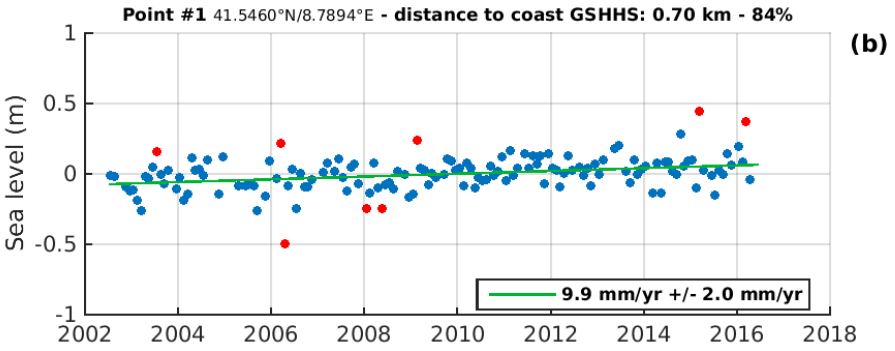

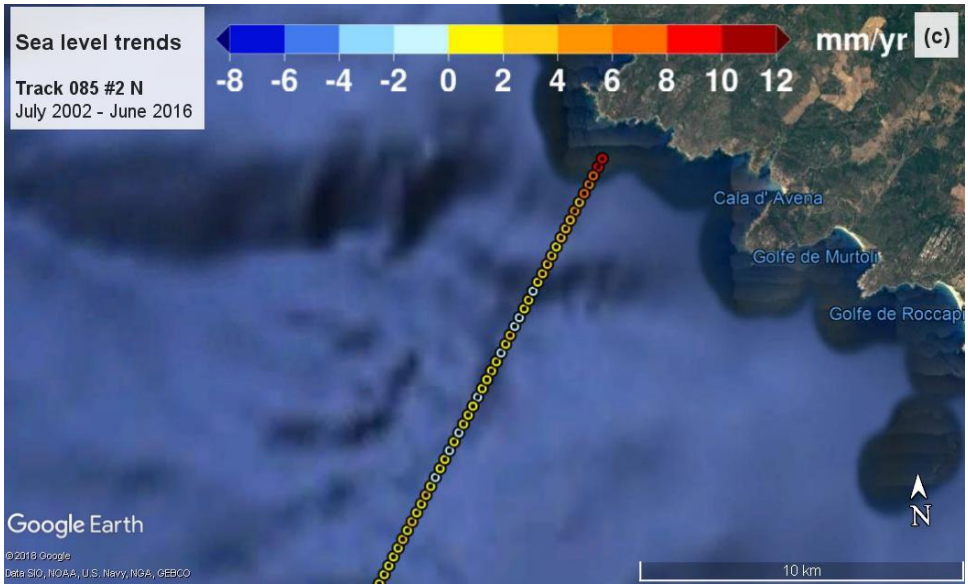

Track 161 #2 N (Italy, near Rome)

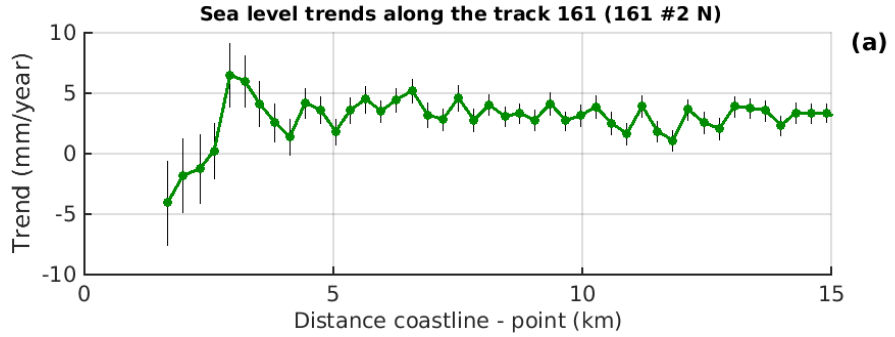

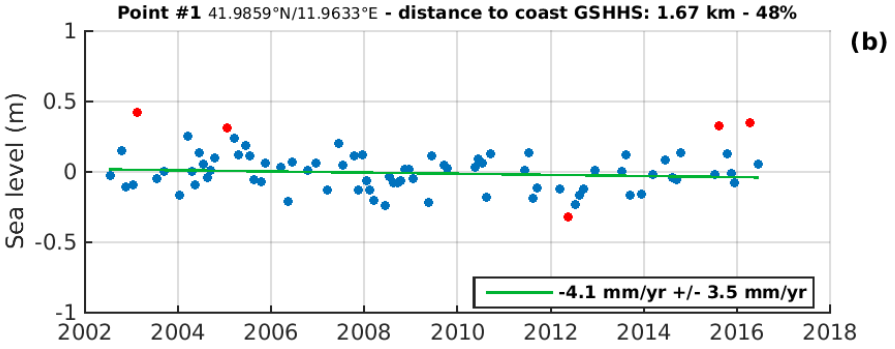

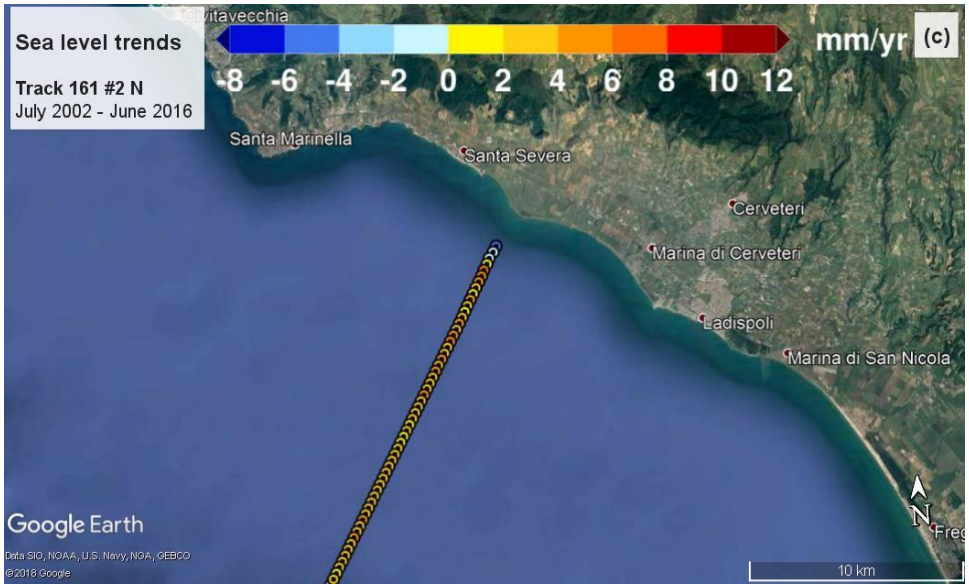

Track 146 #1 S (near Algeria/Tunisia border)

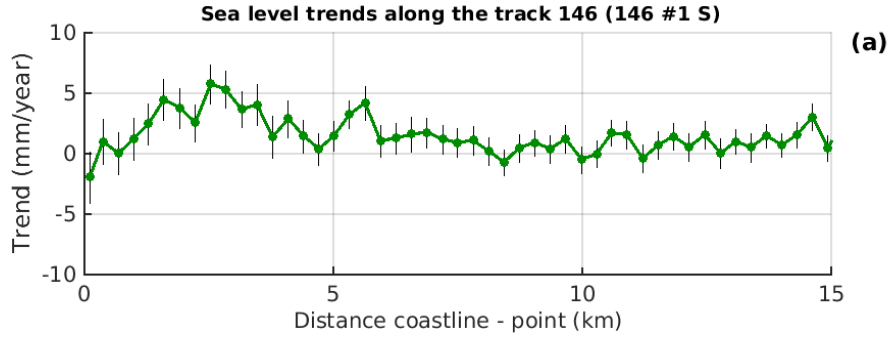

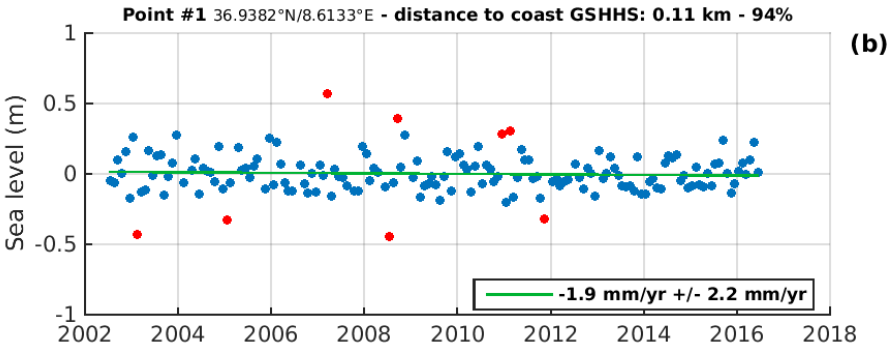

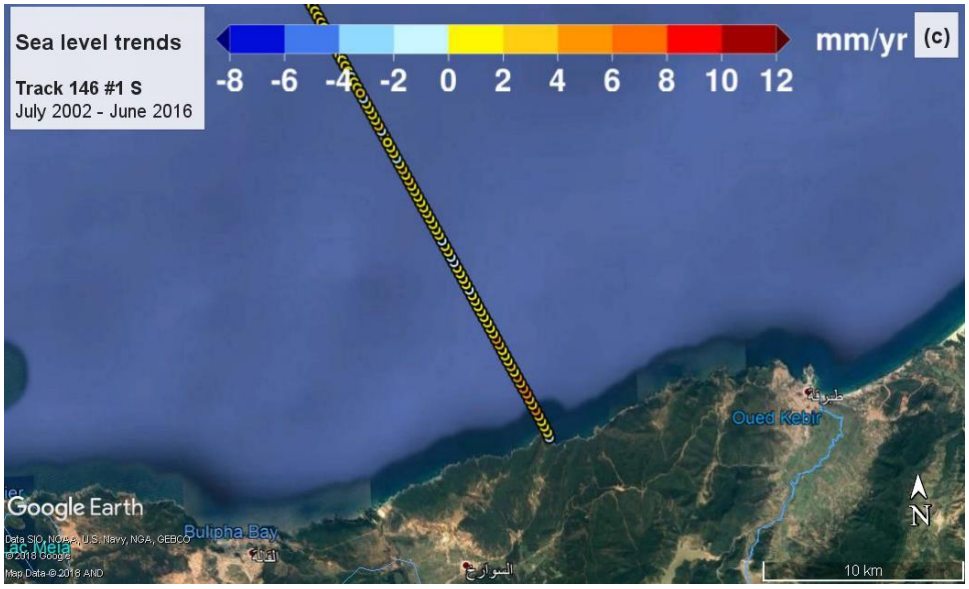

Track 222 #1 S (Italy, north of Sardinia)

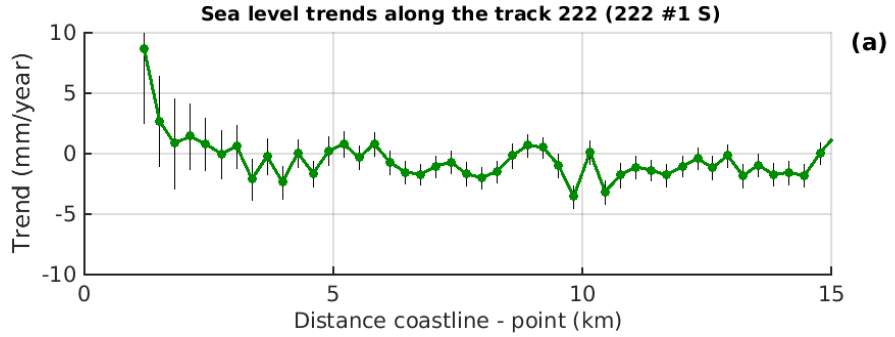

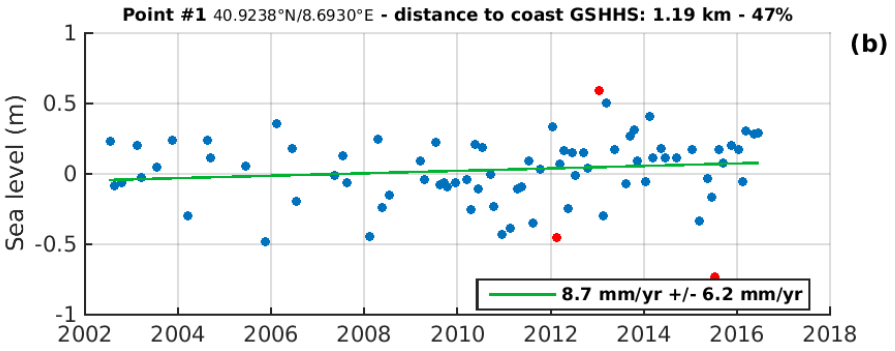

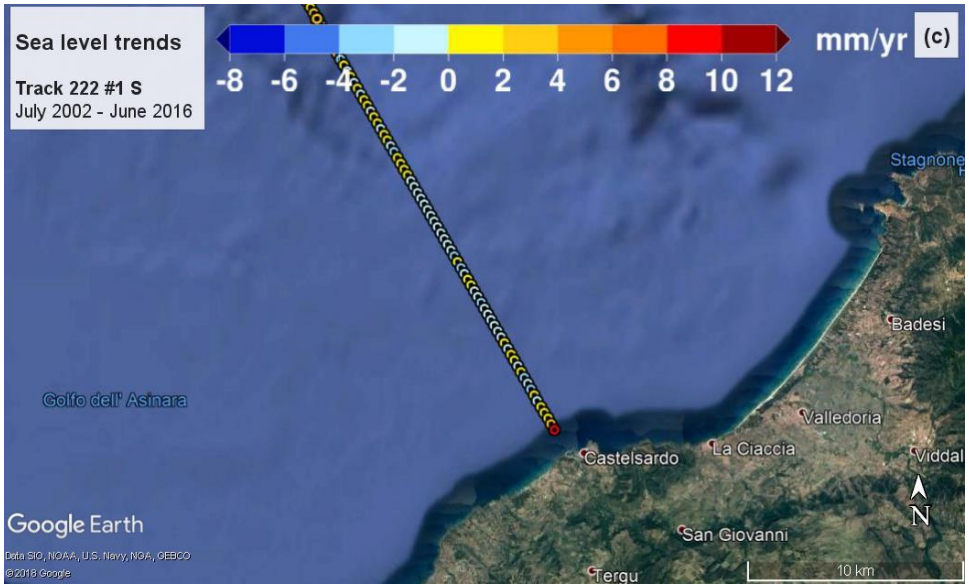

Track 222 #2 S (Libya, east of Tripoli)

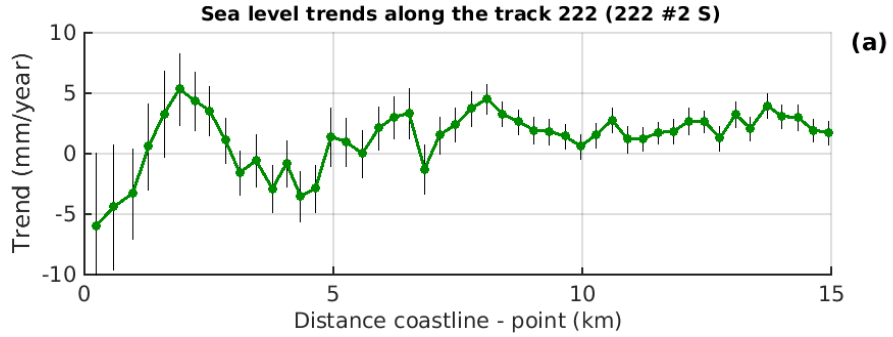

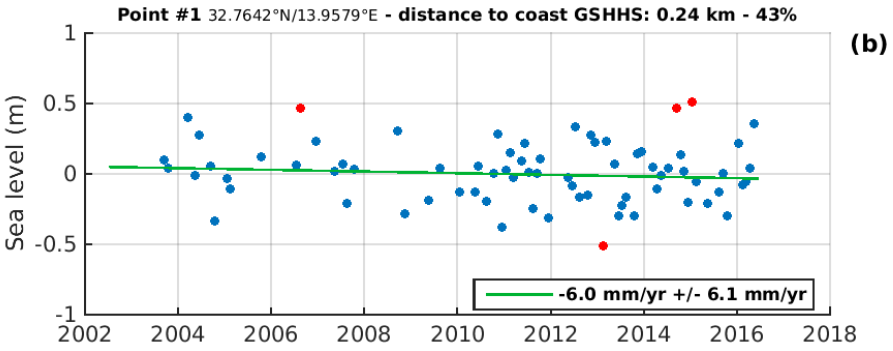

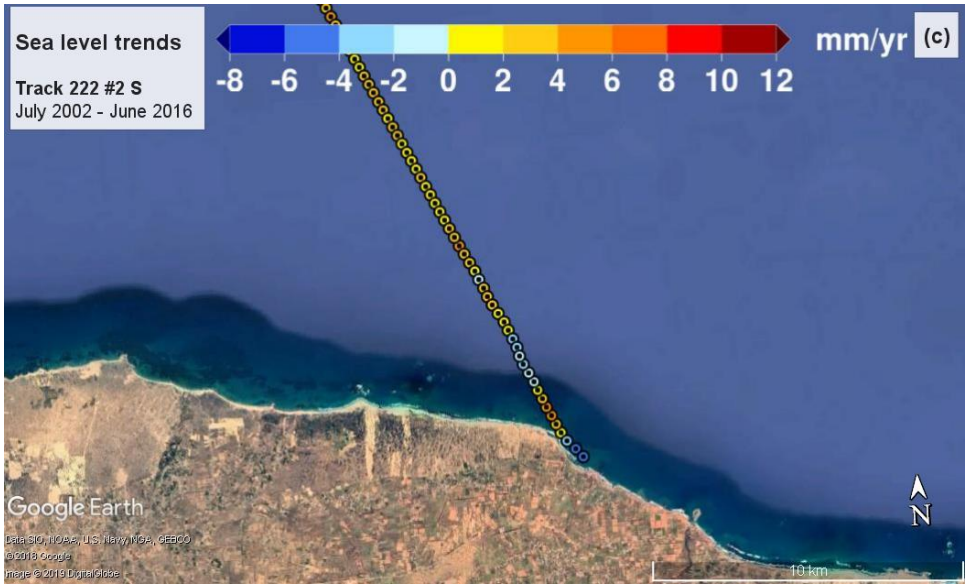

Track 059 #1 N (Croatia, near Dubrovnik)

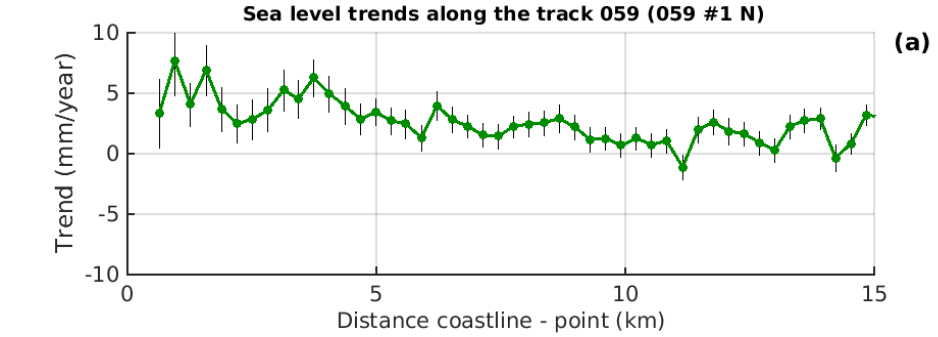

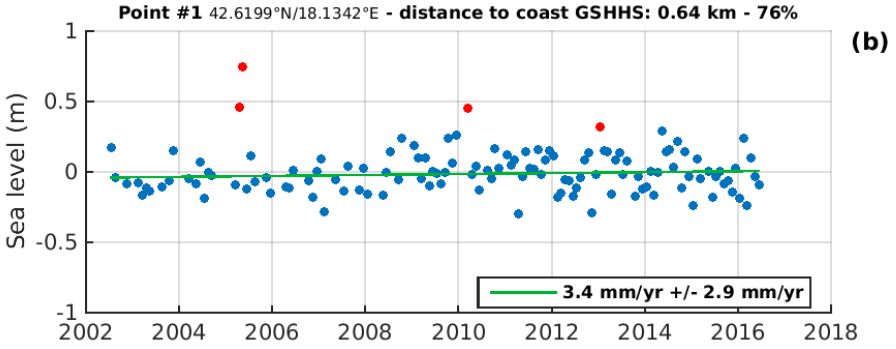

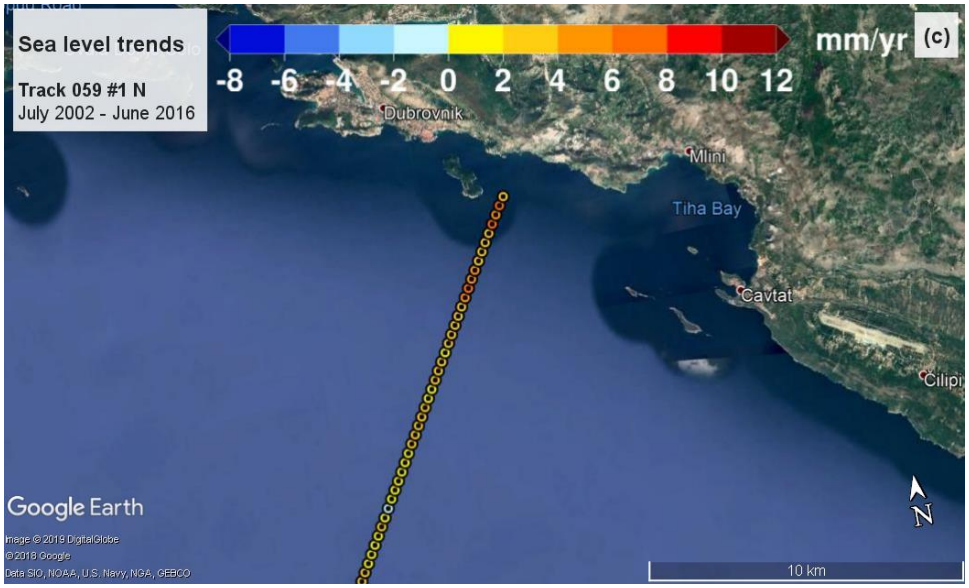

Track 059 #2 N (Italy, north of Calabria)

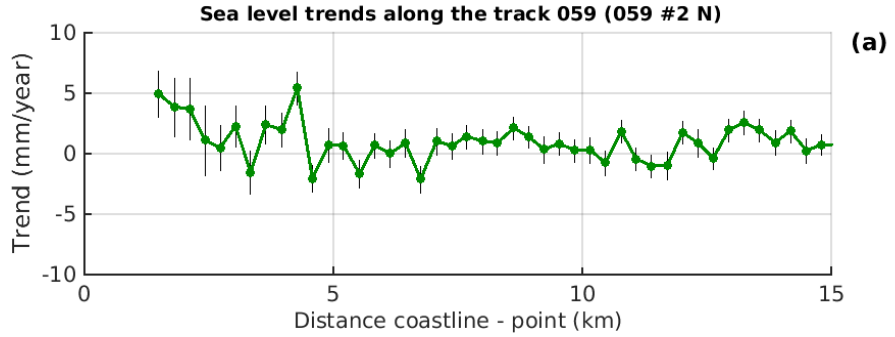

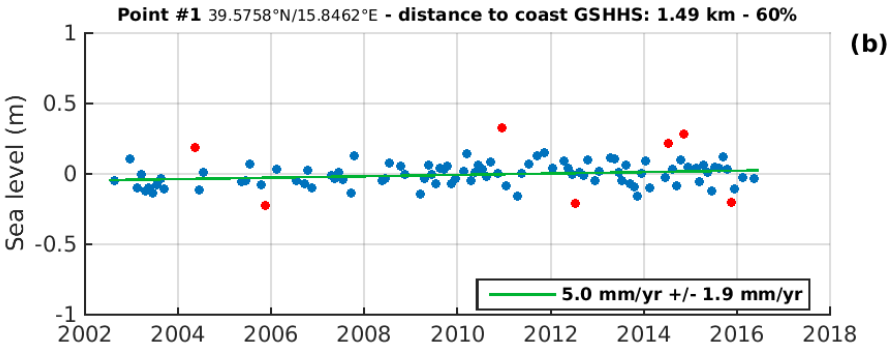

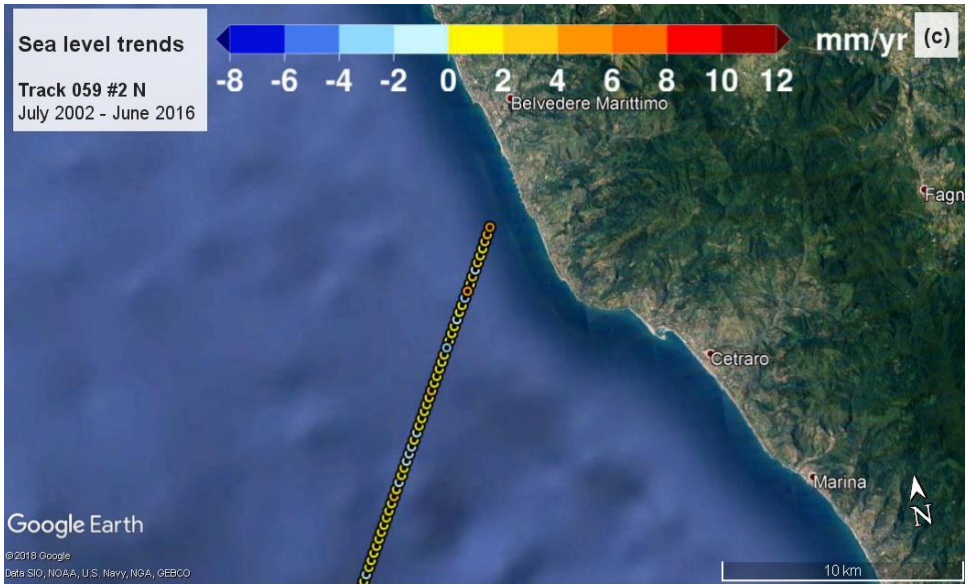

Track 211 #1 N (Greece, Ionian islands)

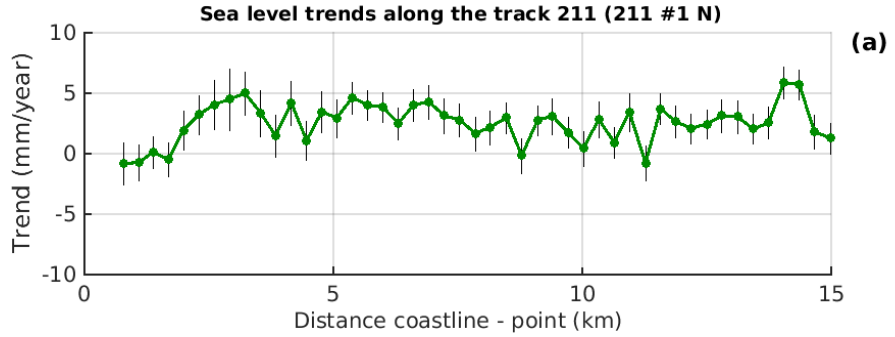

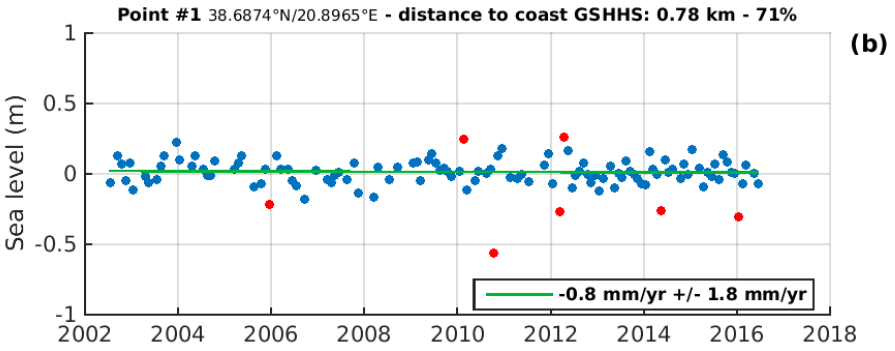

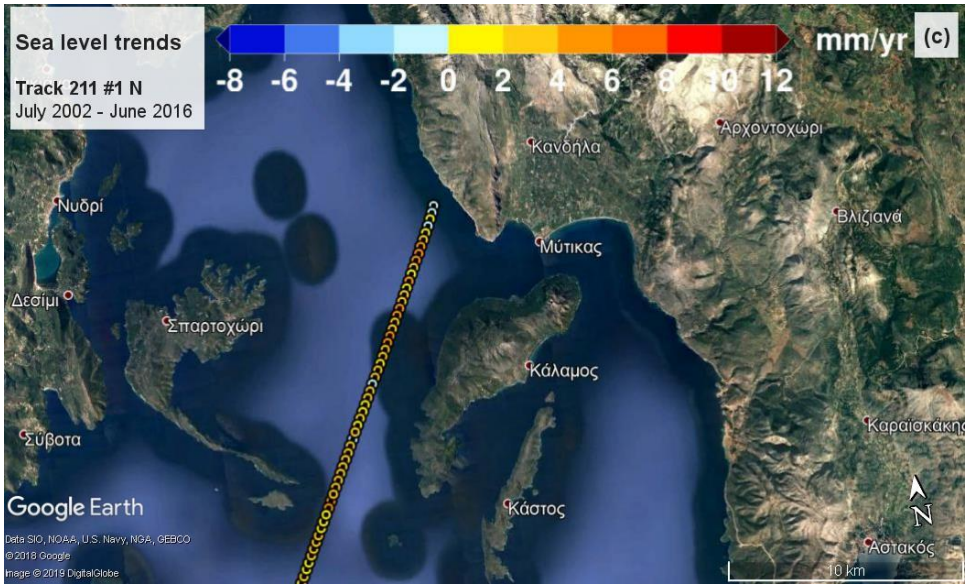

Track 109 #3 N (Greece, south of Crete)

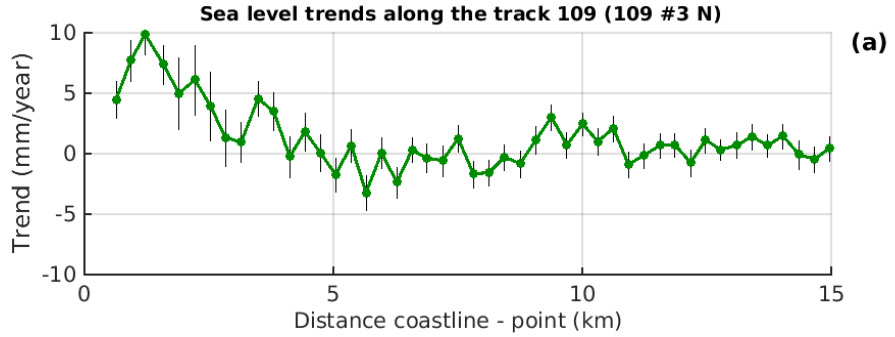

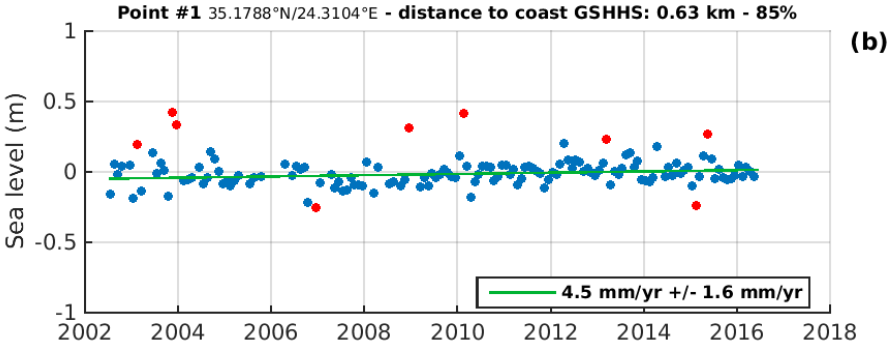

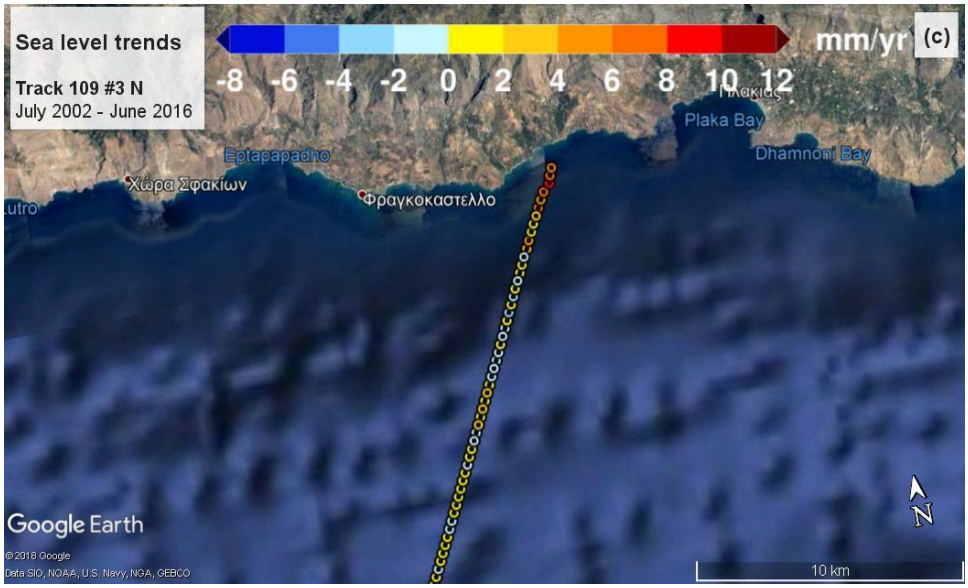

Annex H (results for the Mediterranean and North seas from the University of Bonn)

A. Mediterranean Sea

1. Sea level Trends

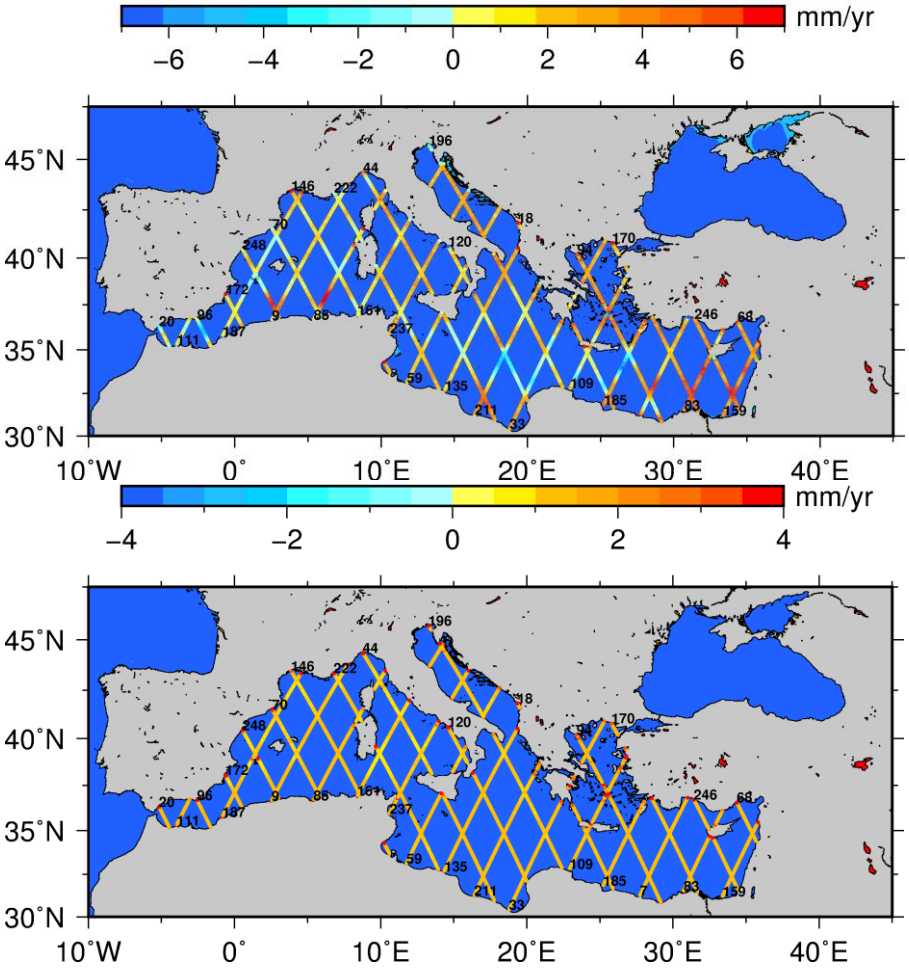

Figure 1: Trend (above) and standard error (below) of the 20Hz points along-track.

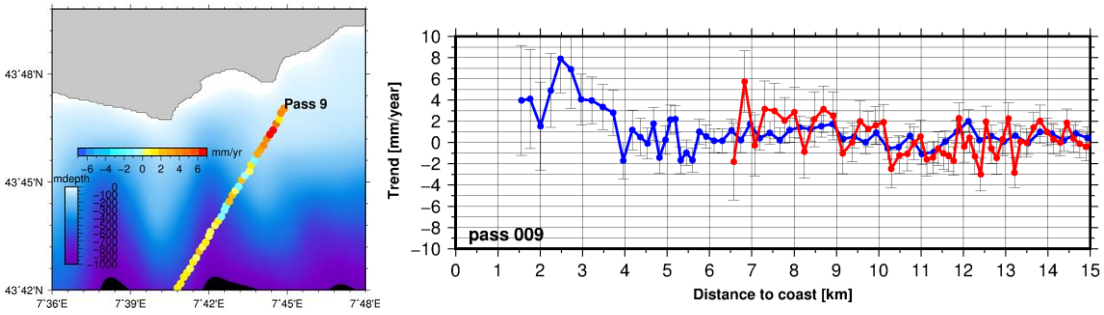

Figure 2: (Right) Trend of 20Hz SLA against distance to coasts for northern (blue) and southern (red) pass 9. (Left) Part of the pass near the northern coast (Sanremo)

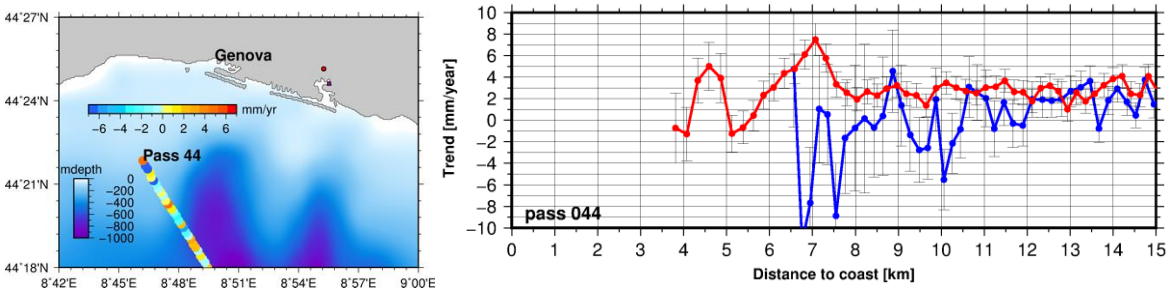

Figure 3: (Right) Trend of 20Hz SLA against distance to coasts for northern (blue) and southern (red) pass 44, (left) Pass near the northern coast (Genova)

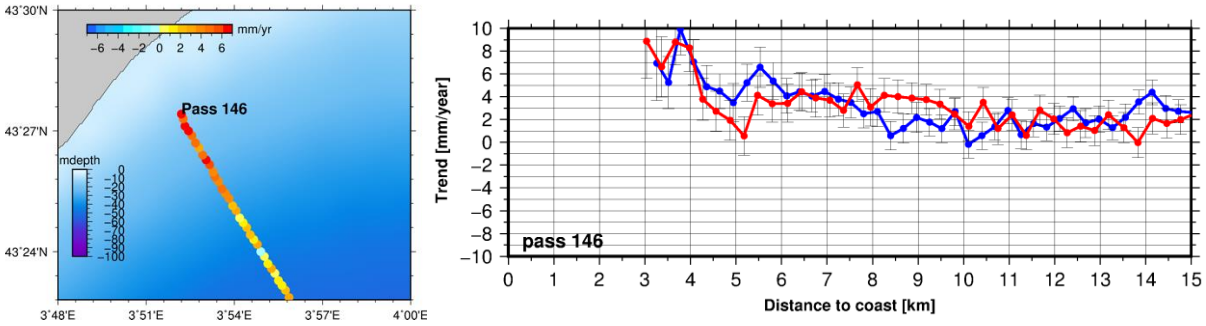

Figure 4: (Right) Trend of 20Hz SLA against distance to coast for northern (blue) and southern (red) pass 146, (left) Pass near the northern coast (Montpellier)

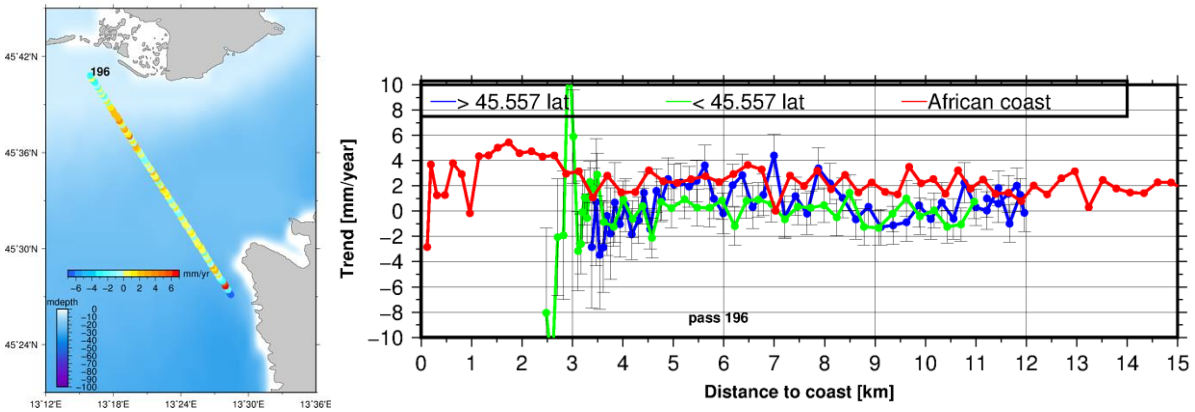

Figure 5: (Right) Trend of 20Hz SLA against distance to coasts for northern (blue) and southern (red) pass 196, (left) Part of the pass near the northern coast (Trieste)

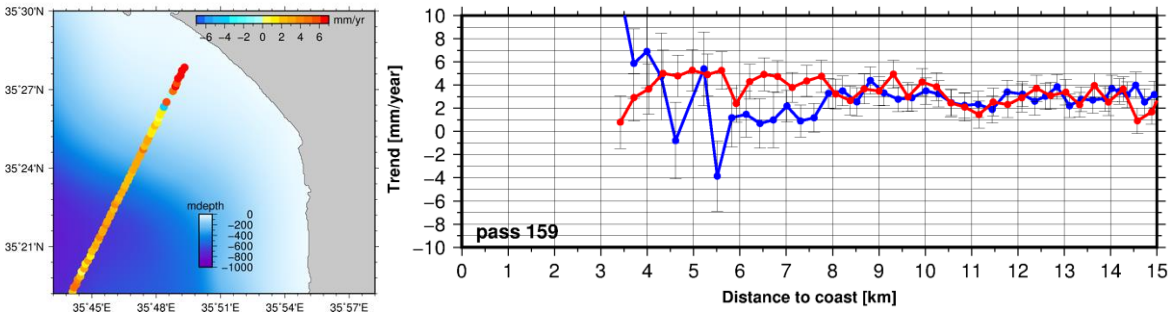

Figure 6 (Right) Trend of 20Hz SLA against distance to coasts for northern (blue) and southern (red) pass 159, (left) Part of the pass near the northern coast (Latakia)

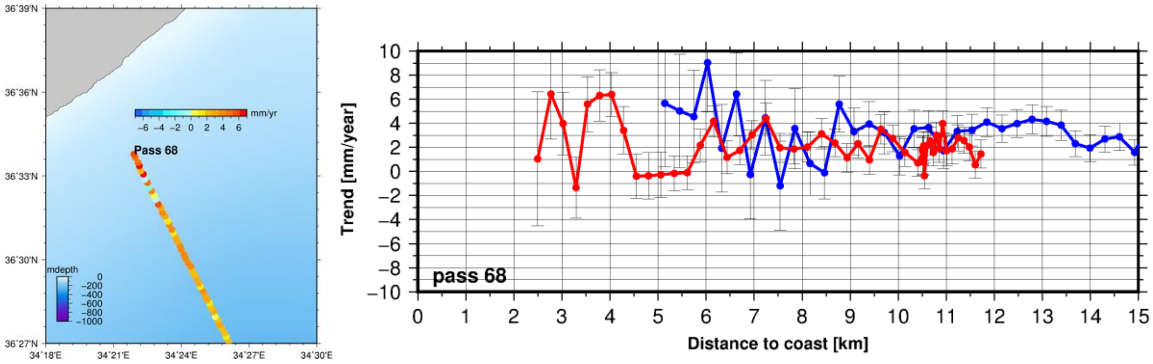

Figure 7: (Right) Trend of 20Hz SLA against distance to coasts for northern (blue) and southern (red) pass 68, (left) Part of the pass near the northern coast (Mersin)

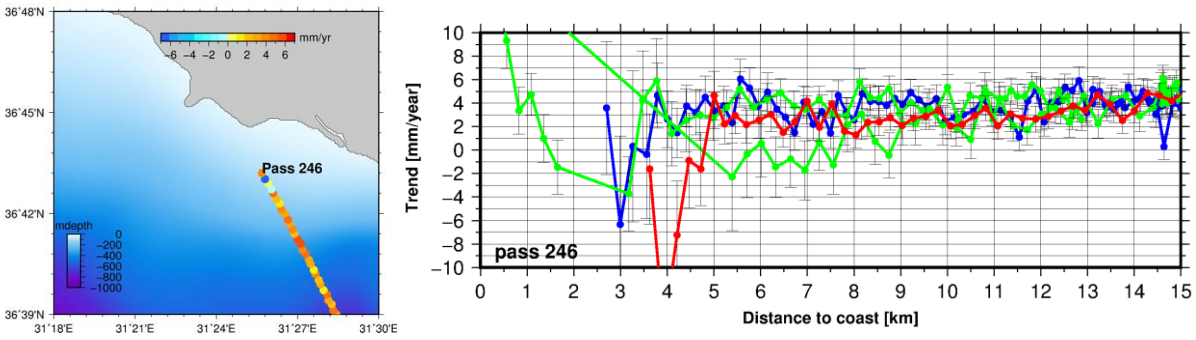

Figure 8: (Right) Trend of 20Hz SLA against distance to coast for northern (blue), southern (red) and Cypros (green) sections of pass 246, (left) pass near northern coast (Manavgat)

The trends of the points distant more than 3 km from coast are homogeneous in values and positive, while trends of points near to coast assume more different values (Fig. 9 and 10). Analysis of selected tracks in Figures 2 to 8 confirm a higher spatial variability of the trend approaching to the coast. The trends could be affected by coastal currents and by the steric effect. Very near to coast (< 5 km) however, higher and lower trends are to be considered carefully, as possibly related to land contamination in the altimetric measurements.

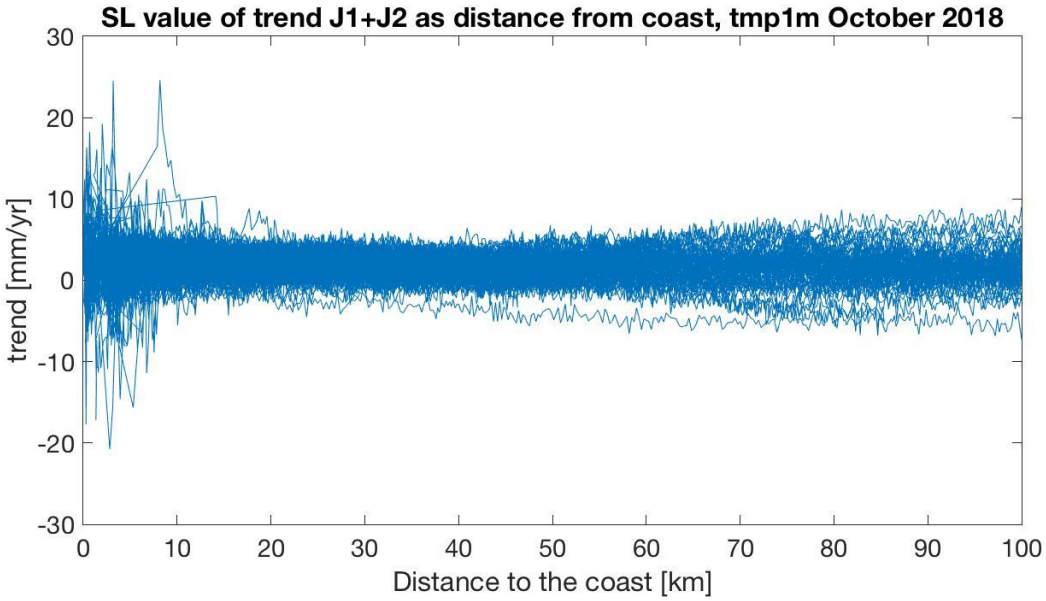

Figure 9: Trend of 20Hz SLA against distance to coast for the complete Mediterranean basin

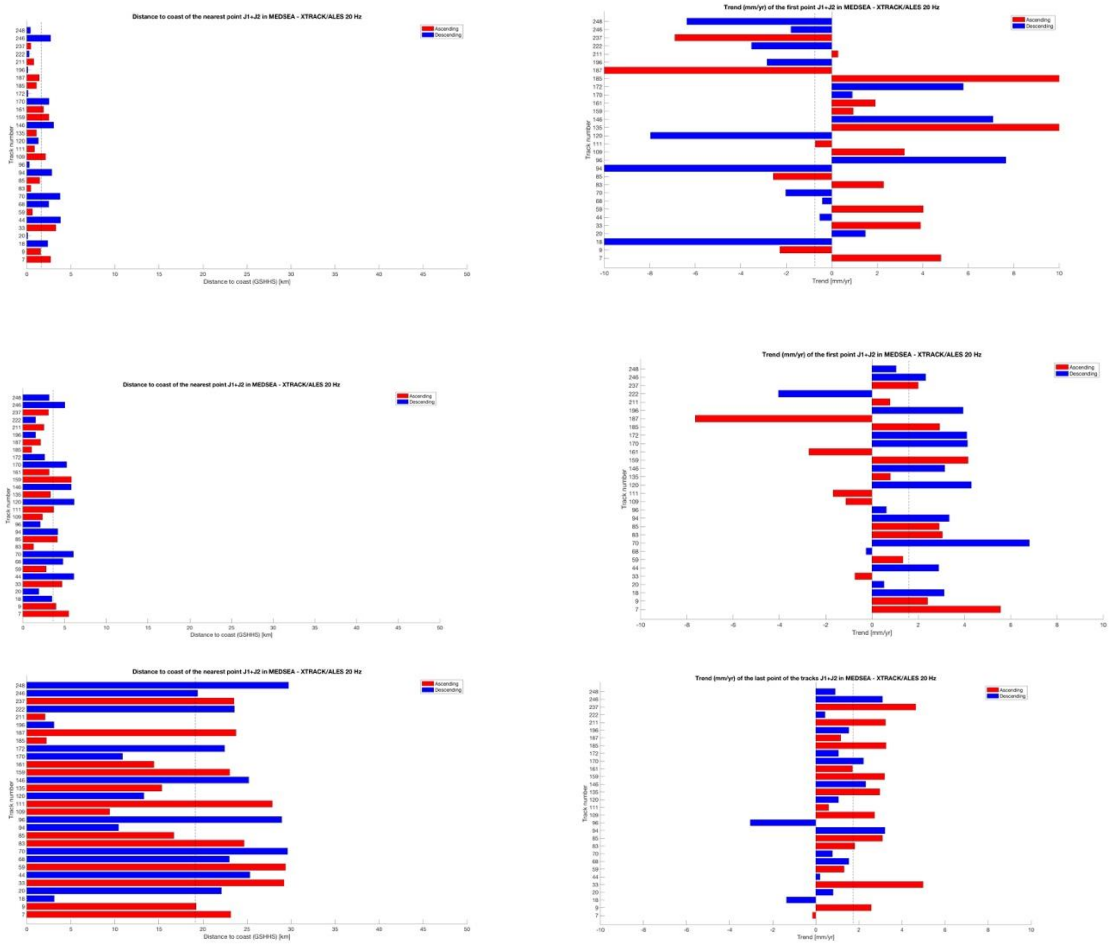

Figure 10: Distance to coast (left) and trend (right) of 20Hz SLA obtained by choosing respectively the 1st, 10th and 100th points along each pass

2. Valid points from comparison between altimetry and tide gauges

We have used the J2 cycles corresponding to a valid value of the Trieste tide gauge station (1 hour sampling). We finally use observations from cycle 21 to cycle 252 for a total of 227 cycles, which are the same for all the three datasets. The pass number is 196.

From Figure 11 we observe that the XTRACK/ALES (blue) dataset has less data available near land compared to the STAR (red), which are derived from the waveforms contained in the SGDR.

The quality of XTRACK/ALES and PODACC/ALES is compared using two different methodologies.
First, we compute for each single 20 Hz point the percentage of the cycles which can be used to provide a correlation between altimetric and in-situ tide gauge time-series larger than 0.9. From Figure 12 we see that XTRACK/ALES has in the open sea time-series less cycles with useful data compared to PODACC/ALES and STAR. At few locations near the Italian coast the XTRACK/ALES time-series contain more points than PODAAC/ALES. STAR has generally more points available.

Secondly, we compute correlation and standard deviation between a near situ station and each of the 20Hz altimetric time-series. Altimeter data are here uncorrected for ocean tide and dynamical ocean correction to be directly compared to tide gauge data. We first remove any outliers by applying a selection criteria, consisting in an outlier detection criteria on the SLA (|SLA| > 3.5 m) and in a minimum number of cycles with valid data at each measurement position (at least 10 cycles). See Figure 13 (top) for the number of cycles retained after this selection criteria. Note that this selection criteria is different from the one applied in Fig. 12.
Correlation and standard deviation of the differences with in-situ data are shown in Figure 13 (center and bottom). From Figure 13 (top) we see that XTRACK/ALES has in the open sea time-series less data compared to PODACC/ALES and STAR. With the suggested selection criteria, correlation and standard deviation of XTRACK/ALES is superior to PODACC/ALES and comparable to STAR. However, PODACC/ALES provides a larger number of cycles with meaningful data according to our selection criteria. In summary, the XTRACK/ALES 20 Hz time-series contain less data for a given space position and some of the sea space position are all NaN in the release of October 2018.

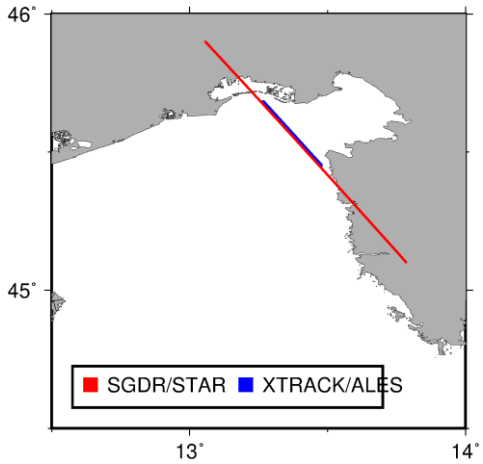

Figure 11: Location of 20 Hz points along track for pass 196 near Trieste

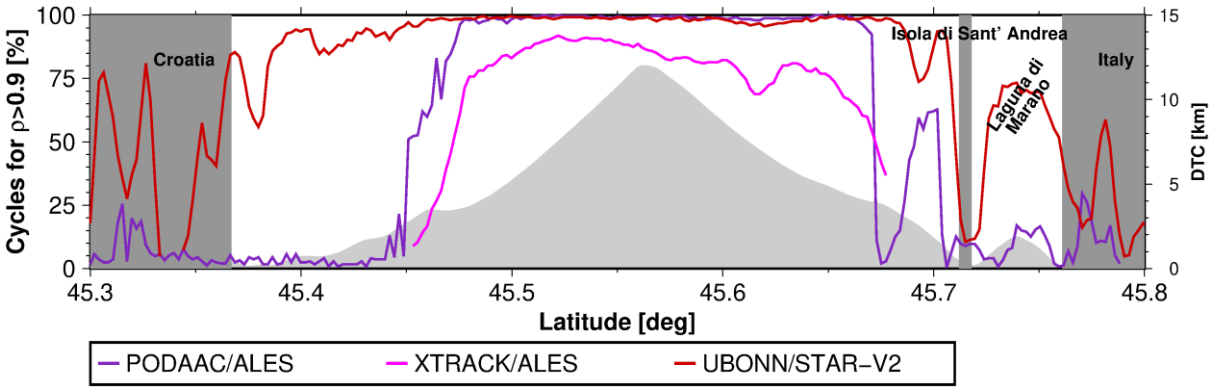

Figure 12: Percentage of retained cycles to achieve a correlation with TG of at least 0.9. Study site in Gulf of Trieste Pass 196 (see also Roscher et al. 2017)

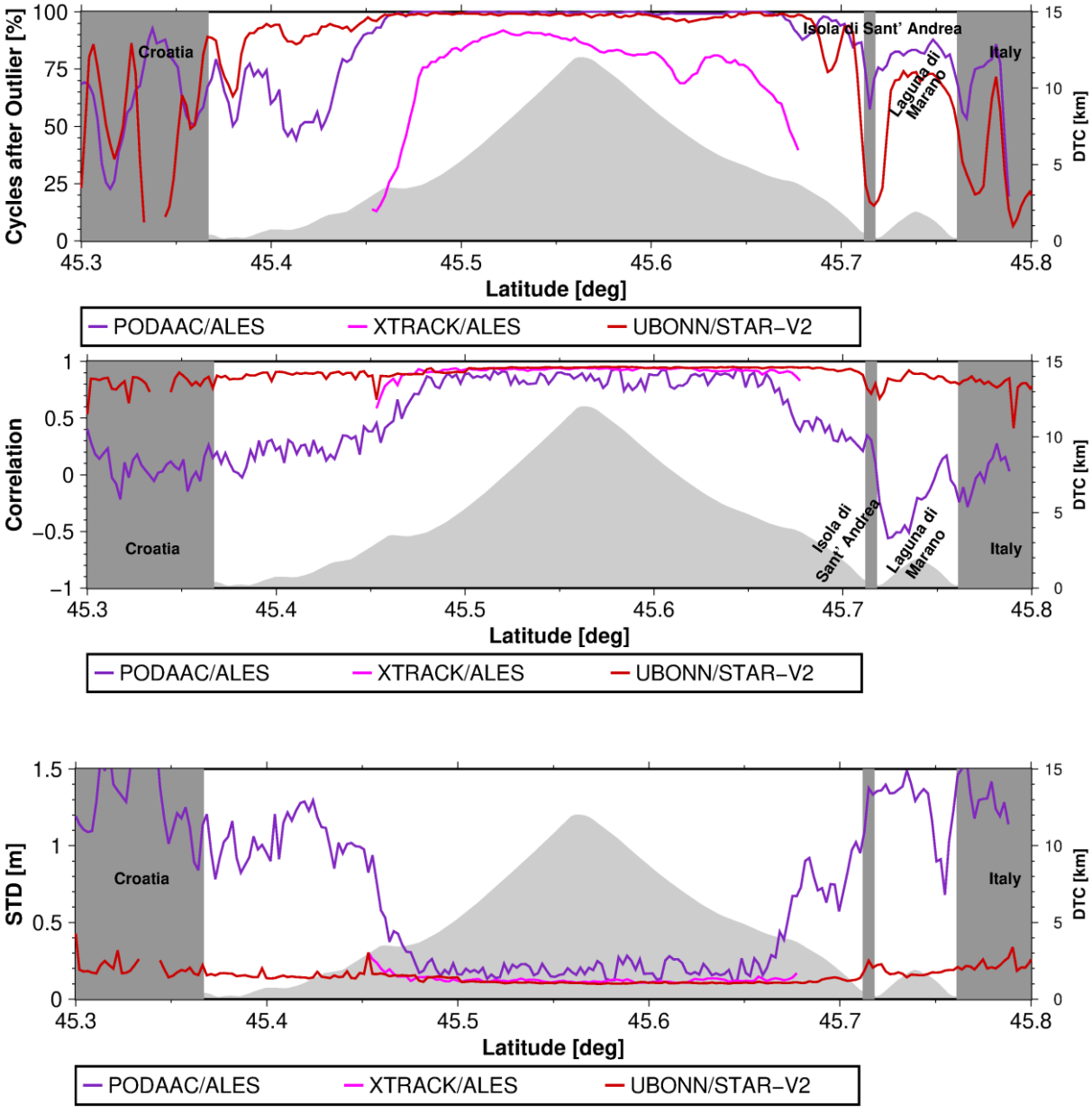

Figure 13: Second comparison: correlation (middle) and standard devation of differences (bottom) for cycles retained (top) after chosen selection criteria (|SLA| > 3.5 m and minimum number of 10 cycles requirement. Study site in Gulf of Trieste Pass 196 (see also Roscher et al. 2017)

B. North Sea

1. Sea level Trends

In the North Sea, the trends of the points distant more than 3 km from coast are homogeneous in values, while trends of points near to coast assume more different values (Fig. 14).

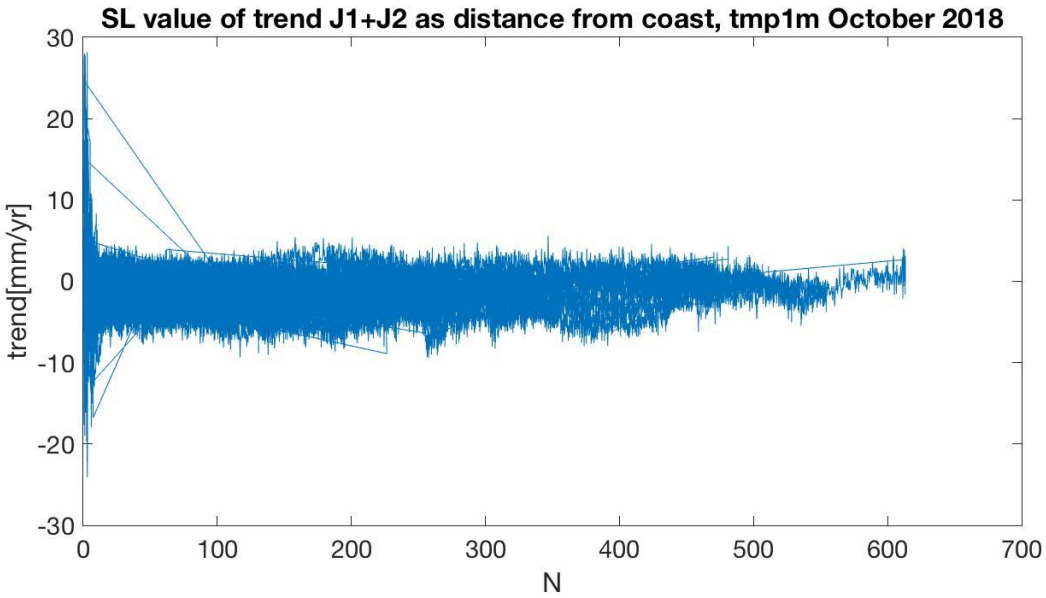

Figure 14: Trend of 20Hz SLA against distance to coast for the complete Mediterranean basin

2. Comparison between altimetry and tide gauges

We have performed the same comparison in the North Sea at the Helgoland tide gauge. The in-situ tide gauge data have one minute sampling. The cycles used are from cycle 55 to 252 for a total of 193 cycles, due to in-situ data gaps. The pass number is pass 312.

From Figure 15 we observe that the XTRACK/ALES dataset has less data available near land compared to the PODACC/ALES. However, differently from pass 196 in Trieste, open sea time-series do not have less data than PODACC/ALES and STAR.

Similar conclusions are drawn from the second comparison. From Figure 16 (top) we see that starting from 10 Km from coast, XTRACK/ALES has time-series with less data than PODAC/ALES and STAR have. With the selection criteria suggested correlation and standard deviation of XTRACK/ALES are superior to PODACC/ALES and comparable to STAR (Figs. 16). However already at 10 km from coast values the 20 Hz time-series are decimated.

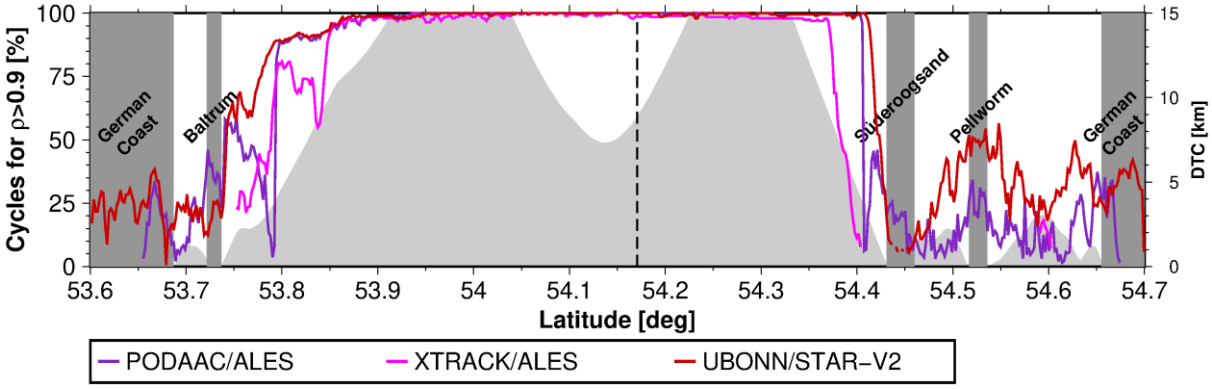

Figure 15: Percentage of retained cycles to achieve a correlation with TG of at least 0.9. Study site in the German Bight, Pass 312.

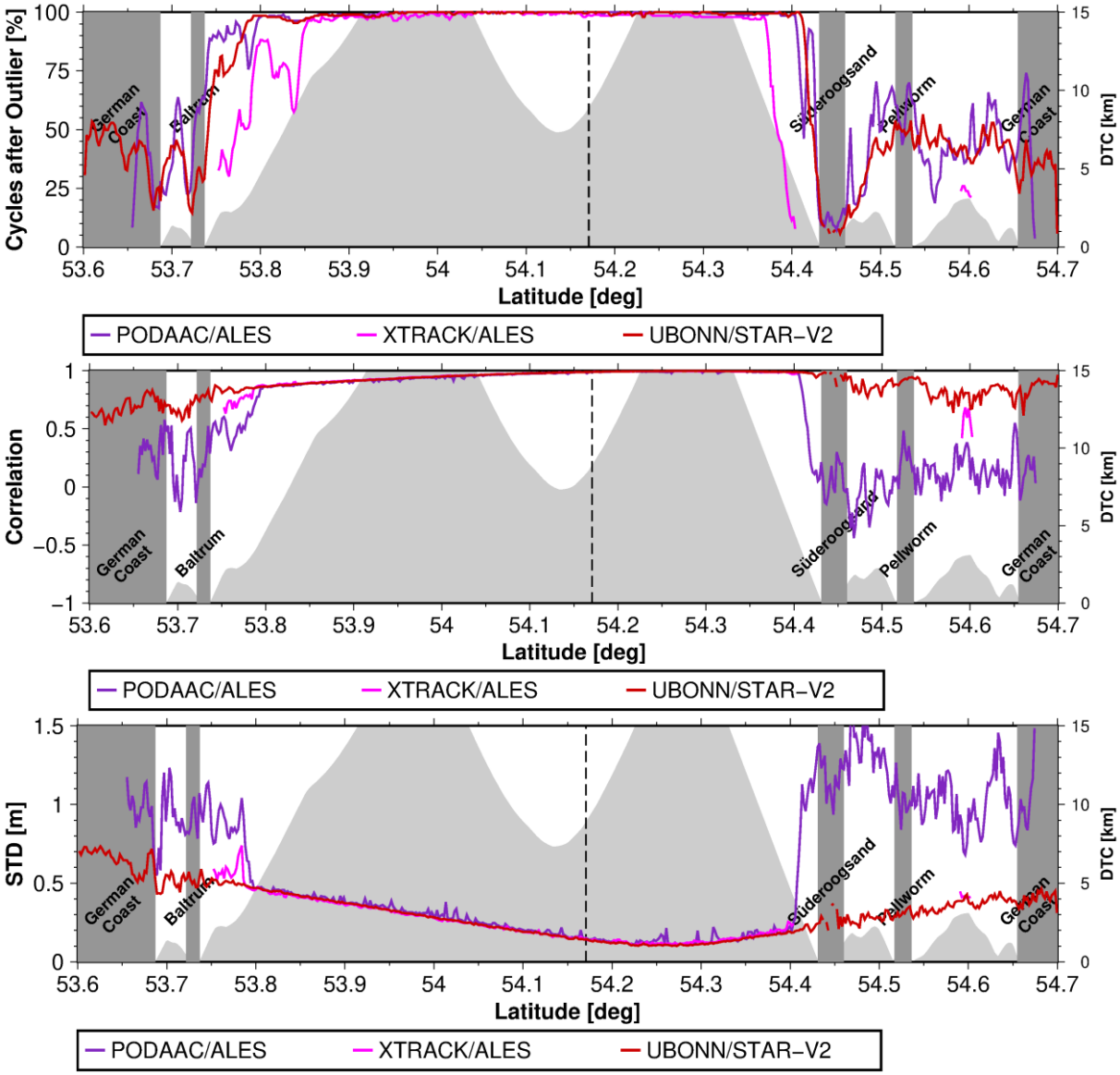

Figure 16: Second comparison: correlation (middle) and standard devation of differences (bottom) for cycles retained (top) after chosen selection criteria (|SLA| > 2.5 m and minimum number of 10 cycles requirement. Study site in the German Bight, Pass 312.

Annex I (Article submitted to ASR)

1

Altimetry-based sea level trends along the coasts of western Africa

Florence Marti[1], Anny Cazenave[1], Florence Birol[1], Marcello Passaro[2], Fabien Leger[1], Fernando Nino[1], Rafael Almar[1], Jérôme Benveniste[3] and Jean François Legeais[4]

1. LEGOS, Toulouse, France
2. DGFI-TUM, Munich, Germany
3. ESA, Frascati, Italy,
4. CLS, Ramonville St Agne, France

Submitted to Advances in Space Research

Special Issue '25 years of satellite altimetry'

23 February 2019

Abstract

We present results of contemporary coastal sea level changes along the coasts of western Africa, obtained from a dedicated reprocessing of satellite altimetry data done in the context of the ESA 'Climate Change Initiative' sea level project. High sampling rate (20-Hz) sea level data from the Jason-1 and Jason-2 missions over a 14-year-long time span (July 2002 to June 2016) are considered. The data were first retracked using the ALES adaptative leading edge subwaveform retracker. The X-TRACK processing system developed to optimize the completeness and accuracy of the corrected sea level time series in coastal ocean areas was then applied. From the 14-year long sea level time series finally obtained, we estimate sea level trends along the Jason-1 & 2 tracks covering the study region. We analyze regional variations in sea level trends, with a focus on the changes observed between the open ocean to the coastal zone. Compared to the conventional 1-Hz sea level products dedicated to open ocean applications, the retracked 20-Hz measurements used in this study allow us to retrieve valid sea level information much closer to the coast (less than 3-4 km to the coast, depending on the satellite track location). The main objective of this study is twofold: (1) provide sea level products in the coastal areas from reprocessed altimetry data and (2) check whether sea level changes at the coast differ from that reported in the open ocean with conventional altimetry products. In the selected region, results show that over the study period, sea level trends near the coast of western Africa are significantly different than offshore. In order to assess the robustness of the results, detailed analyses are performed at several locations to discriminate between drifts in the geophysical corrections and physical processes potentially able to explain the sea level changes observed at the coast.

1. Introduction

Coastal zones are among the most populated regions of the world. Being located at the interface between land and sea, they are exposed to a variety of natural and man-made hazards, e.g., extreme weather such as damaging cyclones, storm surges and associated inundations, sea level change, extreme river discharge, destruction of ecosystems, water pollution, salt water intrusion into coastal aquifers, vertical land motions, etc. They are also impacted by direct human activities, such as increasing urbanization, coastal & river engineering, land use change, subsidence due to groundwater pumping in coastal megacities and oil extraction on shallow shelves. Many shorelines are currently eroding (25% of sandy beaches worldwide and 75% in northern Europe; Luijendijk et al., 2018). This raises the question of understanding the underlying causes. It is not yet fully clear whether reported broad-scale erosion is due to natural processes only, to direct human activities or to the combination of both. The contribution of present-day sea level rise to shoreline retreat has not yet been fully assessed, except at a few limited locations where detailed studies have been conducted (e.g., Le Cozannet et al., 2013). This mostly results from limited knowledge about coastal sea level changes. Indeed, there are reasons to believe that sea level changes at the coast significantly deviate from open ocean changes. A number of small-scale processes of oceanographic and hydrological origin, specific to coastal areas, may indeed modify the rate of sea level rise near the land: e.g., continental slope and shelf currents, changes in the wave characteristics, fresh water input from rivers in estuaries, etc. (Woodworth et al., 2019). Hence, sea level change at the coast may not just be an extrapolation of the regional sea level trends that are routinely provided by standard ocean altimetry products (see **Fig.1**, showing a global map of altimetry-based sea level trends over 2002-2016 -our study period-, based on the altimetry products from the Copernicus Climate Change Service).

Tide gauges are located at the coast, thus are in principle able to provide information on coastal sea level. However, while the mid latitude regions of the northern hemisphere are rather well covered, this is not the case for a numbered of world coastlines where tide gauges are either lacking or the data are not available. This is particularly true along the coasts of western Africa (see **Fig.2** showing the GLOSS tide gauge network; https://www.psmsl.org/products/gloss/status) where only Dakar (Senegal) displays a long sea level record.

Since the early 1990s, sea level changes are estimated at global and regional scales using high precision satellite altimetry (e.g., Escudier et al., 2018, Legeais et al., 2018, Cazenave et al., 2018). However, classical altimetry processing and products provide sea level data up to 10-15 km from the coast only (Cippollini et al., 2018, Benveniste et al., 2019). The main limitation comes from the land contamination within the footprint of the radar signal reflected from the Earth surface, leading to radar echoes (or waveforms) that are significantly different from those collected over pure ocean surfaces. Estimating the range (the distance between the satellite and the Earth surface) in such environments is thus complex (see an illustration in **Fig.3**). In addition, the geophysical corrections to be applied to the altimetry measurements (e.g., wet tropospheric correction, sea surface bias, ocean tides, etc.) are optimized for the open ocean and so far, may remain a source of significant errors on the coastal zones.

Nevertheless, it has been shown that it is possible to retrieve significantly more valid sea level data in the coastal zones by using adapted reprocessing of the altimetry-based measurements in order to extract a robust estimate of the 'range' from the radar echoes (a process called 'retracking'; Gommenginger el al., 2011; Passaro et al., 2014; Wang and Ichikawa, 2017; Xu et al., 2018). In parallel, the quality of geophysical corrections is also constantly improved (Cipollini et al., 2017; Fernandez and Lazaro, 2016) and solutions exist to reduce the associated remaining errors in the coastal domain (Birol et al., 2017).

In this paper, we have combined both approaches to process a dedicated new coastal sea level dataset and present sea level trend results along the coasts of western Africa using Jason-1 and Jason-2 altimetry over 2002-2016. The results presented here are an outcome of a project supported by the European Space Agency (ESA) in the context of the Climate Change Initiative (CCI) sea level project (http://www.esa-sealevel-cci.org/).

2. The ESA CCI Sea level project and its extension to coastal zones.

Earlier this decade, ESA implemented the Climate Change Initiative project (http://cci.esa.int/) dedicated to provide long, accurate time series of a set of Essential Climate Variables (ECVs) observable from space, as defined by the Global Climate Observing System (GCOS, 2011) to monitor and understand climate change. The first phase (2011-2017) of the CCI project allowed the processing of 13 ECVs, including sea level, using all available satellite data sets. Within the CCI sea level project (noted SL_cci), 9 different satellite altimetry missions were reprocessed, and new, optimized algorithms and geophysical corrections were developed for

5

the production of an accurate gridded sea level time series at monthly interval over 1992-2015. This product has been shown to be significantly improved and more suitable for climate studies, in comparison to previous altimetry-based sea level data sets, approaching the GCOS requirements in terms of accuracy and stability (Legeais et al., 2018). In particular, the uncertainty of the global mean sea level trend, now at the level of ~ 0.3 mm/yr, has been significantly reduced (Ablain et al., 2017). At regional scale, sea level trend errors have also been reduced by 1 to 2 mm/yr. The sea level ECV (at global and regional scales) is now operationally produced by the Copernicus Climate Change Service (C3S), adopting the altimetry standards developed in the SL_cci project.

In the context of additional activities of the CCI Sea Level project, it has been proposed to extend the processing efforts done during the SL_cci project to the coastal zones, and to develop new coastal sea level products for estimating rates of sea level change in selected regions. Such a new data set would help answering the following questions:

(1) Is sea level rising at the same rate at the coast as in the open ocean?

(2) Does the answer to question (1) depends on the region considered?

(3) How small-scale ocean dynamics impact sea level variations and trends at the coast?

(4) What is the influence on coastal sea level of fresh water input from rivers in estuaries?

(5) Is present-day shoreline erosion due to sea level rise or not?

The delivery of coastal sea level products that include most recent algorithms developments, will allow better understanding of the role of climate-related sea level rise on present-day coastal changes and impacts.

In this study, we focus on the western African region (indicated by the green square in Fig.1). Two main reasons justify this choice: (1) the western African coastal region is highly populated and under significant threat under climate change and human-induced forcings, and (2) in situ tide gauge networks are very sparse (almost inexistent). The western African coastal zone consists of a narrow, low-lying belt where a large percentage of the population lives in coastal megacities (e.g., Dakar, Conakry, Abidjan, Accra, Lagos, and Douala). In between these big cities, a large number of intermediate size cities have developed, e.g., in Senegal, Ivory coast, Togo, Benin, Nigeria and Cameroun. In Nigeria, about 20 million people live close to the coast. In Senegal, about 5 million people live in Dakar and 90% of industries are located within the Dakar coastal zone (Wong et al., 2014). In Ghana, Benin, Togo and Nigeria, most economic activities are also located in the coastal zone. Because these urban centres stand on low-lying sandy coasts, they are particularly vulnerable to marine hazards, including sea level rise (Brown et al., 2011, Neumann et al., 2015; Dada et al., 2019). The recently observed increase in

shoreline erosion has become a major issue (Ndour et al., 2018; Almar et al., 2015; Giardino et al., 2018; Anthony et al., 2019) but it remains unclear if this is due to sea level rise or human activities (e.g., sand extraction). Moreover, flooding events are becoming more frequent (Angnuureng et al., 2018; Almar et al., 2019). It is urgent to systematically monitor sea level at the coast to better understand its current behaviour and provide insight on future changes (Abessolo Ondoa et al., 2017; 2019). Unfortunately, the west African coastlines are almost devoid of tide gauges. The few existing records are very short and suffer from many data gaps, preventing from estimating decadal or longer-term sea level trends at the coast. A single long-term record is available at Dakar (Senegal), although it is affected by an important data gap in the middle of the altimetry period.

For all these reasons, estimating coastal sea level changes in this region with satellite altimetry is an important goal. It is the purpose of the present study.

3. Data and Method

3.1 Data

In this study, we considered along-track, high-resolution (i.e., at 20 Hz, corresponding to a resolution of ~350 m between consecutive measurements) sea surface height data from the Jason-1 and Jason-2 missions over the July 2002 to June 2016 time span (full 14-year long time span).

The sea level data are derived from range values retracked with the ALES adaptative leading edge sub-waveform system developed by Passaro et al. (2018a, b, c) to improve the number and quality of coastal sea level estimates from altimetry, and provided by the Technical University of Munich (TUM). The ranges from ALES have been then processed by the X-TRACK software developed by the CTOH (Centre de Topographie de l'Océan et de l'Hydrosphère) at the LEGOS (Laboratoire d'Etudes en Géophysique et Océanographie Spatiales) laboratory, in order to obtain corrected sea level times series along a nominal ground-track (Birol et al., 2017). Initially, X-TRACK was designed to provide along-track sea surface height time series at 1-Hz for different conventional nadir altimetry missions (Topex/Poseidon, GFO, Envisat, Jason-1, Jason-2, Jason-3 and SARAL/AltiKa). For the purpose of the present study, it has been adapted to the processing of the 20-Hz ALES data (Birol et al., in preparation). Once the altimetry waveforms have been retracked with ALES, combining with the X-TRACK processing system ensures quality of the resulting coastal sea level time series. Briefly, the method adopted consists in analysing the behaviour of the different altimeter geophysical

corrections as a whole and then editing and recomputing the suspicious correction values in order to maximize the number of valid near-shore sea level data. More details about X-TRACK are provided in Birol et al. (2017).

Table 1 summarizes the geophysical corrections applied to the 20 Hz Jason-1 and Jason-2 data. The sea state bias (SSB) correction is computed at 20 Hz during the ALES retracking process (Passaro et al., 2018a,b,c). Other corrections are provided at 1-Hz and further interpolated at 20-Hz.

Corrections	**Jason-1**	**Jason-2**
Ionosphere	From dual-frequency altimeter range measurements	
Dry troposphere	From ECMWF model	
Wet troposphere	From radiometer	
Sea state bias (SSB)	ALES SSB (Passaro et al., 2018a,b)	
Solid tides	From tidal potential model (Cartwright and Taylor, 1971)	
Pole tides	From Wahr (1985)	
Loading effect	FES 2012 (Carrere et al., 2012)	
Dynamic Atmospheric Correction	TUGOm 2D global models for periods smaller than 20 days (Carrere and Lyard, 2003) + Inverted barometer for periods greater than 20 days, derived from ECMWF pressure fields.	
Ocean Tide	FES 2012 (Carrere et al., 2012)	

Table 1: List of corrections used in the computation of ALES/X-TRACK sea level data.

The sea level data, not exactly located at the same position from one cycle to the other, were then projected onto equally-spaced reference points along a 'mean' reference ground-track by the X-TRACK software (after the editing step). Time series of sea level anomalies –SLA- (with respect to the mean reference track) were then finally estimated (i.e., differences between individual cycle corrected sea level data projected on the corresponding nominal point of the reference track and the mean sea level value estimated at this nominal point).

Jason-1 and Jason-2 data were then merged to obtain a single SLA time series. To do this, a bias between both missions was estimated at regional scale. The procedure adopted consisted in:

(1) Calculation of the mean sea level over the region considered for both Jason-2 cycles 1 to 19 and Jason-1 cycles 240 to 258, excluding all data located at a distance < 50 km from land and altimetry points where less than 80% valid sea level data,

(2) Calculation of the difference between the resulting Jason-2 and Jason-1 mean sea levels. The Jason-1 SLAs were then extended by the Jason-2 time series, as of Jason-2 cycle 21, after subtracting the regional bias to Jason-2 SLAs.

In the following, all results presented are based on the resulting combined dataset, called X-TRACK/ALES SLA.

Apart from the product described above and developed for this project, we also considered the multi-mission gridded product provided by the Copernicus Climate Change Service (C3S) (https://climate.copernicus.eu/), in order to estimate the regional sea level trends for the period 2002-2016. The corresponding trend map is shown in **Fig.4** over the western tropical Atlantic. The Jason tracks are superimposed.

Finally, to locate the western African coastline, we considered the GSHHS (Global Self-consistent, Hierarchical, High-resolution Geography Database) data base (Wessel and Smith, 1996; http://www.soest.hawaii.edu/wessel/gshhg/), providing geographical coordinates of the coastline. This data set is based on multiple sources. Its accuracy in the study region is not well known (W.H Smith and P. Wessel, personal communications) but a comparison with the coastline position from Google map images shows differences of less than 100 m in the study area.

4.2 Estimate of open ocean and coastal sea level trends along the Jason-1/2 tracks: Method

We computed sea level trends over the 14-year period considered in this study along all Jason tracks of the study region. For each track, sea level trends were computed over successive segments of varying lengths along different portions of the reference track from the open ocean to the coast. Constant length segments were considered along the tracks, starting from the closest 20-Hz point to the coast. The construction of the segments along each track is illustrated in Fig.5. The computation of the distance of each 20 Hz point to coast used the GSHHS data base.

To spatially average the data over a given segment, a first method would be to sort all the 20-Hz points with respect to their distance to the nearest coast (defined by GSHHS), and gather them in bins of constant length (e.g. [0 – 2km], [2 – 4 km]...). In this case, one bin may include two measurement points located in the same distance range from the shore but with completely different latitudes (e.g. if a track passes nearby an island).

For this reason, we applied a second method, as illustrated in **Fig.5**: the closest valid point to coast according to the GSHHS data base was considered as a starting point to build the segments. Taking into account its own distance to the coast, we computed a second distance to coast data for all following 20-Hz points. Then, various 20-Hz points were gathered to form constant length segments along the track. The mean position of each along-track segment was defined by the location of the closest 20 Hz point to the middle of the segment.
We successively considered three spatial scales to estimate the along track evolution of the sea level trends:

a) **The entire track over the selected region**; Trends were then computed along 50 km-long successive segments by averaging all SLA data within the segment.
b) **The first 50 km from the coast**; Trends were computed along 2 km-long segments. As for the 50 km-long segments, all SLAs in the segment were averaged to compute the trend.

An additional case (c) was considered:

c) **The first 15 km from the coast**; Trends were computed at individual 20 Hz point location.

For each case (a), (b) or (c), all orbital cycles from July 2002 to June 2016 were considered and SLA data were averaged on a monthly basis. A mean SLA value was computed over the study period and removed from each individual SLA. For cases (a) and (b), the SLA data were spatially averaged along the segment length for each orbital cycle. Removal of annual and semi-annual signals was performed, using a simple least-squares fit to sinusoidal functions, before computing trends. The trend computation was based on a simple linear regression fit.

4. Open ocean and coastal sea level trends along the Jason-1/2 tracks in the western African region

4.1 Results

Sea level trend were estimated for each of the 23 Jason-1/2 tracks covering the western African region. For each track, we computed sea level trends over the 14-year time span at each 20 Hz point for the closest track portion to the coast (a few km).

Fig.6, 7 and 8 show computed along-track trends and associated uncertainties (+/- 1 standard error) at each valid 20 Hz point, for 3 ascending tracks (numbered 187, 237 and 33) selected as examples. The background maps show the geographical setting based on a 2018 version of Google Earth. Track 187 is an ascending satellite track crossing land just south of Freetown in Sierra Leone. Track 237 crosses land east of Abidjan in Ivory Coast, not far from the Ghana border and track 33 crosses land east of Port Harcourt in Nigeria. On each figure, colors correspond to trend/error values. When present, red & white triangles identify points with non-significant trend estimates (sea level time series at each 20 Hz point data too scattered or not enough numerous for a robust trend estimation; see below).
To check the robustness of estimated trends, in particular those closest to the coast, we plotted the sea level time series over the study period for the first few along-track valid points close to the coast. These are shown for each track below the Google map plots in Fig.6-8. Red dots are outliers identified by a simple 2-sigma statistical test. The solid line is the regression line computed over the 14-year time span (excluding the outliers). The corresponding trend value and associated error (+/-1 standard deviation) is indicated in the legend of each figure. We note that the 20 Hz time series show good continuity and little scatter, providing confidence in the computed trends.

Fig. 9, 10 and 11 present another set of 3 examples along descending tracks numbered 174, 46 and 20. Track 174 crosses the land-sea interface south of Dakar (Senegal). Track 46 reaches the sea right east of Accra (Ghana). Track 20 is a short track crossing the land-sea interface in Cameroon. In Fig.11, results are shown for the northern portion of track 20 (called 20N) crossing land northwest of Douala. As in Fig. 6-8, these figures show Google maps and superimposed along-track trends and uncertainties at successive 20 Hz points, as well as associated SLA time series of the first three valid points closest to the coast.

We also computed trends for each 20 Hz point within 15 km from the coast. These are presented in **Fig. 12** as a function of distance to the coast (in Fig.12, 24 trend plots are shown corresponding to the 23 tracks, but with two portions for track 20: north and south, called 20N and 20S). Trend errors (+/- 1 sigma) are also shown. First, we note good continuity of estimated trends from offshore to the coast. We also note quite different behaviors from one track to another when approaching the coast. In most instances, we observed a trend increase in the last few km towards the coast. Some tracks show slight trend decrease followed by a sharp increase when approaching the coast (e.g., tracks 9, 85, 161, 237). Some others show continuous trend

increase over the 15-km distance to coast (e.g., tracks 111, 187, 109, 185, 20N, 122, 46, 224, 72, 174). Others show either no trend increase (e.g., tracks 35, 33, 7, 198) or trend decrease (e.g., track 135 and 211). The observed trend decrease along track 211 looks rather continuous within 5 km to the coast. This track crosses the coast very close to the Niger River estuary in Nigeria, hence the decrease in trend may reflect real coastal signal associated with the river impact on coastal waters (see discussion). In most cases, the trend values deviate significantly within 5 km to the coast compared to those computed farther to the coast.

4.2 Closest distances to coast and associated sea level trends

The results presented above show that depending on the Jason track, it is possible to estimate reliable sea level trends as close as 2-4 km to the coast. This is summarized in **Fig. 13** showing the closest distance to the coast reached for the first valid point and the associated trend. From Fig.13, we note that there is no systematic effect depending on the track direction (ascending and descending). From the 24 track portions covering the study region, 19 provide valid trends at distances less than 3 km. For 8 of them, the distance is even shorter (< 2 km). For 3 tracks, the distance is ~1 km or less. Associated trends are significant (between 5 and 10 mm/yr in some cases). It is worth noting however that the study period is short (14 years) and by no means, what is measured here represents log-term climate-related sea level trends. Nevertheless, even if the computed trends result from decadal variability, they have large enough magnitude to locally impact the coastal zone on decadal time scale.

We also compared the XTRACK/ALES-based trends with the C3S data. For that purpose, we interpolated the gridded data along each Jason track. **Fig.14** shows sea level trends averaged over 50 km-long segments along track 148 (chosen as an example), as a function of distance to the coast. The C3S trends interpolated along the track are superimposed. The latter are smoother but the same large-scale behaviors are seen in both data sets. Fig.14 also shows the same but 2 km-long segments for the last 50 km to the coast. In that case, the C3S trends are constant, unlike the trends computed in this study, indicating that these new data indeed contain small-scale local variability information that the gridded data are unable to retrieve.

4.3 Trends in the geophysical corrections along tracks 237 and 20 over the Jason-1/2 period; Trend comparison between track 174 and Dakar tide gauge record

To check whether the estimated trends result from real physical signals rather than from spurious behavior of some corrections when approaching the coast, we computed the trends of some corrections usually considered as imperfectly known in the coastal zone over the Jason-1/2 period (July 2002 to June 2016). We focused on the wet tropospheric correction, the SSB and Dynamic Atmospheric Correction (DAC).

We extracted each of these corrections at the along-track SLA points located close to the coast and averaged them over successive 2-km long segments (i.e., 0-2 km, 2-4 km, etc.). We then estimated the corrections trends. Results (not shown) reveal no suspect behavior as the distance to the coast decreases. Besides, the correction trends are small and unable to explain the trend increase reported on tracks 237 and 20N (see Fig.7 and 11).

Table 2 summarizes the trend values for each correction along the two 2-km long segments for tracks 237 and 20N.

Table 2: trends in geophysical corrections close to the coast

Geophysical correction trends (mm/yr) over the Jason-1/2 period	Track 237 0-2 km to coast	Track 237 2-4 km to coast	Track 20N 0-2 km to coast	Track 20N 2-4 km to coast
Wet tropospheric correction	-1.14	-0.81	-2.1	-1.86
Sea surface bias (SSB)	0.21	0.46	-0.32	0.1
Dynamic atmospheric correction (DAC)	-0.26	-0.19	-0.42	0.19

As mentioned above, there is a single tide gauge record at Dakar (Senegal) with sufficiently long time series to inter-compare the altimetry-based trends computed in this study and the tide gauge-based sea level trend. Unfortunately, there is a data gap in the Dakar tide gauge record during the Jason-1 time span. Thus the comparison can only be performed over the Jason-2 period. Tide gauge data availability led us to consider the period from July 2009 to June 2016 (7 years). We used monthly RLR tide gauge data from the Permanent Service for Mean Sea Level (www.psmsl.org). The data are not corrected for vertical land motions. The trend at the tide gauge (located in the Dakar harbor) amounts to 0.90 +/- 1.35 mm/yr over this time span. The trend estimate at the closest valid point to coast (distance equal to 2.5 km) on track 174 is 2.1 +/- 5.1 mm/yr. Although the altimetry-based trend at the closest distance to coast displays large uncertainty, the two trend values agree within their respective error bars. In addition,

because of lack of vertical land motion estimate at the tide gauge during this 7 years period, we cannot expect to obtain perfect agreement.

5. Discussion

In this study we provide for the first time, decadal sea level trends very close to the coast of western Africa, using high-resolution (20 Hz) altimetry data, based on ALES retracked waveforms inserted into the XTRACK system. Over the Jason-1 and Jason-2 period (2002-2016), estimated trends along the Jason tracks show interesting behaviors from offshore to the coast. In most instances, the trends are roughly constant from 15 km to ~ 5 km to the coast, then change when approaching the coast. At some locations, a slight trend decrease is observed within the 0-4 km band followed by a sharp trend increase when approaching the coast. Such a behavior is definitely associated to coastal processes that were not visible with former altimetry product (e.g., Cazenave et al., 2017, Birol et al., 2017). This could be the result of wind-induced setup, river freshwater runoff, wave forcing on shallow shelves. At embayed coasts and estuaries and shallow areas, cross-shore winds can drive important surge, such as observed off Senegal over the wide shelf during winter upwelling (Capet et al., 2017). Large river fresh water plumes can change water density and affect coastal sea level (e.g. Han and Webster, 2002; Brammer, 2014). Waves radiate energy over long distances in deep water without any perceptible signature on open ocean sea level (Hoeke et al., 2013). Their influence increases while their interaction with the bathymetry gradually increases in the near-shore where they dissipate energy. This induces a set down in the shoaling zone and setup after the breakpoint that generally reach 20 % of offshore wave height (Bowen et al., 1968). Amazingly, this is what we observed in the trends along tracks 9, 85, 161 and 237. Waves have been recently shown to be strongly influence sea level trends at the coast in many regions of the world (Melet al., 2018) and in particular in the Gulf of Guinea (Melet et al., 2016) and Senegal coast (Almar et al., 2019). We will explore this issue in a future study.

Only two tracks show trend decrease within the 0-5 km to the coast. This is particularly clear on track 211 crossing the coast close to the Niger River estuary. Influence of the river plume could be at the origin of the observed behavior. This again will be the object of a future study.

Among the 24 Jason track portions covering the study region, 19 tracks allow estimating trends as close as 2-3 km to the coast. For 3 of them, distances of ~1 km or less are reached. Such new data will allow investigating small-scale processes occurring in the coastal zone. This represents a real progress compared to what is available with standard GDRs (Geophysical Data Records).

Planned future work will follow several directions: (1) extend the Jason sea level time series beyond 2016, using Jason-3 in particular, to estimate trends on longer periods (2) provide coastal sea level time series from Envisat and SARAL/Altika missions, (3) use of SAR altimetry on Sentinel 3A and 3B to obtain higher-resolution sea level time series and associated trends in coastal zones, and (4) consider a broader range of coastal zones (northern Europe, Indian continent, southeast Asia, small tropical islands). In parallel, we will interpret coastal trend behaviors in terms of coastal processes, focusing first on the western African region.

The new coastal sea level data set developed in this study will be freely available for a wide range of additional investigations, including studies of small-scale shelf currents.

Acknowledgements: This study is an outcome of the ESA CCI Sea Level 'Bridging Phase' project dedicated to coastal sea level. Florence Marti is supported by an engineer grant in the context of this project.

References

Abessolo Ondoa G., R. Almar, B. Castelle et al., 2019. On the use of shore-based video camera to monitor sea level at the coast: A case study in grand popo, benin (gulf of Guinea, west Africa). Submitted to *Journal of Atmospheric and Oceanic Technology*.

Ablain M., Legeais J.F., Prandi P., et al., 2017. Altimetry-based sea level, global and regional, *Surveys in Geophysics*, 38, 7-31, DOI 10.1007/s10712-016-9389-8.

Ablain, M., Cazenave, A., Larnicol, G. et al., 2015. Improved sea level record over the satellite altimetry era (1993–2010) from the Climate Change Initiative project, *Ocean Sci.,* 11, 67-82, doi:10.5194/os-11-67-2015.

Almar, R., E. Kestenare, J. Reyns, J. et al., 2015. Response of the Bight of Benin (Gulf of Guinea, West Africa) coastline to anthropogenic and natural forcing, Part1: Wave climate variability and impacts on the longshore sediment transport, *Continental Shelf Research*, 110, 48-59.

Almar, R., Kestenare, E., Boucharel, J. 2019. On the key influence of remote climate variability from Tropical Cyclones and South Atlantic storms on the Senegalese coast (West Africa), submitted to *Environmental Research Letters*.

Angnuureng, D.B., Appeaning Addo, K., Almar, R. et al. 2017. Influence of sea level variability on a microtidal beach, *Natural Hazards*, 93(3), 1611-1628.

Anthony, E.J., Almar, R., Besset, M. et al., 2018. Response of the Bight of Benin (Gulf of Guinea, West Africa) coastline to anthropogenic and natural forcing, Part 2: Sources and patterns of sediment supply, sediment cells, and recent shoreline change. *Continental Shelf Research*, 173, 93-103.

Benveniste J., Cazenave A., Vignudelli S. et al., 2019. Requirement of a coastal zone observing system, in revision, *Frontiers in Marine Sciences*.

Birol F., N.X Fuller, F. Lyard, et al., 2017. Coastal applications from nadir altimetry: example of the X-TRACK regional products. *Advances in Space Research*, 10.1016/j.asr.2016.11.005.

Bowen, A.J., Inman, D.L., Simmons, VP., 1968. Wave 'set-down' and set-Up., *J. Geophys. Res*. 73, 2569–2577.

Brammer, H., 2014. Bangladesh's dynamic coastal regions and sea-level rise, *Climate Risk Management*, 1, 51-62.

Brown S. et al., 2011. Sea level rise and impacts in Africa, 2000 to 2100, Africa Report.

Capet, X., Estrade, P., Machu, E., 2017. On the dynamics of the southern senegal upwelling center: Observed variability from synoptic to superinertial scales. *Journal of Physical Oceanography,* 47(1), 155-180.

Carrere, L. and Lyard, F. 2003. Modeling the barotropic response of the global ocean to atmospheric wind and pressure forcing- comparisons with observations. *J. Geophys. Res*. 30 (6), 1275. http://dx.doi.org/ 10.1029/2002GL016473.

Carrere, L., Lyard, F., Cancet, et al., 2012. FES2012: a new global tidal model taking advantage of nearly twenty years of altimetry. In: Proceeding of the 20 Years of Progress in Radar Altimetry Symposium. Venice, Italy.

Cartwright, D. E. and R. J. Taylor, 1971. New computations of the tide-generating potential, *Geophys. J. R. Astron. Soc*., 23, 45-74.

Cazenave A., Le Cozannet G., Benveniste J. et al., 2017. Monitoring the change of coastal zones from space, *EOS*, *98,* https://doi.org/10.1029/2017EO085581. Published on 02 November 2017.

Cazenave A., Palanisamy H. and Ablain M., 2018. Contemporary Sea level changes from satellite altimetry; What have we learned? What are the new challenges? *Advances in Space Research*, published online 25 July 2018, https://doi.org/10.1016/j.asr.2018.07.017.

Cipollini P., J. Benveniste, F. Birol, et al., 2018. Satellite altimetry in coastal regions. In 'Satellite altimetry over the oceans and land surfaces, Stammer & Cazenave Edts, CRC Press.

Dada, O.A., Agbaje, A.O., Adesina, R.B., et al., 2019. Effect of coastal land use change on coastline dynamics along the Nigerian Transgressive Mahin mud coast. *Ocean and Coastal Management*, 168, 251-264.

Escudier P. et al., 2018. Satellite radar altimetry: principle, accuracy and precision, in 'Satellite altimetry over ocean and land surfaces', Stammer & Cazenave editors, CRC Press.

Global Climate Observing System (GCOS), 2011. Systematic observation requirements for satellite-based data products for climate (2011 update) – supplemental details to the satellite-based component of the "Implementation plan for the global observing system for climate in support of the UNFCCC (2010 update)", GCOS-154 (WMO), available at: https: //library.wmo.int/opac/doc_num.php?explnum_id=3710 (last access: 10 August 2017).

Giardino, A., Schrijvershofa, R., Nederhoffa, C.M. et al., 2016. A quantitative assessment of human interventions and climate change on the West African sediment budget. *Ocean and Coastal Management*, 156, 249-265.

Gommenginger C. , P. Thibaut, L. Fenoglio-Marc, et al., 2011. Retracking altimeter waveforms near the coasts, in Coastal Altimetry, S. Vignudelli, et al. (Eds.), Springer, Berlin Heidelberg, pp. 61-101, 10.1007/978-3-642-12796-0_4.

Han, W. and Webster, P. J., 2002. Forcing mechanisms of sea level interannual variability in the Bay of Bengal. *Journal of Physical Oceanography*, 32(1), 216–239.

Hoeke, R.K., McInnes, K.L., Kruger, J.C. et al., 2013. Widespread inundation of Pacific islands triggered by distant-source wind-waves. *Glob. Planet. Change*, 108, 128–138.

Le Cozannet G. et al., 2013. Exploring the relation between sea level rise and shoreline erosion using reconstructions: an example in French Polynesia, *J. Coastal Research*, 65, 2137-2142, 10.2112/SI65-361.1.

Legeais J.F., Ablain M., Zawadzki L. et al., 2018. An improved and homogeneous altimeter sea level record from the ESA Climate Change Initiative, *Earth Syst. Sci. Data*, 10, 281-301, https://doi.org/10.5194/essd-10-281-2018.

Luijendijk A. et al., 2018. the state of the world beaches, *Scientific Reports*, 8, 6641, DOI:10.1038/s41598-018-24630-6.

Melet, A., Almar, R. and Meyssignac, B., 2016. What dominates sea level at the coast: a case study for the Gulf of Guinea. *Ocean Dyn.* 66, 623–636.

Melet A., Meyssignac B. Almar R. et al., 2018. Under-estimated wave contribution to coastal sea-level rise, *Nature Climate Change*, 8, pages234–239.

Neumann B, Vafeidis AT, Zimmermann J. et al., 2015. Future Coastal Population Growth and Exposure to Sea-Level Rise and Coastal Flooding - A Global Assessment. *PLoS ONE* 10(3): e0118571.

Ondoa, G., Vacchi, M., 2018. Response of the Bight of Benin (Gulf of Guinea, West Africa) coastline to anthropogenic and natural forcing, Part 2: Sources and patterns of sediment supply, sediment cells, and recent shoreline change. Continental Shelf Research, 173, 93-103.

Passaro M., Cipollini P., Vignudelli S. et al., 2014. ALES: A multi-mission subwaveform retracker for coastal and open ocean altimetry. *Remote Sensing of Environment* 145, 173-189, 10.1016/j.rse.2014.02.008.

Passaro M., Cipollini, P., Benveniste J., 2015. Annual sea level variability of the coastal ocean: The Baltic Sea-North Sea transition zone. *Journal of Geophysical Research* 120(4): 3061-3078, 10.1002/2014JC010510.

Passaro M., Dinardo S., Quartly G.D. et al., 2016. Cross-calibrating ALES Envisat and CryoSat-2 Delay–Doppler: a coastal altimetry study in the Indonesian Seas. *Advances in Space Research*, 58(3), 289-303, 10.1016/j.asr.2016.04.011.

Passaro M., Smith W., Schwatke C. et al., G., 2018a. Validation of a global dataset based on subwaveform retracking: improving the precision of pulse-limited satellite altimetry. 11th Coastal Altimetry Workshop, Frascati (ESA-ESRIN), Italy, 2018-06-15.

Passaro M., Rose S.K., Andersen O.B. et al., 2018b. ALES+: Adapting a homogenous ocean retracker for satellite altimetry to sea ice leads, coastal and inland waters. *Remote Sensing of Environment*, 211, 456-471, 10.1016/j.rse.2018.02.074.

Passaro M, Cipollini P, Vignudelli S et al., 2018c. ALES: a multi-mission subwaveform retracker for coastal and open ocean altimetry. *Remote Sensing Environ.* 145, 173–189.

Piccioni G., Dettmering D., Passaro M. et al., 2018. Coastal Improvements for Tide Models: The Impact of ALES Retracker. *Remote Sensing*, 10(5), 10.3390/rs10050700.

Quartly G.D., Legeais J.F., Ablain M. et al., 2017. A new phase in the production of quality-controlled sea level data, *Earth Syst. Sci. Data*, 9, 557–572, doi.org/10.5194/essd-9-557-2017.

Vessel, P., and W. H. F. Smith, 1996. A Global Self-consistent, Hierarchical, High-resolution Shoreline Database, *J. Geophys. Res., 101*, 8741-8743.

Wang, X. and Ichikawa, K., 2017. Coastal Waveform Retracking for Jason-2 Altimeter Data Based on Along-Track Echograms around the Tsushima Islands in Japan. *Remote Sens*. 9, 762.

Wahr, J.M., 1985. Deformation Induced by Polar Motion. *J. Geophys. Res.,* 90 (B11), 9363–9368.

Wong, P. P., et al., 2014. Coastal systems and low-lying areas. In: Climate Change 2014: Impacts, Adaptation, and Vulnerability. Part A: Global and Sectoral Aspects. Contribution of Working Group II to the Fifth Assessment Report of the Intergovernmental Panel on Climate Change [Field, C.B. et al. (eds.)]. *Cambridge University Press*, Cambridge, United Kingdom and New York, NY, USA, pp. 361-409.

Woodworth P. et al., 2019. Forcing Factors Causing Sea Level Changes at the Coast, *Surveys in Geophysics*, in press.

Xu X.Y., Birol F. and Cazenave A., 2018. Evaluation of Coastal Sea Level of Jason-2 Altimetry Offshore Hong Kong, , *Remote Sensing*, 10, 282, doi:10.3390/rs10020282.

Figure captions

Fig.1 Regional sea level trends over the altimetry era (1993-present) from the Copernicus Climate Change Service (C3S) sea level products

Fig.2: Gloss-based tide gauge network coverage along world coastlines with >40 years records

Fig.3: radar altimetry waveforms over open ocean (left) and coastal region (right)

Fig.4: Sea level trends from the C3S gridded product over July 2002 to June 2016 over the study region. Jason tracks (identified by numbers) are superimposed

Fig.5: Sketch illustrating the method to compute the distance to the coast

Fig.6: *Track 187*. Upper left panel: Sea level trends (mm/yr; colored circles) computed over the 14-year time span at each 20 Hz point for the closest track portion to the coast (a few km). Red/white triangles identify points with non-significant trend estimates (sea level data too scattered or not enough numerous for a robust trend estimation). The background map shows the geographical setting based on a 2018 version of Google Earth. Upper right panel: Associated sea level trend uncertainties (+/- 1 standard error) at each 20 Hz point along the same track as on the left hand side map (note the change in color scale). Lower plots: sea level time series (blue dots) since June 2002 for the first three 20 Hz points closest to the coast (distance indicated in the heading). Red dots are outliers identified by simple statistical test. In green is shown the regression line computed over the 14-year time span (excluding the outliers). The corresponding trend value and associated error (+/-1 standard deviation) is indicated in the legend of the figure.

Fig.7 : same as Fig.6 for *Track 237*.

Fig.8 : same as Fig.6 for *Track 33*.

Fig.9 : same as Fig.6 for *Track 174*.

Fig.10 : same as Fig.6 for *Track 46*.

Fig.11 : same as Fig.6 for *Track 20*.

Fig.12: Sea level trend values and associated formal errors (+/-1 standard deviation; thin vertical bars) as a function of distance to the coast (last 15 km) estimated at each 20-Hz point, for all 23 Jason tracks considered in this study. Plots are ranked for all ascending tracks first, then all descending tracks.

Fig.13: Distribution of the closest distance to coast of the first valid 20 Hz point for all Jason tracks considered in the study region (left panel; black/grey bars correspond to ascending/descending tracks) and associated trend estimates over 2002-2016 (right panel).

Figure 14: Left panel: sea level trends averaged over 50 km-long segments along track 148, as a function of distance to the coast (black points); The C3S trend interpolated along the track is also shown (open squares). Right panel: same as left panel but for 2 km-long segments for the last 50 km to the coast.

20

Figure 1

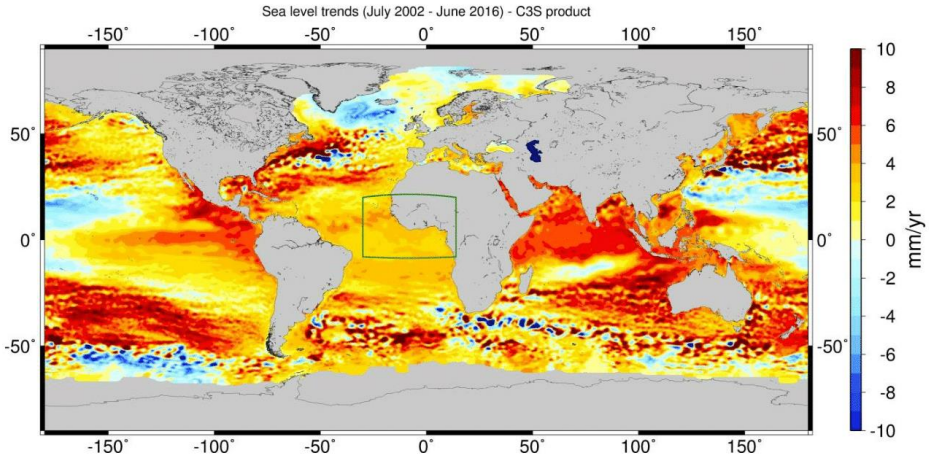

Figure 2

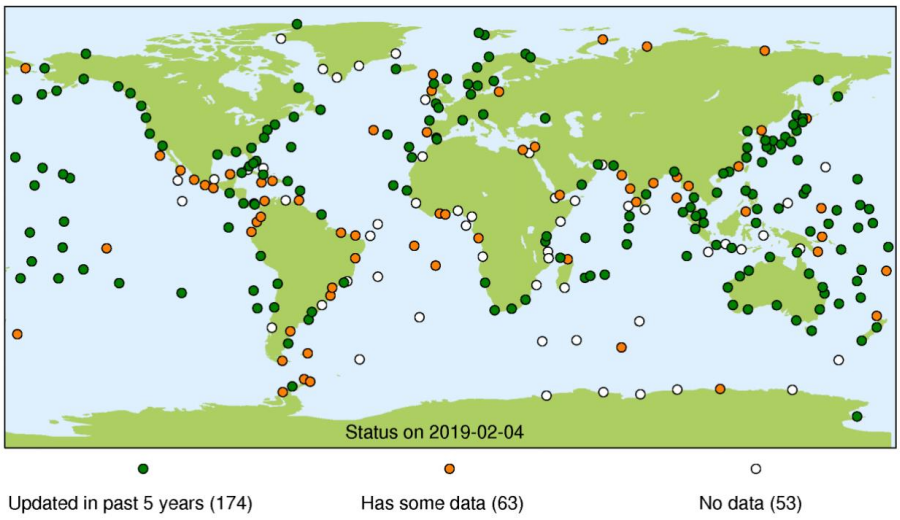

Figure 3

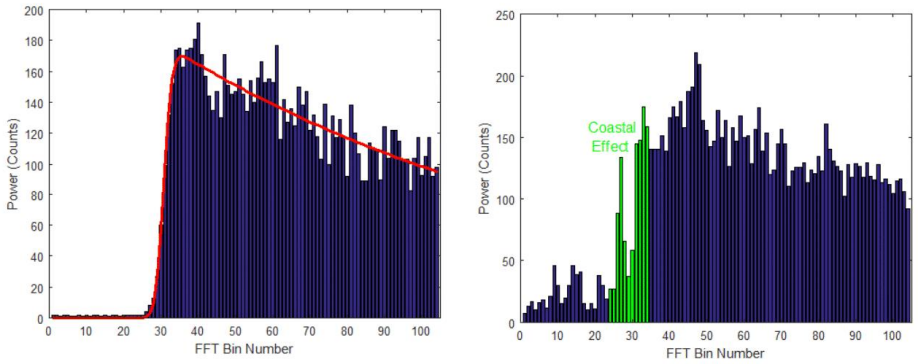

Figure 4

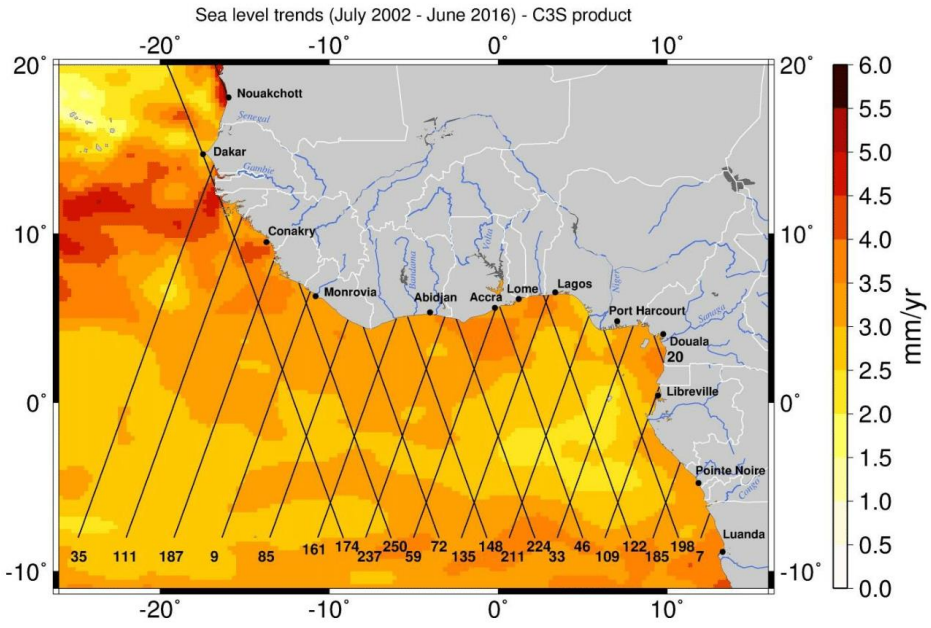

Figure 5

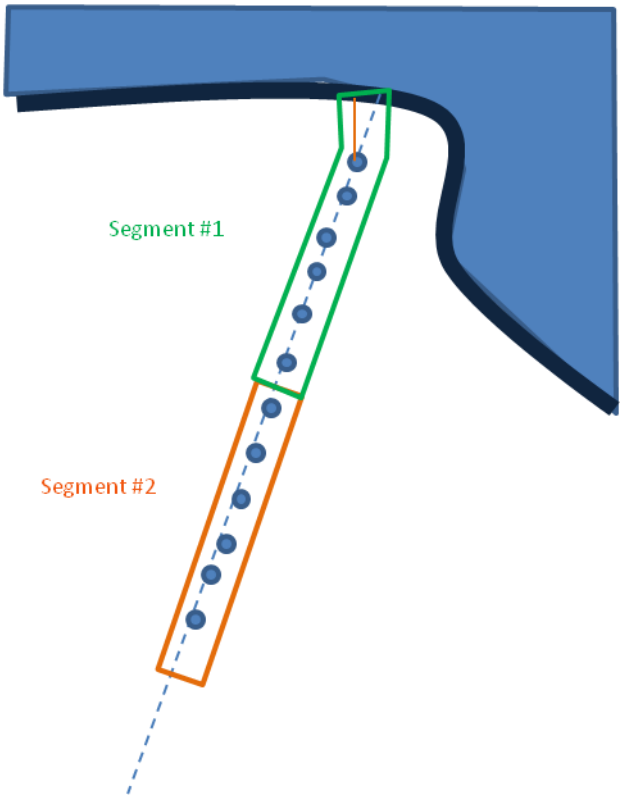

Figure 6

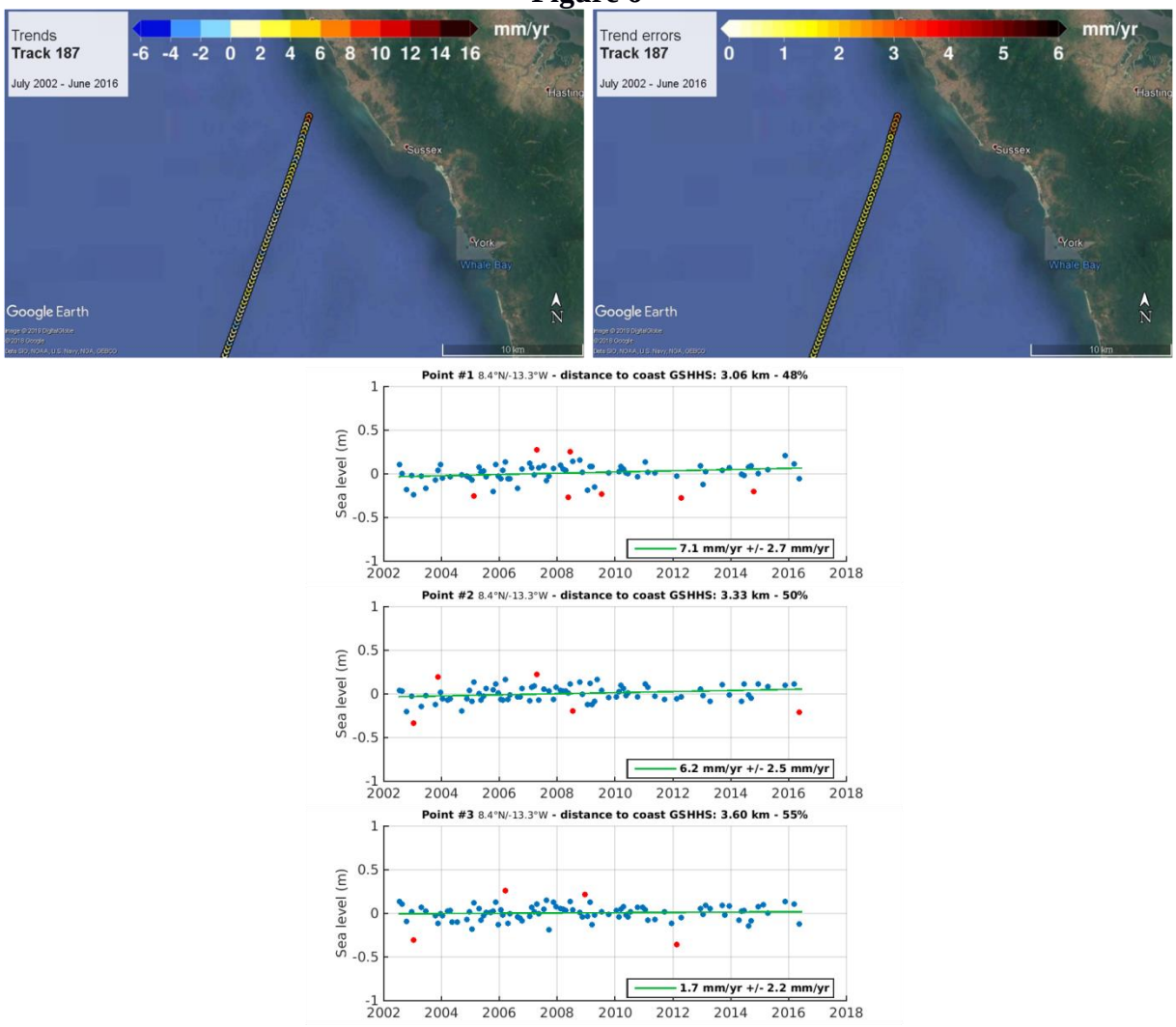

Figure 7

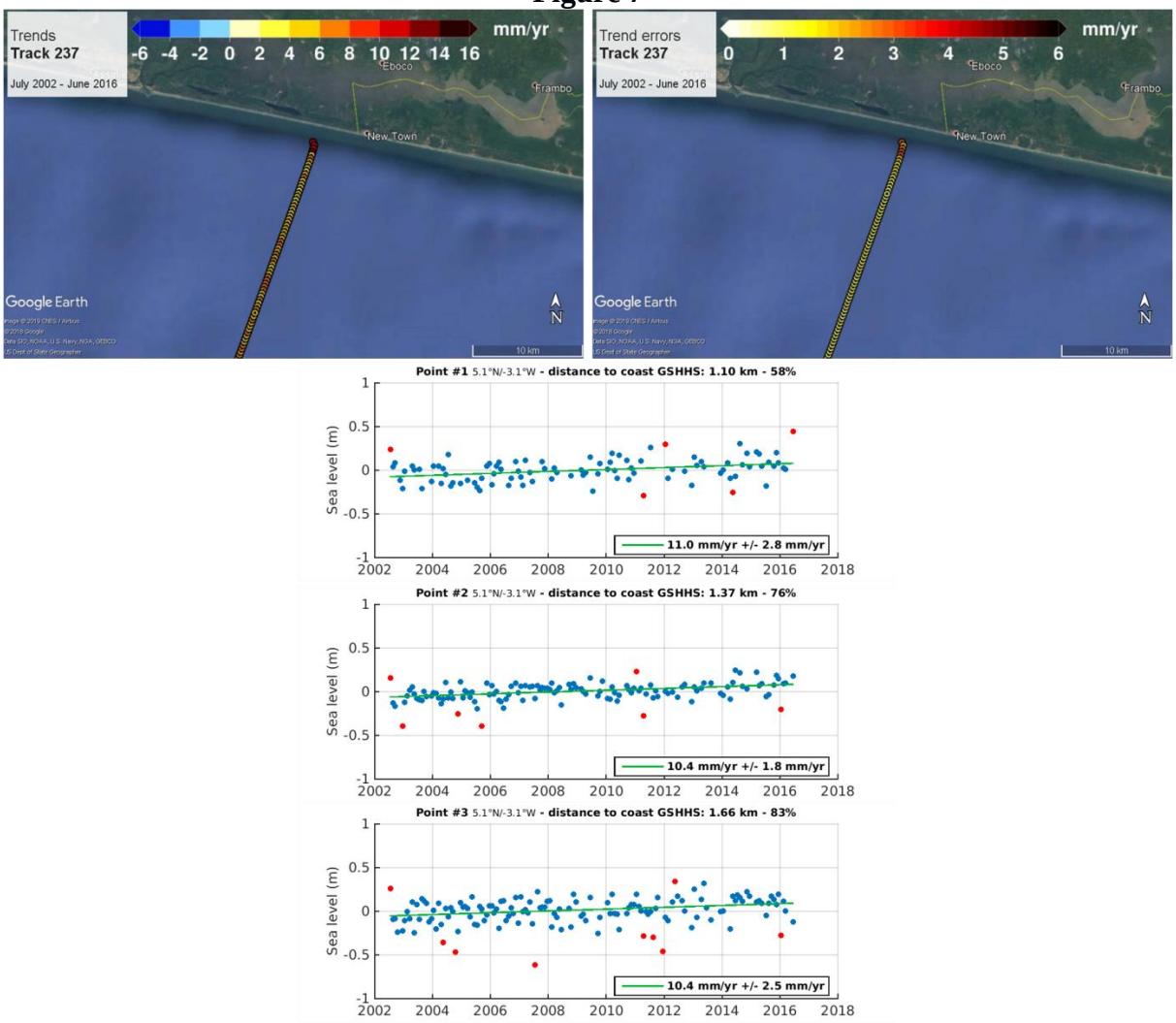

Figure 8

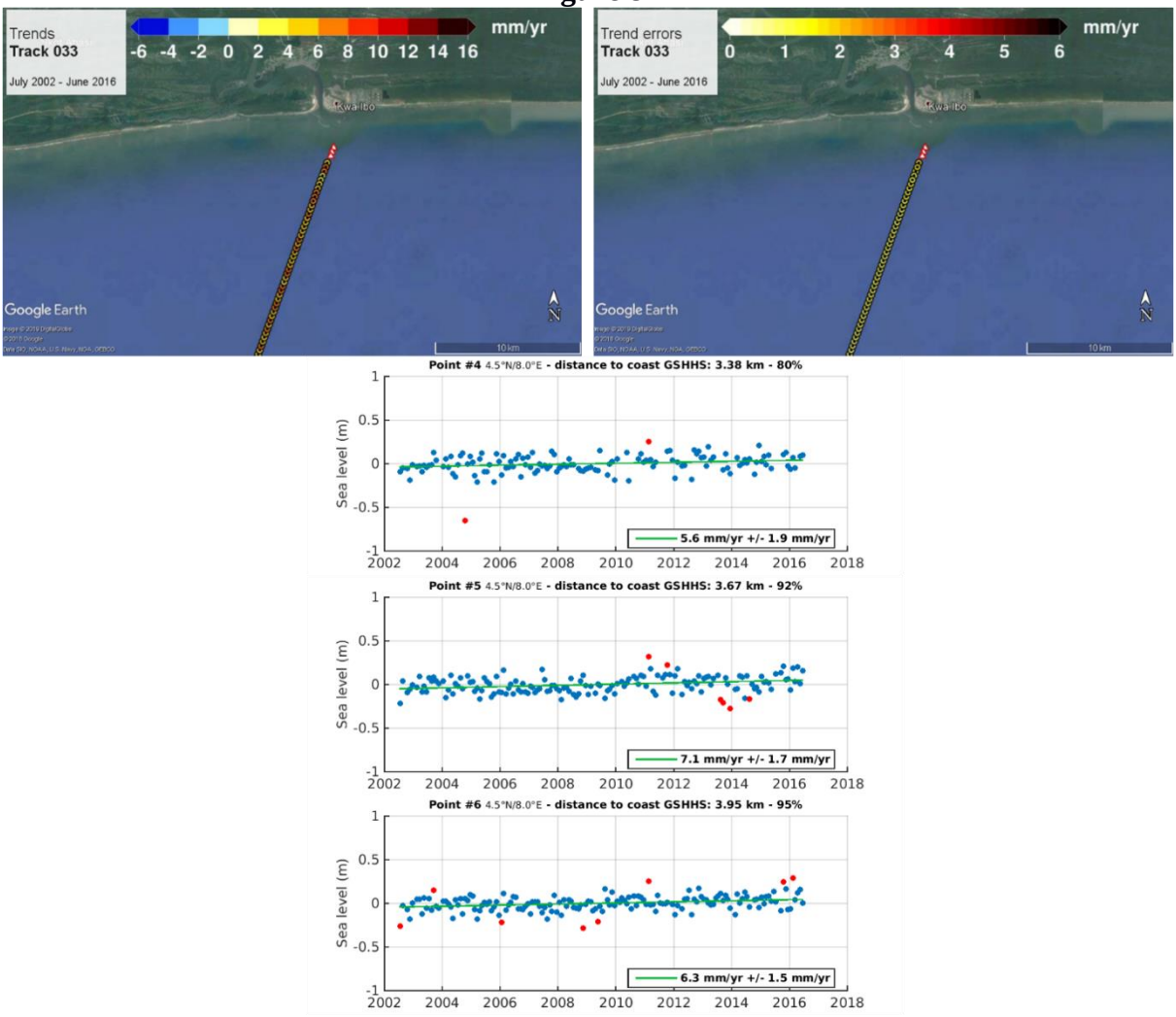

Figure 9

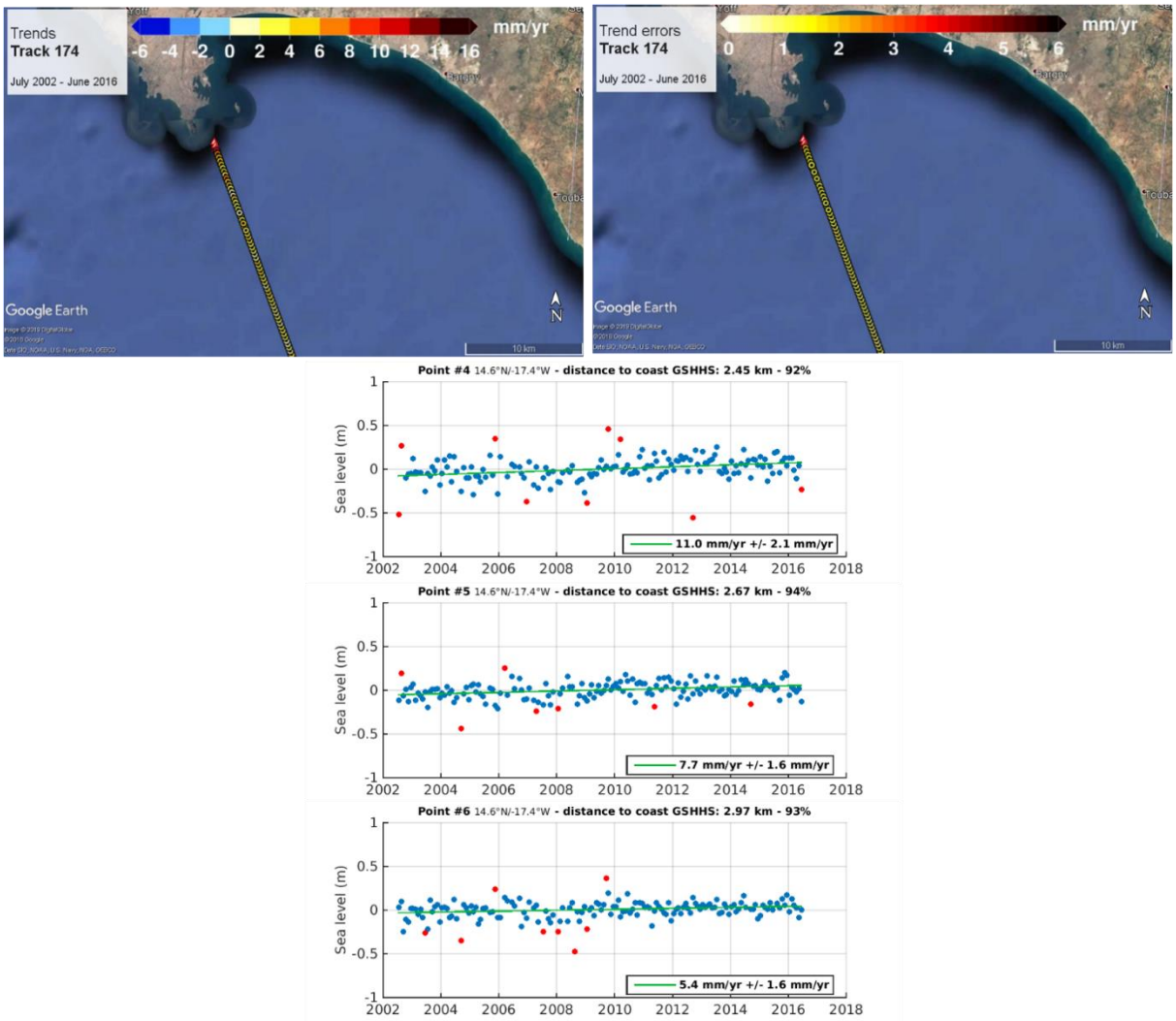

FIGURE 10

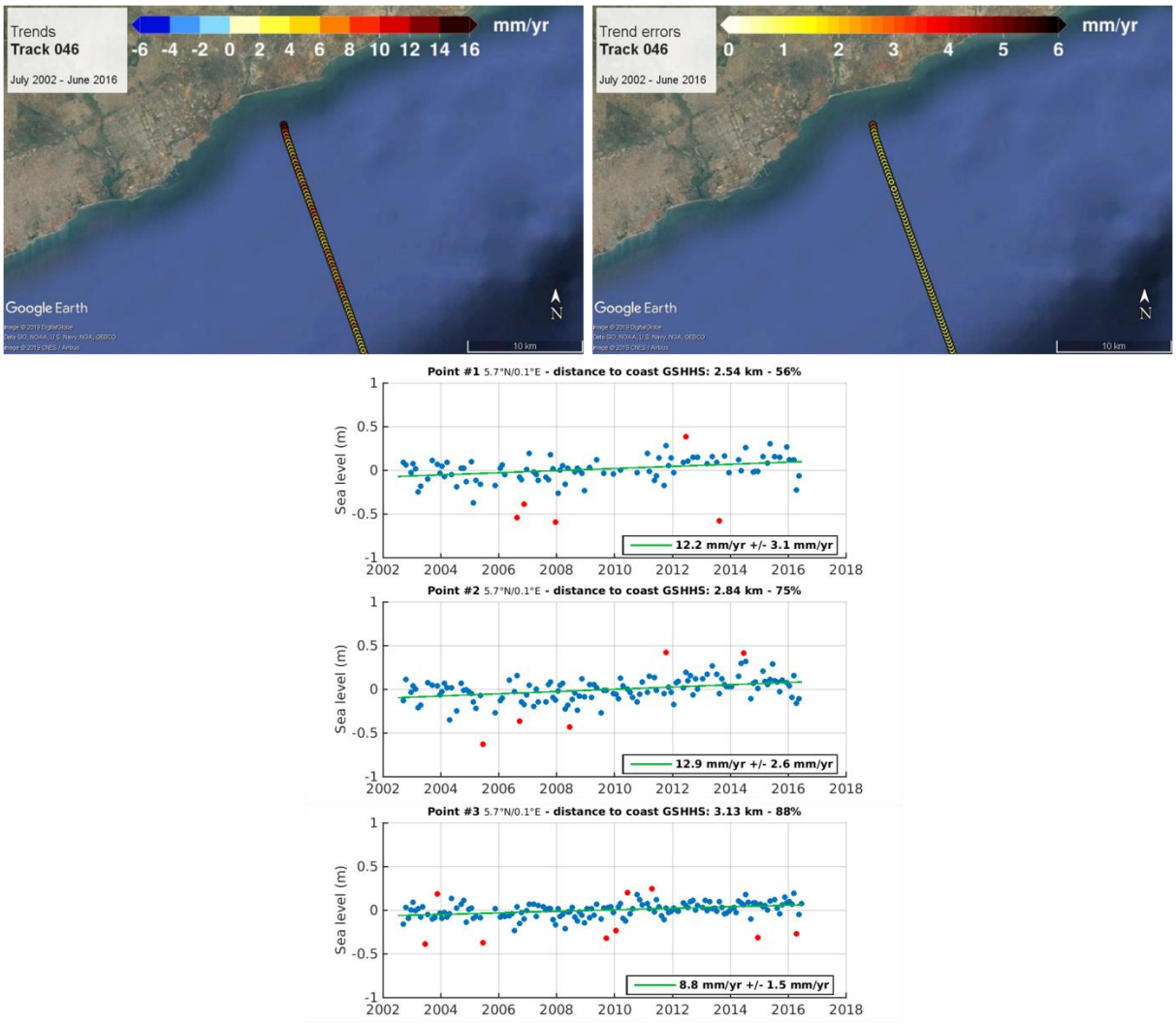

Figure 11

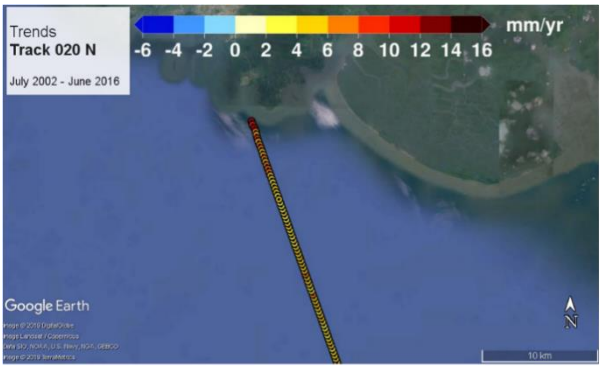

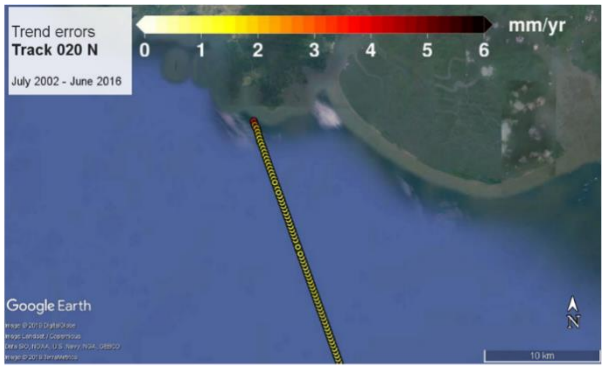

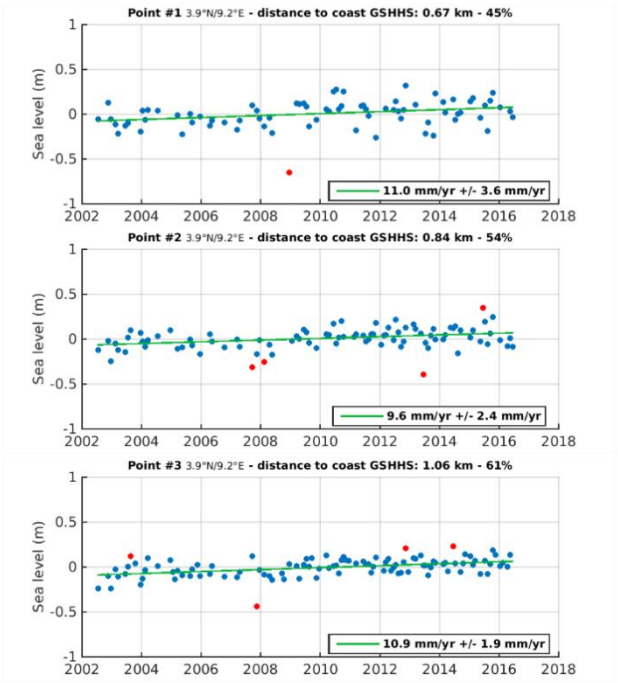

29

Figure 12 (1)

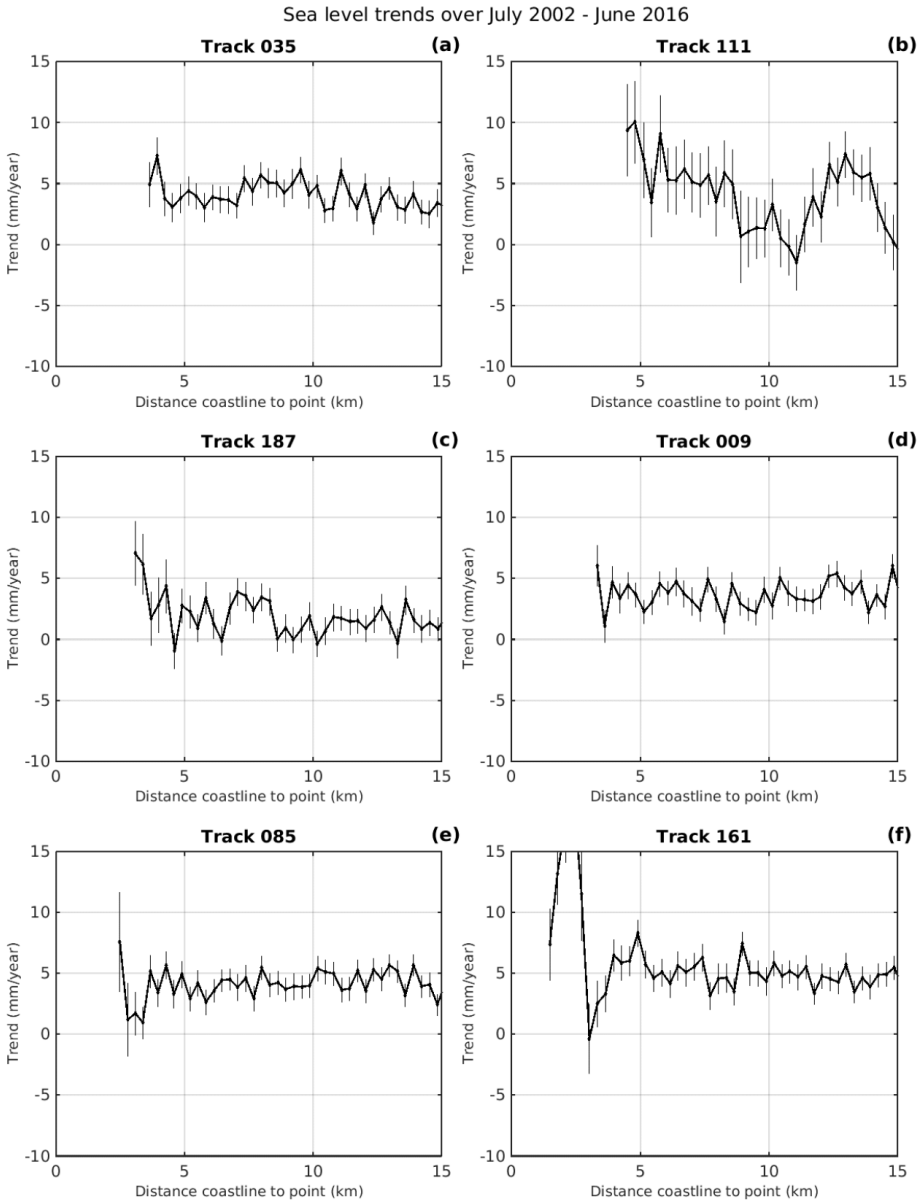

30

Figure 12 (2)

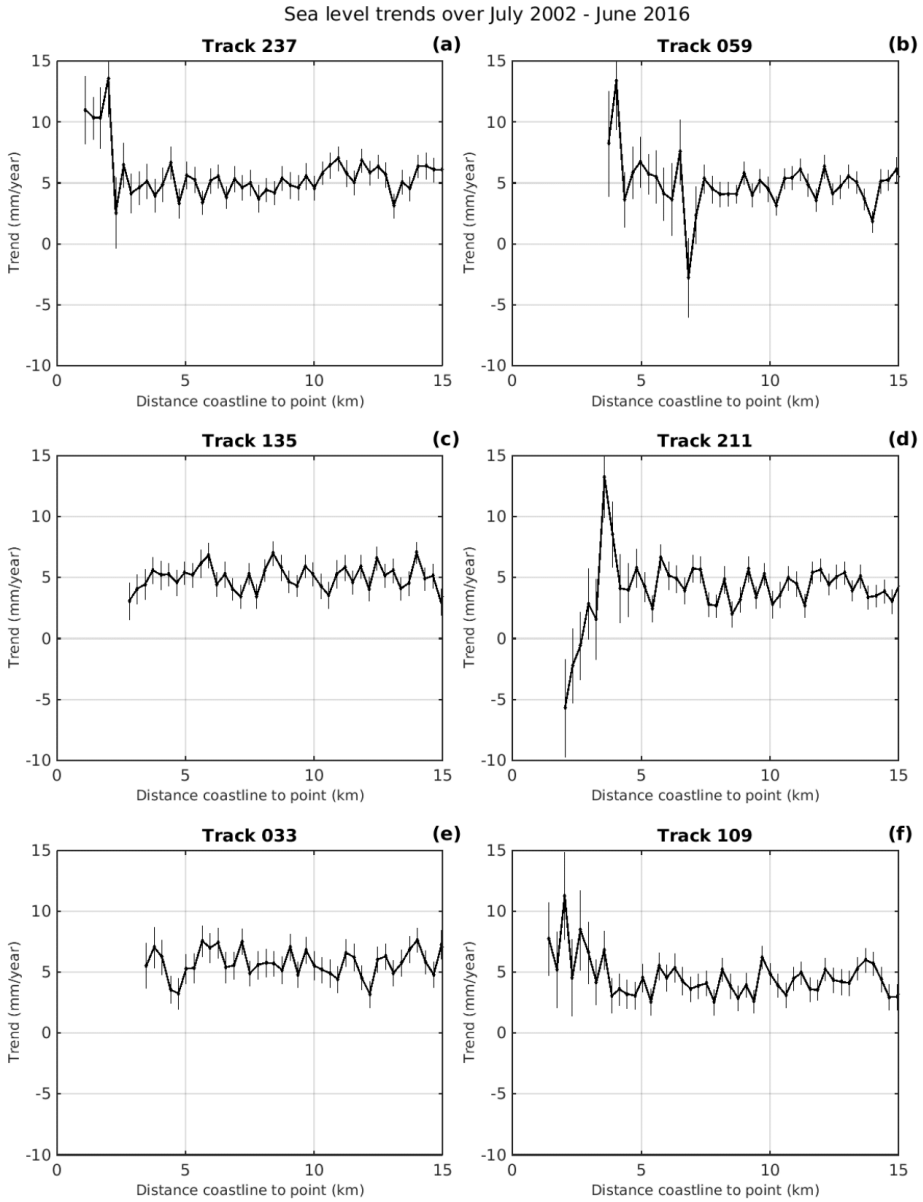

Figure 12 (3)

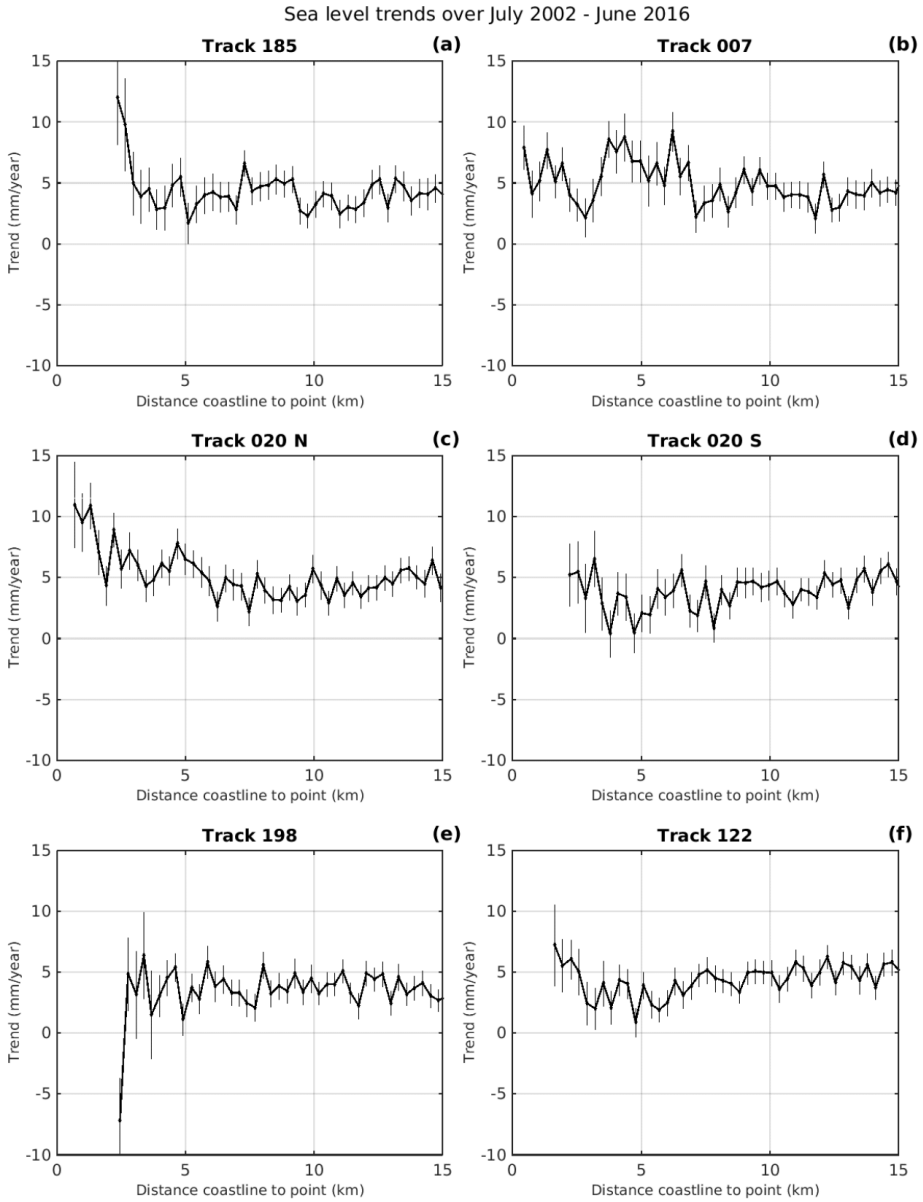

32

Figure 12 (4)

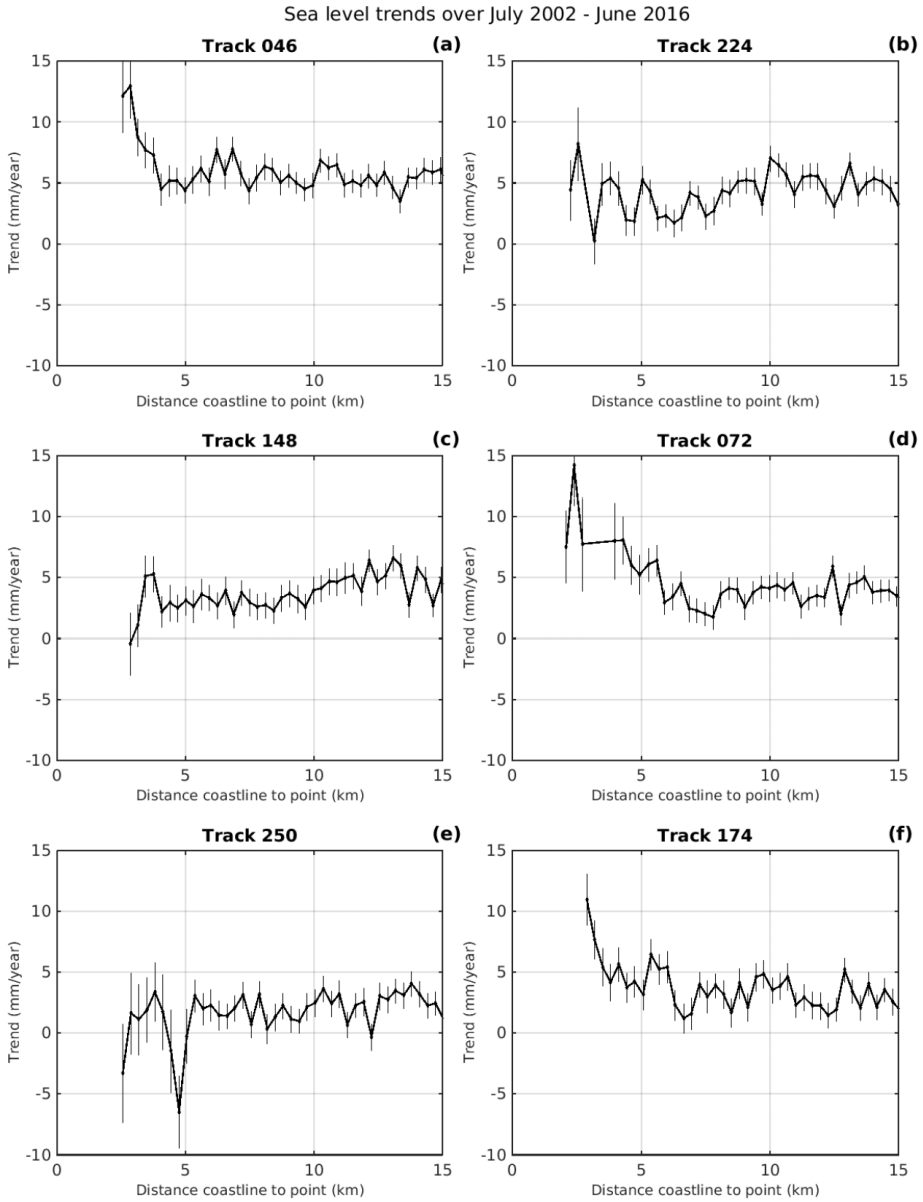

Figure 13

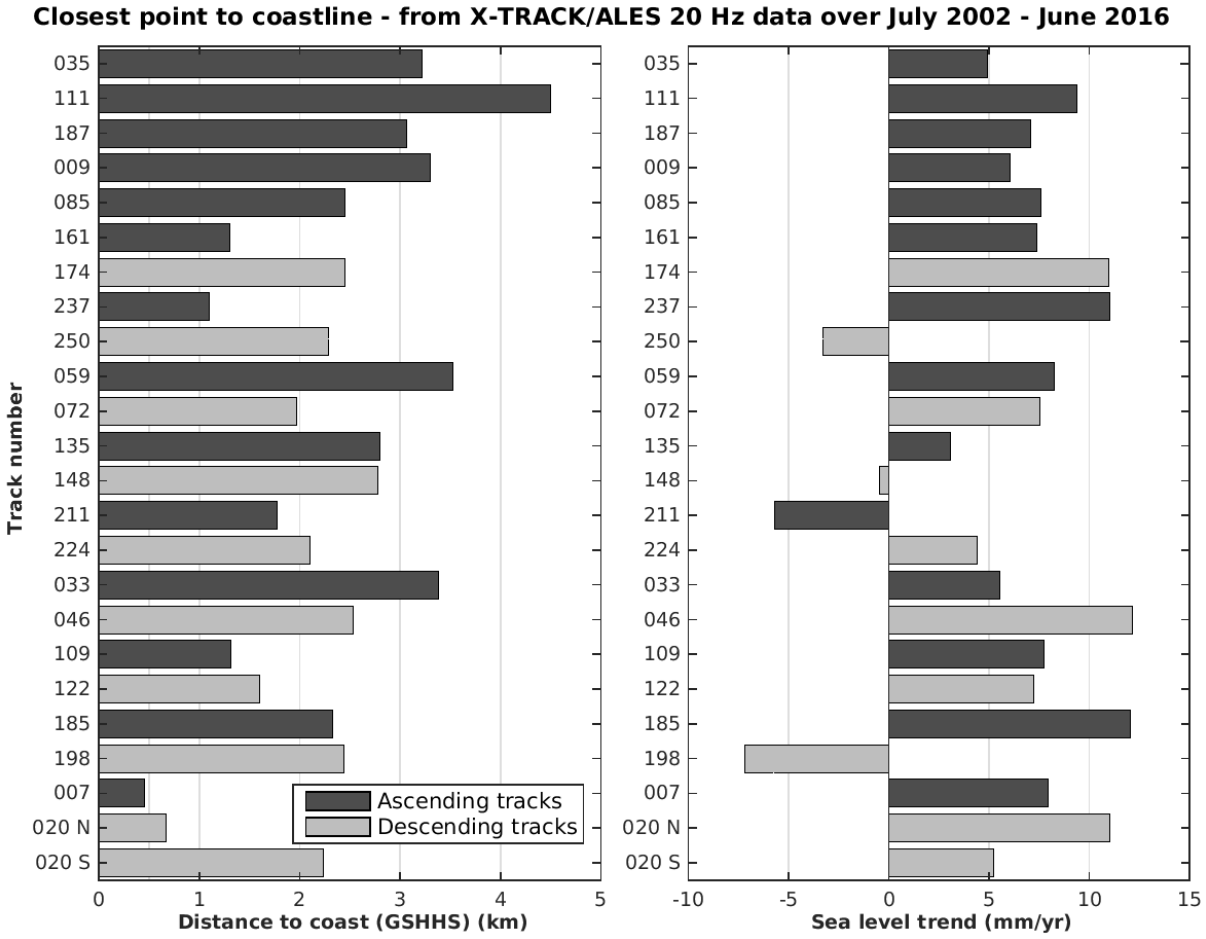

Figure 14